Investigating the mechanisms and the temporal regulation of the first cell polarity establishment in the mouse embryo

Meng Zhu

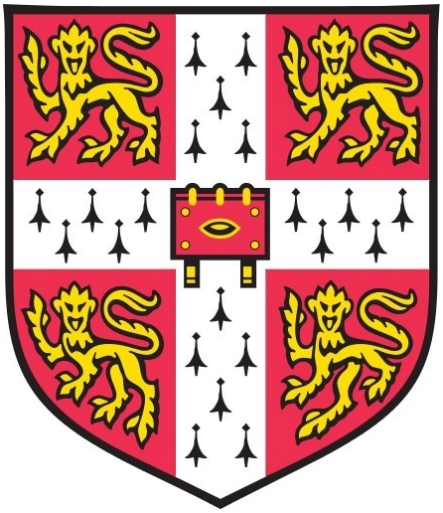

Christ's College

University of Cambridge

This dissertation is submitted for the degree of Doctor of Philosophy
July 2018

Declaration

This dissertation is the result of my own work and includes nothing which is the outcome of work done in the collaborations, except as specified in the text. This dissertation does not exceed the word limit prescribed by the Degree Committee.

Meng Zhu

Acknowledgements

The completion of this dissertation would never be possible without the tremendous help from people that I have met and worked with. Their intelligence, persistence, and the brave of tackling difficult yet significant biological questions are the inspiration for me to pursue the relevant work written in this thesis.

Firstly, I would like to thank my supervisor Professor Magdalena Zernicka-Goetz, for all her instructions, encouragement and caring throughout my entire Ph.D. study. Thank you for giving me suggestions for all the aspects of scientific skills. They transformed me entirely and will influence my life beyond Ph.D.

I would like to thank my parents, for their enduring spiritual and material support of my life and study, and, more importantly, for their respects to each single life choice of mine.

I also would like to thank the following colleagues in the lab: Dr. Agnieszka Jedrusik, for her guidance of mouse embryology and development; Dr. Chuen-Yan Leung, for introducing me to the question of this dissertation and his help for the first year of my Ph.D. Dr. Marta Shahbazi, for her help with my presentation and writing skills. To Shruti Singla, for being my best lab and life friend during my Ph.D.

I am grateful to Professor Martin Johnson and Professor David Glover, for their very helpful instructions and scientific discussions.

Finally, thank you Cambridge, for making my dream come true.

Abstract

Embryonic cells of many species polarise and the cell polarity is often important for the normal developmental progression. In the mouse embryo, the prototype of epithelial cell polarity, namely apico-basal polarisation, become established at the 2.5 days' post-fertilisation, when the embryos are at the 8-cell stage. The formation of apical domain is necessary and sufficient for the first segregation of extra-embryonic and embryonic cell lineages, as well as the following up morphogenetic transitions, such as the blastocyst formation. This study aims to explore the molecular pathways triggering the first cell polarity establishment in the mouse embryo, and to reveal the mechanism that programmes the timing of this event in the mouse embryo.

The results showed that cell polarity establishment during the 8-cell stage development can be divided into two major phases: in the first phase actomyosin complex became polarised to the cell-contact free surface; and in the second phase apical proteins recruited to the actomyosin enriched cell-contact free cortex, they further became centralised in the cell-contact free surface, excluding the local actomyosin meshwork, resulting in the formation of actomyosin ring. The activation and assembly of actomyosin meshwork during the first phase, but not its contractility, was essential for apical protein recruitment. Factors responsible for actin cytoskeleton reorganisation included Phospholipase C (PLC) – Protein Kinase C (PKC) pathway components, they directly activated actomyosin in the first phase through the Rho proteins such as RhoA.

Further results showed that the apical protein centralisation step required a proximate transcriptional input that was induced by two transcription factors, Tfap2c and Tead4. RNAi and Genetic depletion of these two factors prevented apical protein centralisation and the final apical domain assembly. The protein expression profile indicated that Tfap2c and Tead4 expression, and therefore their activity, were induced by zygotic genome activation. Significantly, overexpression of Tfap2c, Tead4, together with constitutively activated Rho proteins were sufficient to advance the timing of apical domain formation, indicating that the timer of cell polarity establishment at the 8-cell stage is set by the Rho proteins activation, and the zygotic transcriptional accumulation of Tfap2c and Tead4. Together, these results characterised the molecular events during the cell polarity establishment at the 8-cell stage mouse embryo, and identified the timing regulation of this event.

Table of Contents

Acknowledgements ii

Abstract iii

List of Figures viii

List of Tables xi

List of abbreviations xii

1 Introduction 1

1.1 Pre-implantation development overview 1

1.2 Compaction and the establishment of cell polarisation 3

1.3 Symmetric and asymmetric cell divisions, and two models of cell fate decisions 7

1.3.1 Inside-outside model 9

1.3.2 Cell polarity model 9

1.4 The mechanisms behind the first cell fate decision 10

1.4.1 Active cell internalisation directed by cellular surface tension settles the final cell position 10

1.4.2 The apical domain suppresses actomyosin contractility and is a necessary and sufficient condition for TE fate induction 11

1.4.3 Polarity couples a mechano-sensing mechanism to regulate Hippo pathway activity and determine inside and outside cell fates. 12

1.5 Project Aim 16

2 Material and Methods 17

2.1 Animals 17

2.2 Embryo culture and inhibitor treatments 17

2.3 Blastomere resection 18

2.4 Microinjection 18

2.5 Preparation of DNA Constructs 18

2.7 Immunofluorescence 31

2.8 RhoA-FRET imaging and data analysis 32

2.9 Optogenetics and regional PKC activation 32

2.10 Imaging and data processing 33

2.11 Real-time PCR **33**
2.12 Statistics **34**

3 Results I: dissecting the molecular mechanism triggering cell polarity establishment – a requirement of the PLC-PKC signalling pathway in triggering actomyosin early asymmetry **35**

3.1 Introduction **35**
3.2 Actomyosin apical polarisation precedes apical domain maturation **35**
3.4 The PLC-PKC pathway is required for apical domain assembly **49**
3.4.1 PKC is required not only for cell compaction but also for apical domain establishment *49*
3.4.2 PLC activation lies upstream of PKC and is required for apical domain assembly and the subsequent TE specification events *51*
3.5 PLC-PKC activity is necessary and sufficient for actomyosin asymmetry during the 8-cell stage development **56**
3.5.2 Ectopic PKC activation is sufficient to polarise actomyosin at the 4-cell stage *58*
3.5.3 PKC directly activates actomyosin *62*
3.6 Rho-GTPases lie downstream of PKC and establish the apical domain **65**
3.6.1 A myosin light chain phosphorylation independent mechanism is involved in PKC mediated actomyosin activation *65*
3.6.2 PKC inhibition inhibits RhoA apical polarisation *68*
3.6.3 RhoA re-activation rescues actomyosin apical recruitment and polarity defects driven by PLC-PKC inhibition *70*
3.7 Discussion **75**
3.7.1 The two phases of the apical domain formation process *75*
3.7.2 The convergence and divergence of compaction and cell polarisation processes during the 8-cell stage development *76*
3.7.3 The mechanism of PKC/RhoA in the activation of the actomyosin complex *77*
3.7.4 The timing of cell polarity establishment part I: how do PKC and RhoA get activated? *79*
3.7.5 Timing of cell polarity establishment part II: what is the missing factor required for apical domain assembly? *80*

3.7.6 The similarities and differences in polarity establishment between the mouse embryo and other developmental systems.....81

4 Results II: investigation of the timing regulation of cell polarity establishment 84

4.1 Introduction.....84

4.2 Protein synthesis inhibitor treatment did not advance the timing of cell polarisation but caused developmental arrest.....84

4.3 Examining the requirement of zygotic transcripts in triggering cell polarisation by blastomere resection 86

4.5 dsRNA screen for candidate zygotic genes for cell polarity establishment at the 8-cell stage.....97

4.5.1 Strategy no 1: Screen candidates based on gene expression profile as well as Gene Ontology terminology 97

4.5.2 Strategy no 2: screen transcription factors active around the 8-cell stage based on ATAC-seq data.....101

4.6 A CRISPR-Cas9 method to genetically deplete Tfap2c and Tead4 105

4.7 Tfap2c and Tead4 protein showed nuclear accumulation after ZGA and their depletion affected gene expression at the early 8-cell stage. 109

4.8 Tead4 expression regulates early Yap nuclear localisation 111

4.9 Overexpression of Tfap2c/Tead4/RhoA triggers premature apical domain formation 114

4.9.2 Actin regulators are activated by Tfap2c and Tead4 and are regulating apical domain concentration step.....119

4.9.3 Co-overexpression of Tfap2c, Tead4 and RhoA accelerates the morphogenetic events related to apical domain establishment. 122

4.10 Tfap2c/Tead4/RhoA co-overexpression accelerated the morphogenetic program in the preimplantation mouse embryo.....126

4.11 Discussion 129

4.11.1 Re-examination of "inhibitor hypothesis": is cell polarity driven by the degradation of inhibitor(s) or the accumulation of zygotic activator(s)? 129

4.11.2 Blastomere resection experiment implicates a role for zygotic RNA concentration in the determination of the timing of cell polarity. 131

4.11.3 Transcription factor Tfap2c and Tead4 activity is required for cell polarity establishment. 132
4.11.4 A genetic interaction between Tfap2c and Tead4 133
4.11.5 The molecular panorama of cell polarity establishment at the 8-cell stage mouse embryo and its potential implications 134

5 Conclusions 136

6 References 138

7 Appendix I: original publications and manuscripts 152

List of Figures

Figure 1.1 Preimplantation mouse embryo development overview..... 2
Figure 1.2 The establishment of cell polarisation at the 8-cell stage of embryonic development..... 6
Figure 1.3 Internalisation of apolar cells during 8-16 cell division..... 8
Figure 1.4 The Hippo pathway directs polarised outer cells to become TE.....15
Figure 3.1Measurement of inter-blastomere angle and the signal intensity.. 36
Figure 3.2 Actomyosin and Pard6 dynamics during 8-cell stage development.....37
Figure 3.3 Dynamics of GFP-MRLC and Pard6 during the 8-cell stage of development.....39
Figure 3.4 Dynamics of aPKC, Crb3 and Ezrin in relation to F-actin during the 8-cell stage development.....41
Figure 3.5 The RNAi method failed to effectively eliminate Myl12b protein due to the maternal store.. 43
Figure 3.6 The effects of different actomyosin inhibitors on polarisation revealed that actomyosin activation but not contractility is required for apical domain assembly.....45
Figure 3.7 ML-7 treatment from the mid 8-cell stage after compaction abolished apical domain establishment.. 47
Figure 3.8 ppMRLC levels are upregulated from the early 8-cell stage.....48
Figure 3.9 Schematic view of PLC-PKC pathway.. 50
Figure 3.10 Inhibition of PLC activity abolished compaction, cell polarisation and subsequent TE specification events upstream of PKC signalling.. 54
Figure 3.11 Overexpression of PLC-DN abolished cell compaction, polarity establishment and TE specification.. 56
Figure 3.12 PKC activity is required for actomyosin activation and polarisation.....58
Figure 3.13 Ectopic activation at early 8-cell stage led to the expansion of apical domain.. 59
Figure 3.14 PKC activation at the 4-cell stage induces actomyosin polarisation but not apical domain formation.....61
Figure 3.15 Regional PKC activation induces local actomyosin activation.. 64
Figure 3.16 Phosphomimetic MRLC mutant bypasses the requirement of MRLC phosphorylation to form Myosin II filaments.. 66

Figure 3.17 PKC recruits MRLC to the membrane in a phosphorylation independent manner.. ..... *67*
Figure 3.18 RhoA inhibition abolished actomyosin and Par complex apical polarisation.. *69*
Figure 3.19 RhoA activity rescues the actomyosin and Par complex polarisation defects upon PLC-PKC pathway inhibition...... *71*
Figure 3.20 Summarised model of molecular pathways leading to cell polarity establishment.. ..... *74*
Figure 4.1 Protein synthesis inhibitors did not trigger premature cell polarisation at the late 4-cell stage...... *85*
Figure 4.2 Protein synthesis inhibitors caused embryo developmental arrest and the failure of cell polarisation establishment.. ..... *86*
Figure 4.3 Zygotic activator driven hour-glass hypothesis and blastomere resection experiment illustration.. ..... *88*
Figure 4.4 Resected cells from 2-cell stage embryo always polarised earlier than control sister cells.. ..... *90*
Figure 4.5 Resected cells from 4-cell stage embryo always polarised earlier than control sister cells.. ..... *91*
Figure 4.6 Inhibition of transcription prevents advancement of timing of cell polarisation.. ..... *93*
Figure 4.7 DRB treatment blocked cell polarisation.. ..... *95*
Figure 4.8 Triptolide treatment blocked cell polarisation.. ..... *96*
Figure 4.9 Validation of dsRNA targeting different transcription factors active at the 8-cell stage.. ..... *103*
Figure 4.10 dsRNA-mediated knockdown of Tfap2c and Tead4 led to the delay of cell polarisation at the late 8-cell stage.. ..... *105*
Figure 4.11 CRISPR strategy to deplete Tfap2c and Tead4 from the zygote stage generated cells expressing different levels of Tfap2c and Tead4...... *107*
Figure 4.12 Genetic depletion of Tfap2c and Tead4 by CRISPR technology abolished cell polarity at the late 8-cell stage...... *108*
Figure 4.13 Expression profile of Tfap2c and Tead4 from the 2-cell to the 8-16 cell stage.. ..... *110*
Figure 4.14 Yap nuclear localistaion correlates with Tead4 expression profile from 2-8 ell stage.. ..... *112*

Figure 4.15 Tead4 expression regulates Yap nuclear localisation.. 113
Figure 4.16 A high concentration of Tfap2c leads to cell division defects..... 115
Figure 4.17 Overexpression of Tfap2c or Tfap2c+Tead4 lead to the formation of membrane protrusion like structures at the late 4-cell stage and premature compaction events..... 116
Figure 4.18 Tfap2c and Tead4 overexpression induces apical domain centralisation without apical domain expansion.. 118
Figure 4.19 Cofilin/ADF factors and the Arp2/3 complex mediate the apical domain centralisation step downstream of Tfap2c and Tead4.. 122
Figure 4.20 RhoA regulates the apical domain size.. 123
Figure 4.21 RhoA-Q63L together with Tfap2c and Tead4 overexpression led to the formation of a premature apical domain.. 125
Figure 4.22 RhoA, Tfap2c, Tead4 overexpression led to premature apical domain formation and accelerated the following morphogenetic events..... 128
Figure 4.23 Model of the timer regulating polarity formation in the 8-cell stage mouse embryo..... 129

List of Tables

Table 2.1 Primer sequences for constructs preparation *19*
Table 2.2 Primers sequence for sgRNAs preparation *21*
Table 2.3 Primers for dsRNA preparation *21*
Table 2.4 Primers for real-time PCR *34*
Table 4.1 The selected candidate list for the RNAi screen. *98*
Table 4.2 The combination of candidate genes for dsRNA injections *100*

List of abbreviations

TE	Trophectoderm	PLC	Phospholipase C
ICM	Inner cell mass	PH	Pleckstrin homology domain
PrE	Primitive endoderm	Cas9	CRISPR associated protein 9
EPI	Epiblast	RNA	Ribonucleic acid
AJ	Adherens Junction	DNA	Deoxyribonucleic acid
ERM	Ezrin, radixin and moesin	sgRNA	single guide RNA
TF	Transcription factor	dsRNA	double strand RNA
Cdx	caudal type homeo box transcription factor 2	mRNA	messenger RNA
Gata	GATA binding protein	Cfl1	Cofilin 1
Amot	angiomotin	Dstn	Destrin
Sox2	SRY-box 2	Marksl1	myristoylated alanine-rich C-kinase substrate
Nanog	Nanog homeobox	Pfn1	Profilin 1
Oct4	octamer-binding transcription factor 4	Pou5f1	POU class 5 homeobox 1
aPKC	atypical protein kinase C	Rbpj	Recombination Signal Binding Protein
ZO-1	Zonula occludens-1	Rps11	Ribosomal Protein S11
Pard6	Partitioning defective 6 homolog alpha	Xab2	XPA Binding Protein 2
E3.5	Embryonic day 3.5	PBS	Phosphate-buffered saline
E4.5	Embryonic day 4.5	PFA	Paraformaldehyde
Yap	Yes associated protein	CRB3	Crumbs 3
Tead4	Transcriptional enhancer factor TEF-3	DAPI	4′,6-diamidino-2-phenylindole
ROCK	Rho-associated protein kinase	ROI	Region of interest
Las1/2	Large tumor suppressor kinase 1/2	PCR	Polymerase chain reaction
DRB	5,6-dichloro-1-beta-D-ribofuranosylbenzimidazole	ANOVA	Analysis of variance
DMSO	Dimethyl sulfoxide	IEA	Inter-blastomere angle
ML-7	ML 7 hydrochloride	PIP2	Phosphatidylinositol 4,5-bisphosphate
PKC	Protein kinase C	DAG	Diacylglycerol
GFP	green fluorescent protein	DN	Dominant Negative
MRLC	Myosin regulatory light chain	FRET	Fluorescence resonance energy transfer
CRY2	Cryptochrome-2	FRAP	Fluorescence recovery after photobleaching
KD	Kinase domain	JAM-1	Junctional adhesion molecule 1
CIBN	Cry2 binding domain	Cdc42	Cell division control protein 42 homolog
CAAX	CAAX motif	ECM	Extra-cellular matrix
Tfap2c	Transcription factor AP-2 gamma	ZGA	Zygotic Genome activation

1 Introduction

1.1 Pre-implantation development overview

During the first four and a half days of mouse embryogenesis, the glycoprotein shell protected zygote transforms into a hollow structure termed the blastocyst, which is characterised by a huge fluid filled blastocoel surrounded by roughly a hundred cells. The blastocyst consists of three distinct cell lineages: the outermost layer is a primary epithelial tissue called Trophectoderm (TE), which consists of the majority of cells of a blastocyst and functions as a material exchange hub between the maternal environment and the embryonic tissues throughout gestation. A compact small ball of cells called the Inner Cell Mass (ICM) sits on the interior and on one side of the blastocyst, hosting two cell populations, the Epiblast (EPI) and the Primitive Endoderm (PrE), which give rise to the embryo proper and the yolk sac respectively (Bedzhov et al., 2014) (Figure 1.1).

Building the blastocyst involves both morphogenetic and potency transitions. Totipotency, the ability of a cell to give rise to all lineages, becomes restricted with the establishment of cellular polarisation that happens at the 8-cell stage or 2.5 days' post-fertilisation. The apical domains developed at the 8-cell stage are not inherited by all cells during the following cell divisions, leading to the generation of polar or apolar cells that ultimately engage different cell positions and fates. At the late morula stage the embryo is consisted of the outside and inside cells, which will become TE and ICM respectively. Despite that the cell position starts to diverge after the 8-cell stage, the transcriptional segregation of TE and ICM precursors are progressive and the fate commitment only completes around the E3.5. This timing overlaps with the initiation of the next cell fate segregation event in which the ICM differentiates into EPI and PrE, accompanying with the cavitation event. All three lineages arise at E4.5 and by then the blastocyst is ready to implant into the uterus (Figure 1.1).

Studying the molecular pathways governing cell fate specification during preimplantation embryogenesis has been challenging due to the scarcity of materials one can obtain from each small-sized embryo. The understanding of the molecular mechanism behind the preimplantation embryogenesis had been therefore largely relied on the embryological manipulations and the generation of genetic mutations. Early embryology studies suggest that the cell positioning and cell polarity cues are responsible for the early lineage segregation

(Johnson and Ziomek, 1981; Tarkowski and Wroblewska, 1967), and the generation of different gene knockout mouse identified important signalling pathways and transcription factors key for cell fate transitions. Nevertheless critical information is lacking to answer important questions such as how cellular morphogenetic changes crosstalk with lineage differentiation, as well as how the dynamics of different signalling pathway activities integrate and direct cell fate specification. The recent advance in bio-imaging methods, sequencing technology and the biophysics and mathematical analysis provided an unprecedented view into preimplantation development and helped to resolve many enduring developmental questions, particularly the processes segregating TE and ICM progenitors. The mechanical and chemical interactions linking cell polarity, cell position and cell fate have been recently revealed, yet many other important questions that are necessary to fully reveal the trajectory from totipotency to cell fate differentiation events, are still outstanding.

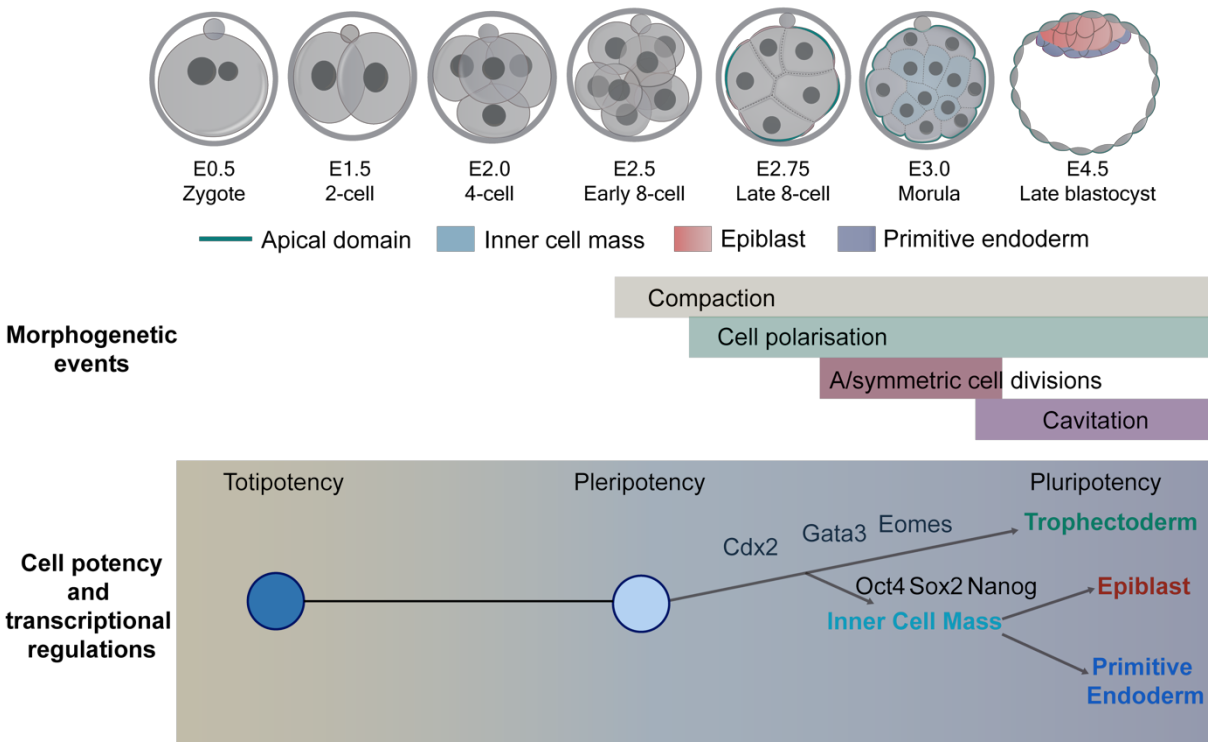

Figure 1.1 Preimplantation mouse embryo development overview. Preimplantation development spans the first 4.5 days of mouse embryogenesis. It begins with a fertilised zygote, followed by three rounds of cleavage cell divisions. At the 8-cell stage the embryos undergo compaction during which cell-cell contacts are maximised. The individual cells establish apico-basal polarity, with apical domains facing outwards (labelled in green). Following the

establishment of cell polarity, symmetric and asymmetric cell divisions generate outer polarised cells and inner apolar cells. The outer polarised cells ultimately give rise to Trophectoderm (TE), whereas the inner apolar cells give rise to Inner Cell Mass (ICM) that will further differentiate into Epiblast (EPI) and Primitive Endoderm (PrE). The cavitation event generates a fluid filled cavity in the middle (blastocoel) which completes the blastocyst structure. The embryos at the blastocyst stage then escape the *zona pellucida* (the outer shell labelled in grey), ready to implant into the uterus.

1.2 Compaction and the establishment of cell polarisation

After fertilisation, the zygote undergoes three rounds of cleavage divisions that increase cell numbers without affecting the total volume. At 2.5 post-fertilisation days, the eight morphologically identical cells flatten against each other, cell-cell boundaries become obscured and the cell contact-free area minimised (Pratt et al., 1982). Coinciding with compaction, each cell establishes an “apico-basal polarity" (Ziomek and Johnson, 1980), in which the cell-junctional proteins are exclusively enriched at the cell contacts (basal domain) (Clayton et al., 1999; Thomas et al., 2004), and the evolutionary conserved apical proteins aPKC and Pard6 become polarised to the cell contact-free surface (apical domain) (Hirate et al., 2013; Vinot et al., 2005). The embryo presents a radial pattern of polarity, with the basal domain localised on the inside of the embryo and apical domains facing outwards. This polarity pattern is highly conserved in evolution, as it also present in many non-mammalian early embryos such as *C.elegans* and *Xenopus* (Nance, 2014). Recent studies point to a critical role of compaction and cell polarity in regulating early mouse embryogenesis, as disturbance of these often leads to preimplantation developmental abnormalities (Kono et al., 2014; Stephenson et al., 2010).

1.2.1 Compaction

Cell adhesion bridges adjacent cells and facilitates multi-cellular scale interactions. Thus it is important for both tissue morphogenesis and homeostasis (Dejana, 2004; Gumbiner, 2005). In the mouse embryo, cell compaction consolidates the blastomeres into an integrated entity, lays the foundations for subsequent morphogenetic events such as blastocyst formation (Ducibella and Anderson, 1975; Larue et al., 1994; Riethmacher et al., 1995), and plays an important role in cell fate specification events (Stephenson et al., 2010). Given the importance of compaction

for embryo progression, significant efforts were made to determine the mechanism triggering this first morphogenetic event. It is widely accepted that the Adherens Junction (AJ) complex, a universal and fundamental unit of cell-cell contacts, is critical for the compaction process. The basic elements composing the AJ include the transmembrane cadherin proteins, E-cadherin and beta/alpha-catenin (Hartsock and Nelson, 2008). Various different attempts to disrupt AJ proteins such as calcium-free medium culture (Pey et al., 1998), glycoprotein antibody incubation (Hyafil et al., 1980), RNAi or genetic gene trap targeting E-cadherin or alpha-catenin (Torres et al., 1997; Wianny and Zernicka-Goetz, 2000) consistently abolished compaction at the 8-cell stage. No significant changes in the expression level of E-cadherin, nor any other AJ components can be detected before or after compaction (Ohsugi et al., 1996; Vestweber et al., 1987). Thus, the literature characterising upstream events driving cell compaction has focused primarily on the post-translational modifications of AJ proteins (Sefton et al., 1992; Vestweber et al., 1987). Some AJ components have indeed been reported to undergo certain post-translational modifications such as phosphorylation and the its level upregulates around the 8-cell sage, yet this seems dispensable for compaction as circumstances exist in which the compaction can happen without E-cadherin phosphorylation (Aghion et al., 1994). Whether compaction is driven by transcription or post-translational modifications of AJ proteins per se remains so far unclear.

Studies in other embryonic tissues or matured epithelial cells suggest that the level and spatial rearrangement of the surface tension are closely associated with the cell shape changes (Lecuit and Lenne, 2007; Miller and Davidson, 2013). In particular, the net balance between interfacial and cortical tension largely accounts for the cellular morphology (Winklbauer, 2015). The key regulator responsible for tension generation is the actomyosin meshwork, which is composed of actin and myosin II filaments, and is positioned underneath the plasma membrane (Munjal and Lecuit, 2014; Murrell et al., 2015). Theoretical modelling according to physical principles predicts that when cortical tension overrides interfacial tension, this can drive the junctional membranes to expand and flatten against each other (Manning et al., 2010). This is commonly the case when cell-contacts become established and cortical tension interacts with the actomyosin network to reduce the interfacial tension. Such mechanism appears largely true for mouse embryo compaction, as it has recently been shown that during the 8-cell stage development the actomyosin network becomes apically polarised and accompanies cell-contact elongation and thereby compaction. More importantly, when the overall surface tension is

reduced, through inhibition of the contractility of myosin II, cell compaction does not occur (Maitre et al., 2015). This result is reminiscent of the theoretical model suggesting that compaction is driven by intracellular mechanics and that actomyosin apical polarisation is a key event in this process.

Alongside the role of differential surface tension in driving cell compaction, morphological changes in the membrane involving the formation of protrusions also contributes to cell compaction. A recent study using advanced time-lapse imaging methods, found that one type of membrane protrusion named filopodia substantially formed during cell compaction between adjacent blastomeres. AJ proteins, such as E-cadherin, alpha-catenin and beta-catenin, as well as a special myosin motor protein, myosin X, have all been identified as components of the filopodia (Fierro-Gonzalez et al., 2013). Filopodia have been documented previously in cultured cells and are associated with cell migration, but their function in the context of development is not clear (Nishita et al., 2006). These filopodia form during compaction, actively extend at the points of contact with adjacent blastomeres, and then retract prior to cell divisions (Fierro-Gonzalez et al., 2013). Laser ablation of filopodia leads to the failure of cell compaction, while conversely, induction of premature formation of filopodia by overexpression of myosin X induces premature compaction (Fierro-Gonzalez et al., 2013). This suggests that these structures assist the compaction process, presumably by promoting the binding of trans-AJ molecules and thus the establishment of new AJ across cell-membranes (Fierro-Gonzalez et al., 2013; White and Plachta, 2015) (Figure 1.3).

In brief, recent studies suggest that actomyosin tension, together with the formation of membrane specialised structures activate compaction process at the 8-cell stage.

1.2.2 Apico-basal polarity establishment

Similar to most other embryonic model systems, mouse embryonic cells are polarised but only after the 8-cell stage (Johnson and Ziomek, 1981; Nance, 2014). As mentioned earlier, the time-window of polarity overlaps with that of compaction (Ziomek and Johnson, 1980) and thus these two processes are thought to be correlated. Proteins from many different types of junctions localise to the basal domain but not all of them are completely functional at the 8-cell stage. These include: the AJ proteins; the gap junction proteins such as connexin43; and some but not all tight junction proteins, such as Jam-1 (also named F11r) (De Sousa et al., 1993;

Ducibella et al., 1975; Thomas et al., 2004). Meanwhile, a handful of conserved epithelial apical polarity proteins are also enriched at the apical domain. Typical examples include: the functional Par complex, which consists of a scaffold protein Pard6 and a kinase protein atypical Protein Kinase C (aPKC) (Vinot et al., 2005), and in general drives apical domain differentiation; the ERM protein family, which controls microvilli formation and acts as a linker between the plasma membrane and Filamentous actin (F-actin) (Louvet et al., 1996); various cytoskeleton components, such as actin and the microtubule network (Johnson and Maro, 1984; Maro et al., 1991). The changes in molecular distribution are coupled with ultracellular structural changes. Consistent with the apical enrichment of ERM family proteins and F-actin, the microvilli, a cluster of specific cellular membrane protrusions which function to facilitate the ion exchange between the intracellular and intercellular environments, are also polarised to the cell contact-free surface (Reeve and Ziomek, 1981).

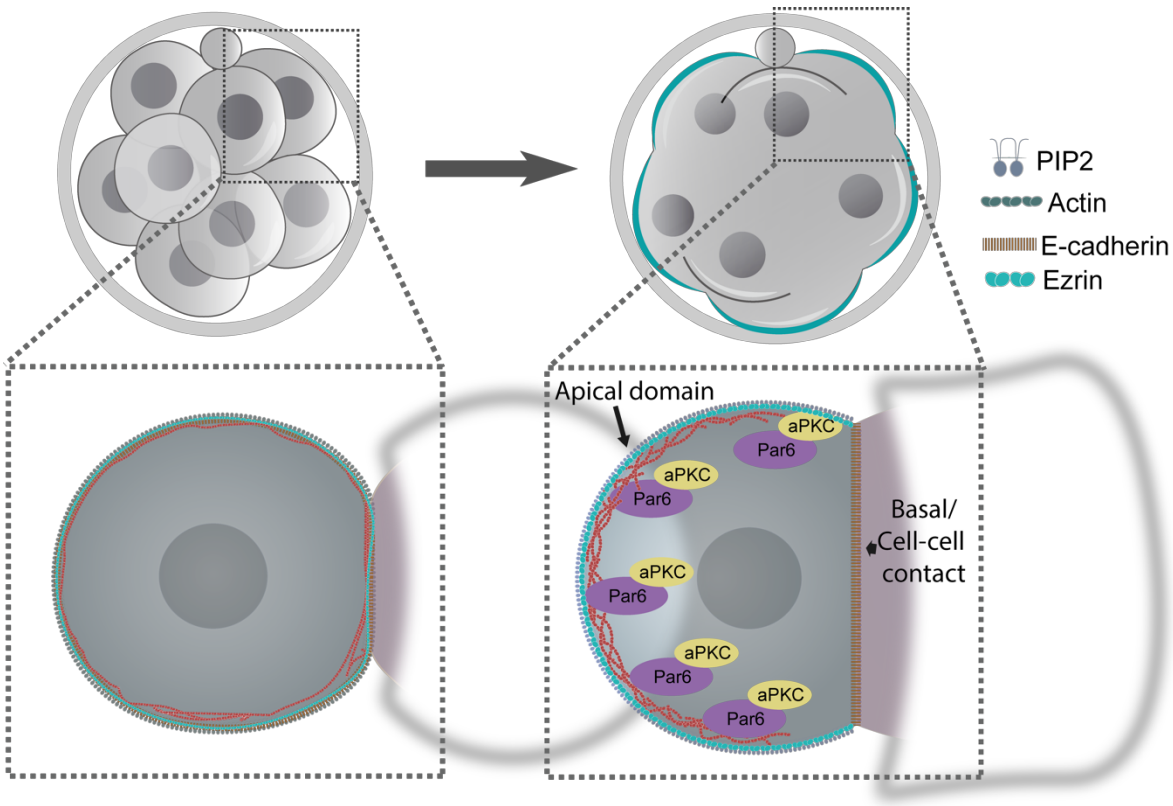

Figure 1.2 The establishment of cell polarisation at the 8-cell stage of embryonic development. During the 8-cell stage, the cell contacts enriched by E-cadherin are polarised to the cell contacts site and become elongated (basal domain), resulting in the close apposition between adjacent blastomeres. Concomitantly, the Par complex, including aPKC, Pard6 and

ERM family members such as Ezrin, becomes recruited to the cell contact-free surface, denoting the apical domain.

Apico-basal polarisation is established at the 8-cell stage and drives the commencement of the epithelisation process that takes place during TE differentiation. At the 16-32 cell stage, the apical domains start to expand to the cell-junctions where they couple to newly recruited tight junction proteins such as ZO-1 and Cingulin, a process that is termed "apical domain zippering" (Zenker et al., 2018). Tight junctions become fully matured at the late morula stage with the recruitment of Claudin and Occuldin (Eckert and Fleming, 2008). Tight junction maturation also coincidence with the recruitment of membrane Na+ K+ ATPase pumps, with which the embryo starts to cavitate. Desmosomes, another important type of junctions in epithelial cells, can only be detected from the blastocyst stage in the TE cells (Fleming et al., 1991). Therefore, the epithelialisation process of the outside TE starts from the 8-cell stage but is only completed at the blastocyst stage (Fleming et al., 1989).

Epithelisation at the 8-cell stage mouse embryo begins with the establishment of polarity of a small group of non-polarised cells and extends to the subsequent process of TE maturation. It is a unique in vivo model for the study of de novo cell polarity establishment as well as that of initiation of epithelisation. However, in comparison to other model systems such as *C.elegans* and *Drosophila* our knowledge of cell polarity establishment in the early mouse embryo is limited (Nance, 2014; St Johnston and Ahringer, 2010).

1.3 Symmetric and asymmetric cell divisions, and two models of cell fate decisions

The initiation of epithelial polarity at the 8-cell stage is a critical event for embryonic progression as it facilitates cellular diversity and thereby lineage differentiation, through symmetric or asymmetric cell divisions. This model has recently been illustrated in the context of mouse embryo development, but is also likely to be conserved in other mammalian species, as its key components show similar distribution patterns in human and bovine embryos (Frankenberg et al., 2016; Kuijk et al., 2012).

In the mouse embryo at the time of cytokinesis which follows on from the 8-cell stage, as the embryonic cells polarise, the apical domain can be distributed in two different ways. On one

hand, the apical domain may be equally partitioned by the cleavage plane, in which case it is inherited equally by the two daughter cells, resulting in the formation of two polarised cells or two polar cells. On the other hand, the cell cleavage planes may incline in which case apical domains are assigned to only one side, permitting the generation of two cells that differ in their cell polarisation status, thus a polar and an apolar cell. In the former case the process is termed symmetric cell division while in the latter case it is termed asymmetric (Figure 1.3) (Bedzhov et al., 2014; Chazaud and Yamanaka, 2016).

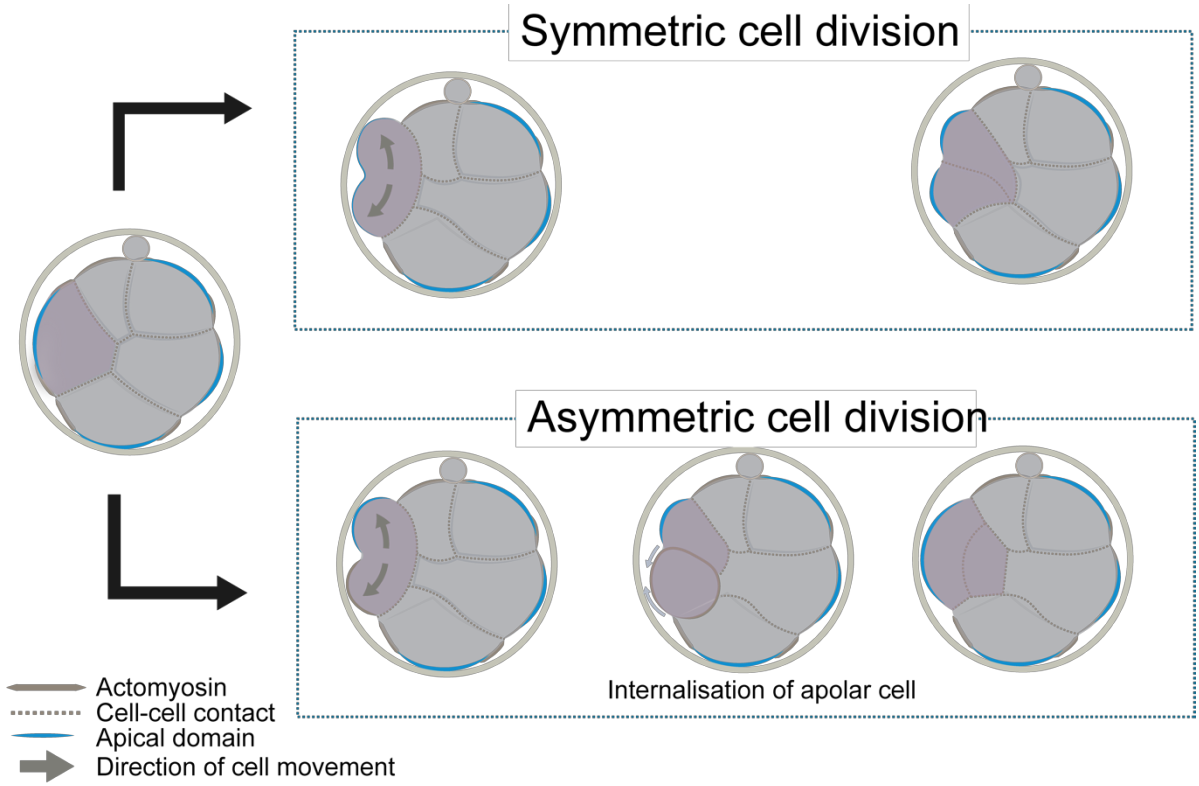

Figure 1.3 Internalisation of apolar cells during 8-16 cell division. During the 8-16 cell stage, the cells can divide in two different ways: 1) in symmetric cell division the apical domain is equally inherited by the two daughter cells (labelled in pink). The presence of the apical domain antagonises actomyosin contractility and therefore reduces cortical tension, allowing the two daughter cells to remain outside. 2) In asymmetric cell division, one of the daughter cells appears apolar and therefore displays high actomyosin contractility and cortical tension, and is internalised as a result of the net cortical tension difference with its neighbouring cells.

The difference in cell polarity between polar and apolar cells relates to subsequent differences in cell position and fate. Specifically, the polarised cells are positioned on the outside and

become TE, whereas the apolar cells are positioned on the inside and are specified as pluripotent ICM. As both the cell polarity conditions as well as the cell position seem to correlate with cell fate, two models namely the inside-outside model and the cell polarity model, have been proposed to explain the mechanism segregating TE and ICM cell fate.

1.3.1 Inside-outside model

The inside-outside model originated from an early observation that when cell numbers were not sufficient for correct positioning of cells on the inside of a blastocyst, such as in the case of an isolated 8-cell stage blastomere allowed to develop to blastocyst stage, all cells would specify as TE (Tarkowski and Wroblewska, 1967). Tarkowski et al., therefore proposed that the cell position endows the cells with distinct external environment which specifies their fate. This hypothesis is further supported by the experimental observation that when the cell position of inside and outside cells in 16-cell to 32-cell stage embryos were experimentally reversed, the cells altered their fate in response to the new positions accordingly (Handyside, 1978; Spindle, 1978). Although the determinant of inside-outside cell positioning remains unclear, as does the initial cue that breaks symmetry to generate different cell positions, this model has been highly influential for a certain period due to its simplicity and its strength in explaining experimental observations. The discovery of new transcription factors that are responsible for specifying different lineages however bring some doubts to this model, as those transcription factors start to express non-correlated with cell positions initially (Anani et al., 2014; Dietrich and Hiiragi, 2007). Some other cues seem to come into play to influence cell fate before the cells settle their positions.

1.3.2 Cell polarity model

By dissecting single 8-cell stage blastomeres and examining their polarisation status using Concanavalin A, it was determined that the 8-16 cell stage divisions generate two populations of cells, one of which appears polarised and the other apolar (Johnson and Ziomek, 1981a (Johnson and Ziomek, 1981; Ziomek and Johnson, 1981). Together with the observation that the polarised cells always localise to the outside of the embryo while the apolar cells are enclosed (Handyside, 1981; Reeve and Ziomek, 1981; Ziomek and Johnson, 1981), a second hypothesis was raised, according to which the differential inheritance of polarised domains leads to the formation of TE and ICM cells.

The latter cell polarity model is not independent of the former inside-outside model but rather it is complementary to it. However, the intermediate steps between the asymmetric assignment of the apical domains and the final allocation of cell position remained undetermined (Johnson and Ziomek, 1981a). That is, what allows the polarised cells to maintain their outside position and what leads the apolar cells to the inside? Thanks to the advance of time-lapse imaging techniques and the introduction of mechanical principles, this question has been recently addressed. Moreover, the generation of several knockout mice has aided in the discovery of the critical modulators of TE/ICM segregation. Current literature allows us to draw a relatively complete picture of TE and ICM lineage segregation, with the inclusion of both of the two aforementioned models.

1.4 The mechanisms behind the first cell fate decision

1.4.1 Active cell internalisation directed by cellular surface tension settles the final cell position

It has always been assumed that the inside cells adopt their position directly by asymmetric cell divisions, that is, the spindle orientation is almost perpendicular to the apical domain and thus the cell is directly pushed to the inside (Rossant and Tam, 2009; Zernicka-Goetz et al., 2009). In the effort to discern the link between cell polarity and cell position, another interesting observation from the work describing the cell polarity model should be considered. Despite reports that a single 8-cell blastomere preferentially divided asymmetrically (82%) (Johnson and Ziomek, 1981a), and therefore one would expect around 6 apolar cells to arise from the 8-16 cell stage division, the average number of inside cells at the 16-cell stage was found to be only 2-3 (Anani et al., 2014; Morris et al., 2010). Arguably, in the case of the isolated blastomere the lack of cell-cell contacts in the environment may have modulated the ratio of division patterns which would explain the difference in number. Yet although recent results using intact embryos showed that the frequency of asymmetric cell divisions is slightly lower than that in isolated couplets, it is still too high to explain the number of inside cells (around 60%) ((Anani et al., 2014; Humiecka et al., 2017). It thus seems unlikely that asymmetric cell divisions would directly allocate the apolar cells to the inside. In order for this process to be confidently captured an approach allowing the visualisation of the global cell behaviour is necessary. A recent study utilised high resolution confocal microscopy, combined with a 3D membrane segmentation technique to demonstrate that, in the majority of asymmetric cell

divisions, the spindle is not oriented along the radial axis of cell polarity in each cell, but rather it is randomised (McDole et al., 2011; Samarage et al., 2015; Watanabe et al., 2014). As a result, many apolar cells are left on the outside of the embryo, but from the 12-cell stage onwards, 2-3 cells are selectively engulfed by the embryo, via a process known as "internalisation" (Samarage et al., 2015). So what triggers cell internalisation and why are only 2-3 cells engulfed? The key player is again the actomyosin complex and the resulting surface tension it generates. In the first instance, it was shown that the active actomyosin complex appears asymmetric between polar and apolar cells in both 16-cell couplets and intact embryos (Anani et al., 2014; Samarage et al., 2015). Specifically, surface tension is high in apolar cells and low in polar cells, and as a result when a polar cell encounters an apolar cell the membrane of the polar cell will move over the apolar cell, leading to an "entosis" like behaviour (Figure 1.3) (Anani et al., 2014). Similar results can be expected in an intact embryo, especially in cases where the newly formed apolar cells are surrounded by polar cells. However when too many apolar cells appose nearby, the engulfment purely depends on the differential surface tension. A successful engulfment of apolar cells will only happen when the difference in surface tension is above 1.5 fold (Maitre et al., 2016), thus explaining why only a small proportion of cells can be engulfed. In support of the model, reducing actomyosin activity by for example depletion of myosin or inhibition of myosin phosphorylation, blocked cell internalisation, and led to subsequent cell fate alteration (Figure 1.3) (Maitre et al., 2016; Samarage et al., 2015).

Together this evidence points to actomyosin as a critical regulator of cell internalisation, yet the number of cells that can be engulfed depends on both the surrounding environment and the geometrical limitations of the inner space.

1.4.2 The apical domain suppresses actomyosin contractility and is a necessary and sufficient condition for TE fate induction

How does the activity of actomyosin differ in polar and apolar cells? As it appears that the apical domain activity is negatively correlated with the level of actomyosin, it would be reasonable to assume that the apical domain suppresses actomyosin activity. This has proven to be largely true: once the apical domain is established, it occupies a proportion of the cell contact-free surface between the 8-16 cell stage and actomyosin activity appears to be lower on the inside of the apical domain than the periphery. However, the depletion of apical domain

components, such as aPKC isoforms, leads to homogeneous actomyosin activity over the entire cell contact-free surface, indicating an aPKC mediated inhibition of actomyosing activity (Maitre et al., 2016).

Besides the role of actomyosin in mediating cell internalisation, it is clear that the differential allocation of the apical domain also influences the cell position. Polar cells remain on the outside of the embryo as a result of a lack of actomyosin activity, while the apolar cells have the potential to localise to the inside, but this process is dependent the neighbouring environment. Cells that are not engulfed will then re-polarise and remain on the outside.

But is the apical domain really the key modulator in directing the cells to the TE fate? To unequivocally clarify this point, an apical domain transplantation experiment was performed. In this experiment, the apical domain from a polarised 8-cell stage blastomere was grafted to the apolar cells of a 16-cell stage embryo. The results indicate that the exogenous apical domain was sufficient to direct the apolar host cells to upregulate Cdx2 expression and thus become specified as TE progenitors (Korotkevich et al., 2017).

Thus far it is clear that the cell polarity model and the inside-outside model can be reconciled. The apical domain is either symmetrically or asymmetrically assigned to the daughter cells, leading to the generation of polar and apolar cells. The cells tend to have high actomyosin contractility yet this is inhibited by the apical domain. As a result, the apolar cells when surrounded by polar cells, present with a greater surface tension, which results in the engulfment of these cells to the inside of the embryo. When positioned inside, E-cadherin covers all cell membranes and therefore apical domains can no longer be re-generated, which restricts the fate of these cells to the ICM.

1.4.3 Polarity couples a mechano-sensing mechanism to regulate Hippo pathway activity and determine inside and outside cell fates.

The specification of TE and ICM fate is reliant on the activation of a lineage specific transcriptional network. The TE transcriptional network is established by several master transcription factors (TF) such as Cdx2, Gata3, Elf5 and Eomes (Latos et al., 2015; Niwa et al., 2005; Ralston et al., 2010; Russ et al., 2000). Of these, Cdx2 and Gata3 function during TE specification at the preimplantation stage, while Elf and Eomes are important for maintaining

the extraembryonic ectoderm identity in the post-implantation embryo. The knockout of zygotic Cdx2 results in TE differentiation defects, as a result of which the embryos collapse soon after implantation (Strumpf et al., 2005). The pluripotent ICM state, on the other hand, is stablished by pluripotency factors including Nanog (Mitsui et al., 2003), Sox2 (Avilion et al., 2003) and Oct4 (Nichols et al., 1998), all of which are known to be essential in the self-renewal of pluripotent embryonic stem cells (Kashyap et al., 2009; Loh et al., 2006). In the embryo, the transcriptional network responsible for TE fate specification, inhibits the ICM cell fate and restricts the pluripotent ICM progenitors to the inside of the embryo (Dietrich and Hiiragi (Dietrich and Hiiragi, 2007; Strumpf et al., 2005). Specifically, both Cdx2 and Gata3 expression are limited to the outside cells from the 16-cell stage onwards, and before ICM markers are restricted to the inside (Dietrich and Hiiragi, 2007; Ralston et al., 2010). The knockout of TE factors, such as Cdx2, leads to the expression of ICM markers by the outside cells (Strumpf et al., 2005). This suggests that the cells may adopt the ICM cell fate by default, but subsequently adopt the TE fate as a result of repression of the ICM transcriptional network by the expression of TE regulators.

What activates TE regulators in the outside cells? Recently, the events upstream of this pathway have been uncovered. Specifically, the transcription factor Tead4, an important regulator of Hippo pathway activity (Zhao et al., 2008), is responsible for both Cdx2 and Gata3 zygotic activation. The knockout of Tead4 leads to a complete failure of TE specification, accompanied by a dramatic down-regulation of Cdx2 and Gata3 (Nishioka et al., 2008; Yagi et al., 2007). However, the expression of Tead4 itself is not exclusively restricted to the outside cells but is rather homogeneous in all cells of the late morula, indicating that other factors are involved in providing the cells with spatial information (Nishioka et al., 2008). According to the properties of the Hippo pathway described in *Drosophila*, Tead4 does not bind DNA alone but requires a partner termed Yap/Taz (Huang et al., 2005). Unlike Tead4, Yap/Taz appears to be localised specifically in the nucleus of the outside cells (Nishioka et al., 2009). It thus seems that the nuclear translocation of Yap/Taz is the key for TE specification. Then what restricts nuclear Yap/Taz to the outside cells? As expected, the apical domain plays a decisive role. The down-regulation of essential apical components, such as the knockdown of Pard6b (Alarcon, 2010), the overexpression of aPKC dominant negative forms (Hirate et al., 2013), or the depletion of Cdc42 (Korotkevich et al., 2017), consistently leads to the loss of nuclear Yap in the outside cells, and the subsequent repression of Cdx2 in the whole embryo. Conversely, the

transplantation of an exogenous apical domain to the apolar 16-cell stage embryo promotes nuclear localisation of Yap in those cells (Korotkevich et al., 2017). Together, these results consistently demonstrate that the presence of the apical domain directs Yap/Taz translocation to the nucleus where it cooperates with Tead4 to activate the TE transcriptional program.

So what links the apical domain to Yap/Taz nuclear translocation? It seems that both biochemical and mechanical cues come into play. In a study of cultured cells, the AMOT protein family, including Amot and its homologue Amotl1, were shown to inhibit the nuclear translocation of Yap by promoting its phosphorylation (Zhao et al., 2011). It appears that AMOT family proteins function in a similar manner in the mouse embryo and in fact they serve as the critical linker between the apical domain and Yap nuclear localisation. The downregulation of Amot and Amotl2 leads to Yap nuclear localisation in the inside cells, and accordingly results in the ectopic Cdx2 expression on the inside (Hirate et al., 2013; Leung and Zernicka-Goetz, 2013). As expected, AMOT proteins present differential activities between the inside and outside cells and this is under the regulation of the apical domain. In the inside cells where the apical domain is missing, AMOT proteins bind to the cell contacts where they get phosphorylated and become active, sequestering Yap to the cytoplasm; in the outside cells, the apical domain, presumably due to aPKC, traps AMOT proteins from the cell contacts to the apical side, thus allowing Yap to translocate to the nucleus (Hirate et al., 2013; Leung and Zernicka-Goetz, 2013).

Recent studies have shown that Yap/Taz can also function as a mechano-sensor and its nuclear/cytoplasm localisation can be controlled by upstream mechanical cues (Halder et al., 2012). Interestingly, such a pathway also functions during TE/ICM fate segregation. Specifically, a couple of recent studies have demonstrated that during the asymmetric cell divisions, the apolar cells not only adopt higher actomyosin contractility, but also present cytoplasmic Yap (Anani et al., 2014; Maitre et al., 2016). On the other hand, in the polar cells which have an apical domain, Yap appears in the nucleus before the final cell position is settled (Anani et al., 2014). As mentioned earlier, the apolar cells adopt a greater actomyosin contractility and therefore a higher surface tension, and it appears that Yap is localised deferentially prior to the determination of cell position, and this process is controlled directly by actomyosin contractility, rather than the cell contact environment. The inhibition of actomyosin contractility by blebbstatin treatment results in homogeneity of the Yap

nuclear/cytoplasm ratio between the apolar and polar cells, and cell differentiation is blocked (Maitre et al., 2016).

The precise mechanism behind Yap localisation remains unclear. That is, it is unknown whether mechanical cues controlling Yap localisation are AMOT protein dependent, and whether the time window during which surface tension controls differential Yap localisation is specific to the early morula, as in the later stages symmetric and asymmetric cell divisions become less random and seem to be controlled by classical epithelium pathways (Figure 1.4).

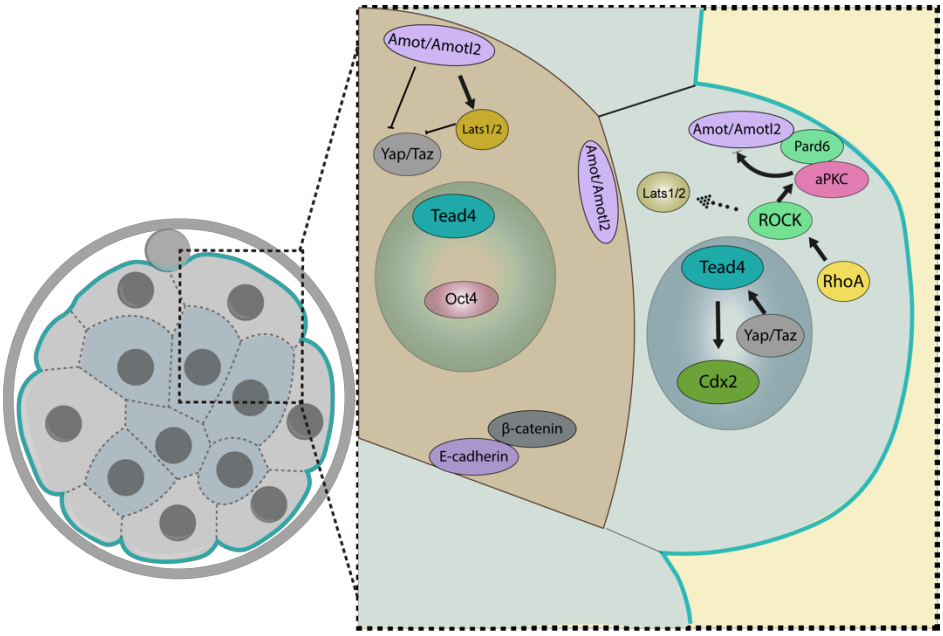

Figure 1.4 The Hippo pathway directs polarised outer cells to become TE. At the morula stage, in the outer polarised cells the Par complex (including Pard6 and aPKC) recruits and inhibits Amot/Amotl2 which blocks the activation of Lats1/2 kinase. Yap can diffuse to the nucleus to form the Tead4/Yap transcription complex, which activates Cdx2 expression. The Par complex activity is partially maintained by ROCK activity. In the inner apolar cells, Amot/Amolt2 binds to the AJ and activates the Lats1/2 kinase. The Lats1/2 kinase phosphorylates Yap and therefore blocks its transportation to the nucleus. The lack of activated Tead4/Yap transcription machinery induces the expression of pluripotency factors (such as Oct4) that direct the cells to the ICM fate.

In conclusion, recent studies have shed light on the mechanisms governing the first cell fate decision, where the TE and ICM lineages are segregated in the early mouse embryo. Briefly,

the apical domains seem to drive the process of segregation of the TE and ICM progenitors, through activation of the TE transcriptional network in the polarised cells via the inhibition of the Hippo pathway. Subsequently, cell position, which is determined by differential actomyosin activity and surface tension prompts the allocation of the appropriate cell fate.

1.5 Project Aim

Dissecting the mechanisms driving the first cell fate decision is a complex but fundamental step in understanding preimplantation mouse embryo development. Although recent studies have addressed questions pertaining to the correlation between cell position, cell polarity and cell fate, many fundamental questions remain open, such as what triggers cell polarity establishment, and precisely how species specific timing of such events is regulated. Thus, the current project aims to investigate the possible mechanisms driving cell polarity establishment, and address the question of how cell polarity timing is regulated. The first part of the results will mainly address the molecular cascades required for cell polarity establishment at the 8-cell stage. The second chapter will discuss the transcriptional requirement for cell polarity establishment and the possible connection between these programs and the timing of cell polarity establishment.

2 Material and Methods

2.1 Animals

This research has been carried out following regulations of the Animals (Scientific Procedures) Act 1986 - Amendment Regulations 2012 - reviewed by the University of Cambridge Animal Welfare and Ethical Review Body. Embryos were collected from F1 females (C57BI6xCBA) that had been superovulated by injection of 7.5 IU of pregnant mares' serum gonadotropin followed by human chorionic gonadotropin (Intervet) 48 h later. F1 females were mated with F1 males.

2.2 Embryo culture and inhibitor treatments

Embryos were recovered at the zygote or 2-cell stage in M2 medium and subsequently transferred to KSOM medium for long-term culture, as described previously (Graham et al., 2014).

For staging the 8-cell stage embryo development, the cytokinesis time-point of the last cell of the 4-cell stage embryo has been used as a reference, embryos within 1-2 hours' post-division have been considered as "early 8-cell stage"; 3-4 hours' post-division as "mid 8-cell stage" and 6-9 hours' post-division as "late 8-cell stage".

Inhibitor treatment: Puromycin (Invivogen, ant-pr-1) was diluted in KSOM to a working concentration of 10μg/ml. Cycloheximide (Sigma-Aldrich, C7698) was dissolved in DMSO and diluted in KSOM to a working concentration of 20μg/ml. 5,6-Dichlorobenzimidazole 1-b-D-ribofuranoside (DRB; Sigma-Aldrich, D1916) and Tritolide (Cayman Chemical, CAY11973) were dissolved in DMSO and diluted in KSOM to a working concentration of 50μM (DRB) or 5μM (Triptolide). D-erythro-sphingosine C-18 (2.5 μM; Caymanchem; in DMSO); Calphostin C (200 nM; Santa Cruz Biotechnology; in DMSO); U73122 (4.5–7.5 μM; Caymanchem; in DMSO); blebbistatin (25 μM; Sigma-Aldrich; in DMSO); ML-7 (20 μM; Sigma-Aldrich; in DMSO); Y-27632 (20 μM; Stemcell Technologies); C3-transferase (7 μg/ml; Cytoskeleton; in distilled water; the zona pellucida of 4–8-cell embryos was removed as described; 1-oleoyl-2-acetyl-sn-glycerol (OAG) (200 μM; Caymanchem; in DMSO), Latrunculin B (15 μM; Abcam; in DMSO). For the control groups, the same dilutions of the vectors of different inhibitors were added to the medium.

2.3 Blastomere resection

The resection procedure was performed as previously described (31). Briefly, the zona pellucida was removed for both 2-cell stage and 4-cell stage embryos. Embryos were transferred to a 1% agarose coated petri-dish covered by M2-medium containing 2μM Cytochalasin D (Sigma-Aldrich, C8273) prior to the resection procedures. For the 2-cell stage embryo, the embryo was first elongated by using a thin glass capillary with a flame-polished end. One of the blastomeres was resected using a thin glass needle, leaving approximately 30-40% of the cytoplasm (cytoplast) attached to its sister cell. For the 4-cell stage resection, the 4 blastomeres were first transferred to Calcium-Magnesium free M2 medium for 5 min and cells were disassociated by gently pipetting, as previously described (Graham et al., 2014). All four blastomeres were elongated using a thin glass capillary, and only two were resected (Figure 4.3 B, E). The resected and control cells were transferred to M2 medium immediately after resection. The whole resection process for each embryo took up to 5 min with a survival rate greater than 80%.

2.4 Microinjection

Microinjection was carried out as described previously. In brief, embryos were placed in M2 medium on a glass slide with a depression and covered by a drop of mineral oil. Microinjection was performed with an Eppendorf Femtojet Microinjector. Negative capacitance was used to facilitate penetration through the membrane. dsRNA was injected at a concentration of 1μg/μl. Synthetic mRNAs were injected at the following concentration: PLCδ1-PH-Ruby (1 μg/μl); Ruby (900 g/μl); GFP-MRLC (600 ng/μl); PKCα-A25E (200 ng/μl); CIBN-Zsgreen-CAAX (400 ng/μl); CIBN-Zsgreen (400 ng/μl); CRY2-mCherry-PKC-KD (500 ng/μl); GFP-Myl12b-T18DS19D (600 ng/μl); Raichu-RhoA-CR (600 ng/μl); Clover (200 ng/μl); mRuby2 (200 ng/μl); RhoA-Q63L (150 ng/μl (for experiments in Chapter III; 3ng/ul for experiments in Chapter IV)); CRY2-mCherry-RhoA-Q63L-C190R (600 ng/μl); CRY2-mCherry (500 ng/μl); Ezrin-Ruby (400 ng/μl); Ezrin-Venus (400ng/μl);LifeAct-eGFP (300 ng/μl). Tfap2c (15ng/μl); Tead4 (15ng/μl); Cas9 (100ng/μl). All sgRNAs were injected at 25ng/μl.

2.5 Preparation of DNA Constructs

pRN3P was used as the vector for all constructs as previously described (Zernicka-Goetz et al., 1997). To construct PLCδ1-PH-Ruby. The PH domain of Plcδ1 was PCR-amplified from pBSK-Plcδ1-PH-eGFP40 (Varnai and Balla, 1998) and cloned into the pRN3P vector. pRN3P-

Ruby and pRN3p-GFP-Myl12b are used as previously described (Ajduk et al., 2011). pRN3p-GFP-Myl12b-T18DS19D is made by site-directed mutagenesis using GFP-Myl12b as a template. RhoA-Q63L was PCR amplified from PCR-amplified from pRK5myc-RhoA-L63 and cloned into pRN3p. To construct pRN3p-CIBN-Zsgreen, The CIBN domain was PCR-amplified from pCMV-CIB1-mCerulean-MP (gift of Won Do Heo (Addgene plasmid #58366)). The Zsgreen was subcloned from pZsgreen-C1 (Clontech) and inserted downstream of CIBN. The CAAX motif of K-Ras was PCR-amplified from mouse liver complementary DNA (cDNA), and inserted downstream of Zsgreen to make pRN3p-CIBN-Zsgreen-CAAX. To construct pRN3p-CRY2-mCheery-PKC-KD, CRY2 domain and the mCherry coding sequence were subcloned from pCMV-CRY2-mCherry (gift of Won Do Heo (Addgene plasmid #58368)) into pRN3P; the kinase domain of PKCα (337-673aa) was PCR-amplified from pMTH-PKCalpha (gift of Frederic Mushinski (Addgene plasmid #8409)) and inserted downstream of CRY2-mCherry. To construct pRN3p-PKC α-A25E, the coding sequence of Prkca was PCR-amplified from pMTH-PKCalpha and cloned into pRN3P. The A25E mutation was generated by site-directed mutagenesis. pRN3p-Raichu-RhoA-CR was made by PCR amplification of Raichu-RhoA-CR from pCAGGS-Raichu-RhoA-CR (gift from Michael Lin (Addgene plasmid #40258)) and inserted into pRN3P. pRN3p-Clover and pRN3p-mRuby2 were made by PCR amplifying Clover and mRuby2 fragments from pCAGGS-Raichu-RhoA-CR and inserted into pRN3P vector. CRY2-mCherry-RhoA-Q63L-C190R was made by site-driected mutagenesis (using pRN3p-RhoA-Q63L as a template) and inserted into pRN3p-CRY2-mCherry downstream of mCherry. To construct Ezrin-Ruby and Ezrin-Venus, Ezrin-Ruby: Ruby was inserted into pRN3P, Ezrin was PCR-amplified from mouse adult kidney cDNA and inserted upstream of Ruby or Venus. To construct LifeAct-eGFP or LifeAct-Ruby, LifeAct peptide coding sequence was cloned into pRN3P plasmid, eGFP coding sequence or Ruby coding sequence were subcloned and inserted downstream of LifeAct. To construct pRN3p-Tead4, Tead4 was amplified from mouse kidney cDNA and cloned into pRN3p vector. To construct pRN3p-Tfap2c, Tfap2c cDNA was purchased from Origene (MR207174) and cloned into the pRN3p vector. pRN3p-Cas9 was a gift of J. Na (Tsinghua University, School of Medicine). All primers for constructs preparation are listed as below:

Table 2.1 Primer sequences for constructs preparation

Primer name	Sequence (5' to 3')
Tead4-BamHI-F	TTACGGATCCTATGACCTCCAACGAGTGGAG

Tead4-XbaI-R	ACGTTCTAGAGCAGAATTCGCCCTTTTCAC
EcoRI-Tfap2c-F	ACGTGAATTCCAGCGACATGGGAGGAGG
BamHI-Tfap2C-R	ACGTGGATCCCCTCCTTGCAGCCATTTTACTTCC
dsGFP-F	GAATTAATACGACTCACTATAGGGAGAACGTAAACGGCCACAAGTTCAGC
dsGFP-R	GAATTAATACGACTCACTATAGGGAGAGGGTGTTCTGCTGGTAGTGGTCG
dsTfap2c_F	ACGTTAATACGACTCACTATAGGGCCACGTCACTCTCCTCACG
dsTfap2c_R	ACGTTAATACGACTCACTATAGGGTATCGATGGCGATTAGAGCC
dsTead4-F	ACGTTAATACGACTCACTATAGGGTGTTGGAGTTCTCGGCTTTC
dsTead4-R	TAATACGACTCACTATAGGGTAATCATGTTCTCCGGGCTC
Tfap2c-gRNA1-F	TAATACGACTCACTATAGCGCCGACCATTACTCGCATC
Tfap2c-gRNA1-R	TTCTAGCTCTAAAACCCAGATGCGAGTAATGGTC
Tfap2c-gRNA2-F	TAATACGACTCACTATAGTGGTAAGGCGGCGGGAAGTA
Tfap2c-gRNA2-R	TTCTAGCTCTAAAACCCTTACTTCCCGCCGCCTT
Tfap2c-gRNA3-F	TAATACGACTCACTATAGGCGCCGCCTCTCTCGCACAC
Tfap2c-gRNA3-R	TTCTAGCTCTAAAACCCGGTGTGCGAGAGAGGCG
Tead4-gRNA1-F	TAATACGACTCACTATAGGATAATTTTGCGGCGGCCGC
Tead4-gRNA1-R	TTCTAGCTCTAAAACCCTGCGGCCGCCGCAAAAT
Tead4-gRNA2-F	TAATACGACTCACTATAGGTCGGGAGAGCTCCACTCGT
Tead4-gRNA2-R	TTCTAGCTCTAAAACCCAACGAGTGGAGCTCTCC
Tead4-gRNA4-F	TAATACGACTCACTATAGCGAAATTGAGCGAAGCTTCC
Tead4-gRNA4-R	TTCTAGCTCTAAAACCCTGGAAGCTTCGCTCAATT

2.6 mRNA, dsRNA, sgRNA preparation

For mRNA preparation, constructs for each mRNA were linearised using a restriction site downstream of poly-A region. In vitro transcription was performed using the mMessage mMachine T3 kit (Thermo Fisher, AM1348) following the manufacturer's instructions. mRNAs were purified using lithium chloride precipitation method.

For sgRNA preparation, the sequence of sgRNAs were designed using CRISPR design tool website (http://cirpsr.mit.edu). The DNA fragment containing T7 promoter, crRNA and

sgRNA sequence were amplified using Geneart gRNA kit (Thermo Fisher, A29377). sgRNAs were in vitro transcribed and purified using gRNA Clean Up Kit (Thermo Fisher, A29377), following manufactuer's instructions. All primers for making sgRNAs were listed below:

Table 2.2 Primers sequence for sgRNAs preparation

Primer name	Sequence (5' to 3')
Tfap2c-gRNA1-F	TAATACGACTCACTATAGCGCCGACCATTACTCGCATC
Tfap2c-gRNA1-R	TTCTAGCTCTAAAACCCAGATGCGAGTAATGGTC
Tfap2c-gRNA2-F	TAATACGACTCACTATAGTGGTAAGGCGGCGGGAAGTA
Tfap2c-gRNA2-R	TTCTAGCTCTAAAACCCTTACTTCCCGCCGCCTT
Tfap2c-gRNA3-F	TAATACGACTCACTATAGGCGCCGCCTCTCTCGCACAC
Tfap2c-gRNA3-R	TTCTAGCTCTAAAACCCGGTGTGCGAGAGAGGCG
Tead4-gRNA1-F	TAATACGACTCACTATAGGATAATTTTGCGGCGGCCGC
Tead4-gRNA1-R	TTCTAGCTCTAAAACCCTGCGGCCGCCGCAAAAT
Tead4-gRNA2-F	TAATACGACTCACTATAGGTCGGGAGAGCTCCACTCGT
Tead4-gRNA2-R	TTCTAGCTCTAAAACCCAACGAGTGGAGCTCTCC
Tead4-gRNA4-F	TAATACGACTCACTATAGCGAAATTGAGCGAAGCTTCC
Tead4-gRNA4-R	TTCTAGCTCTAAAACCCTGGAAGCTTCGCTCAATT

All dsRNAs were designed using the E-RNAi website (Horn and Boutros, 2010) and were 350-500bp in length. The specific targeting regions for each dsRNA were amplified from a mixture of mouse kidney, lung, liver cDNAs. The in vitro transcription reactions were performed using the MEGAscript T7 transcription kit (Thermo Fisher, AM1334) following the manufacturer's instructions. dsRNAs were purified by lithium chloride precipitation. All primers for dsRNA preparation are listed below:

Table 2.3 Primers for dsRNA preparation

Primer name	Sequence from 5' to 3'
ds-Als2-F	ACGTTAATACGACTCACTATAGGGGTGAGAGCAGTAACCGAGCC
ds-Als2-R	ACGTTAATACGACTCACTATAGGGCCTCAAAGCCTGATCCACAG
ds-Amhr2-F	ACGTTAATACGACTCACTATAGGGCAGGAAGGAGGTCATGCAGT

ds-Amhr2-R	ACGTTAATACGACTCACTATAGGGAGGGTACAGTTCCAGTACCAG C
ds-Ap2m1-F	ACGTTAATACGACTCACTATAGGGTTGATGACTGCACCTTCCAC
ds-Ap2m1-R	ACGTTAATACGACTCACTATAGGGCATGCGCTTGATCTTCCATA
ds-Arhgap10-F	ACGTTAATACGACTCACTATAGGGTGCCTCCTTACGGGAATTTT
ds-Arhgap10-R	ACGTTAATACGACTCACTATAGGGTTCTGCTCCACTTGGAGGTC
ds-Arhgap11a-F	ACGTTAATACGACTCACTATAGGGGCTTTTTAGGAAGTCGGGGT
ds-Arhgap11a-R	ACGTTAATACGACTCACTATAGGGCAGGATAAAATCTGGCACTCG
ds-Arhgap12-F	ACGTTAATACGACTCACTATAGGGCCTCCTGGTGAAGAAGACCA
ds-Arhgap12-R	ACGTTAATACGACTCACTATAGGGTCAGGTCCAGGCTTAGGTTG
ds-Arhgap19-F	ACGTTAATACGACTCACTATAGGGATTGGTGGTCAGCAACATCA
ds-Arhgap19-R	ACGTTAATACGACTCACTATAGGGTCGAACACTGTTGCCTGGTA
ds-Arhgap1-F	ACGTTAATACGACTCACTATAGGGTACCTGAGTGAGCTGAGCGA
ds-Arhgap1-R	ACGTTAATACGACTCACTATAGGGGGAAGATGCCCTCAGTGGT
ds-Arhgap28-F	ACGTTAATACGACTCACTATAGGGCTGCTGCTGCTGAAGTCAAG
ds-Arhgap28-R	ACGTTAATACGACTCACTATAGGGTGTCTTGGTAACTCCTGGCA
ds-ARHGAP29-F	ACGTTAATACGACTCACTATAGGGCCTGAAGACAAGAAACACCC A
ds-Arhgap29-F	ACGTTAATACGACTCACTATAGGGCCTGAAGACAAGAAACACCC A
ds-ARHGAP29-F2	ACGTTAATACGACTCACTATAGGGTGTCTGTAAAAGCCCCAAGC
ds-ARHGAP29-R	ACGTTAATACGACTCACTATAGGGACTAATCGTGCCTGATTGGAA
ds-Arhgap29-R	ACGTTAATACGACTCACTATAGGGACTAATCGTGCCTGATTGGAA

ds-ARHGAP29-R2	ACGTTAATACGACTCACTATAGGGTTGGCAGTAAAATTGTTCCGT
ds-Arhgap35-F	ATGCTAATACGACTCACTATAGGGGCTCCCTGGAGGATTGTGT
ds-Arhgap35-R	ATGCTAATACGACTCACTATAGGGATTCACATTGGACCTTGCAG
ds-Arhgap5-F	ACGTTAATACGACTCACTATAGGGAGAGGGAACAAGAAAGGCCA
ds-Arhgap5-F2	ACGTTAATACGACTCACTATAGGGAAGACCTTCAACCCACCAAC
ds-Arhgap5-R	ACGTTAATACGACTCACTATAGGGTCGAATGGGATCCGTCTATC
ds-Arhgap5-R2	ACGTTAATACGACTCACTATAGGGGCATGAAAGCGCTCTGTTTT
ds-Arhgap8-F	ACGTTAATACGACTCACTATAGGGAATCAAGGTGAACTCATCCCC
ds-Arhgap8-R	ACGTTAATACGACTCACTATAGGGCGAGAATCTGCTCGTAGGCT
ds-Arhgdia-F	ATGCTAATACGACTCACTATAGGGCAGAACAGGAACCCACTGCT
ds-Arhgdia-R	ATGCTAATACGACTCACTATAGGGCGGACACGATCTCTCTGTTC
ds-Arhgdig-F	ATGCTAATACGACTCACTATAGGGGCTTGGTCAAGTACAAGCAGG
ds-Arhgdig-R	ATGCTAATACGACTCACTATAGGGGTTCAGCCTGTCGTCATCAG
ds-Arhgef16-F	ACGTTAATACGACTCACTATAGGGGGAGGACATCAGCGACATCT
ds-Arhgef16-R	ACGTTAATACGACTCACTATAGGGAGGCCGCTTCTCGATCTC
ds-ArhGef19-F	ACGTTAATACGACTCACTATAGGGCTGGGGACTCAGGACAAGC
ds-ArhGef19-R	ACGTTAATACGACTCACTATAGGGGACTCCTCTAGGCGAGCCA
ds-Arhgef3-F2	ACGTTAATACGACTCACTATAGGGCCTTGATATTCCCCGGAGC
ds-Arhgef3-R2	ACGTTAATACGACTCACTATAGGGAGCTCTCCATGACAACACAGG
ds-Arpc3-F	ACGTTAATACGACTCACTATAGGGTTCAAGGCCAATGTCTTCTTC
ds-Arpc3-R	ACGTTAATACGACTCACTATAGGGTCACTCTGAGGGTCAAAAACC
ds-Arpc5-F	ACGTTAATACGACTCACTATAGGGAGGTGGACTCGTGCCTACG
ds-Arpc5-R	ACGTTAATACGACTCACTATAGGGTCAAAACTCGAACAATGGACC
ds-B4galt1-F	ACGTTAATACGACTCACTATAGGGGTCTCTCCTCACAAGGTGGC
ds-B4galt1-R	ACGTTAATACGACTCACTATAGGGCGAACTTGTCCATTGCAACA
ds-Cap1-F	ACGTTAATACGACTCACTATAGGGCCTCCTCCCCCAATCTCTAC
ds-Cap1-R	ACGTTAATACGACTCACTATAGGGCTTCCAGTTCCAGCAGAGC

ds-Capzb-F	ACGTTAATACGACTCACTATAGGGAGACCACGGTGGGCAAGGATTACCTTT
ds-Capzb-R	ACGTTAATACGACTCACTATAGGGAGACCACCCTCCACCAGGTCGTTCTTA
ds-Ccdc43-F	ACGTTAATACGACTCACTATAGGGGTGGAGCGATGGTCAGAAA
ds-Ccdc43-R	ACGTTAATACGACTCACTATAGGGTGTTTCGGAACAAGGTTCTGT
ds-CD151-F	ACGTTAATACGACTCACTATAGGGCAAGCTGCAGCAAGAGTTCC
ds-CD151-F	ACGTTAATACGACTCACTATAGGGAGTGTTCCAGCTTGAGGCTT
ds-Cdc42ep1-F	ACGTTAATACGACTCACTATAGGGGATGCTGTGACAAGCCTTCC
ds-Cdc42ep1-R	ACGTTAATACGACTCACTATAGGGCATCAGCAAACTCAAAGGCA
ds-Cdc42ep4-F	ACGTTAATACGACTCACTATAGGGCTGACCCACTCCTTGACGA
ds-Cdc42ep4-R	ACGTTAATACGACTCACTATAGGGCCATCCGTCATCCTCCAC
ds-Celsr1-F	TAATACGACTCACTATAGGGGGTATCCACAGTGTCACCGC
ds-Celsr1-R	TAATACGACTCACTATAGGGGTCGTTCTGGATGTTGAAGACA
ds-Celsr2-F	TAATACGACTCACTATAGGGGTCCACAGTGTGACAGCCC
ds-Celsr2-R	TAATACGACTCACTATAGGGCTGGGGCATCAGTATCCCT
ds-Celsr3-F	TAATACGACTCACTATAGGGGCCCCTGAGCAACCAAAC
ds-Celsr3-R	TAATACGACTCACTATAGGGCTGAAGGGTGAGGAGAGCTG
ds-Cfl1-F	ACGTTAATACGACTCACTATAGGGGGACAAGAAGAACATCATCCTGG
ds-Cfl1-R	ACGTTAATACGACTCACTATAGGGGGTGGCTCACAAAGGCTTG
ds-Cttn-F	ACGTTAATACGACTCACTATAGGGGTGCAAGCTGACCGTGTAGA
ds-Cttn-R	ACGTTAATACGACTCACTATAGGGGGCACACTTGTCCTGTCTGT
ds-Dlg5-F	ACGTTAATACGACTCACTATAGGGCAGAGGTCCAGGCGCATA
ds-Dlg5-R	ACGTTAATACGACTCACTATAGGGGCATATCCACCAGCCCATAG
ds-Dstn-F	ACGTTAATACGACTCACTATAGGGGTGTCATTTTCTGTCTCAGTGC
ds-Dstn-R	ACGTTAATACGACTCACTATAGGGGCACCTAGCTTTTCAGCAATACAG
ds-Epb41-F	ACGTTAATACGACTCACTATAGGGCCCAGATTCTGAAACGAAGG
ds-Epb41-R	ACGTTAATACGACTCACTATAGGGGCTGTCCCACAGGGCTAAAC
ds-Esrrb-F	ACGTTAATACGACTCACTATAGGGGAGGACTCCGCCATCAAAT

ds-Esrrb-R	ACGTTAATACGACTCACTATAGGGCTTTTTAGCAGGTGGGGAAA
ds-Fabp3-F	ACGTTAATACGACTCACTATAGGGCGGTACCTGGAAGCTAGTGG
ds-Fabp3-R	ACGTTAATACGACTCACTATAGGGGAGTCAGGATGAGTTTCCCG
ds-Fabp5-F	ACGTTAATACGACTCACTATAGGGCAAAACCGAGAGCACAGTGA
ds-Fabp5-R	ACGTTAATACGACTCACTATAGGGTTTGACCGCTCACTGAATTG
ds-Fam89b-F	ACGTTAATACGACTCACTATAGGGGGCCTTCTTAACGCTAGTGG
ds-Fam89b-R	ACGTTAATACGACTCACTATAGGGGAGGCTCCTCGTCATCAGAC
ds-Gabpa-F	ACGTTAATACGACTCACTATAGGGTGCAGTGTTCTTTGGATGCT
ds-Gabpa-R	ACGTTAATACGACTCACTATAGGGCCGAAATGTTGAGTGTGGTG
ds-Gata1-F	ACGTTAATACGACTCACTATAGGGTATGCTAGCTGGGCCTATGG
ds-Gata1-R	AGCTTAATACGACTCACTATAGGGTGCTGACAATCATTCGCTTC
ds-Gata3-F	ACGTTAATACGACTCACTATAGGGGCCACTCCAGTCCTCATCTC
ds-Gata3-R	ACGTACGTTAATACGACTCACTATAGGGCGCAGTTCACACACTCCCT
ds-Gata4-F	ACGTTAATACGACTCACTATAGGGGCTCCTACTCCAGCCCCTAC
ds-Gata4-R	ACGTTAATACGACTCACTATAGGGGCCGCAGGCATTACATACAG
ds-GFP-F	GAATTAATACGACTCACTATAGGGAGAACGTAAACGGCCACAAGTTCAGC
ds-GFP-R	GAATTAATACGACTCACTATAGGGAGAGGGTGTTCTGCTGGTAGTGGTCG
ds-Glrx3-F	ACGTTAATACGACTCACTATAGGGGATAGGTGGGCCAATTAGAG
ds-Glrx3-R	ACGTTAATACGACTCACTATAGGGGGAAGCATCAGAAGAGCTGG
ds-Gmfg-F	ACGTTAATACGACTCACTATAGGGTTGAGGAAATTTCGTTTCCG
ds-Gmfg-R	ACGTTAATACGACTCACTATAGGGCACCAGCCTGTTTTTACTTCC
ds-GPR137b-F	ACGTTAATACGACTCACTATAGGGCTGGCTGCTCTACTGCTTCC
ds-GPR137b-R	ACGTTAATACGACTCACTATAGGGCACACTGATGAGCCCTTTGA
ds-Gpr160-F	ACGTTAATACGACTCACTATAGGGTATGGCTTCTTGCATTACCCA
ds-Gpr160-F2	ACGTTAATACGACTCACTATAGGGCTTCTCACTCGCACTTGTCG
ds-Gpr160-R	ACGTTAATACGACTCACTATAGGGTCTGAGTGCTGACATAGGCG
ds-Gpr160-R2	ACGTTAATACGACTCACTATAGGGCGGGTCAACCAAAACGTAAG
ds-Gpr161-F	ACGTTAATACGACTCACTATAGGGGCCTTCATGGTCACCTGG

ds-Gpr161-F2	ACGTTAATACGACTCACTATAGGGGCCTTCATGGTCACCTGG
ds-Gpr161-R	ACGTTAATACGACTCACTATAGGGGTGAGATGTGGGGACAGACC
ds-Gpr161-R2	ACGTTAATACGACTCACTATAGGGCTGTGATCCTGTTGGAAATGC
ds-Gpr171-F	ACGTTAATACGACTCACTATAGGGTCTTAGCCTTTGTCAGCATCG
ds-Gpr171-R	ACGTTAATACGACTCACTATAGGGGTCTGATTGCAAGGAAGTTGG
ds-Gpr172b-F	ACGTATGGCTAGCATGACTGGTGGACAGCAAATGGGTGCTCCTGCCCTGTGTGCTAG
ds-Gpr172b-F2	ACGTTAATACGACTCACTATAGGGGTGCCTGTCTACTGGGCCT
ds-Gpr172b-R	ACGTATGGCTAGCATGACTGGTGGACAGCAAATGGGTGCTGCAAAGGTGAGGCCTCTTC
ds-Gpr172b-R2	ACGTTAATACGACTCACTATAGGGAGGGACTTAAGGCTGCCAGT
ds-Gpr19-F	ACGTTAATACGACTCACTATAGGGGGTCCGCTACTTCCAGTACCT
ds-Gpr19-R	ACGTTAATACGACTCACTATAGGGTCCGTGCCTATTCTCCAGAT
ds-Gpr50-F	ACGTTAATACGACTCACTATAGGGATCCTGTTCATCTCTCACCTCA
ds-Gpr50-F2	ACGTTAATACGACTCACTATAGGGCTGCCAAAGCCCGACTAC
ds-Gpr50-R	ACGTTAATACGACTCACTATAGGGGTGGATAGAGGCAGGTTTGC
ds-Gpr50-R2	ACGTTAATACGACTCACTATAGGGCAGATAGATGCAAGTGTTGCG
ds-Gprc5a-F	ACGTTAATACGACTCACTATAGGGTTCTGAGCTGCCTGCTCCT
ds-Gprc5a-R	ACGTTAATACGACTCACTATAGGGACCAAGGCTGTGCTGAGAAT
ds-Gprc5c-F	ACGTTAATACGACTCACTATAGGGCTCACCCTTGTGGAGGTCAT
ds-Gprc5c-R	ACGTTAATACGACTCACTATAGGGAAGAGGACAAAGGTCCAGGC
ds-Hand1-F	ACGTTAATACGACTCACTATAGGGCTGCCCCAGATTTCCCTG
ds-Hand1-R	ACGTTAATACGACTCACTATAGGGAGCACGTCCATCAAGTAGGC
ds-Igf1r-F	ACGTTAATACGACTCACTATAGGGGGAGAGACGTCATGCAAGTG
ds-Igf1r-R	ACGTTAATACGACTCACTATAGGGGCATGGTTCTCGCAAAGAC
ds-Igf2r-F	ACGTTAATACGACTCACTATAGGGCCTGCATGGTGTCAGAAGAC
ds-Igf2r-R	ACGTTAATACGACTCACTATAGGGCTGGCAGTTGTCTCCTTCCT
ds-Itgae-F	ACGTTAATACGACTCACTATAGGGCCCTGGACCACTACAAGGAA
ds-Itgae-R	ACGTTAATACGACTCACTATAGGGATTGAAGGCTGCGTGTCTCT
ds-Jarid2-F1	ACGTTAATACGACTCACTATAGGGGAGATTTTTCTAGATTGGAAAAGGGATAGAAG

ds-Jarid2-F2	ACGTTAATACGACTCACTATAGGGAGTTCAGCTGTCAACCACACA ATCTC
ds-Jarid2-R1	ACGTTAATACGACTCACTATAGGGCCTTTTCCTCAAGGATGCTATT GAAG
ds-Jarid2-R2	ACGTTAATACGACTCACTATAGGGGCTTTGGCCGATTCCTTTCCA AAC
ds-Jup-F	ACGTTAATACGACTCACTATAGGGCACTTGACAAGCAACAGTCCC
ds-Jup-F2	ACGTTAATACGACTCACTATAGGGGTCCTCACCTGTGCCACG
ds-Jup-R	ACGTTAATACGACTCACTATAGGGCTCTCAGGATGGCGTGGAT
ds-Jup-R2	ACGTTAATACGACTCACTATAGGGGTTTGGCTGGTTGAGCAGTT
ds-Krtcap2-F	ACGTTAATACGACTCACTATAGGGATGCAGATCTACAGCCGCC
ds-Krtcap2-R	ACGTTAATACGACTCACTATAGGGAGTTTCTCTTCTTGCCCTTGC
ds-Lgr4-F	ACGTTAATACGACTCACTATAGGGCTGCAAGGTAGCTGGGTCTC
ds-Lgr4-R	ACGTTAATACGACTCACTATAGGGAATGGCCATCAATAAAAATGC
ds-Llgl1-F	ACGTTAATACGACTCACTATAGGGCACCAACTCGGGCTCTGT
ds-Llgl1-R	ACGTTAATACGACTCACTATAGGGTGAATTGTTCCTCAGATGCAA
ds-Llgl2-F	ACGTTAATACGACTCACTATAGGGTGCTGGAGTTGAACGATGAG
ds-Llgl2-R	ACGTTAATACGACTCACTATAGGGTTGACAAAGACCTGCCGC
ds-Lpar1-F	ACGTTAATACGACTCACTATAGGGCTCATTGACACCAGCCTGAC
ds-Lpar1-R	ACGTTAATACGACTCACTATAGGGACAAAGGTCACCAGGTTGAA A
ds-Lpar5-F	ACGTACGTTAATACGACTCACTATAGGGCCAGATGAACATGTACG GCA
ds-Lpar5-R	ACGTTAATACGACTCACTATAGGGAGCCTGCCCTTCCACAGTT
ds-Lpar6-F	ACGTTAATACGACTCACTATAGGGACAGTGATGGGAGGAAGTGC
ds-Lpar6-F2	TAATACGACTCACTATAGGGTCGCTCATGAGGACACAGAC
ds-Lpar6-R	ATCGTAATACGACTCACTATAGGGAAACAGAAGATGACCAAGTG GA
ds-Lpar6-R2	TAATACGACTCACTATAGGGGGAGCCGGAGAGATAGTTCC
ds-Lrg1-F	ACGTTAATACGACTCACTATAGGGAGCTGAGTTCGCTGCCCT
ds-Lrg1-R	ACGTTAATACGACTCACTATAGGGTCCAACATATCCAGGTGCTG
ds-Mapt-F	ACGTTAATACGACTCACTATAGGGTGACGAGAAGAAAGCCAAGG
ds-Mapt-R	ACGTTAATACGACTCACTATAGGGGGACCACTGCCACCTTCTT

ds-Marcks-F	ACGTTAATACGACTCACTATAGGGCGAAAAGGATGAGGCTGC
ds-Marcksl1-F	ACGTTAATACGACTCACTATAGGGGCGTGAGAAGCAATGGAGAC TTAAC
ds-Marcksl1-F2	ACGTTAATACGACTCACTATAGGGGGCAGCCAGAGCTCTAAGG
ds-Marcksl1-R	ACGTTAATACGACTCACTATAGGGGCATCTCGCCCTGCTCCTG
ds-Marcksl1-R2	ACGTTAATACGACTCACTATAGGGTGCTCCTGCTCTTCCTCTGT
ds-Marcks-R	ACGTTAATACGACTCACTATAGGGCTTCTTGAAGGAGAAGCCGCT C
ds-Mark3-F	ACGTTAATACGACTCACTATAGGGAACTCCAGTTGCTTCAACCC
ds-Mark3-R	ACGTTAATACGACTCACTATAGGGATCATGTCACTGGGGTCCAT
ds-Mesdc2-F	ACGTTAATACGACTCACTATAGGGTCCAGAACACAAGAGACCCTC
ds-Mesdc2-R	ACGTTAATACGACTCACTATAGGGATAGCTCCCATCCCGGAG
ds-Mybpc2-F	ACGTTAATACGACTCACTATAGGGGGTACTTGATGGAGCGGAAG
ds-Mybpc2-R	ACGTTAATACGACTCACTATAGGGACCAATCCGATCTGGAGGT
ds-Net1-F	ACGTTAATACGACTCACTATAGGGAAATGAGCGCCACTTGTACC
ds-Net1-R	ACGTTAATACGACTCACTATAGGGCACTCTTCGTGGAGGTCTGG
ds-Oog1-F	ATGCTAATACGACTCACTATAGGGTGAGCCTCTTGGTTTTCTCC
ds-Oog1-R	ATGCTAATACGACTCACTATAGGGACATTGGGTATGCCGATCAT
ds-P2ry14-F	ACGTTAATACGACTCACTATAGGGATCGTGTTCTTTGGGCTCAT
ds-P2ry14-R	ACGTTAATACGACTCACTATAGGGCGAGCACGATGCTGAAGATA
ds-Pdzd3-F	ACGTTAATACGACTCACTATAGGGCCGACTTGGGCAGTTCTTGT
ds-Pdzd3-R	ACGTTAATACGACTCACTATAGGAGCAGCAATCTCAGTGTTCTCC
ds-Pfn1-F	ACGTTAATACGACTCACTATAGGGCGTAGGCTACAAGGACTCGC
ds-Pfn1-R	ACGTTAATACGACTCACTATAGGGATGAGGTCAGTACTGGGAACG
ds-Pkm-F	ATGCTAATACGACTCACTATAGGGAGACCATCAAGAATGTCCGTG
ds-Pkm-R	ATGCTAATACGACTCACTATAGGGCAAACACCATGTCCACATCC
ds-Pkn2-F	ACGTTAATACGACTCACTATAGGGGGTCAAACTAGCTGGAAACCC
ds-Pkn2-R	ACGTTAATACGACTCACTATAGGGTGTTTTGCCTTGTTGTTTTGA
ds-Pkn3-F	ACGTTAATACGACTCACTATAGGGGCAGCCTTATCCACAAGGAA
ds-Pkn3-R	ACGTTAATACGACTCACTATAGGGGCAGACAGGCAAGGAGAGAG

ds-Plekhf1-F	ACGTTAATACGACTCACTATAGGGGCCACATCGAAGAGTGTGTG
ds-Plekhf1-R	ACGTTAATACGACTCACTATAGGGACTGGATGCACCACAGACAG
ds-Plekhg2-F	ACGTTAATACGACTCACTATAGGGCTTAGAGGAGGCAGCACCAG
ds-Plekhg2-R	ACGTTAATACGACTCACTATAGGGACAGACTCCTGGGTGCAGTT
ds-Pou5f1-F	ACGTTAATACGACTCACTATAGGGGTTGGAGAAGGTGGAACCAA
ds-Pou5f1-R	ACGTTAATACGACTCACTATAGGGCCACATCCTTCTCTAGCCCA
ds-Ppp1ca-F	ACGTTAATACGACTCACTATAGGGGGGGCCTGTCTCCAGACTT
ds-Ppp1ca-R	ACGTTAATACGACTCACTATAGGGCTCCACAGTAGTTGGGAGCTG
ds-Psap-F	ACGTTAATACGACTCACTATAGGGGCCACCGAGACCATTAAGAA
ds-Psap-R	ACGTTAATACGACTCACTATAGGGCGATCACACCGCACAGAG
ds-Psen1-F	ACGTTAATACGACTCACTATAGGGCATCCACTGGAAAGGCCC
ds-Psen1-R	ACGTTAATACGACTCACTATAGGGTCACCAACCACACCATTGTT
ds-Ptpn18-F	ACGTTAATACGACTCACTATAGGGAAGGAAGCCTTCTCCCTCAG
ds-Ptpn18-R	ACGTTAATACGACTCACTATAGGGTCCAGTCTGTGCTCCATCTG
ds-Rack1-F	ACGTTAATACGACTCACTATAGGGCCGGCAGATTGTCTCTGG
ds-Rack1-R	ACGTTAATACGACTCACTATAGGGCTCCAGAAGCACAGAGGGAT
ds-Rbpj-F	ACGTTAATACGACTCACTATAGGGACAAGAGTCTCAACCCTGTGC
ds-Rbpj-R	ACGTTAATACGACTCACTATAGGGCGTGGAAATTCCCTCCTTCT
ds-Ripor1-F	ACGTTAATACGACTCACTATAGGGCTCTCCCCTCACCTCCACAG
ds-Ripor1-R	ACGTTAATACGACTCACTATAGGGACAGCACCGGTGGTATGAGT
ds-Rnd1-F	ACGTTAATACGACTCACTATAGGGCGAAAGACTGCTATCCCGAG
ds-Rnd1-R	ACGTTAATACGACTCACTATAGGGTGTCTTGCAGCCAATAAGCA
ds-Rnd2-F	ACGTTAATACGACTCACTATAGGGAGAGACTCAGGAGTTTTGCCC
ds-Rnd2-R	ACGTTAATACGACTCACTATAGGGGTACGACGTAGCTGCCTATGG
ds-Rnd3-F	ACGTTAATACGACTCACTATAGGGCAAGGACTGCTTCCCAGAAA
ds-Rnd3-R	ACGTTAATACGACTCACTATAGGGCGCAGATCAGACTTGCAGC
ds-Rps11-F	ACGTTAATACGACTCACTATAGGGTCGGTCTAGGCTTCAAGACG
ds-Rps11-R	ACGTTAATACGACTCACTATAGGGACGCTTCTCAAAGCGATTGT
ds-S1pr2-F	ACGTTAATACGACTCACTATAGGGGCTGATTCTGGGTGGCTTG
ds-S1pr2-F3	ACGTTAATACGACTCACTATAGGGGGGTGTCAGCATTCTGTCTG
ds-S1pr2-R	ACGTTAATACGACTCACTATAGGGCAGCCAGCAGATGATGAAAA
ds-S1pr2-R3	ACGTTAATACGACTCACTATAGGGTTTCCTTTCCCCGAATATGA

ds-S1pr3-F	ACGTTAATACGACTCACTATAGGGCCAACAGTGTGGTTCCTCAG
ds-S1pr3-R	ACGTTAATACGACTCACTATAGGGCGCATACAAGATGACGATGG
ds-Sfn-F	ACGTTAATACGACTCACTATAGGGAGAGACCGAGCTCAGAGGTG
ds-Sfn-R	ACGTTAATACGACTCACTATAGGGGACTGAAAAGTTCAGGGCCA
ds-Six1-F	ACGTTAATACGACTCACTATAGGGGGCGAGGAGACCAGCTACT
ds-Six1-R	ACGTTAATACGACTCACTATAGGGAGCAGAAGGACCGAGTTCTG
ds-Slk-F	ACGTTAATACGACTCACTATAGGGCAAGACCAGCAAACTGTGGA
ds-Slk-R	ACGTTAATACGACTCACTATAGGGCTGTCCCCACCTCACTGC
ds-Smpdl3a-F	ACGTTAATACGACTCACTATAGGGCTCCCTTATGCAACTGACACC
ds-Smpdl3a-R	ACGTTAATACGACTCACTATAGGGCACCATGTCCAGCAATGTGT
ds-Snx5-F	ACGTTAATACGACTCACTATAGGGCAAGGAGATGTTTGGAGGCT
ds-Snx5-R	ACGTTAATACGACTCACTATAGGGTGATGAGACTCGACCTTCCAC
ds-Spint1-F	ACGTTAATACGACTCACTATAGGGTCCCACGCTGGTACTACGAC
ds-Spint1-R	ACGTTAATACGACTCACTATAGGGCAAAGCCGCTGGTGTATTTT
ds-Stub1-F	ACGTTAATACGACTCACTATAGGGACCAGGAGAGTGAGCTGCAT
ds-Stub1-R	ACGTTAATACGACTCACTATAGGGCTGGGTGTAATGCAGGGTTC
ds-Sycn-F	ACGTTAATACGACTCACTATAGGGCGCAGACCTGAAGAAGTCAG
ds-Sycn-R	ACGTTAATACGACTCACTATAGGGGGTACTCTTCCAGGCGAGG
ds-Tagln2-F	ACGTTAATACGACTCACTATAGGGCACTGTATCCTGAGGGGCAG
ds-Tagln2-R	ACGTTAATACGACTCACTATAGGGATCTGCAACCCAATCACGTT
ds-Taxbr2-F	ACGTTAATACGACTCACTATAGGGAGCTATGGTGTTCTTCGGGC
ds-Taxbr2-R	ACGTTAATACGACTCACTATAGGGCCCAGGAGTGCGAATATGAG
ds-Tdgf1-F	ACGTTAATACGACTCACTATAGGGGTACGCGATCGGTCTTTCC
ds-Tdgf1-R	ACGTTAATACGACTCACTATAGGGGAGGAAGACAGTGGAGCTGG
ds-Tead4-F	ACGTTAATACGACTCACTATAGGGTGTTGGAGTTCTCGGCTTTC
ds-Tead4-R	TAATACGACTCACTATAGGGTAATCATGTTCTCCGGGCTC
ds-Tfap2c-F	ACGTTAATACGACTCACTATAGGGCCACGTCACTCTCCTCACG
ds-Tfap2c-R	ACGTTAATACGACTCACTATAGGGTATCGATGGCGATTAGAGCC
ds-Tm4sf1-F	TAATACGACTCACTATAGGGTCCTCTGGGTCCTCTCTCCT
ds-Tm4sf1-R	TAATACGACTCACTATAGGGGAGGTTCTGCTTTCCCACAG
ds-Tmem92-F	ACGTTAATACGACTCACTATAGGGTCTTAAACTGCCCCAAAGGA
ds-Tmem92-R	ACGTTAATACGACTCACTATAGGGACAAAAGGGGAGGGGTCTTA

ds-Trp63-F	ACGTTAATACGACTCACTATAGGGCTGCCAGATTGCGAAGACAT
ds-Trp63-R	ACGTTAATACGACTCACTATAGGGATTCAGTGCCAACCTGTGGT
ds-Vangl1-F	TAATACGACTCACTATAGGGATTGCCAGGATTAGCAAGGA
ds-Vangl1-R	TAATACGACTCACTATAGGGATTGCCAGGATTAGCAAGGA
ds-Vangl2-F	TAATACGACTCACTATAGGGGATGACAACTGGGGAGAAACA
ds-Vangl2-R	TAATACGACTCACTATAGGGAACAGCAGGATGAGCAGCTT
ds-Wdr83-F	ACGTTAATACGACTCACTATAGGGGACACAGGGGAGCTGCTG
ds-Wdr83-R	ACGTTAATACGACTCACTATAGGGCATCAGCAAACTCAAAGGCA
ds-Xab2-F2	ACGTTAATACGACTCACTATAGGGTACCGATATCTGAAGGCACG
ds-Xab2-R2	ACGTTAATACGACTCACTATAGGGAGCGCAGGAAACGTAGATAC A
ds-Ywhab-F	ACGTTAATACGACTCACTATAGGGGAGGAATGAGAAGAAGCAGC A
ds-Ywhab-R	ACGTTAATACGACTCACTATAGGGTTCAAATGCTTCTTGGTAAGC C
ds-Ywhae-F	ACGTTAATACGACTCACTATAGGGTGAAAGGGGACTACCACAGG
ds-Ywhae-R	ACGTTAATACGACTCACTATAGGGAGCTTTCTTCACTCAGCGTGT
ds-Ywhah-F	ACGTTAATACGACTCACTATAGGGTACTACCGCTACCTGGCAGA
ds-Ywhah-R	ACGTTAATACGACTCACTATAGGGTGCTTCTTCATCCTGCTGGT
ds-Ywhaq-F	ACGTTAATACGACTCACTATAGGGAGAAGGAGATGCAGCCTACG
ds-Ywhaq-R	ACGTTAATACGACTCACTATAGGGTTCTTGAGGGGAAGGAGGTT
ds-Zfp281-F	ACGTTAATACGACTCACTATAGGGAGTCAGTCATTCAGTCTGCAG
ds-Zfp281-R	ACGTTAATACGACTCACTATAGGGCATTAGTGGATTTTTCGAAAG CCTG
ds-Zfp740-F	ACGTTAATACGACTCACTATAGGGAAAGGGCCACCGAAAAGAC
ds-Zfp740-R	ACGTTAATACGACTCACTATAGGGACTGTGTACCCGCTTGTGG

2.7 Immunofluorescence

Embryos were fixed in 4% PFA at room temperature for 20min, and washed in PBST (0.1% Tween in PBS) three times. Embryos were permeabilised in 0.5% Triton X-100 in PBS for 20 min at room temperature, washed in PBST three times, transferred to blocking solution (3% bovine serum albumin) for 2h and incubated with primary antibodies (diluted in blocking

solution) at 4 °C overnight. After the incubation, embryos were washed in PBST and incubated with secondary antibodies (1:500 in blocking solution) for 1h at room temperature. Embryos were stained with DAPI (1:1000 dilution, in PBST, Life Technologies, D3571) for 15 min, followed by two washes in PBST. Primary antibodies: rabbit polyclonal anti-Pard6b (Santa Cruz, sc-67393, 1:200); anti ppMRLC2 (Cell Signalling, 3674P, 1:200), mouse monoclonal anti PKCζ (Santa Cruz, sc-17781, 1:50), rabbit polyclonal anti-CRB3 (Atlas antibodies, HPA013835, 1:50); mouse monoclonal anti-GFP (Nacalai Tesque Inc., 04404-84, 1:500); mouse monoclonal anti-Tfap2c (Santa Cruz, sc-12762, 1:200); rabbit monoclonal anti-Tead4 (Abcam, ab97460, 1:200); rabbit monoclonal anti-Gata4 (Santa Cruz, sc-9053, 1:200); mouse monoclonal anti-Pou5f1 (Santa Cruz, sc-5729, 1:200); goat monoclonal anti Sox17 (R&D Systems, af1924); mouse monoclonal anti Cdx2 (Launch Diagnostics, MU392-UC (Biogenex)); rabbit monoclonal anti Nanog (Abcam, ab80892). Secondary antibodies: Alexa Fluor 568 Donkey anti-Goat (A-11057, ThermoFisher Scientific); Alexa Fluor 488 Donkey anti-Mouse, (A-21202, ThermoFisher Scientific); Alexa Fluor 568 Donkey anti-Mouse (A10037, ThermoFisher Scientific); Alexa Fluor 647 Donkey anti-Mouse (A31571, ThermoFisher Scientific); Alexa Fluor 568 Donkey anti-Rabbit (A10042, ThermoFisher Scientific); Alexa Fluor 647 Donkey anti-Rabbit (A-31573, ThermoFisher Scientific).

2.8 RhoA-FRET imaging and data analysis

The structure of RhoA FRET sensor Raichu-RhoA-CR was as described previously68. Raichu-RhoA-CR, Clover mRNA and mRuby2 mRNA were injected into 2-cell stage embryos, and at the 4–8 cell stage, embryos were imaged under Leica TSC SP8 confocal microscope (Leica fluotar VISIR 0.95NA ×25 water objective). Images were acquired using the following excitation and emission settings: clover: 488 nm excitation, 505–540 nm emission; FRET: 488 nm excitation, 580–650 nm emission; mRuby2: 568 nm excitation, 580–650 nm emission. Clover mRNA-injected embryos and mRuby2 mRNA-injected embryos were imaged first to determine the signal bleed-through (BT). Next, Raichu-RhoA-CR-expressing embryos were imaged with 20 min interval. For data analysis, the FRET and co-localisation analyser plugins in Fiji software were used to analyse the co-localisation between donor, FRET and acceptor channels to eliminate the noise generated by detectors. The radiometric image of FRET-co-localisation and donor images were generated using the image calculation function in Fiji. Cell-contact-free/cell-contact RhoA-FRET ratio is calculated by I cell-contact-free/I cell-contact.

2.9 Optogenetics and regional PKC activation

2-cell stage embryos were injected with CIBN-Zsgreen-CAAX and CRY2-mCherry-PKC-KD or CRY2-mCherry-RhoA-Q63L-C190R or CRY2-mCherry and cultured in the dark. After 3 h, embryos were transferred to an optical glass bottom culture dish (MatTek Corporation) mounted with M2 medium and imaged under Leica TSC SP5 confocal microscopy (×63 oil objective). Laser power of 458 nm wavelength (8% for CRY2-mCherry-PKC-KD and CRY2-mCherry, 4% for CRY2-mCherry-RhoA-Q63L-C190R) was used to illuminate a defined region in the cell-contact-free domain of the blastomeres using the region of interest tool in Leica Las AF software. The laser was illuminated for 5 s and followed with a 20 s interval. Each individual embryo was imaged for 15 min.

2.10 Imaging and data processing

Imaging was carried out on a Leica-SP5 or Leica-SP8 confocal using a Leica 1.4 NA 63X oil (HC PL APO) objective. Images were processed with Fiji software (35). For the analysis of nucleo-cytoplasmic signal intensity ratio, the region of the nucleus, and a cytoplasmic region of the same size, were cropped and the mean signal extracted using the Fiji ROI function. To normalise signals to the level of DAPI fluorescence, the Fiji ROI function was used to extract the nuclear region stained to reveal specific proteins and for the equivalent DAPI channel and normalisation performed using the formula: I(protein of interest)/ I (DAPI). For Ezrin apical enrichment analysis, a freehand line with the width of 0.5μm was drawn along the cell-contact free surface (apical domain), or cell-contact (basal) area of the cell, signal intensity were obtained via ROI function of Fiji. The apical/basal signal intensity ratio is calculated as: I(apical)/I(basal). Compaction was assessed by measuring the inter-cellular blastomere angle in the mid-plane between adjacent cells (as described previously (11)) by using the Fiji angle function.

For live-imaging, time-lapse recordings of embryos were carried out using a spinning disk or a Leica-SP5 scanning confocal. For the blastomere resection experiment, time-lapse frames were acquired every 1h; for other live-imaging experiments, time-lapse frames were acquired every 20-30min. Images were acquired using a 3-4μm Z-step. Images were processed with Fiji software. Correlations were calculated using Prism software (http://www.graphpad.com).

2.11 Real-time PCR

RNA was extracted from 8-cell stage embryos using the Arcturus PicoPure RNA isolation kit (Arcturus Bioscience). RT-PCR was performed using a StepOne Plus Real-time PCR machine (Applied Biosystem). The expression level was calculated using ddCT methods, normalised to a Gapdh PCR reaction and the endogenous control group. The primers used for RT-PCR are listed below:

Table 2.4 Primers for real-time PCR

Primer name	Sequence (5' to 3')
Myl12b-qF	CTTAGTTTCTCAGTCACTTCCCCTC
Myl12b-qR	GTCCTGGGCTTTCACAGTGGTT
Cfl1-qF	ATGACATGAAGGTTCGCAAGT
Cfl1-qR	GACAAAAGTGGTGTAGGGGTC
Dstn-qF	GAGTTCAGGTTGCGGATGAAG
Dstn-qR	TGCACTGAGACAGAAAATGACAG
Arpc5-qF	GTGGACGTGGACGAATATGAC
Arpc5-qR	CTTGCCGTAGGCACGAGTC
Pfn1-qF	TGGAACGCCTACATCGACAG
Pfn1-qR	GTAATGCTAACGAAGGTCTTCCC

2.12 Statistics

Statistical methods are indicated for every experiment in the corresponding figure legends. Qualitative data is presented as a contingency table and was analysed using Fisher's exact test. Normality of quantitative data was first analysed using D'Agostino's K-squared test. A one-sample t-test was used to test whether an observed distribution followed a hypothetical mean. If data showed a normal distribution, then for comparison of two or multiple samples, an unpaired two-tailed Student's t test (two experimental groups) or a One-way ANOVA test (more than two experimental groups) was used to analyse statistical significance. Differences in variances were taken into account by performing a Welch's correction. For data that did not present a normal distribution, a Mann–Whitney U-test (two experimental groups) or a Kruskal–Wallis test with a Dunn's multiple comparison test (more than two experimental groups) was used to test statistical significance. Statistical analyses were performed using Prism software (http://www.graphpad.com).

3 Results I: dissecting the molecular mechanism triggering cell polarity establishment – a requirement of the PLC-PKC signalling pathway in triggering actomyosin early asymmetry

3.1 Introduction

Cell polarity establishment in the mouse embryo is a crucial event for the first cell fate specification. The apical domain, which is enriched by the Par complex (including aPKC and Pard6) and ERM protein family members, is necessary and sufficient for TE fate specification (Korotkevich et al., 2017). Despite the importance of the apical domain in developmental progression, how the apical domain first becomes established at the 8-cell stage, remains poorly understood. Work in other model systems points to a role of cytoskeleton dynamics in triggering *de novo* cell polarity establishment. However, the role of the cytoskeleton in apical domain formation is also under-investigation in the early mouse embryo. In this chapter, the dynamics of cytoskeletal networks, including actin and microtubules, and their contribution to apical domain establishment has been examined. This reveals that actomyosin reorganisation and polarisation is required for the formation of a matured apical domain. The upstream regulators controlling actin cytoskeleton reorganisation have been explored. Using a combination of pharmacological treatments, dominant negative constructs, as well as optogenetic activation, the PLC-PKC signalling pathway, and the downstream pathway regulating actomyosin apical polarisation and organisation has been defined.

3.2 Actomyosin apical polarisation precedes apical domain maturation

The maturation of apical domain is characterised by the apical enrichment of the Par complex, which consists of Pard6 and aPKC, localised in the centre of the cell-contact free surface, surrounded by an actin network which forms a "ring" like structure (Anani et al., 2014; Vinot et al., 2005) (Figure 3.1 A). The actomyosin network was recently found to be involved in de novo cell polarity establishment in several embryonic systems (Li and Gundersen, 2008; Schonegg and Hyman, 2006). To determine whether the actomyosin network plays an equivalent role in the apical domain assembly in the mouse embryo (Wedlich-Soldner et al., 2003), the spatial-temporal dynamics of the actomyosin system in relation to apical domain

formation were examined at the 8-cell stage of development. To this end, early, mid, and late 8-cell stage embryos were fixed according to the post-division hours (1-2 hrs for early 8-cell stage, 3-4 hours to mid-8-cell stage, and 5-9 hours to late 8-cell stage) and stained with filamentous actin (F-actin) as an actomyosin marker, and Pard6 as the matured apical domain marker. To precisely measure the 8-cell stage developmental progression, the inter-blastomere angle (the intracellular angle formed by adjacent blastomeres) was measured as a read out of compaction (Figure 3.1). This revealed that F-actin and Pard6b polarisation form a step-wise pattern: during the early to mid 8-cell stage of development as the embryo compacts, F-actin became gradually polarised to the cell contact-free surface. Pard6b however, did not show any obvious asymmetry between cell contacts and cell contact-free surface during this stage (Figure 3.2A-C). Only in the next couple of hours when the embryos compacted fully, did Pard6 begin to accumulate at the cell contact free surface. At the early phase of Pard6 apical accumulation, F-actin co-localised with Pard6b; yet at the later phase when the Pard6 apical signal increased, F-actin redistributed to the periphery of the Pard6 domain, suggesting a negative feedback mechanism between Pard6 and F-actin (Figure 3.2 A-D).

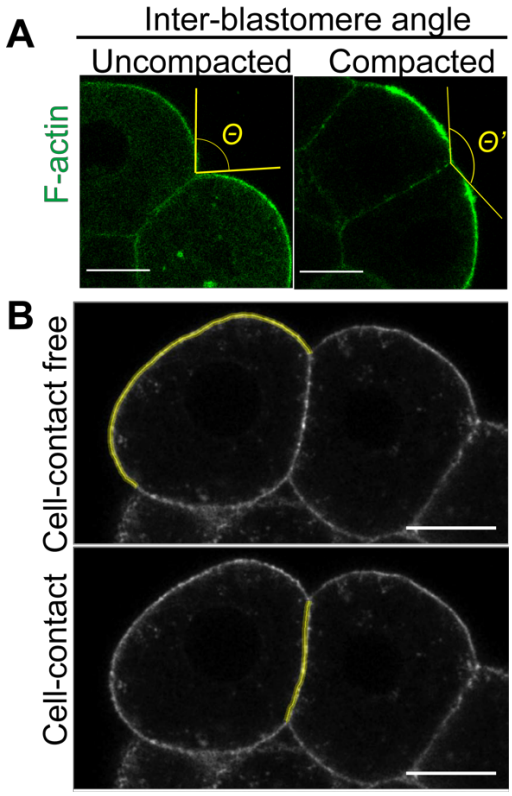

Figure 3.1Measurement of inter-blastomere angle and the signal intensity. (A) The angle between adjacent blastomeres were measured as a readout of compaction. The inter-blastomere

angle increases with cell compaction. (B) A line with 0.8 µm was drawn across the cell contact-free or cell contact region for signal intensity plotting. All scale bars, 15µm.

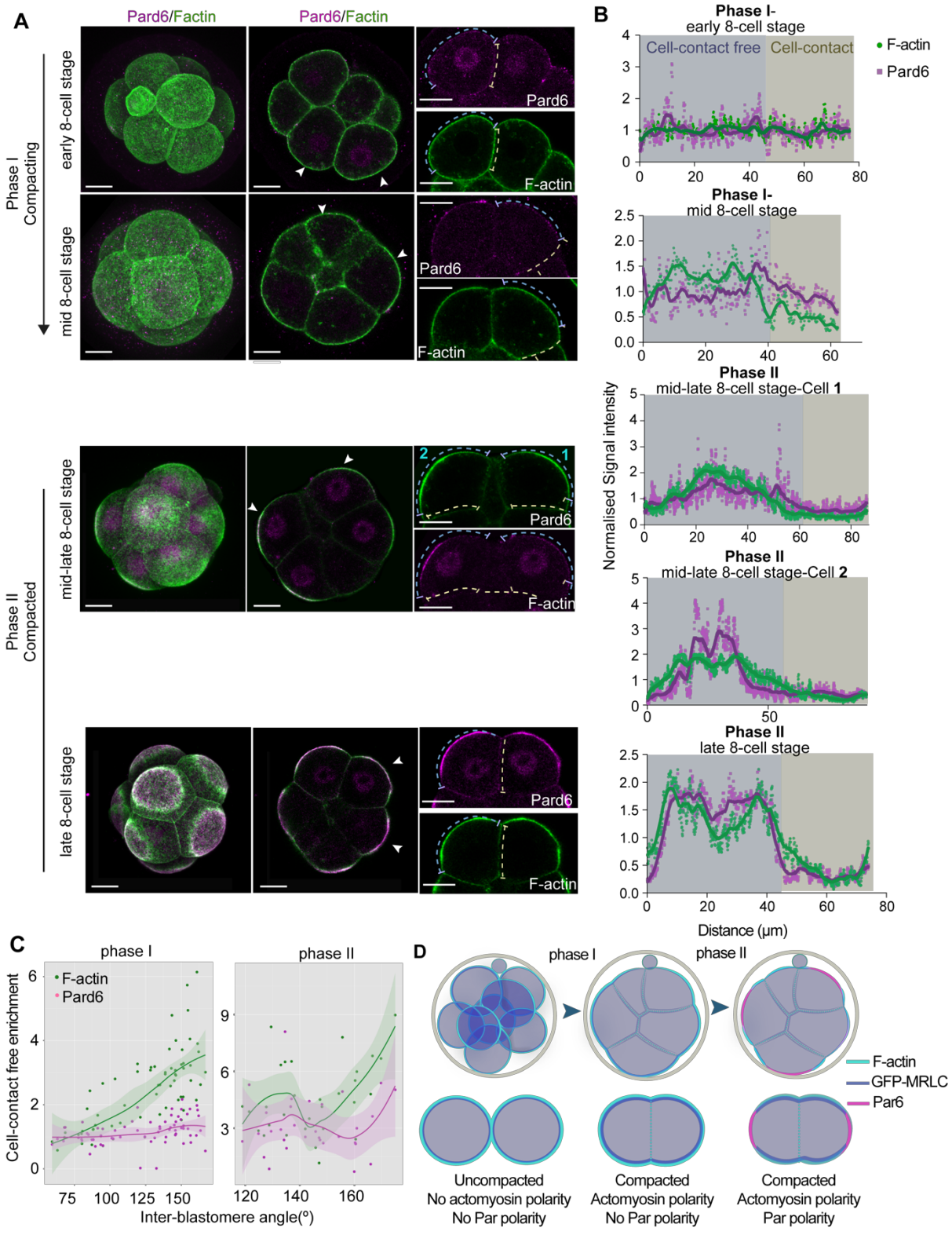

Figure 3.2 Actomyosin and Pard6 dynamics during 8-cell stage development. (A) Embryos at the early, mid and late 8-cell stage were fixed and stained for F-actin and Pard6. Arrows

indicate the magnified cells on the right panel. The dash lines indicate the regions used in the signal plotting graphs in B. Colours of the dotted line correspond to the colours displayed as the background of the signal plotting graph in B. (B) Plotting of the circumferential signal intensity of F-actin and Pard6b in cell contact and cell contact free region. Squares of different colours indicate cell contact (in yellow) and cell contact free surface (in blue) of plotted cells indicated in A. (C) Quantifications of F-actin and Pard6 normalised signal intensity in relation to inter-blastomere angle. Each dot indicates one analysed cell. The LOWESS curve was used to estimate the tendency, the shadows indicate a 95% confidence interval. (D) Summarised model of the two phases of cell polarity establishment. In the first phase, actomyosin is polarised to the cell contact-free surface, accompanied with cell compaction. In the second phase, apical domain components are recruited to the cell contact-free surface and co-localise with actomyosin. Upon apical domain component enrichment, actomyosin is excluded from the centre and is reorganised into a ring domain. N = 25 embryos analysed, three independent experiments. All scale bars, 15μm.

As an alternative readout for actomyosin localisation, the localisation of the myosin II complex was also examined. To this end, 2-cell stage embryos were injected with mRNA encoding a GFP tagged myosin light chain (GFP-MRLC) and fixed at the early, mid and late 8-cell stage with a post-division timing consistent with F-actin. Embryos were stained with anti-GFP (for GFP-MRLC) and Pard6. In agreement with the F-actin distribution pattern, GFP-MRLC also polarised apically during compaction and before Pard6 was polarised to the cell contact-free surface (Figure 3.3 A-C). Similar to F-actin, upon Pard6 apical accumulation, GFP-MRLC was re-distributed to the periphery of Pard6 domain (Figure 3.3 A-C). Together with the F-actin localisation pattern, these results suggest that the actomyosin complex polarises to the cell contact-free area prior to Par complex apical polarisation.

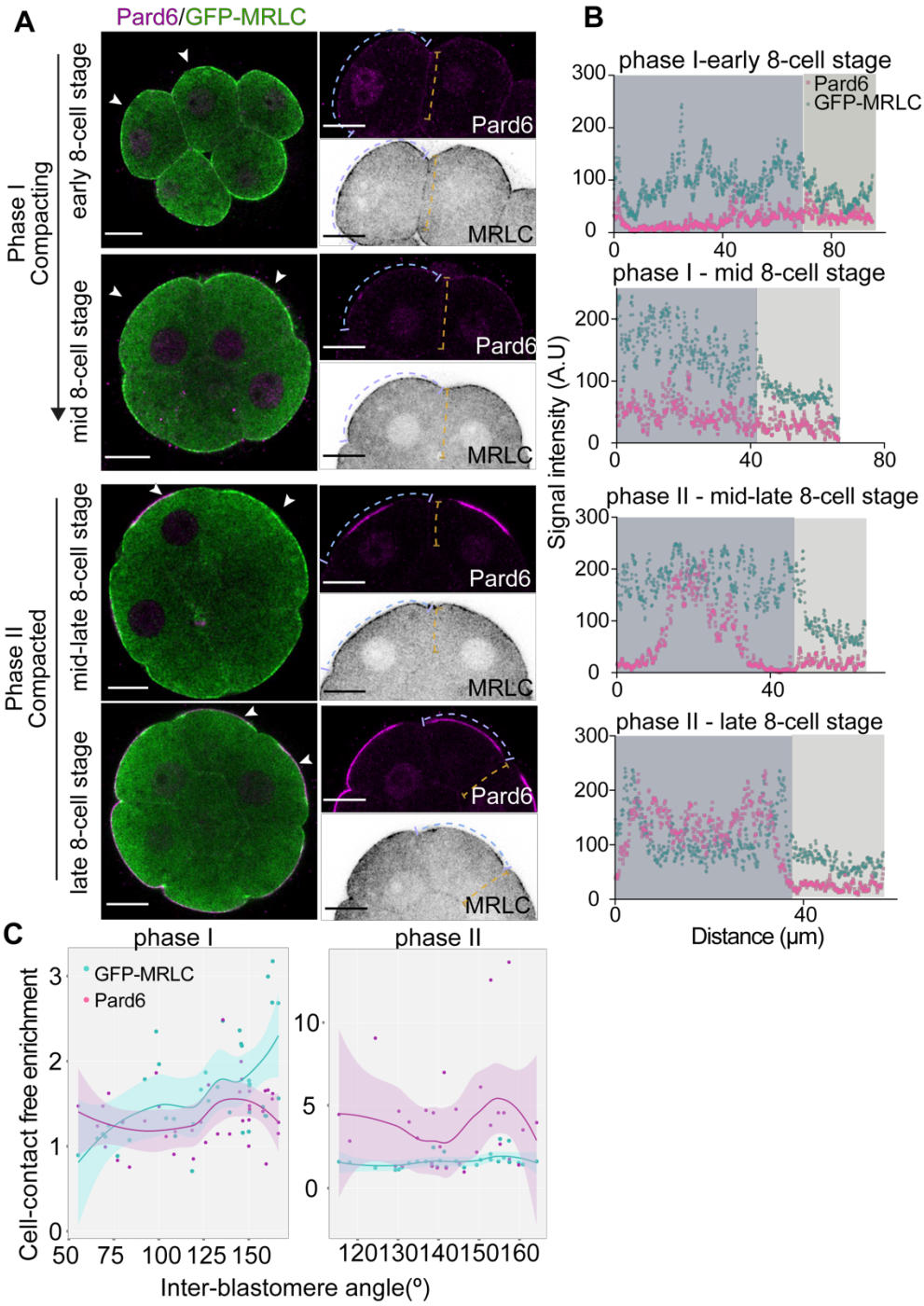

Figure 3.3 Dynamics of GFP-MRLC and Pard6 during the 8-cell stage of development. (A) The embryos expressing GFP-MRLC at the early, mid and late 8-cell stage were fixed and stained anti-GFP and Pard6. Arrows indicate the magnified cells on the right panel. The dotted lines indicate the regions used in the signal plotting graphs in B. Colours of the dotted line correspond to the colours displayed as the background of the signal plotting graph in B. (B) plotting of the circumferential signal intensity of GFP-MRLC and Pard6b in cell contact and cell contact-free region. Squares of different colours indicate cell contact (in yellow) and cell contact-free surface (in blue) of plotted cells indicated in A. (C) Quantifications of GFP-MRLC

and Pard6 normalised signal intensity in relation to inter-blastomere angle. Each dot indicates one analysed cell. The LOWESS curve was used to estimate the tendency, the shadows indicate 95% confidence interval. N=14 embryos, 4 independent experiments.

The above results suggest that actomyosin polarises to the cell contact-free surface before Pard6b. To determine whether actomyosin polarisation is indeed the early cue for cellular asymmetry before the apical domain assembly, other apical domain components including aPKC, Ezrin, and Crb3 were also examined. For aPKC and Crb3, embryos were fixed at the same time-points as for Pard6b and immunostained with antibodies against aPKC zeta (aPKCζ) and Crb3. For Ezrin, mRNAs encoding a RFP tagged Ezrin (Ezrin-Ruby), and a GFP tagged actin-probe (LifeAct-eGFP) were injected at the 2-cell stage into both blastomeres. Embryos were filmed from the early 8-cell stage to the late 8-cell stage and the localisation of Ezrin-Ruby and LifeAct-eGFP were recorded. Similar to Pard6b, aPKC, Ezrin and Crb3 only show apical localisation at the late 8-cell stage when F-actin or LifeAct were already polarised (Figure 3.4 A-D).

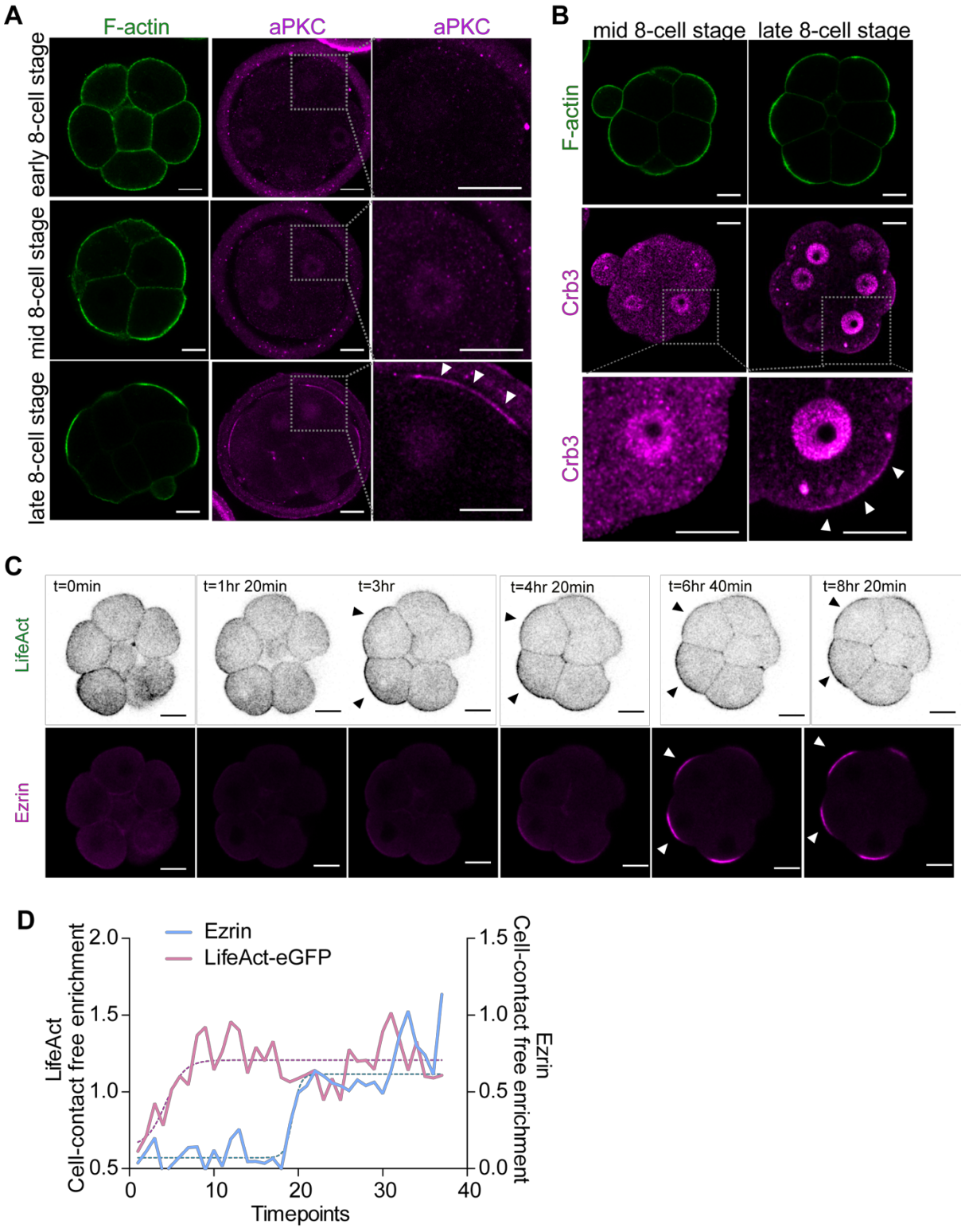

Figure 3.4 Dynamics of aPKC, Crb3 and Ezrin in relation to F-actin during the 8-cell stage development. (A) Localisation pattern of F-actin and aPKC during the 8-cell stage development. Squares indicate the magnified region. Arrows indicate the apically localised aPKC. (B) Localisation pattern of F-actin and Crb3 during the 8-cell stage development. Squares indicate the magnified region. Arrows indicate the apically localised Crb3. (C)

Snapshots of time-lapse recordings of embryos expressing Ezrin-Ruby and LifeAct-eGFP. Arrows indicate the polarised localisation of LifeAct-eGFP or Ezrin-Ruby. (D) Quantification of Ezrin and LifeAct-eGFP cell contact-free enrichment. Quantifications were fitted into a "Boltzmann sigmoidal" model based curve (R2= 0.8886 for Ezrin-Ruby, R2=0.5198 for LifeAct-eGFP). N=10 embryos, 3 independent experiments. All scale bars, 15μm.

Taken together, these results indicate that during the 8-cell stage development, as the embryo compact, actomyosin polarises to the cell contact-free surface, and this precedes apical domain establishment. Thus actomyosin is likely to be among the earliest molecules that is associated with symmetry breaking events coordinating cell polarity establishment in the 8-cell stage mouse embryo.

3.3 Actomyosin apical polarisation is required for Par complex enriched apical domain assembly

3.3.1 Pharmacological perturbation of the actomyosin structure from the early 8-cell stage inhibits compaction and apical domain assembly

The above results suggest that actomyosin accumulates to the cell contact-free surface before the maturation of the apical domain, indicating a role for actomyosin asymmetry in assembling the matured apical domain. To functionally test this hypothesis, different strategies to down-regulate the actomyosin complex were employed. In the first attempt, the siRNA targeting Myl12b, the highest expressed myosin light chain isoform, was injected into the zygote to prevent myosin II formation. However, this RNAi strategy was unsuccessful as although the siRNA effectively eliminated Myl12b (by 74%, Figure 3.5A), no significant down-regulation of the myosin light chain protein was observed. This indicates that the presence and function of the protein of the myosin II complex at the 8-cell stage is regulated by the maternal store (Figure 3.5B).

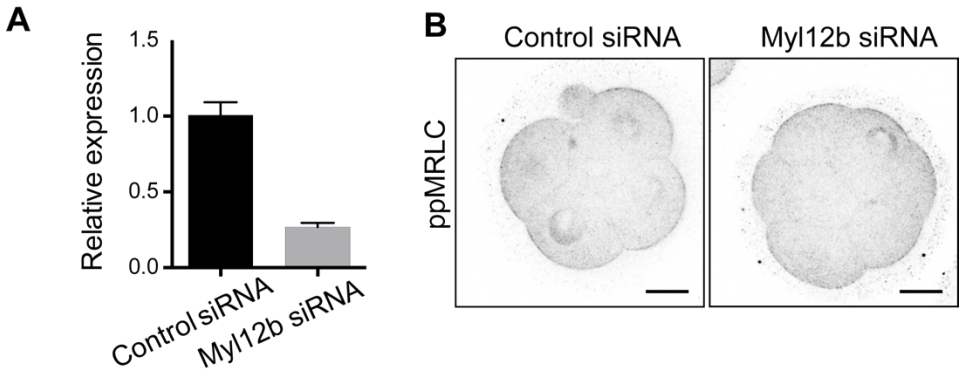

Figure 3.5 The RNAi method failed to effectively eliminate Myl12b protein due to the maternal store. (A) Verification of the efficiency of Myl12b siRNA by qPCR. Data are shown as mean ± S.E.M. N=1 experiments. N=20 embryos per each group. (B) Embryos injected with Control siRNA or Myl12b siRNA were fixed at the late 8-cell stage and stained for ppMRLC. N=8 embryos for DMSO and N=9 embryos for Blebbistatin, 2 independent experiments. All scale bars, 15μm.

Next, pharmacological inhibition methods were used to block actomyosin activity. Actomyosin activation starts by myosin light chain phosphorylation, which triggers the packing of the myosin light chain and heavy chain, resulting in myosin II filament assembly. The myosin II filament, once formed, is able to bind to the polymerised actin network and starts contracting, through constant cycling between ADP to ATP. Two myosin II inhibitors, namely Blebbistatin and ML-7 were used to block myosin II ATPase activity (Blebbistatin) thus contractility, or to block the phosphorylation of the myosin light chain (ML-7), which antagonises myosin light chain kinase (MLCK) activity thus blocking the myosin II filament formation. The inhibitors were added from the early 8-cell stage (to eliminate the effects on cytokinesis) and the embryos were fixed at the late 8-cell stage (Figure 3.6A-D). The localisation of Pard6 and F-actin was subsequently examined. The intra-blastomere angle (IEA) was measured as a readout of compaction. Consistent with the previous study, Blebbistatin treatment effectively blocked cell compaction (Maitre et al., 2015), as the IEA remained at a similar level to that of the early 8-cell stage (Figure 3.6A-B). Surprisingly, both Pard6b and F-actin still effectively polarised to the cell contact-free surface and eventually formed the apical cap structure (Figure 3.6 A-D). This phenotype was independent of the timing of treatment or the concentration of the drug, as when Blebbistatin concentration was increased to 50uM, or the treatment was administered at the late 4-cell stage, a similar phenotype was observed (Figure 3.5E). This indicates that although actomyosin contractility is required for cell compaction, it is not essential for apical

domain establishment. This result also suggests that cell compaction is not required for the formation of the apical domain, but rather they are parallel events. In contrast, ML-7 treatment not only blocked cell compaction (Figure 3.6 A-D), but also abolished the apical recruitment of both Pard6 and F-actin (Figure 3.6 A-D). Particularly, F-actin organisation appeared largely disorganised upon ML-7 treatment. In the DMSO treated control embryos, at the late 8-cell stage actin formed dense filaments on the outside of the actomyosin ring structure and a puncta-like lattice network on the inside of the ring. In ML-7 treated embryos the actin cortex density was significantly reduced, and isotropic and dispersed actin patches were observed on the surface of each blastomere (Figure 3.6A), indicating that lack of myosin II filaments significantly affected the organisation of actin. To unequivocally determine the effectiveness of ML-7, embryos treated with DMSO or ML-7 were fixed at the late 8-cell stage and stained for di-phosphorylated myosin light chain (ppMRLC). In the DMSO treated late 8-cell stage embryos, ppMRLC was polarised to the cell contact-free surface, in agreement with the F-actin and GFP-MRLC staining. In ML-7 treated embryos however, ppMRLC apical accumulation was largely reduced (Figure 3.6 F-G). On the contrary, Blebbistatin treatment did not affect the level of ppMRLC (Figure 3.6 H-I). These results suggest that actomyosin activation, rather than contractility, is required for apical domain assembly.

As an alternative way to destroy the actomyosin network, Lat-B, a potent antibiotic which induces actin depolymerisation, was administered from the early 8-cell stage to the late 8-cell stage and polarisation. Embryos were then fixed and stained for F-actin and Pard6b, as earlier described. Consistent with the ML-7 treatment, Lat-B treatment strongly decreased the density of F-actin, and inhibited compaction (Figure 3.6A-C). More importantly, Pard6 failed to polarise to the cell-contact free surface, and as a result no apical domain was observed (Figure 3.6A-D).

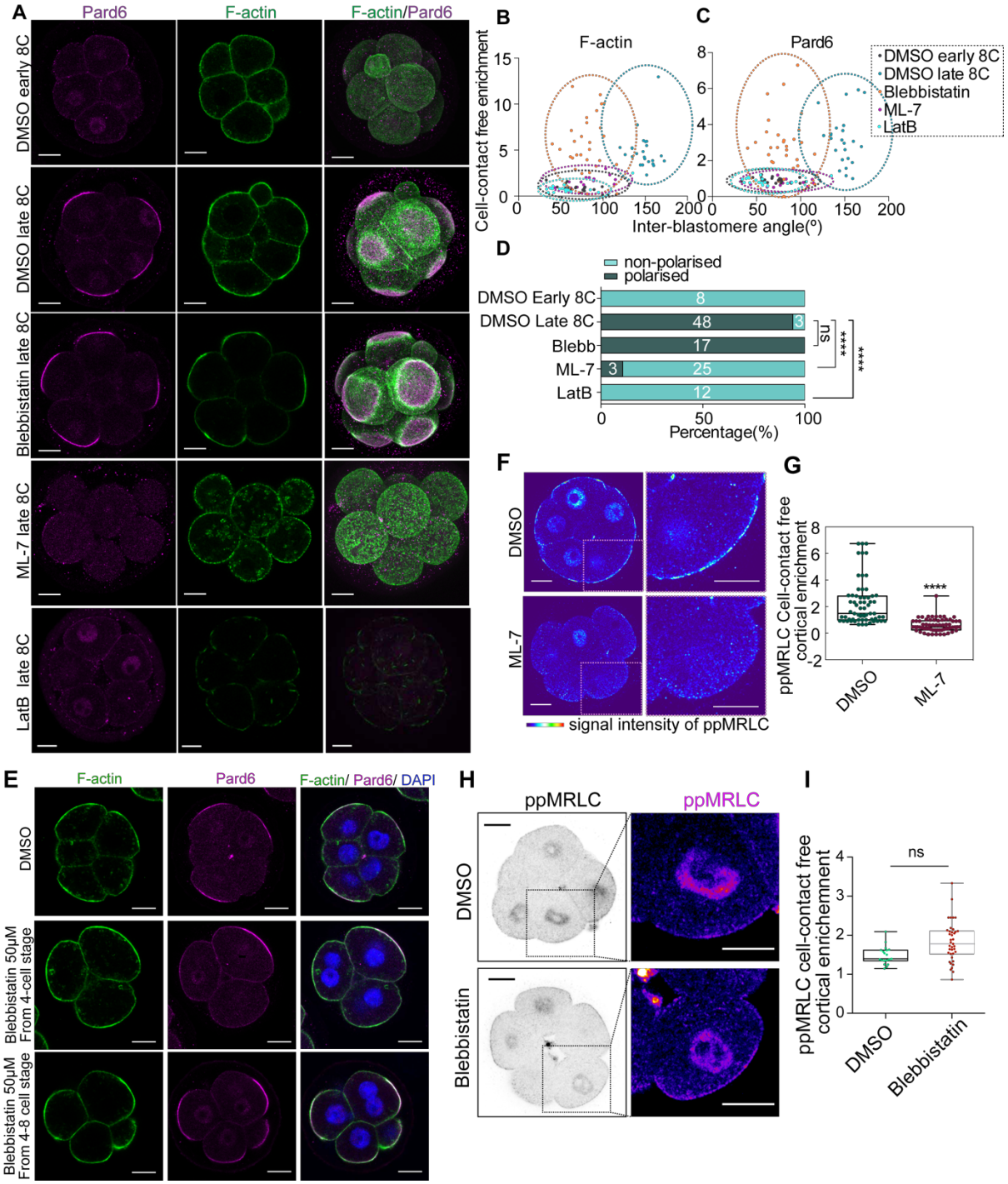

Figure 3.6 The effects of different actomyosin inhibitors on polarisation revealed that actomyosin activation but not contractility is required for apical domain assembly. (A) The embryos treated with Blebbistatin, ML-7 and Lat-B were fixed at the late 8-cell stage and stained for Pard6 and F-actin. (B, C) Quantification of inter-blastomere angle, F-actin and Pard6 apical enrichment in embryos treated with DMSO, Blebbistatin, ML-7 and LatB. Each dot indicates a measured cell. The measurements of cells in the same treatment group were indicated using a circle. Number of embryos per each condition is indicated in (D). N=3

experiments. (D) Quantification of polarisation rate in DMSO, Blebbistatin, ML-7 and Lat-B treatment. Numbers in each bar represent the number of analysed cells showing a polarised/unpolarised phenotype. ****$p < 0.0001$, NS = not significantly different, Fisher's exact test. (E) Embryos treated with Blebbistatin at different stages or different concentrations were fixed at the late 8-cell stage and stained for F-actin and Pard6. (F) Embryos treated with DMSO (as a control) or ML-7 were fixed at the late 8-cell stage and stained for ppMRLC. (G) Quantification of ppMRLC apical enrichment in DMSO or ML-7 treated cells. Data are shown as individual data points with a Box and Whiskers graph (bottom: 25%; top: 75%; line: median; whiskers: min to max). Each dot represents an analysed cell. N = 10 embryos for DMSO and N = 12 embryos for ML-7, 4 independent experiments. ****$p < 0.0001$, Mann–Whitney test. (H) Embryos treated with DMSO or Blebbistatin were fixed at the late 8-cell stage and stained for ppMRLC. (I) Quantification of ppMRLC apical enrichment in DMSO or Blebbistatin treated cells. Data are shown as individual data points with Box and Whiskers graph (bottom: 25%; top: 75%; line: median; whiskers: min to max). Each dot represents an analysed cell. ns, not significant, Mann–Whitney test. N=8 embryos for DMSO and N=9 embryos for Blebbistatin, 2 independent experiments All scale bars, 15μm.

Taken together, various pharmacological methods to destroy actomyosin architecture suggest that the early asymmetry of actomyosin complex to the cell-contact free surface primes the apical accumulation of various apical domain proteins to form the matured apical domain.

3.3.2 ML-7 treatment from the mid 8-cell stage inhibits specifically apical domain assembly

To unequivocally determine whether the intact actomyosin architecture is required for apical domain assembly, as opposed to it being a secondary result of the failure of compaction, ML-7 was applied at the mid 8-cell stage when the embryos had already compacted. At the late 8-cell stage (4 hours after the drug application) embryos were fixed and stained for F-actin and Pard6. It was observed that this treatment allowed the embryos to remain compacted (Fig 7). However, F-actin and myosin apical polarisation was strongly impaired, and Pard6b still failed to polarise to the apical domain (Figure 3.7).

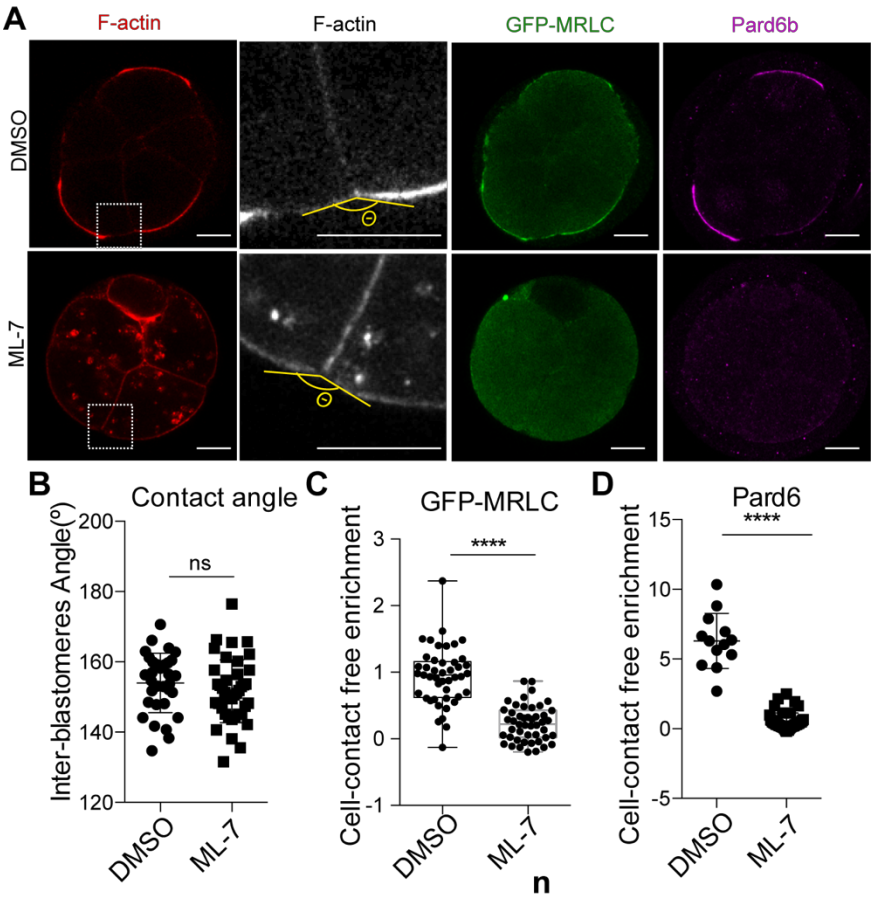

Figure 3.7 ML-7 treatment from the mid 8-cell stage after compaction abolished apical domain establishment. (A) Embryos treated with DMSO or ML-7 were fixed at the late 8-cell stage and stained for F-actin, GFP-MRLC and Pard6b. Squares indicate the magnified region. (B) Quantification of the contact angles in the cells treated with DMSO and ML-7. ns, not significant; unpaired student's t-test. (C) Quantification of the GFP-MRLC cell-contact free surface enrichment in cells treated with DMSO or ML-7. ****p<0.0001; unpaired student's t-test. (D) Quantification of the GFP-MRLC cell-contact free surface enrichment in cells treated with DMSO or ML-7. ****p<0.0001; unpaired student's t-test. N=9 embryos for DMSO and N=10 embryos for ML-7, 4 independent experiments. All scale bars, 15µm.

Combined with the results from section 3.3.1, these results strongly suggest that actomyosin apical polarisation is required for the subsequent apical domain establishment, and it this is achieve through a structure dependent function.

3.3.3 Myosin light chain phosphorylation starts from the early 8-cell stage

As compaction and polarisation events are conserved processes among different mammalian species, the understanding of the timing mechanism of compaction and polarisation is another interesting and fundamental topic in mammalian embryo development. Based on the observation that actomyosin activity is bound to compaction and polarisation, it is highly likely that the dynamic changes of activated actomyosin are associated with temporal events, thus it is important to dissect the timing of actomyosin activation and polarisation. To this end, early, mid and late 4-cell stage as well as early, mid and late 8-cell stage embryos were fixed and stained for ppMRLC. This reveals, that actomyosin activation happens in a stage-dependent manner. The level of cortical ppMRLC remains low or undetectable throughout 4-cell stage development. However, from the early 8-cell stage, ppMRLC can be detected initially in the cortex region all around the cell (early 8-cell stage), and then gradually at the cell contact-free surface until the late 8-cell stage (Figure 3.8A-).This is in agreement with the localisation pattern of GFP-MRLC (Figure 3.3).

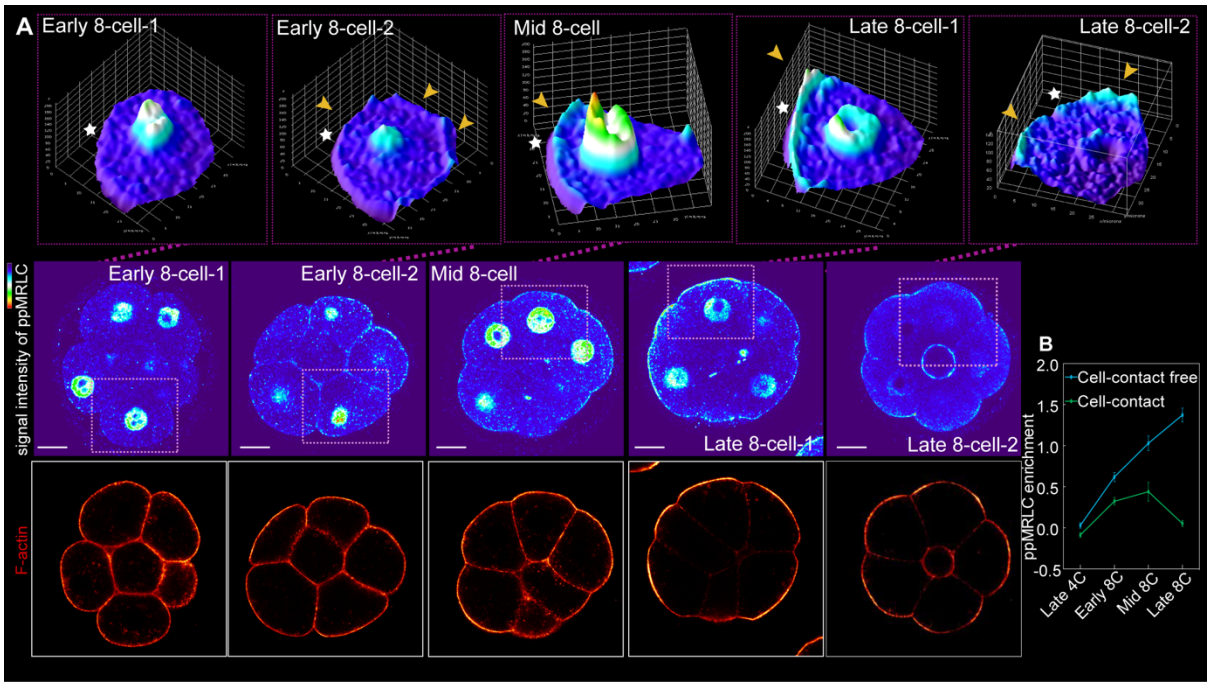

Figure 3.8 ppMRLC levels are upregulated from the early 8-cell stage. (A) The embryos of early, mid and late 8-cell stage are fixed and stained for ppMRLC. The stars indicate the apical domain, the yellow arrows indicate the ppMRLC enrichment. Pink squares indicate the magnified region. (B) Quantification of ppMRLC level at different developmental stages at cell-contact or cell-contact free surface. N = 32 measurements from 7 late 4-cell stage embryos;

N = 69 measurements from 11 early 8-cell stage embryos; N = 86 measurements from 11 mid 8-cell stage embryos; N = 50 measurements from 13 late 8-cell stage. 3 independent experiments. All scale bars, 15µm.

Taken that ppMRLC is a bona fide marker for actomyosin activation, these results suggest that the actomyosin network is specifically activated only around the early 8-cell stage, concomitant with the timing of compaction and the establishment of the apical domain.

3.4 The PLC-PKC pathway is required for apical domain assembly

3.4.1 PKC is required not only for cell compaction but also for apical domain establishment

The PKC protein family consists of 3 sub-families: conventional PKCs, novel PKCs and atypical PKCs. The different sub-families are activated by unique and specific mechanisms. Activation of Conventional PKCs requires production of the second messenger diacyl-glycerol (DAG) and an increase in intracellular calcium levels. Activation of Novel PKCs requires DAG but not calcium. Atypical PKCs, as previously described, are the major kinases of the Par apical polarity complex, and they are activated independently of DAG and calcium. Since the PKC activators PMA, diC8, TPA and OAG, which trigger pre-mature compaction, are the analogue of DAG, the activation of conventional or novel PKCs may be involved in the compaction event.

The classical signalling pathway that activates conventional and novel PKCs is Phospholipase C (PLC)-induced Phosphatidylinositol 4,5-bisphosphate (PIP2) cleavage. PIP2 is a minor phospholipid present in cell membranes, which participates in multiple signalling transduction pathways. Upon stimulation, activated PLC will cleave PIP2 to generate DAG and Inositol 1,4,5-triphosphate (IP3). The latter activates calcium channels situated in the endoplasmic reticulum leading to an elevation of cytoplasmic calcium levels. The elevated calcium levels, together with DAG, induce PKC activation (Figure 3.9).

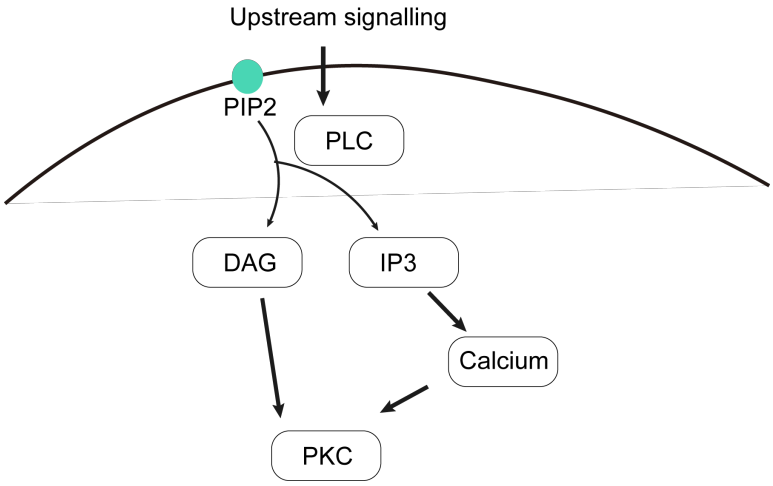

Figure 3.9 Schematic view of PLC-PKC pathway. The activation of PLC by multiple different upstream signalings triggered the hydrolysis of PIP2 into DAG and IP3. DAG directly activate PKC activation and IP3 first activated the ER membrane bound Calcium channel to induce a cytoplasmic calcium wave, which in turn activate PKC. As a results, DAG and IP3 both are able to induce PKC activation.

As the actomyosin system is specifically activated at the 8-cell stage, the identification of the upstream actomyosin activator is critical for understanding the timing of compaction and apical domain establishment as well as the regulatory mechanism behind both of these events. PKC activity has been implicated in triggering compaction, however its potential requirement for actomyosin activation and relationship to cell polarisation unclear. To investigate whether PKC activity is required for polarisation two selective PKC inhibitors, sphingosine and calphostin C, which specifically inhibit conventional and novel PKC but not the cell polarity-related protein atypical PKC, were applied at the late 4-cell stage (Figure 3.10 A). Embryos were fixed at the late 8-cell stage and stained for F-actin and Pard6b. Both sphingosine and calphostin C effectively blocked cell compaction at the late 8-cell stage (Figure 3.10 B-D), consistent with the earlier studies suggesting that PKC is required for cell compaction(Winkel et al., 1990). More importantly, F-actin and Pard6 also failed to polarise to the cell contact-free surface (Figure 3.10 B-D), suggesting that PKC is important for the apical domain establishment.

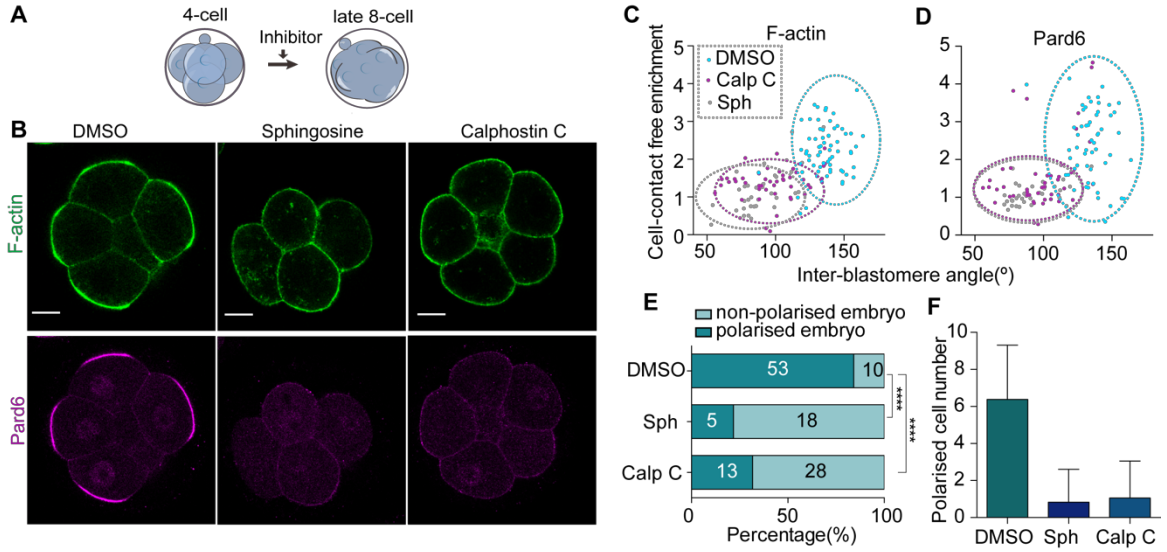

Figure 3.10 PKC inhibitors abolished cell compaction and polarity establishment. (A) Scheme of inhibitor treatment. Two PKC inhibitors that specifically inhibit canonical and novel PKC, but not atypical PKC were added to the medium from the 4-cell stage until the late 8-cell stage. (B) Embryos treated with DMSO (as a control), Sphingosine and Calphostin C were fixed at the late 8-cell stage and stained for F-actin and Pard6. (C, D) Quantification of inter-blastomere angle, F-actin and Pard6 apical enrichment in embryos treated with DMSO, Sphingosine and Calphostin C. Each dot indicates an analysed cell. The measurements of cells in the same treatment group were indicated using a circle. Number of embryos analysed for each condition has been indicated in (E). N=3 independent experiments. (E) Quantification of the percentage of embryos that show polarised cells under DMSO, Sphingosine and Calphostin C treatments. Data are shown as a contingency table, the number in each bar indicates the number of embryos analysed. ****p<0.0001, Fisher's exact test. (F) Quantification of polarised cell number in embryos treated with DMSO, Sphingosine and Calphostin C. Data are shown as mean ± S.D. All scale bars, 15µm.

3.4.2 PLC activation lies upstream of PKC and is required for apical domain assembly and the subsequent TE specification events

Conventional and novel PKC activation is triggered by the generation of two second messengers, DAG and IP3, from a membrane phospholipid PIP2, and catalysed by the enzyme Phospholipase C (PLC). As an alternative to PKC inhibition, the activity of PLC was blocked by treatment with the selective pan-PLC inhibitor, U73122 (Figure 3.11A). The embryos were fixed at the late 8-cell stage and their polarisation status was examined. The immunostaining of F-actin and Pard6 revealed that, U73122 treatment blocked cell polarisation at the late 8-

cell stage (Figure 3.11 B-G). To determine whether these phenotypes resulted from the inactivation of PKC, a rescue experiment was performed. Specifically, the PKC activator OAG (analogue of DAG), was added from the early 8-cell stage and embryos were fixed at the late 8-cell stage and stained for F-actin and Pard6. The examination of compaction and F-actin and pard6 localisation revealed that, the re-activation of PKC can effectively rescue compaction and polarisation defects caused by PLC inhibition (Figure 3.11 B-G), suggesting that the phenotype observed from PLC inhibition was indeed due to PKC inactivation. The effect from U73122 was not likely due to the impaired cell fitness as the washout of U73122 allowed the embryos to develop to blastocyst stage (data not shown).

The cell polarity defects were long-lasting in the U-73122 treated embryos, as the cells were unable to polarise at the 16-cell stage and the subsequent cell differentiation events, such as the induction of Cdx2, were abolished. This suggests that apical domain assembly was indeed suppressed by the inhibition of PLC.

Inhibitors can very often cause off-target effects and so, to further determine whether the phenotype observed from U73122 treatment were specifically due to PLC inactivation, other methods of PLC inhibition were explored. To this end, a dominant negative form of PLC (PH domain of Plcd1, referred as PLC-DN) were constructed and overexpressed at the 2-cell stage (Figure 3.12A). To visualise PLC-DN localisation, Ruby (a modified form of RFP) was tagged to the C-terminal of PLC-DN. Ruby mRNA overexpression alone has been used as the control condition. The embryos were fixed at the late 8-cell stage and the degree of cell compaction and cell polarisation was analysed. Consistent with pharmacological treatment experiments, PLC-DN effectively blocked cell compaction, as well as the apical polarisation of F-actin and Pard6b (Figure 3.12B-F). Consistent with the U73122 experiment, the defects in cell polarity were effectively rescued by OAG treatment from the early 8-cell stage, indicating that the polarity phenotype caused by PLC-DN overexpression was due to the downregulation of PKC activity. Beyond the 8-cell stage, the embryos overexpressing PLC-DN still failed to polarise, and the downstream TE specification was abolished (Figure 3.11G-H), indicating that apical domain function was completely blocked by the inhibition of PLC activity.

Combined, these results consistently show that PKC activation, triggered by PLC activity, is required not only for cell compaction, but also for the establishment of the apical domain.

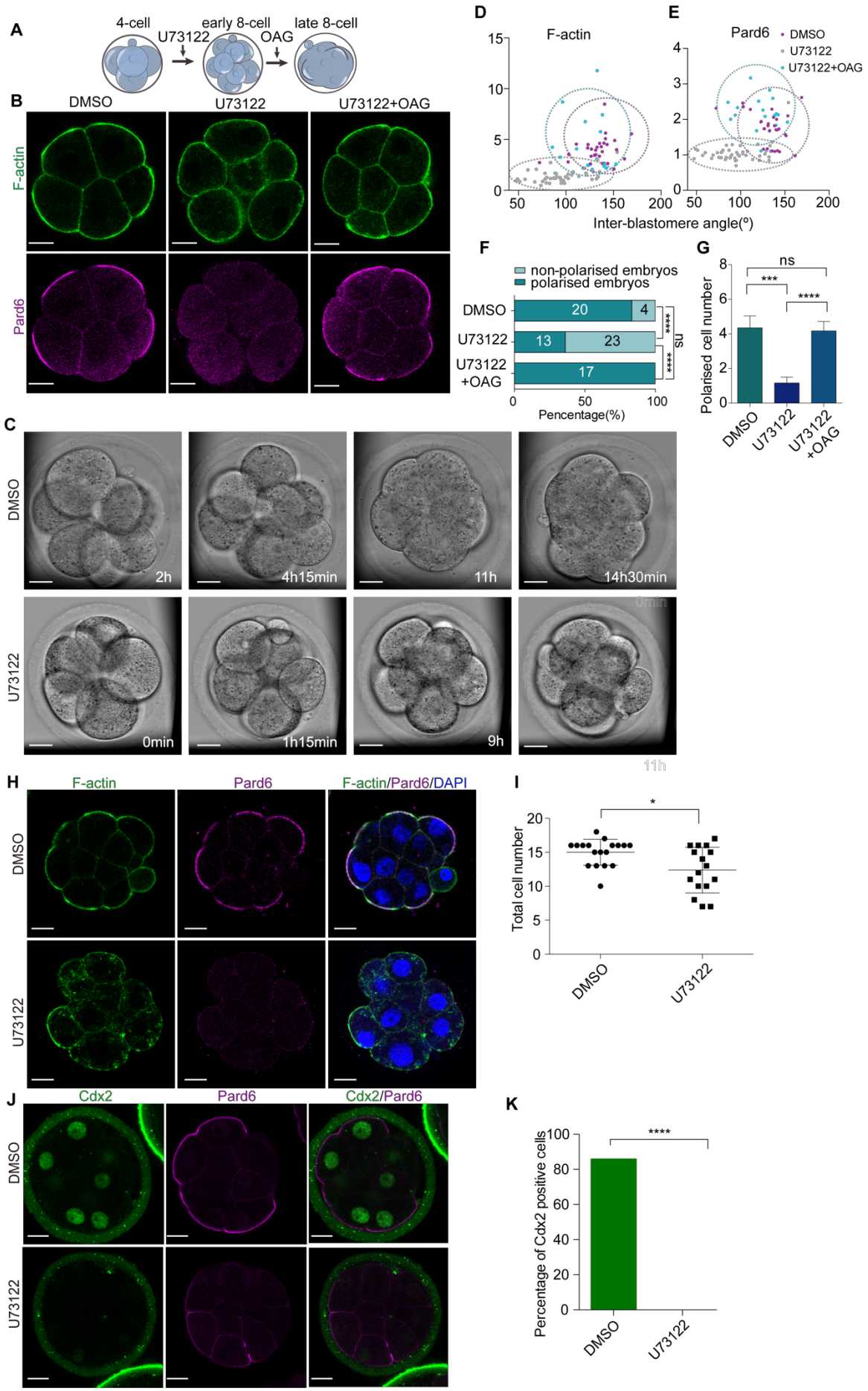
A
4-cell
early 8-cell
late 8-cell
U73122
OAG
B
DMSO
U73122
U73122+OAG
F-actin
Pard6
C
DMSO
U73122
2h
4h15min
11h
14h30min
0min
1h15min
9h
11h
D
F-actin
Inter-blastomere angle(°)
E
Pard6
DMSO
U73122
U73122+OAG
F
non-polarised embryos
polarised embryos
DMSO
U73122
U73122 +OAG
20
4
13
23
17
Pencentage(%)
G
Polarised cell number
ns
***
****
H
F-actin
Pard6
F-actin/Pard6/DAPI
I
Total cell number
J
Cdx2
Pard6
Cdx2/Pard6
K
Percentage of Cdx2 positive cells

Figure 3.10 Inhibition of PLC activity abolished compaction, cell polarisation and subsequent TE specification events upstream of PKC signalling. (A) Scheme of PLC inhibitor treatments. Selective pan-PLC inhibitor U73122 was treated from late 4-cell stage, for OAG rescue group, the OAG was added at the presence of U73122 at the early 8-cell stage. (B) Embryos treated with DMSO (control), U73122 or U73122+OAG were fixed at the late 8-cell stage and stained for F-actin and Pard6. (C) Time-lapse movie of embryos treated with DMSO or U73122 from 4-8 cell stage to 8-16 cell stage. (N=72 embryos for DMSO and N=127 embryos for U73122, 12 independent experiments). (D, E) Quantification of inter-blastomere angle, F-actin and Pard6 apical enrichment in embryos treated with DMSO, U73122 and U73122+OAG group. Each dot indicates an analysed cell. The measurements of cells in the same treatment group were indicated using a circle. Number of embryos analysed were indicated in (F). (F) Quantification of the percentage of embryos that show polarised cells under DMSO, U73122 and U73122+OAG treatments. Data are shown as a contingency table, the number in each bar indicates the number of embryos analysed. N=2 independent experiments. ns, not significant; ****p<0.0001, Fisher's exact test. (F) Quantification of polarised cell number in embryos treated with DMSO, Sphingosine and Calphostin C. Data are shown as mean ± S.D. ns, not significant; ***p<0.01; ****p<0.0001; Kruskal–Wallis test and Dunn's multiple comparisons test. 64 embryos for DMSO group; 23 embryos for Sphingosine group; 51 embryos for Calphostin C group. N=3 independent experiments. (H) Embryos treated with DMSO or U73122 were fixed at the 16-cell stage embryos and stained for F-actin and Pard6. (N=18 embryos for DMSO and N=16 embryos for U73122, 3 independent experiments). (I) Quantifications of the total cell numbers in embryos treated with DMSO or U73122. Data are shown as mean ± S.D. *p<0.05, Student's t-test. (J) Embryos treated with DMSO or U73122 were fixed at the 16-cell stage and stained for Pard6 and Cdx2. (N=10 embryos for each group; N=1 experiment). (K) Quantifications of the percentage of Cdx2 positive cells in embryos treated with DMSO or U73122 at the 16-cell stage. ****p<0.0001, Fisher's exact test. All scale bars, 15μm.

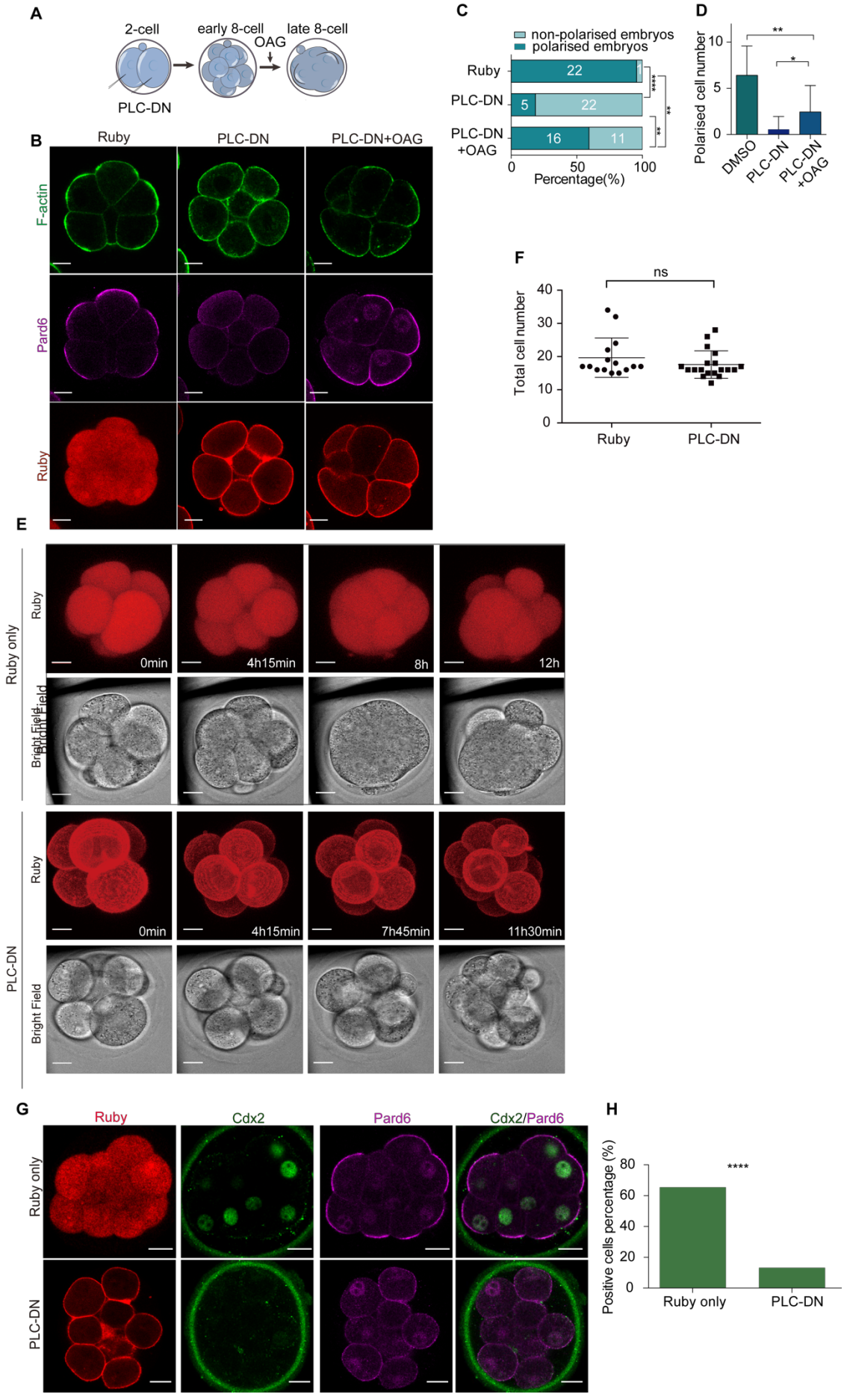
A
2-cell
early 8-cell
late 8-cell
OAG
PLC-DN
B
Ruby
PLC-DN
PLC-DN+OAG
F-actin
Pard6
Ruby
C
non-polarised embryos
polarised embryos
Ruby
PLC-DN
PLC-DN +OAG
22
5
22
16
11
0
50
100
Percentage(%)
****
**
**
D
Polarised cell number
10
5
0
**
*
DMSO
PLC-DN
PLC-DN +OAG
F
Total cell number
40
30
20
10
0
ns
Ruby
PLC-DN
E
Ruby only
PLC-DN
Ruby
Bright Field
0min
4h15min
8h
12h
7h45min
11h30min
G
Ruby
Cdx2
Pard6
Cdx2/Pard6
Ruby only
PLC-DN
H
Positive cells percentage (%)
80
60
40
20
0
****
Ruby only
PLC-DN

Figure 3.11 Overexpression of PLC-DN abolished cell compaction, polarity establishment and TE specification. (A) Scheme of PLC-DN overexpression. (B) Embryos overexpressing Ruby (control) and PLC-DN were fixed at the late 8-cell stage and stained for F-actin and Pard6. (C) Quantification of the percentage of embryos that showed polarised cells in Ruby or PLC-DN overexpression conditions. Data are shown as a contingency table, the numbers in each bar indicate the number of embryos analysed. ** $p<0.01$, ****$p<0.0001$, Fisher's exact test. N=2 independent experiments. (D) Quantification of polarised cell number in embryos overexpressing Ruby or PLC-DN. Data are shown as mean ± S.D. ns, not significant; *$p<0.05$; **$p<0.01$; Kruskal–Wallis test and Dunn's multiple comparisons test. Number of embryos analysed were indicated in (C). (E) Time-lapse movie of embryos expressing Ruby or PLC-DN from 4-8 cell stage to 8-16 cell stage of development. (F) Quantification of the total cell number in embryos expressing Ruby or PLC-DN. Data are shown as mean ± S.D. ns, not significant; Student's t-test. (G) Embryos expressing Ruby or PLC-DN were fixed at the 16-cell stage and stained for Pard6 and Cdx2. (H) Quantification of the percentage of cells expressing Cdx2. ****$p<0.0001$, Fisher's exact test. (N=8 embryos for each group, 4 independent experiments). All scale bars, 15µm.

3.5 PLC-PKC activity is necessary and sufficient for actomyosin asymmetry during the 8-cell stage development

3.5.1 PKC is required for the apical polarisation of the activated actomyosin meshwork

As the results above suggest that both actomyosin polarisation and PKC activation are required for compaction as well as the establishment of the apical domain, it is conceivable that PKC controls compaction and apical domain establishment through the regulation of actomyosin. To test this possibility, PLC or PKC activity were inhibited with the use of methods described in the above sections (calphostin C, sphingosine treatment for PKC inhibition; U-73122 treatment and PLC-DN overexpression for PLC inhibition). For all conditions, embryos were fixed at the late 8-cell stage and stained for ppMRLC and F-actin. While at the late 8-cell stage control embryos (DMSO treatment or Ruby injected embryos), ppMRLC were strongly enriched in the cell contact-free cortex, co-localising with F-actin (Figure 3.13A-H), all methods of PLC or PKC inhibition consistently led to dramatic down-regulation of the apical ppMRLC enrichment (Figure 3.13A-H).

These results suggest that, as expected the PLC-PKC pathway is required for the apical enrichment of the activated actomyosin network, and thus compaction and apical polarisation.

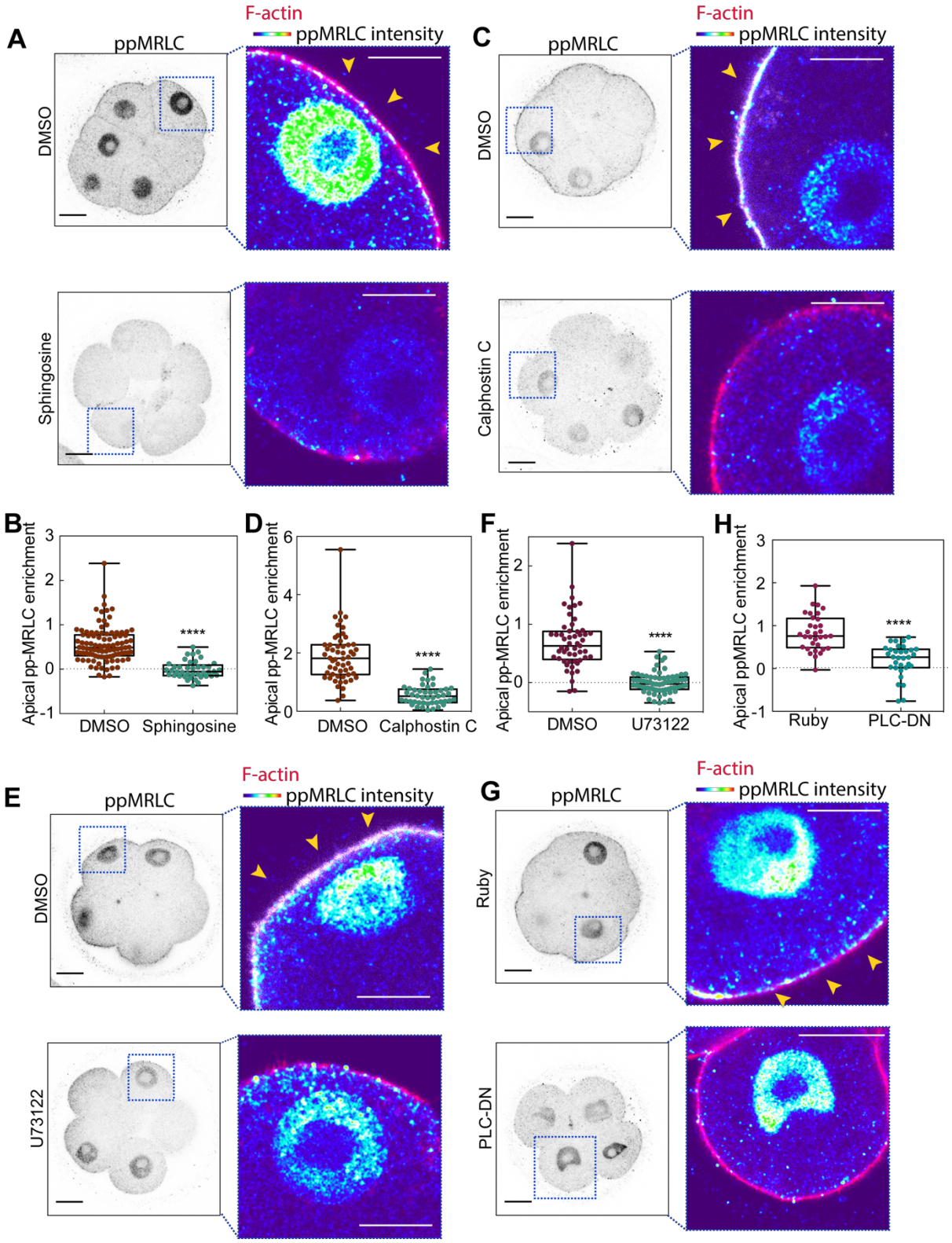

Figure 3.12 PKC activity is required for actomyosin activation and polarisation. (A) Embryos treated with DMSO or Sphingosine were fixed at the late 8-cell stage and stained for ppMRLC and F-actin. (B) Quantification of ppMRLC apical enrichment in the cells treated with DMSO or Sphingosine. N = 9–10 embryos, 2 independent experiments. (C) Embryos treated with DMSO or Calphostin C were fixed at the late 8-cell stage and stained for ppMRLC and F-actin. N = 11 embryos for DMSO and N = 9 embryos for Calphostin C, 2 independent experiments. (D) Quantification of ppMRLC apical enrichment in the cells treated with DMSO or Calphostin C. (E) Embryos treated with DMSO or U73122 were fixed at the late 8-cell stage and stained for ppMRLC and F-actin. (F) Quantification of ppMRLC apical enrichment in the cells treated with DMSO or U73122. N = 20 embryos for DMSO and N = 22 embryos for U73122, three independent experiments. (G) Embryos overexpressing Ruby or PLC-DN were fixed at the late 8-cell stage and stained for ppMRLC and F-actin. (H) Quantification of ppMRLC apical enrichment in the cells overexpressing Ruby or PLC-DN. Arrowheads indicate apically localised ppMRLC and squares indicate the magnified regions. N = 7 embryos for Ruby and N = 8 embryos for PLC-DN, 2 independent experiments. All data are shown as individual data points with Box and Whiskers graph (bottom: 25%; top: 75%; line: median; whiskers: min to max). ****$p<0.0001$, Mann–Whitney test. All scale bars, 15 μm.

3.5.2 Ectopic PKC activation is sufficient to polarise actomyosin at the 4-cell stage

To test the effect of ectopic PKC activation on cell polarity establishment, OAG was applied at the early 8-cell stage. The embryos were then fixed at the late 8-cell stage or 16-cell stage and stained for F-actin and Pard6. This revealed that, upon PKC activation, the Par complex enriched apical domain was expanded. In the DMSO treated control embryos, the Par complex occupied a proportion of the cell contact-free surface (mean surface coverage ratio (SCR) of 57.3%; Figure 3.14A-C). OAG treatment expanded the apical domain to the whole cell contact-free surface (mean SCR 84.8%; Figure 3.14A-C). As a result of OAG of treatment, Pard6 localisation expanded to the cell contacts (Figure 3.14D-E).

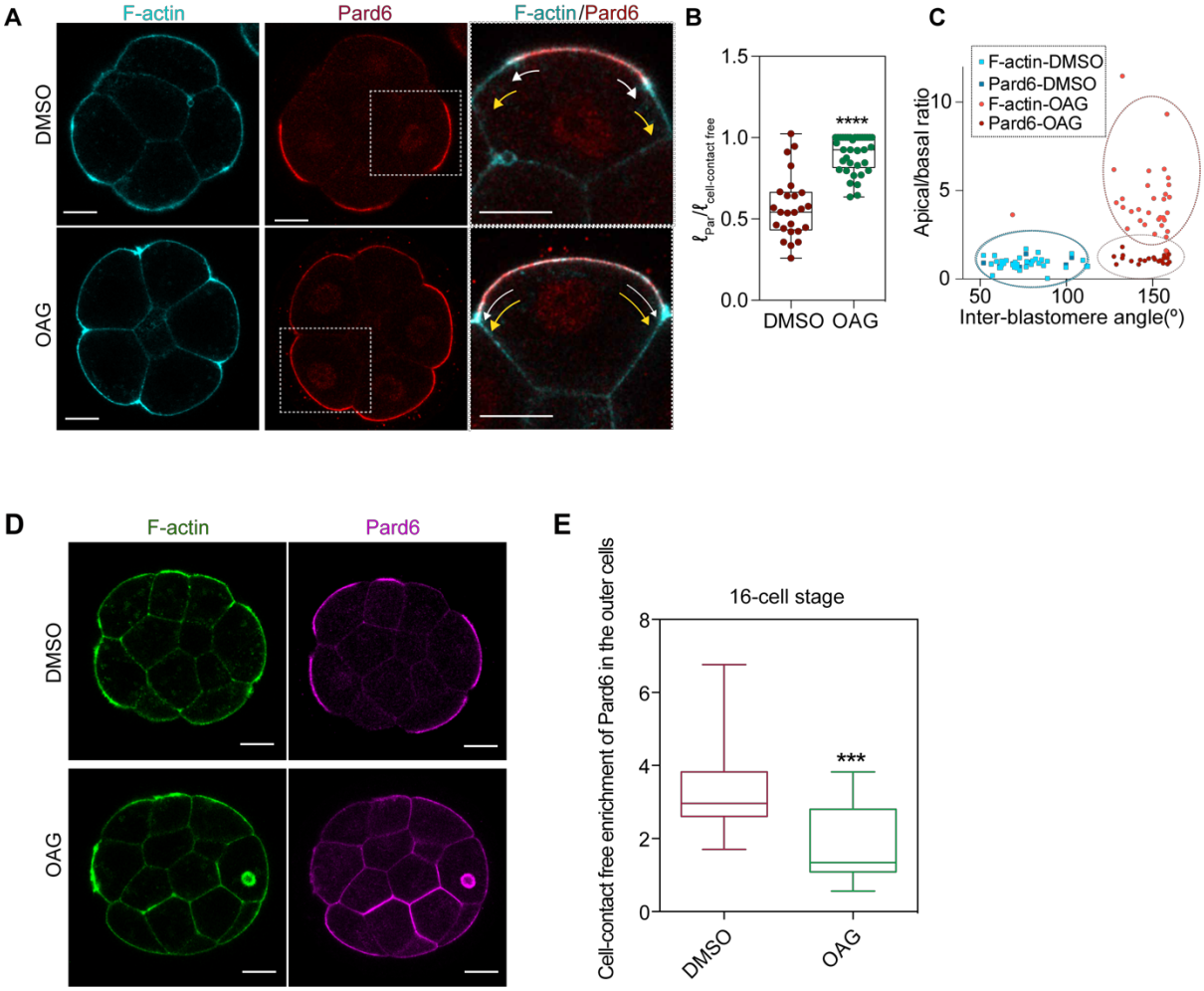

Figure 3.13 Ectopic activation at early 8-cell stage led to the expansion of apical domain. (A) Embryos treated with DMSO or OAG were fixed at the 8-cell stage and stained for F-actin and Pard6. Squares indicate the magnified region. White arrows indicate the apical domain, yellow arrows indicate the cell-contact free surface. (B) Quantification of the coverage of the apical domain in DMSO or OAG treated cells. Data are shown as individual data points with Box and Whiskers graph (bottom: 25%; top: 75%; line: median; whiskers: min to max). ****$p < 0.0001$, two-tailed unpaired Student's t test. (C) Quantification of inter-blastomere angle, F-actin and Pard6 apical enrichment in embryos treated with DMSO and OAG group. Each dot indicates an analysed cell. Cells in the same treatment group were indicated using a circle. For both B and C, N = 8 embryos for DMSO and N = 6 embryos for OAG, 4 independent experiments. (D) Embryos treated with DMSO or OAG were fixed at the 16-cell stage and stained for F-actin and Pard6. (E) Quantification of Pard6 cell contact enrichment in the outer cells of embryos treated with DMSO or OAG. Data are shown as Box and Whiskers graph

(bottom: 25%; top: 75%; line: median; whiskers: min to max). ***p<0.001, Mann–Whitney test. All scale bars, 15 μm.

To determine whether PKC activation is able to trigger the premature activation of the apical domain, two different approaches were taken for PKC activation: A constitutively activated form of PKC-alpha (Prkca-A25E) and the PKC activator OAG were used. OAG was added at the early 4-cell stage, and the embryos were fixed after 4 hours induction and stained for F-actin, ppMRLC and Pard6. Consistent with earlier reports, OAG treatment prompted the embryo to prematurely compact within 30 minutes (Winkel et al., 1990) (Figure 3.15A). In the meantime, F-actin and ppMRLC polarised to the cell contact-free surface upon OAG treatment (Figure 3.15A-B). Although Pard6b was slightly enriched at the cell contact-free surface (Figure 3.15A,C), the level of enrichment was much lower than at the apical domain of a natural 8-cell stage embryo, suggesting that no mature apical domain was successfully induced.

mRNA encoding PKCα-A25E was injected into 2 blastomeres at the early 4-cell stage, while mRNA encoding GFP-MRLC was co-injected to visualise actomyosin localisation. The embryos were fixed at the late 4-cell stage and stained for anti-GFP (for GFP-MRLC), F-actin and Pard6b (Figure 3.15D). mRNA of GFP-MRLC alone was injected as a control. At the late 4-cell stage, while GFP-MRLC alone showed homogeneous distribution among the cell membranes (Figure 3.14D), the co-overexpression of PKCalpha-A25E induced GFP-MRLC to polarise to the cell contact-free surface (Figure 3.15D-E). Consistently, F-actin also polarised toward the cell contact-free surface (Figure 3.15D,F). Although both GFP-MRLC and F-actin polarised to the cell contact-free surface, Pard6 remained unpolarised in all of the embryos examined, consistent with the results of OAG treatment (Figure 3.15G). These results indicate that although PKCalpha-A25E is sufficient to polarise the actomyosin complex prematurely at the 4-cell stage, other factors are required to polarise the Par complex and thus drive apical domain maturation.

Together, PKCα-A25E overexpression and OAG treatment experiments suggest that PKC ectopic activation is sufficient to induce actomyosin asymmetry but other factors are required to establish a matured apical domain.

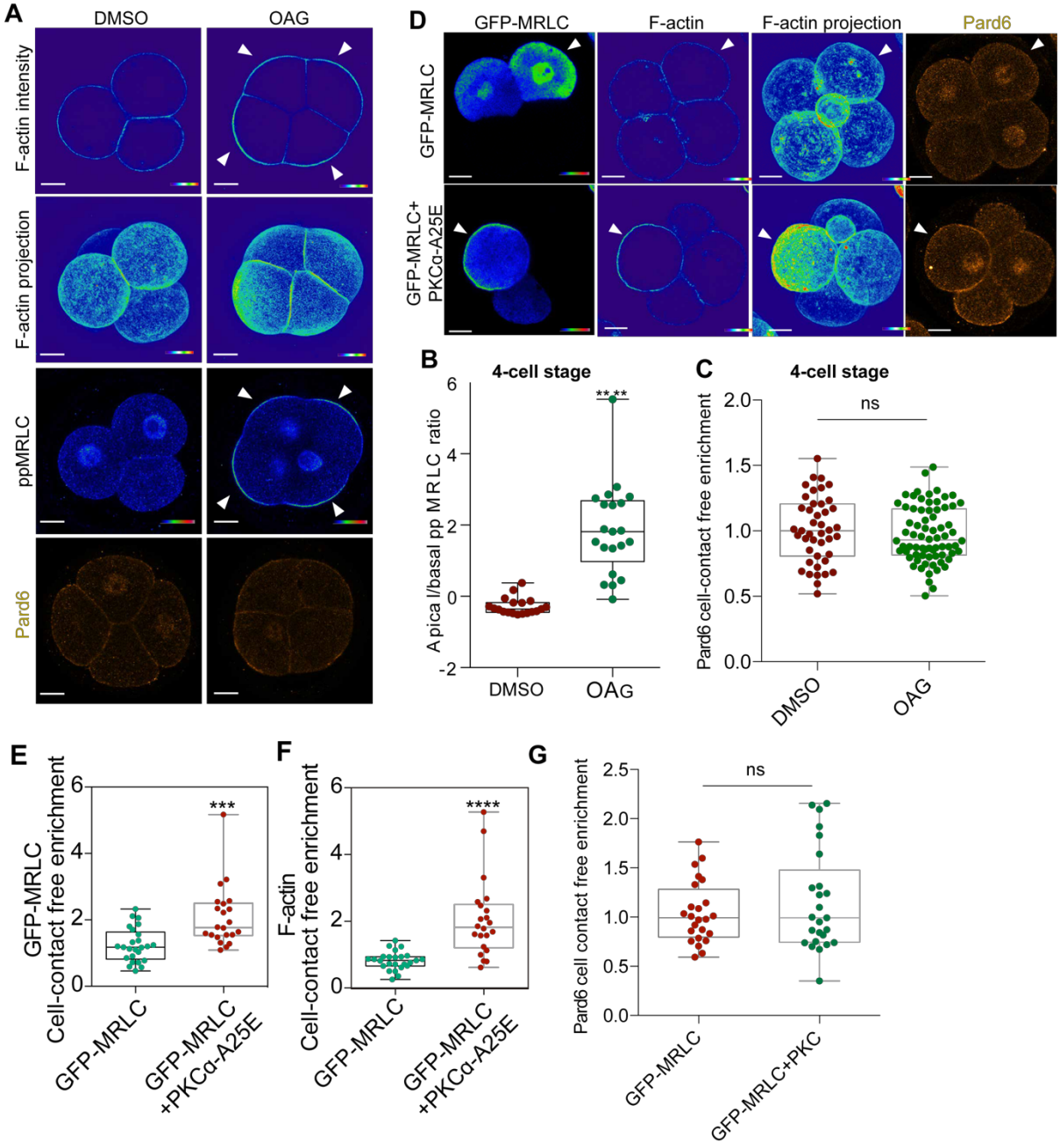

Figure 3.14 PKC activation at the 4-cell stage induces actomyosin polarisation but not apical domain formation. (A) Embryos treated with DMSO or OAG were fixed at the late 4-cell stage and stained for F-actin, ppMRLC and Pard6. Arrows indicate the polarised actomyosin complex. (B) Quantification of apical ppMRLC enrichment in the cells treated with DMSO or OAG at the 4-cell stage. ****$p < 0.0001$; Mann–Whitney test. (C) Quantification of apical Pard6 enrichment in the cells treated with DMSO or OAG at the 4-cell stage. ns, not significant; Mann–Whitney test. For both B and C, N=18 embryos for DMSO; N=10 embryos for OAG. 6 independent experiments. (D) mRNA encoding GFP-MRLC with or without PKCα-A25E were fixed at the late 4-cell stage and stained for GFP, F-actin and Pard6. Arrows

indicate an injected cell. (E) Quantification of GFP-MRLC apical enrichment in cells expressing GFP-MRLC with or without PKCα-A25E. **p<0.01; Mann–Whitney test. (F) Quantification of F-actin apical enrichment in cells expressing GFP-MRLC with or without PKCα-A25E. ****p<0.0001; Mann–Whitney test. (G) Quantification of Pard6 apical enrichment in cells expressing GFP-MRLC with or without PKCα-A25E. ns, not significant; Mann–Whitney test. For both F and G, N = 6 embryos, three independent experiments. All data are shown as individual data points with Box and Whiskers graph (bottom: 25%; top: 75%; line: median; whiskers: min to max). All scale bars, 15 μm.

3.5.3 PKC directly activates actomyosin

As the above results demonstrated that PKC is sufficient to polarise the actomyosin complex, the mechanism driving this process was investigated further. Two potential models were hypothesised to explain how PKC can trigger actomyosin polarisation: 1) actomyosin is activated by other factors, and PKC may help to stabilise cell contacts and therefore restrict the activated actomyosin complex specifically to the cell contact-free domain; 2) PKC directly activates actomyosin and the already established cell contacts help to polarise actomyosin.

To specifically test these two models, a recently developed optogenetic approach was adapted to the mouse embryo and used to activate PKC at the precise region of interest. Specifically, the CRY2-CIB1 system was used. The CRY2-CIB1 system constitutes of two domains, CRY2 and CIB1, the binding which is triggered by blue light excitation. In the absence of blue light input, the binding is automatically reversed within a defined time frame. To activate PKC at a defined cortical region, a CAAX motif was linked to CIB1 domain in order to constitutively localise this domain to the membrane (CIB1-CAAX); the kinase domain of PKCα was fused to the CRY2 domain (CRY2-PKC-KD) (Figure 3.16A). As expected, without blue light CRY2-PKC localised in the cytoplasm and CIB1-CAAX on the membrane (Figure 3.16B). 488nm blue light activation triggered the membrane recruitment of CRY2-PKC-KD within 10 minutes (Figure 3.16B). The embryos were fixed after 30 minutes of activation and stained for F-actin, ppMRLC and Pard6b. An upregulation of ppMRLC and F-actin (Figure 3.16C) was observed specifically in the region of CRY2-PKC-KD recruitment to the membrane, indicating that PKC-KD membrane recruitment results in the local activation of the actomyosin complex. To validate whether the upregulation of actomyosin activity was indeed due to PKC but not as a result of artefacts caused by the imaging of the optogenetic constructs, the CIB1-CAAX and

CRY2 domain were co-expressed and the embryos were imaged using the same conditions as for CRY2-PKC-KD. The CRY2 domain was effectively recruited to the membrane as CRY2-PKC-KD (Figure 3.16D), yet no upregulation of ppMRLC was observed (Figure 3.16E).

Together, these results show that PKC polarises the actomyosin complex through its direct activation.

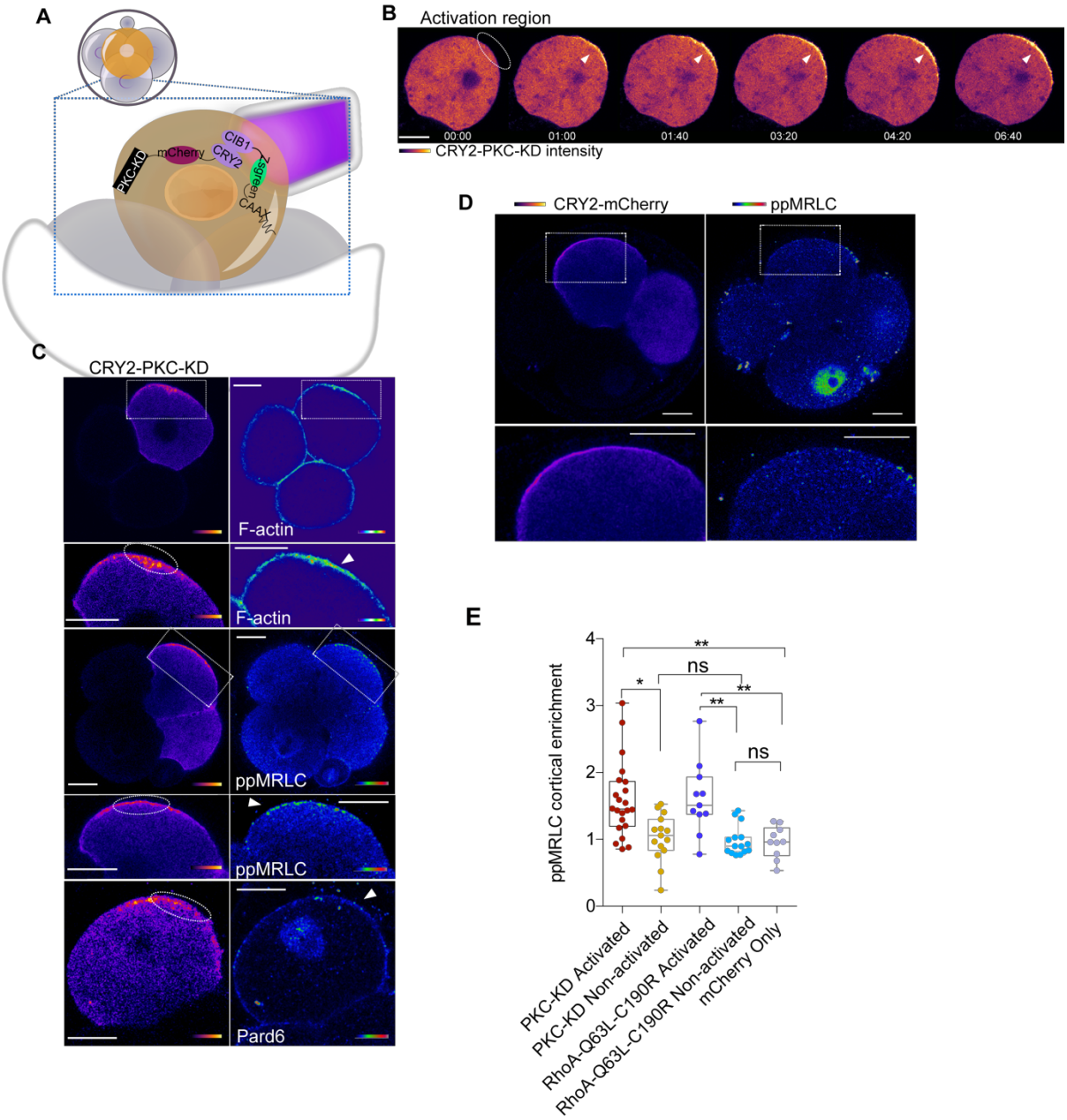

Figure 3.15 Regional PKC activation induces local actomyosin activation. (A) Scheme of the optogenetic methods for PKC activation. (B) Snapshots of PKC-KD localisation upon the introduction of blue light, arrows indicate the membrane enrichment of PKC-KD. Image represents N=24 embryos from N=11 independent experiments. (C) Cells expressing CIB1-CAAX and CRY2-PKC-KD were illuminated with blue light and fixed and stained for F-actin, ppMRLC and Pard6. Arrows indicate the illumination site. (D) Cells expressing CIB1-CAAX and CRY2-mCherry were fixed and stained for ppMRLC. (E) Quantifications of ppMRLC cortical enrichment of cells illuminated or not illuminated with blue light, expressing various combinations of optogenetic constructs. ns, not significant; *p<0.05; **p<0.01; Mann-Whitney test. (N=17 embryos for PKC-KD activated region, N=9 embryos for PKC-KD non-

activated region, N=7 embryos for RhoA-Q63L-C190R activated region, N=13 embryos for RhoA-Q63L- C190R non-activated region and N=10 embryos for mCherry only, 3 independent experiments for mCherry only, 2 independent experiments for all the other conditions). All scale bars, 15μm.

3.6 Rho-GTPases lie downstream of PKC and establish the apical domain

3.6.1 A myosin light chain phosphorylation independent mechanism is involved in PKC mediated actomyosin activation

Since PKC inhibition led to the loss of cortical MRLC accumulation (Figure 3.13), it was hypothesised that PKC may activate actomyosin through triggering MRLC filament assembly by promoting MRLC phosphorylation, or through assisting the actomyosin filaments to localise to the cortex. To test these hypotheses, a phosphomimetic form of MRLC (MRLC-DD) was constructed. In other systems, the overexpression of this phosphomimetic form was able to bypass the phosphorylation step and trigger myosin II filament formation (Vicente-Manzanares and Horwitz, 2010). To test the efficacy of this construct, the mRNA of GFP-MRLC or GFP-MRLC-DD was injected into 2-cell stage embryos, while DMSO (control) or ML-7 was applied at the early 8-cell stage to inhibits MRLC phosphorylation. In control embryos, both GFP-MRLC and GFP-MRLC-DD were polarised to the cell contact-free surface, consistent with earlier observations (Figure 3.3). ML-7 treatment effectively abolished the cortical accumulation of GFP-MRLC (Figure 3.17A-B), however GFP-MRLC-DD was still able to accumulate and polarise to the cell contact-free surface (Figure 3.17A-B) upon ML-7 treatment, indicating that in agreement with previous studies GFP-MRLC-DD can form myosin II filaments in the absence of MRLC phosphorylation.

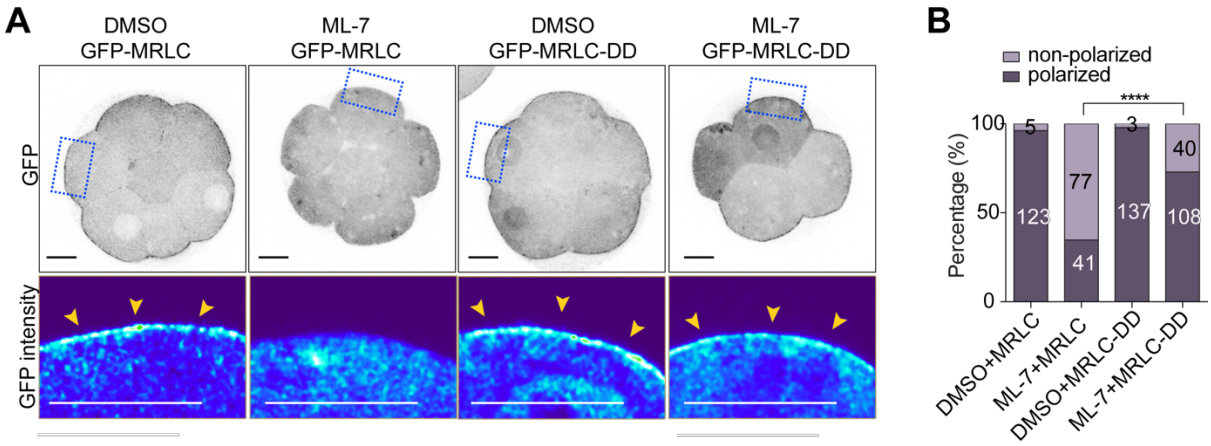

Figure 3.16 Phosphomimetic MRLC mutant bypasses the requirement of MRLC phosphorylation to form Myosin II filaments. (A) Embryos expressing GFP-MRLC, GFP-MRLC-DD were treated with DMSO or ML-7 and stained for GFP. Squares indicate the magnified region; Arrows indicate the membrane localised GFP-MRLC or GFP-MRLC-DD. (B) Quantification of the percentage of polarised cells in embryos expressing GFP-MRLC or GFP-MRLC-DD and treated with DMSO or ML-7. Data are shown as contingency table; the numbers show in each bar indicate the number of cells analysed. N = 18 embryos for DMSO + MRLC, N = 17 embryos for ML-7 + MRLC, N = 15 embryos for DMSO + MRLC-DD, N = 18 embryos for ML-7 + MRLC-DD, two independent experiments.****$p<0.0001$; Fisher's exact test.

To test whether PKC activates actomyosin through MRLC phosphorylation and thus myosin II filament formation, GFP-MRLC or GFP-MRLC-DD were overexpressed at the 2-cell stage, and PKC inhibitors Sphingosine and Calphostin C, PLC inhibitor U-73122 and PLC-DN were used as described earlier. Consistent with earlier observations, upon PKC or PLC inhibition, GFP-MRLC lost its apical accumulation (Figure 3.18). However, in contrast with ML-7 treatment, GFP-MRLC-DD was also unable to localise to the apical domain in all treatment conditions.

Together, these results suggest that PKC triggers actomyosin activation and therefore apical domain establishment through a MRLC phosphorylation independent method.

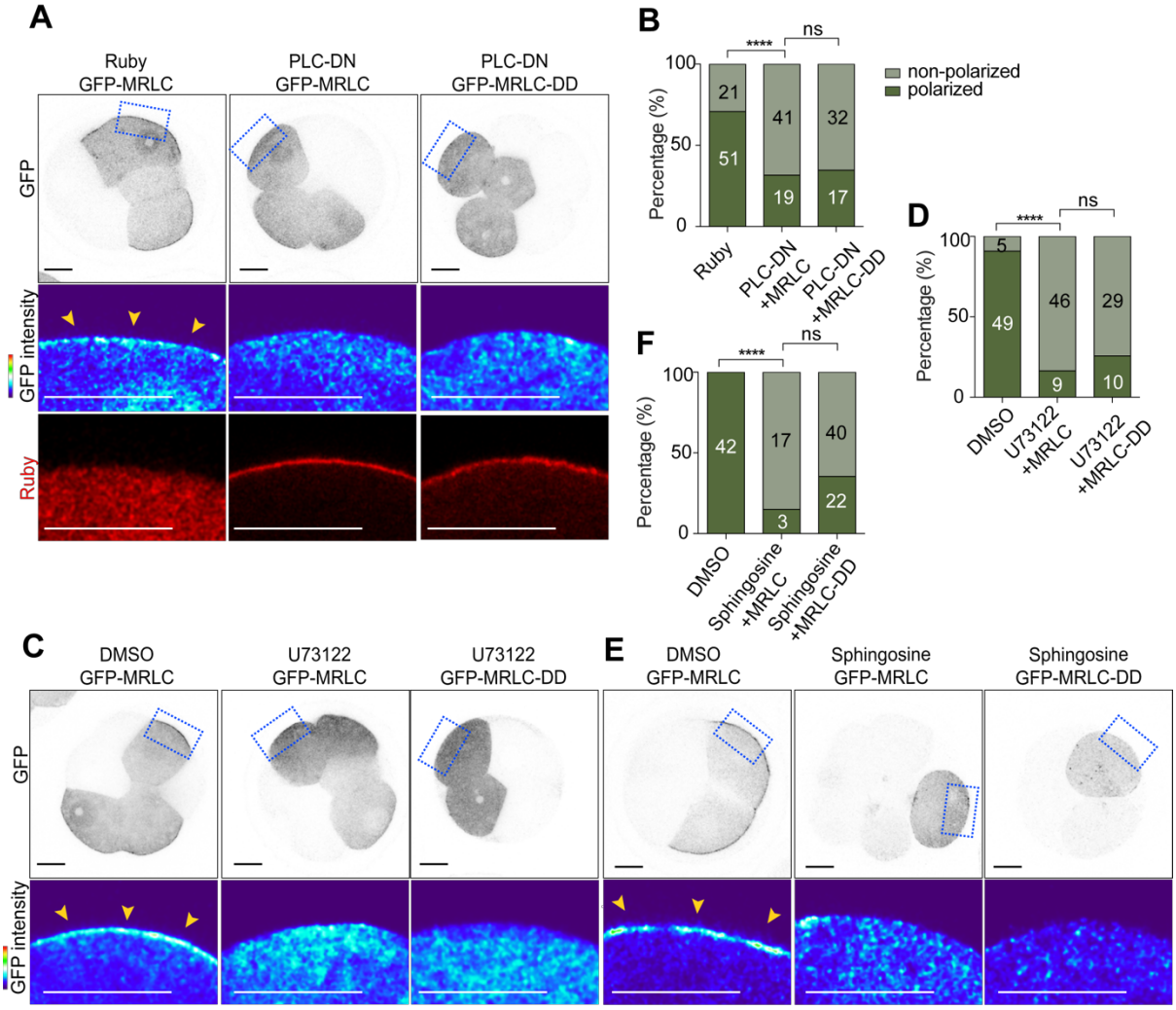

Figure 3.17 PKC recruits MRLC to the membrane in a phosphorylation independent manner. (A) Embryos overexpressing GFP-MRLC or GFP-MRLC-DD with Ruby (control) or PLC-DN were fixed at the late 8-cell stage and stained GFP. Arrows indicate the apical recruitment of GFP-MRLC. (B) Quantification of percentage of polarised cells in embryos expressing GFP-MRLC or GFP-MRLC-DD and overexpressing Ruby or PLC-DN. Data are shown as a contingency table; the numbers in each bar indicate the number of cells analysed. N = 17 embryos for Ruby + MRLC, N = 17 embryos for PLC-DN + MRLC and N = 17 embryos for PLC-DN + MRLC-DD, three independent experiments. ns, not significant; ****p<0.0001; Fisher's exact test. (C) Embryos overexpressing GFP-MRLC or GFP-MRLC-DD treated with DMSO or U73122 were fixed at the late 8-cell stage and stained for GFP. Arrows indicate the apical recruitment of GFP-MRLC. (D) Quantification of percentage of polarised cells in embryos expressing GFP-MRLC or GFP-MRLC-DD treated with DMSO or

U73122. Data are shown as contingency table; the numbers show in each bar indicate the number of cells analysed. N = 11 embryos for DMSO + MRLC, N = 11 embryos for U73122 + MRLC and N = 9 embryos for U73122 + MRLC-DD, four independent experiments. ns, not significant; ****p<0.0001; Fisher's exact test. (E) Embryos overexpressing GFP-MRLC or GFP-MRLC-DD treated with DMSO or Sphingosine were fixed at the late 8-cell stage and stained for GFP. Arrows indicate the apical recruitment of GFP-MRLC. (F) Quantification of the percentage of polarised cells in embryos expressing GFP-MRLC or GFP-MRLC-DD treated with DMSO or Sphingosine. Data are shown as a contingency table; the numbers show in each bar indicate the number of cells analysed. N = 20 embryos for DMSO + MRLC, N = 9 embryos for sphingosine + MRLC and N = 20 embryos for sphingosine + MRLC-DD, two independent experiments. ns, not significant; ****p<0.0001; Fisher's exact test. All scale bars, 15μm.

3.6.2 PKC inhibition inhibits RhoA apical polarisation

Actomyosin cortical accumulation requires not only myosin II filament formation but also the local rearrangement of the actin lattice. A common actin modifier are the Rho GTPases (such as RhoA/B/C family), which are known to promote actin polymerisation and branching. Consistently, RhoA inhibition abolished both GFP-MRLC and Pard6 apical polarisation (Figure 3.19A-D). It was therefore hypothesised that RhoA might act downstream of PKC to trigger actomyosin cortical accumulation. To monitor whether RhoA activity is affected by PKC, the mRNA of an advanced form of the Förster resonance energy transfer (FRET) based RhoA sensor (Raichu-RhoA-CR) was injected into 2-cell stage embryos and the RhoA activity was monitored during the 8-cell stage of development. RhoA activity was initially homogeneous along the cell membrane, as the embryo compacted it was gradually restricted to the cell contact-free surface, and at the late 8-cell stage RhoA was downregulated and its activity was limited to a defined region of cell contact-free surface, recapitulating the actomyosin ring structure (Figure 3.20A). Upon PLC inhibition by U-73122 treatment, the activated RhoA failed to polarise to the cell contact-free surface but instead was slightly enriched at the regions of cell contact (Figure 3.20A-B), suggesting that the PLC-PKC pathway is required for polarisation of the activated RhoA to the cell contact-free surface. The RhoA inhibition by C3-transferase did not block the initiation of cytokinesis yet did lead to the failure of the completion of cytokinesis during the following development and the embryos failed to form a proper blastocyst at E3.5 (data not shown).

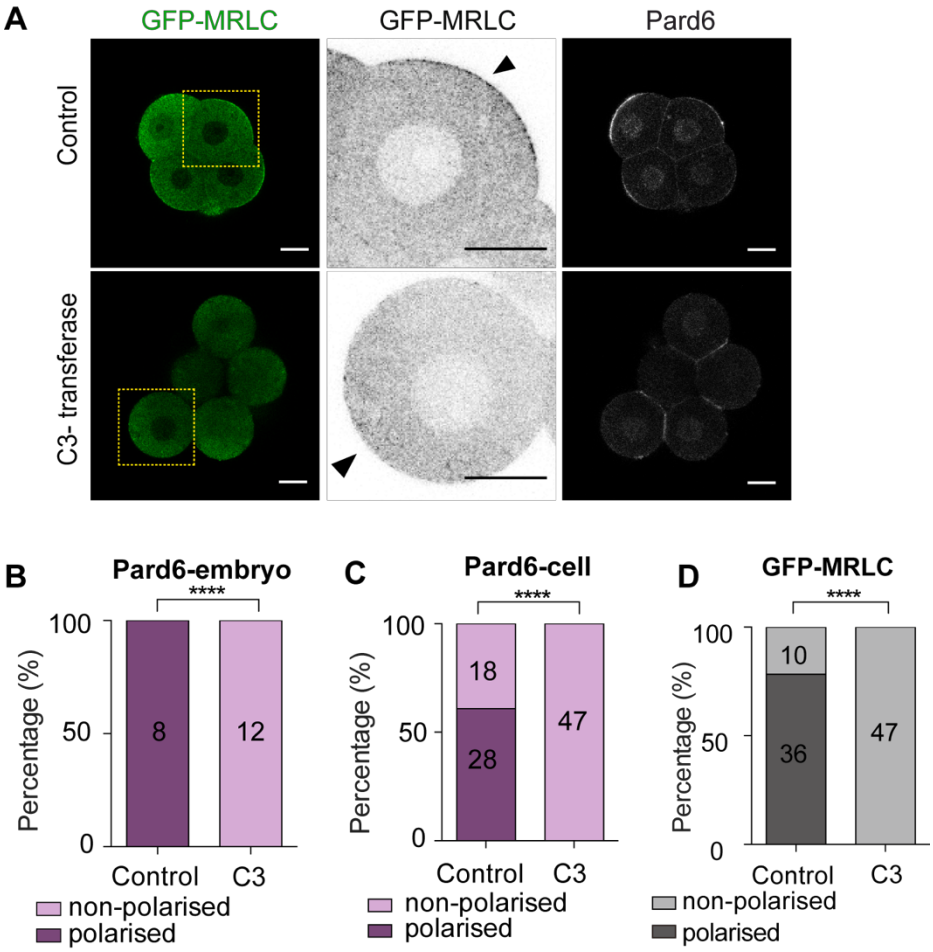

Figure 3.18 RhoA inhibition abolished actomyosin and Par complex apical polarisation. (A) Embryos expressing GFP-MRLC treated with Water (control) or C3-transferase were fixed at the late 8-cell stage and stained for GFP and Pard6. Squares indicate the magnified region. The arrows indicate the cell contact-free surface. (B) Quantifications of the percentage of embryos that showed polarised Pard6. ****p<0.0001, Fisher's exact test. 2 independent experiments). (C) Quantifications of the percentage of cells that showed polarised Pard6. ****p<0.0001, Fisher's exact test. (D) Quantifications of the percentage of cells that showed polarised GFP-MRLC. ****p<0.0001, Fisher's exact test. All scale bars, 15µm.

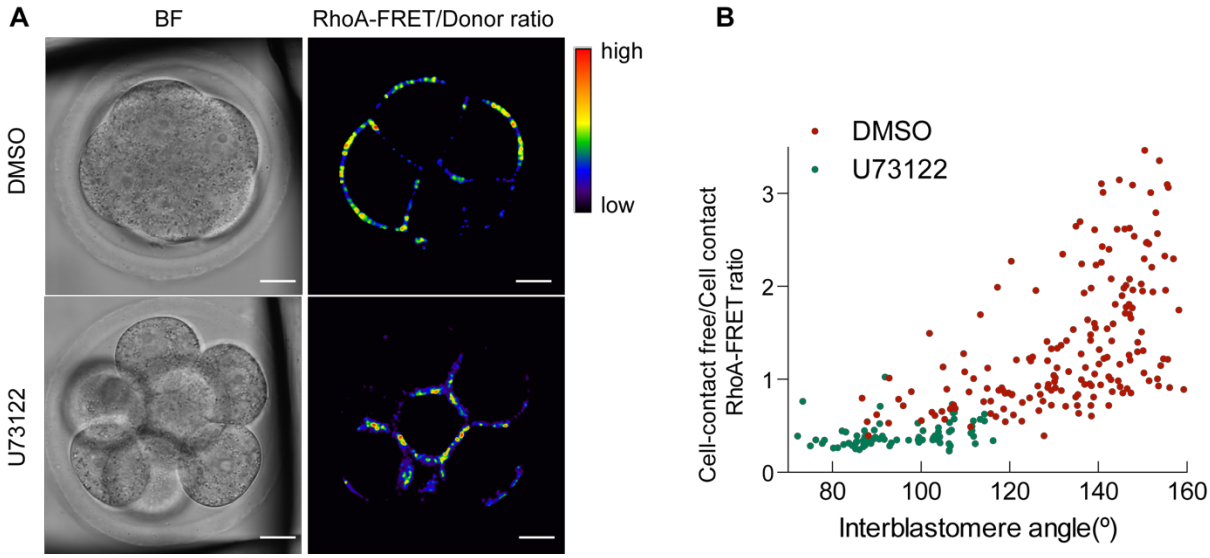

Figure 3.20 Activated RhoA failed to polarise to the cell contact-free surface upon the inactivation of PLC-PKC pathway. (A) Embryos expressing Raichu-RhoA-CR were imaged at the late 8-cell stage. (B) Quantifications of RhoA-FRET ratio between cell contact-free and cellcontact cortex in relation to interblastomere angle with cells treated with DMSO or U73122. Each dot represents one analysed cell. (N=14-16 embryos, 4 independent experiments). All scale bars, 15µm.

3.6.3 RhoA re-activation rescues actomyosin apical recruitment and polarity defects driven by PLC-PKC inhibition

To functionally test whether RhoA acts downstream of PLC-PKC to trigger actomyosin cortical accumulation and thus apical domain formation, the PLC-DN was overexpressed at the 2-cell stage to inhibit PLC activity, and a constitutively active form of RhoA (RhoA-Q63L) was injected into 2 blastomeres of early 4-cell stage embryos. This RhoA mutant lost the ability to convert GTP to GDP and therefore kept the RhoA constitutively active (Longenecker et al., 2003). In all groups, GFP-MRLC was co-injected to visualise MRLC localisation. The embryos were fixed at the late 8-cell stage and stained for GFP (for GFP-MRLC) and Pard6. As expected, GFP-MRLC and Pard6 polarised to the cell contact-free surface in the control embryos (GFP-MRLC and Ruby overexpression) (Figure 3.21A). Upon U-73122, GFP-MRLC lost the apical localisation and Pard6b failed to polarise to the cell contact-free surface (Figure

3.21B-D). However, with RhoA-Q63L overexpression, GFP-MRLC re-accumulated to the cell contact-free surface, and Pard6b was also effectively re-polarised to the cell contact-free surface (Figure 3.21B-D), suggesting that the activated RhoA rescued PLC-DN, and caused GFP-MRLC and Pard6b polarisation defects.

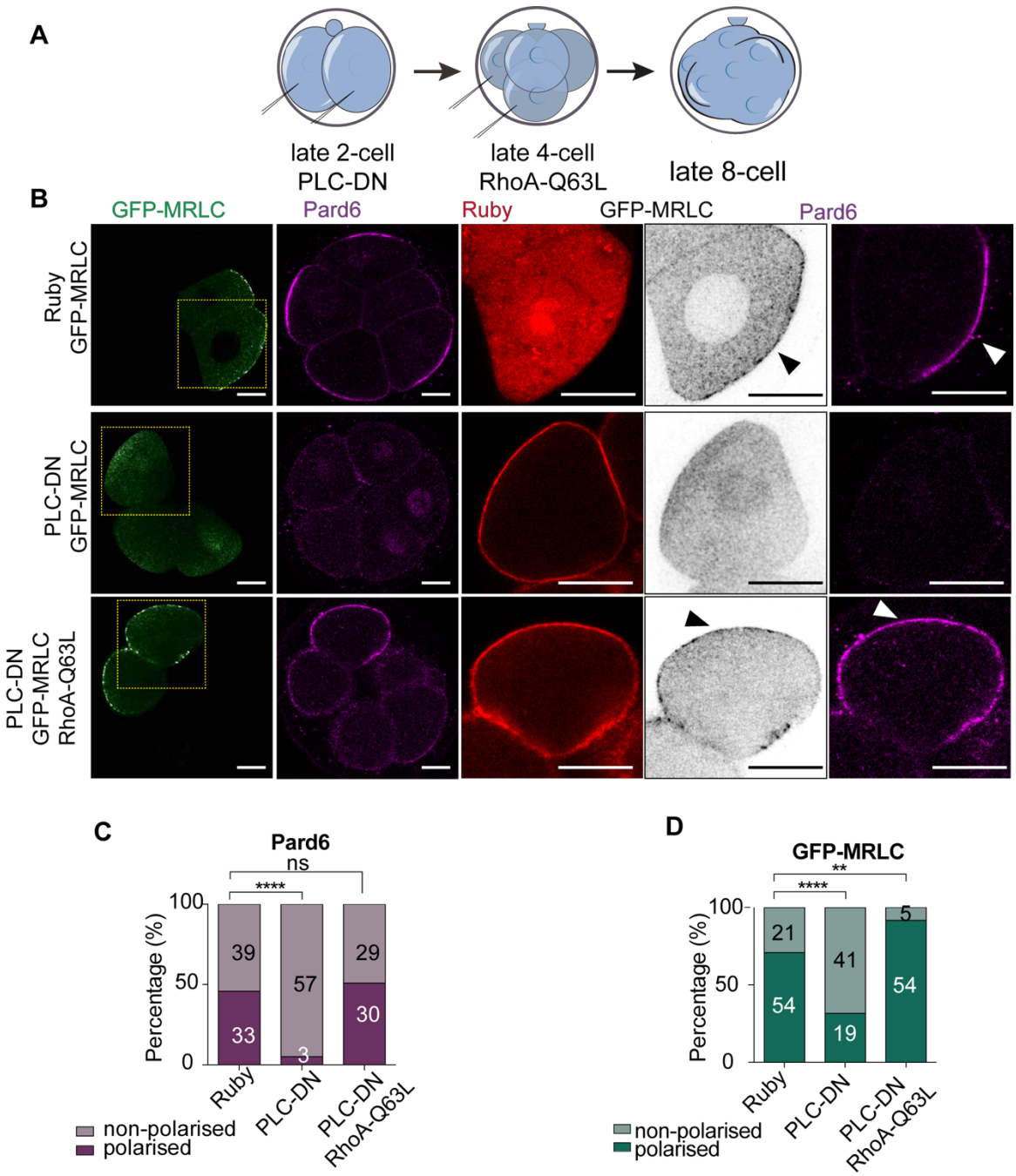

Figure 3.19 RhoA activity rescues the actomyosin and Par complex polarisation defects upon PLC-PKC pathway inhibition. (A) Scheme of rescue strategy. Ruby (control) or PLC-

DN mRNA were injected at the 2-cell stage into both blastomeres. At the early 4-cell stage 2o out of 4 blastomeres were injected with GFP-MRLC only or with RhoA-Q63L. (B) Embryos overexpressing different combinations of Ruby, PLC-DN, GFP-MRLC or RhoA-Q63L were fixed at the late 8-cell stage and stained for GFP and Pard6. Squares indicate the magnified region. Arrows indicate the apical domain. (C) Quantifications of the percentage of cells that showed polarised Pard6 localisation pattern with Ruby, PLC-DN or PLC-DN or RhoA-Q63L overexpression. ns, not significant; ****p<0.0001; Fisher's exact test. (D) Quantification of cells showed polarised GFP-MRLC. **p<0.01; p<0.0001; Fisher's exact test. N = 17 embryos for Ruby, N = 17 embryos for PLC-DN, N = 18 embryos for PLC-DN + RhoA-Q63L, 2 independent experiments. All scale bars, 15μm.

The ability of activated RhoA to rescue PLC-PKC phenotype was also tested using U-73122. U-73122 was applied at the early 4-cell stage, and RhoA-Q63L was injected into 2 cells of the 4-cell stage embryo, and cultured in medium containing U-73122 afterwards (Figure 3.22A). Similar to PLC-DN experiments, RhoA-Q63L overexpression effectively rescued the polarisation of GFP-MRLC and Pard6b (Figure 3.22B-D).

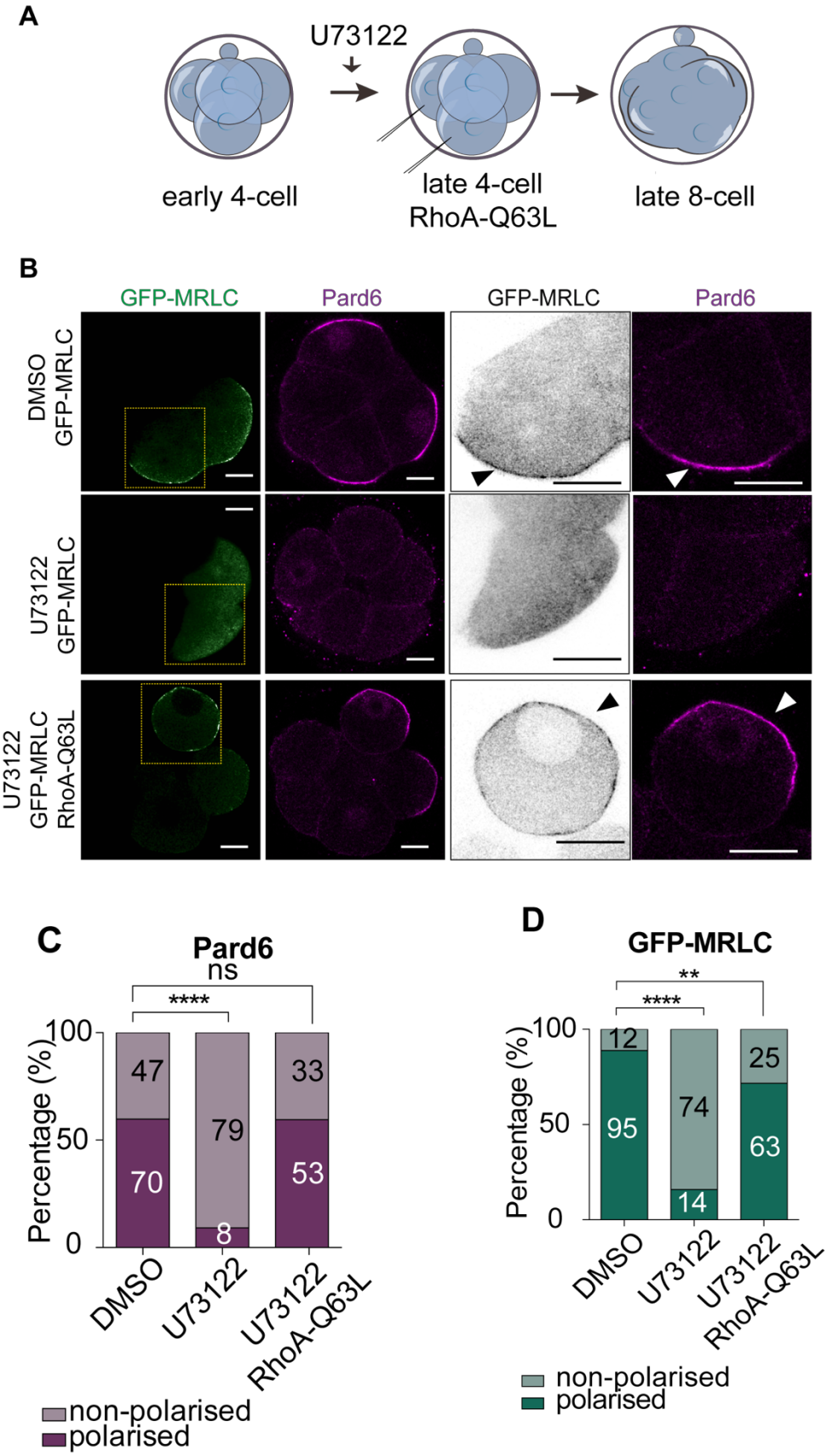
A
U73122
early 4-cell
late 4-cell
RhoA-Q63L
late 8-cell
B
GFP-MRLC
Pard6
GFP-MRLC
Pard6
DMSO GFP-MRLC
U73122 GFP-MRLC
U73122 GFP-MRLC RhoA-Q63L
C
Pard6
ns
****
Percentage (%)
100
50
0
47
70
79
8
33
53
DMSO
U73122
U73122 RhoA-Q63L
non-polarised
polarised
D
GFP-MRLC
**
****
Percentage (%)
100
50
0
12
95
74
14
25
63
DMSO
U73122
U73122 RhoA-Q63L
non-polarised
polarised

Figure 3.22 RhoA activity rescues the actomyosin and Par complex polarisation defects upon PLC-PKC pathway inhibition. (A) Scheme of rescue strategy. DMSO (control) or U73122 were applied from the early 4-cell stage, mRNA encoding GFP-MRLC or with RhoA-Q63L was injected into 2 out of 4 blastomeres at the 4-cell stage. (B) DMSO or U73122 treated embryos expressing GFP-MRLC with or without RhoA-Q63L were fixed at the late 8-cell stage and stained for GFP and Pard6. Squares indicate the magnified region. Arrows indicate the apical domain. (C) Quantifications of the percentage of cells that showed polarised Pard6 localisation pattern with DMSO, U73122 or U73122 with RhoA-Q63L overexpression. ns, not significant; ****p<0.0001; Fisher's exact test. (D) Quantification of cells showed polarised GFP-MRLC. **p<0.01; ****p<0.0001; Fisher's exact test. N = 21 embryos for DMSO, N = 17 embryos for U73122, N = 27 embryos for U73122 + RhoA-Q63L.All scale bars, 15µm.

Together, these results suggest that PLC-PKC activity triggers apical actomyosin accumulation and apical domain establishment through a Rho protein mediated pathway (Figure 3.23).

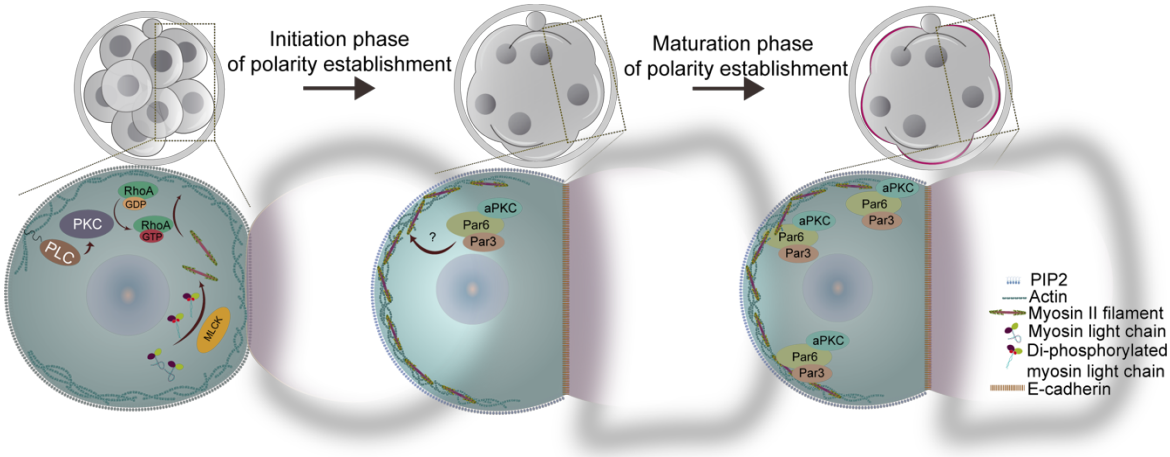

Figure 3.20 Summarised model of molecular pathways leading to cell polarity establishment. The establishment of cell polarisation can be divided into two phases. In the first phase (initiation phase), PLC regulated PKC activity triggers RhoA activation, together with MLCK activity which drives actomyosin complex membrane recruitment. The actomyosin is excluded from cell contacts and polarises at the cell contact-free surface; in the second phase (maturation phase), apical proteins are recruited to the actomyosin enriched cell contact-free surface to form an apical domain.

3.7 Discussion

3.7.1 The two phases of the apical domain formation process

The establishment of cell polarity has been a topic of study in the mouse embryo for decades, due to the unique significance of polarisation in developmental progression. More importantly, the polarity establishment process in the mouse embryo is de novo, and it is followed by the entire epithelialisation process, therefore it is also a valuable in vivo model to study this epithelisation process. The results in this chapter describe the division of the cell polarity establishment process into two distinct stages: in the first stage, actomyosin polarises to the cell contact-free surface, and concomitantly all cells in the embryo compact; in the second phase apical proteins are recruited to the cell contact-free surface where they meet the actomyosin cortex, and further reorganise the actomyosin into a ring structure by locally excluding it. To support this conclusion, we examined a handful of apical domain proteins using either immunostaining (for Pard6, aPKC and Crb3) or the overexpression of fluorescence tagged constructs (for Ezrin-RFP). Despite that nearly all apical proteins we examined showed the same localisation pattern, the sensitivity of the antibodies against specific epitopes would need to be taken into consideration. It is possible that the apical proteins already shoed polarisation yet the low sensitivity of antibody to detect protein concentration would block the detection of such polarisation localisation pattern. Nevertheless, the consistency between different apical proteins would still support the conclusion. This crude division of the cell polarity establishment process during the 8-cell stage of development also highlights the temporal segregation of the compaction and polarisation processes. It has long been thought that these two processes occur within an identical time-window, and a causal relationship between these two events has been conceived. Yet these results highlight that compaction occurs overall slightly earlier than cell polarity establishment. Such a timing discrepancy is not surprising, yet it is also uncommon in mammalian embryos, as the high synchronicity of compaction and polarisation, that is the compaction and polarisation of all cells within a short time-window or developmental stage, seems specific to the mouse. Studies in other mammalian species have revealed a great amount of heterogeneity in the timing of cell compaction and polarisation, and further a greater distinction in the timing between these two events. For example, in porcine embryos compaction takes place at around the 16-32 cell stage, yet cell polarisation establishment is only completed at the blastocyst stage (Reima et al., 1993). In rabbit embryos, compaction occurs between the 32-64 cell stage and polarisation happens at

around the 63 cell stage (Koyama et al., 1994). These timing differences suggest the possibility that these two processes are in fact independent of each other. The results shown in this chapter provide a clear demonstration of this, as when actomyosin contractility was blocked by blebbistatin treatment cell compaction was abolished, yet all cells displayed a normal apical domain and polarised. There are also several examples in which the converse is true: when ROCK activity is inhibited through pharmacological treatments, the localisation of apical domain proteins such as the Par complex was disrupted yet embryos were able to compact without any defects. Overall, these results suggest that compaction and polarisation are independent processes.

3.7.2 The convergence and divergence of compaction and cell polarisation processes during the 8-cell stage development

So what are the common and specific requirements for compaction and polarisation that lead to their independence, and why is actomyosin polarisation specifically associated with compaction? Studies suggest that compaction requires a tension difference between the inter-facial and apical cortex. The generation of membrane tension in turn requires the actomyosin network (Maitre et al., 2015). Therefore, it is not surprising to see that the first phase of cell polarity establishment, actomyosin polarisation, is accompanied by compaction processes. However, for compaction a fully functional actomyosin network is required, that requires not only the actomyosin meshwork to be constructed, but also myosin contractility for the generation of membrane tension. On the other hand, blebbistatin and ML-7 treatments experiment are complementary to each other and suggest that polarisation does not exclusively require membrane tension, but it does require an intact actomyosin cortex. Thus it seems that the actomyosin cortex functions as a scaffold for apical domain protein recruitment. How the actomyosin network helps apical domain protein recruitment is not clear from the results presented here. Yet studies in other biological systems or those using in vitro artificial biological systems could give some indications. Actomyosin drives apical domain protein recruitment and concentration in 8-cell stage blastomeres in a similar manner to that of the T-cell receptor activation process. In this system, receptors bind to antigens and cluster at the cell cortex, locally exclude actomyosin to the periphery. Effective cluster formation requires a dynamics actomyosin network that is maintained by the interaction of myosin with the actin cortex mediated by Arp2/3 and Cofilin/ADF factors (Huang and Burkhardt, 2007). All three factors work together to build a cortex that is mobile enough for inducing, stabilising and transporting receptor clusters. Although the contribution of Arp2/3 and Cofilin/ADF to mouse

embryo polarity is unknown, it is likely that a myosin-actin interaction is required for building a suitable actin network conformation and therefore facilitating Par complex membrane mobility. Indirectly in support of this, the inhibition of Myosin II filament formation dramatically changed the actin meshwork organisation (Figure 3.6A). Secondly the FRAP experiments suggested that the stability of Pard6 was steadily increasing from 4-cell to the late 8-cell stage. The precise details of how myosin remodels the actin network, and how the specific configuration of the actin network aids in the transport of the apical domain proteins will need to be further explored. To address these questions, simulations of the manner in which Pard6 cargos would fit into the actomyosin network, and a detailed analysis of the effect of each component on the stability and mobility of the Pard6 complex through the application of pharmacological treatments targeting myosin, Arp2/3 and Cofilin/ADF may be informative.

3.7.3 The mechanism of PKC/RhoA in the activation of the actomyosin complex

The various pharmacological treatments targeting PLC, PKC and RhoA individually, together with the rescue experiments using the PKC activator or the overexpression of constitutively activated RhoA, revealed that the PLC-PKC-RhoA linear molecular pathway is critical for apical domain assembly through the regulation of the apical recruitment of the actomyosin network.

The downstream pathways of PLC-PKC-RhoA activation of actomyosin remain unexplored. PKC is well-known for its function in contractility in muscle tissues, where it increases the levels of phosphorylated myosin light chain through the inhibition of myosin light chain phosphatase (Etter et al., 2001). The results described in this body of work demonstrate that PKC regulates actomyosin via a different mechanism. Through the use of a phosphomimetic mutant of myosin light chain, MRLC-DD, it was demonstrated that although MRLC-DD seems to be able to bypass the requirement of the MLCK mediated MRLC phosphorylation step, it still fails to localise to the cell contact free surface upon PLC-PKC inhibition. Therefore, PLC-PKC regulates myosin phosphorylation through a phosphorylation independent process.

RhoA has long been known as important for polarity establishment in the mouse embryo, although the mechanism behind the regulation of polarisation by RhoA remained unknown (Clayton et al., 1999). Yet studies in many other systems have always pointed to RhoA's role in the regulation of the actomyosin network (Arnold et al., 2017; Levayer and Lecuit, 2012; Ramkumar and Baum, 2016). RhoA has been implicated in playing a role in enhancing

actomyosin activity via two different pathways. Firstly, RhoA can enhance MRLC phosphorylation by inhibiting myosin phosphatase through its downstream kinase ROCK, in a similar manner to the reported mechanism of PKC in elevating MRLC phosphorylation. Secondly, RhoA activates several downstream actin re-modellers, such as mDia1 and Arp2/3, and thus promotes actin branching and polymerisation. It is possible that RhoA enhances the actin-myosin interaction by organising the actin cortex instead of directly phosphorylating MRLC. The elevated concentration of myosin II filaments in the actin cortex could further induce the changes in actin mesh configurations. A similar phenomenon has been observed in the cortical environment during cytokinesis (Chugh et al., 2017).

A FRET based RhoA sensor, Raichu-RhoA-CR, was used to monitor RhoA activity in an attempt to determine its role in actomyosin activation and further dissect the timing of cell polarity establishment. From the analysis of normalised FRET ratio, it appeared that RhoA activity was homogeneous around the cell membrane prior to the early 8-cell stage, and gradually shifted to the cell contact-free surface during compaction. It then further reorganised into a ring like structure, reminiscent of the reorganisation of the actomyosin complex at the 8-cell stage of development (Figure 3.19). Together with the result that the C3-transferase treatment abolished MRLC apical recruitment, this data suggests that the change in the activated RhoA spatial localisation may guide actomyosin re-organisation over the 8-cell stage developmental progression. The application of a PLC inhibitor inhibited the reorganisation of activated RhoA. Therefore the PLC-PKC pathway influences the activated RhoA spatial organisation which could mechanistically explain how the PLC-PKC pathway affects actomyosin polarisation. However, an important question remains of whether PKC activity is responsible for elevating RhoA basal activity or whether itis merely responsible for RhoA spatial distribution. Three potential mechanisms may apply in this case : 1) PKC may activate RhoA through the phosphorylation of RhoA activators such as RhoGEFs, as similar mechanisms have been demonstrated in other model systems (Peng et al., 2011). Moreover, in support of this idea, the analysis of phosphor-peptides at the cleavage stages of mouse embryo development from recent proteomic study suggest that Arhgap1, a RhoA activity regulator is a possible downstream target of PKCα or PKCβ (Gao et al., 2017). 2) PKC could phosphorylate AJ proteins and inhibit RhoA at cell-cell contacts, the boundaries of which have been shown in other developmental model systems to be inhibitors of actomyosin activity (Klompstra et al., 2015). 3) It has been reported that RhoA activation requires oligomerisation mediated by its C-terminal. Therefore it is also possible that PKC lipid homeostasis aids RhoA oligomerisation.

Optogenetic experiments suggest that PLC-PKC activation of the actomyosin cortex is direct, therefore making the second possibility unlikely. This also conflicts with the early hypothesis whereby PKC phosphorylates AJ and thereby activates some of their functions to trigger cell compaction (Winkel et al., 1990). One cannot completely rule out the possibility that PKC activation affects AJ stabilisation, yet its role in cell polarisation establishment, or cell contact-free surface actomyosin activation is more likely to be direct rather than mediated through cell contact-free surfaces. A recent report has also suggested that the apical domain assembly is independent of the E-cadherin mediated AJ complex (Korotkevich et al., 2017), strengthening such a hypothesis. The further determination of the possible mechanisms of PKC activation of RhoA would require the identification of the downstream effectors of PKC at the cleavage stages. This would require the determination of the mechanism of the corresponding targets in the regulation of RhoA activation and therefore actomyosin polarisation.

3.7.4 The timing of cell polarity establishment part I: how do PKC and RhoA get activated?

The timing of cell polarity establishment in the mouse embryo is a fascinating question in developmental biology. Intriguingly, the immunostaining of the ppMRLC expression profile over different developmental stages suggests that actomyosin activation happens around the early 8-cell stage and thus is closely associated with the timing of cell polarity establishment. The results described in this chapter identified the PKC-RhoA axis as the upstream activator of the actomyosin network. Therefore a further question is whether they are activated specifically at the 8-cell stage and thus constitute part, if not the whole of the timing mechanism for cell polarity establishment. Monitoring the change of PKC activity by traditional biochemistry assay is extremely difficult in the mouse embryo due to the scarcity of available materials. Some PKC sensors, which utilised DAG or the calcium binding domain of some of the PKC isoforms, conjugated with fluorescence proteins have been developed and have been used in other cell systems to monitor PKC activation dynamics. However, the application of such sensors in the mouse embryos fail to produce any reliable signals (data not shown). It is possible that the basal PKC activity in the mouse embryo is low and sensitive, as the application of DAG at a low concentration is sufficient to activate compaction in a rapid time-window, and leads to a great upregulation of ppMRLC (Figure 3.15A). Some studies report that subtle changes of basal activity of PKC can have a significant effect on cell homeostasis (Kirton and Loutzenhiser, 1998; Weiner et al., 1997). It is therefore likely that while PKC activation in the

mouse embryo may not be as dramatic as in other developmental processes such as fertilisation (Gonzalez-Garcia et al., 2013), a subtle activation is nevertheless sufficient to effect actomyosin spatial organisation. Taking these possibilities into consideration, a more sensitive assay, such as real-time qPCR, could be applied to precisely determine the change of PKC activity during different stages of mouse embryo development. The identification of transcriptional targets downstream of PKC activation may partially help to address this question in the future.

3.7.5 Timing of cell polarity establishment part II: what is the missing factor required for apical domain assembly?

Given that the PLC-PKC-RhoA-actomyosin axis is required for triggering cell polarity establishment, it is obvious that actomyosin activation and polarisation per se are insufficient to trigger the assembly of an intact apical domain, as the matured apical polarity marker Pard6 failed to respond to actomyosin polarisation and was not recruited to the cell contact-free surface, after actomyosin cortical activation at the 4-cell stage (Figure 3.15; Figure 3.16). Combined with the fact that the ectopic enhancement of actomyosin activity at the 8-cell stage allowed the region of apical domain proteins to expand, it seems likely that unknown factors besides actomyosin are specifically responsible for apical protein recruitment, but these only appear at the 8-cell stage. These factors may help to connect the actomyosin cortex to the apical domain proteins, perhaps by directly binding to apical domain proteins such as the Par complex or ERM family members. Potential candidates include the tight junction protein JAM-1 and Cdc42. It has been reported that JAM-1 expression is upregulated from the 4-8 cell stage (Thomas et al., 2004), and a direct interaction between JAM-1 and the Par complex has been reported in epithelial tissues (Ebnet et al., 2004). Although the injection of a JAM-1 antibody failed to block cell polarisation (Thomas et al., 1991), it is possible that other members, such as JAM-2,3,4, the transcripts of all of which can be detected prior to the 8-cell stage (sequencing data from the Zernicka-Goetz lab, unpublished results), function similarly to JAM-1. A RNAi based knockdown strategy to eliminate all family members may be necessary to dissect the potential correlation of JAM proteins with the apical domain assembly. Data from studies in epithelial cells, as well as other developmental model systems suggest that Pard6 membrane localisation can be regulated by other membrane localised Rho GTPases such as Cdc42 through the direct binding of Cdc42 to the membrane. It has been recently reported that the maternal-zygotic depletion of Cdc42 abolished cell polarisation and led to the reduction of

Pard6 apical localisation (Korotkevich et al., 2017), further strengthened this hypothesis. Given that Cdc42 depletion disrupts cell polarity establishment at the morula stage, it will be important to determine whether the inhibition of Cdc42 can abolish cell polarity from the early 8-cell stage onward. And if this were to be the case how does Cdc42 act together with the PLC-PKC-RhoA pathway to build the apical domain.

3.7.6 The similarities and differences in polarity establishment between the mouse embryo and other developmental systems

The process of establishing cell polarity at the 8-cell stage in the mouse embryo shares many common features with epithelial cell tissues or single cell systems, but is also unique in many ways. Studies of cell polarity establishment in numerous systems reveal the importance of cytoskeletal networks, including the actomyosin cortex, the microtubule network, the intermediate filament cytoplasmic network and septin based cytoskeletal systems in establishing cell polarity. Actomyosin or microtubule mediated symmetry breaking processes are the most well studied examples. In the 8-cell stage mouse embryo, although it is clear that the actomyosin cortex is vital for the establishment as well as the maintenance of cell polarity, the inhibition of microtubules failed to interfere with the cell polarity establishment process, regardless of the duration of treatment, concentration, or the drugs used (Fleming et al., 1986; Pratt et al., 1982) (unpublished observations). Therefore the polarity establishment process in the mouse embryo seems to be exclusively regulated by actomyosin. This could partially due to the fact the mouse embryo at the earlier stage lacks a classical microtubule organisation centre such as a centrosome (Howe and FitzHarris, 2013), and is therefore unable to generate polarised transport of the cargos containing polarity proteins to generate the cortical polarity as it would in other cases (Siegrist and Doe, 2007). Actomyosin breaking cortical symmetry is most well demonstrated in the c.elegans zygote. In this case, the actomyosin flow carries anterior Par proteins to the anterior region of the zygote, and through the mutually exclusive relationship between anterior and posterior Par proteins the two polarity domains are established. The fact that actomyosin polarisation failed to trigger Par complex polarisation makes it unlikely that a similar mechanism is used by the mouse embryo specifically at the 8-cell stage. Nevertheless, it seems that the process of actomyosin flow driven apical domain formation is indeed conserved in the mouse embryo but is responsible for apical domain formation at other stages. It has recently been reported that during the 8-16 cell stage divisions, the apical domain is first disassembled/expanded and is subsequently re-established by the actomyosin flow which originates from the cleavage furrow (Zenker et al., 2018). Although a

similar process was not observed at the 8-cell stage, this highlights the diverse pathways that are used by the mouse embryo to shape a specialised cortical domain. As has been mentioned before, the precise mechanism of actomyosin establishment of the 8-cell stage apical domain (de novo cell polarity establishment) requires further and detailed characterisation of actin dynamics during the 8-cell stage of development.

In many matured epithelial cells, the extra-cellular matrix (ECM), which is composed of integrin, fibronectin and collagen provides extracellular polarity cues to direct the orientation and formation of cell polarity. Yet it seems unlikely that a similar mechanism is used for 8-cell stage polarity establishment. Firstly, at the 8-cell stage the ECM components are not fully synthesized and therefore no matured ECM can be formed at such an early stage. Secondly, embedding of the 8-cell stage mouse embryo into ECM coated gels failed to affect the radial polarity pattern. Therefore, overall the mouse embryo is another example of de novo cell polarity taking place independently of the guidance of the ECM. Although cell adhesion has been demonstrated to be the second most common signal that directs cell polarity establishment, it also seems dispensable for cell polarity establishment in the mouse embryo, but instead merely aids in the acceleration of the process. When un-compacted 8-cell stage blastomeres were isolated, in the absence of any cell-cell adhesions, the apical domain could still be established at the late 8-cell stage prior to cytokinesis in over half of the cases. And more importantly the location of the apical domains appear random with reference to the mid-body (cytokinesis bridge), suggesting that the cells do not have a memory of their position in the embryo, ruling out the possibility that cell adhesion may still play a role in establishing cell polarity (unpublished observations) (Korotkevich et al., 2017). Studies in an artificial in vitro actin system suggest that in response to the appropriate concentration of actin monomers and its regulators (such as myosin, Arp2/3), the actin cortex can self-organise into a specialised domain, similar to the apical domain in the mouse embryo (Abu Shah and Keren, 2014; Carvalho et al., 2013). A similar principle may apply in the mouse embryo which could explain how the apical domain can be formed in the absence of any external cues.

Studies in epithelial cells revealed that the different polarity domains are maintained by distinct and functional polarity complexes, which include: the Crumbs complex and Par complex for the apical domain; the Lgl complex and Scribble complex for the basal/basolateral domain (Laprise and Tepass, 2011; St Johnston, 2018). All complexes have been demonstrated to localise in a similar manner in the mouse embryo, and a similar mutually exclusive relationship

exists between different complexes (Hirate et al., 2013; Kono et al., 2014; Stephenson et al., 2010), suggesting the functional conservation of the core polarity complexes in regulating cell polarity in different developmental model systems.

Overall, the results described in this chapter characterised the processes of establishment of cell polarity in the mouse embryo, and revealed the signalling molecules that mediate this process.

4 Results II: investigation of the timing regulation of cell polarity establishment

4.1 Introduction

Unlike other model systems, the early embryonic cells of the mammalian embryo do not polarise until the zygotic developmental stage. In the mouse embryo this happens at the 8-cell stage, i.e. 2.5 days' post-fertilisation. This raises the intriguing question of what regulates the timing of cell polarity establishment, allowing its construction at a defined developmental time-window. The answer to this question would also shed light on mammalian evolution, as the timing of cell polarisation displays species specificity.

In this Chapter, the original "inhibitor timing hypothesis" has been re-visited. A new hypothesis named "zygotic activator driven hour glass model" has been proposed and the key factors regulating the transcriptional programme triggering cell polarisation have been revealed. The necessity and sufficiency of such factors has been explored through the use of RNAi, gene-editing and overexpression assays. The remaining questions related to these results have also been discussed.

4.2 Protein synthesis inhibitor treatment did not advance the timing of cell polarisation but caused developmental arrest

It has been postulated that the requirements for cell polarity that commits cells of the mouse cleavage stage embryo to their first fate decision are established well in advance, and so the destruction of polarity inhibitors remains as the major barrier for cell polarisation prior to the 8-cell stage. This "inhibitor hypothesis" stemmed from an earlier observation that premature polarisation can be induced within several hours when protein synthesis inhibitors are applied at the late 2- or early 4-cell stage (Levy et al., 1986). To re-examine the validation of this hypothesis, the protein synthesis inhibitor puromycin, used in the early study (Levy et al., 1986), and cycloheximide (Schneider-Poetsch et al., 2010) were added from the early 4-cell stage (0-1 hours post-2-cell stage division) onward and embryos were examined at the late 4-cell (8 hours post-treatment) and late 8-cell (7 hours post-4 cell stage division) stages. However, neither puromycin nor cycloheximide were able to induce precocious cell polarisation at the

late 4-cell stage as determined by the localisation of the apical domain protein Pard6 (Figure 4.1A,B). On the contrary, embryo development fully arrested upon puromycin or cycloheximide treatment as neither cytokinesis nor cell polarisation were observed at later stages (Figure 4.2A-C).

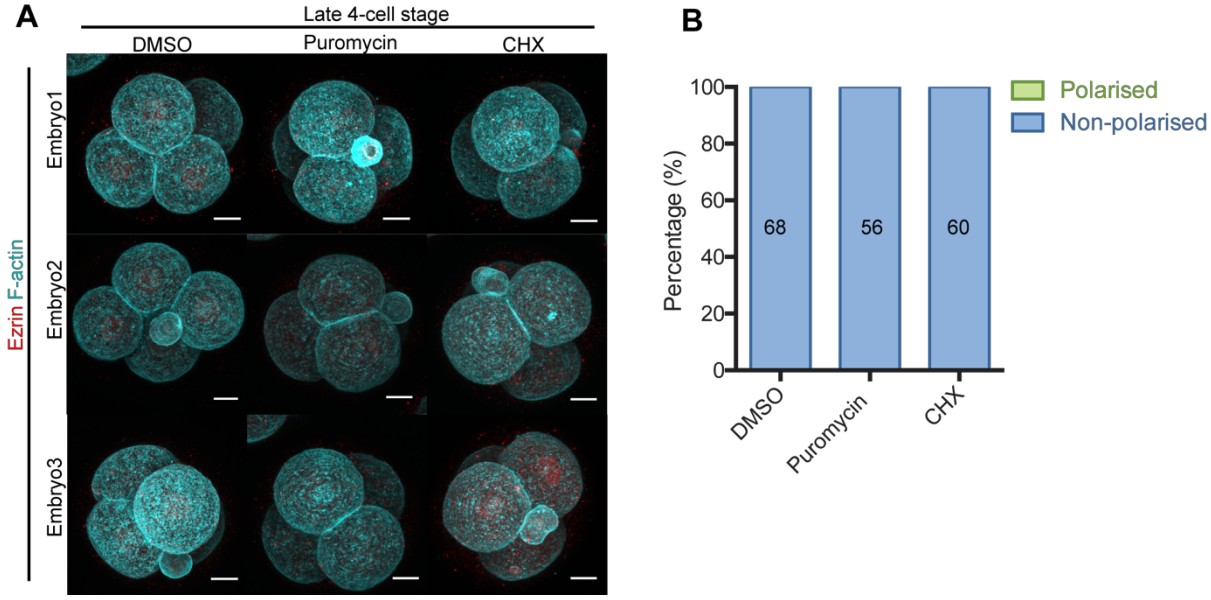

Figure 4.1 Protein synthesis inhibitors did not trigger premature cell polarisation at the late 4-cell stage. (A) Embryos treated with DMSO (as a control), Puromycin or Cycloheximide from the early 4-cell stage were fixed at the late 4-cell stage and stained for Pard6 and F-actin. (B) Quantifications of polarised cell numbers in embryos treated with DMSO, Puromycin or Cycloheximide. Data are shown as a contingency table, the numbers in each bar represent the number of cells analysed. N=17 embryos for DMSO, N=16 embryos for Puromycin, N=15 embryos for Cycloheximide treatments. N=2 independent experiments. Scale bars, 15µm.

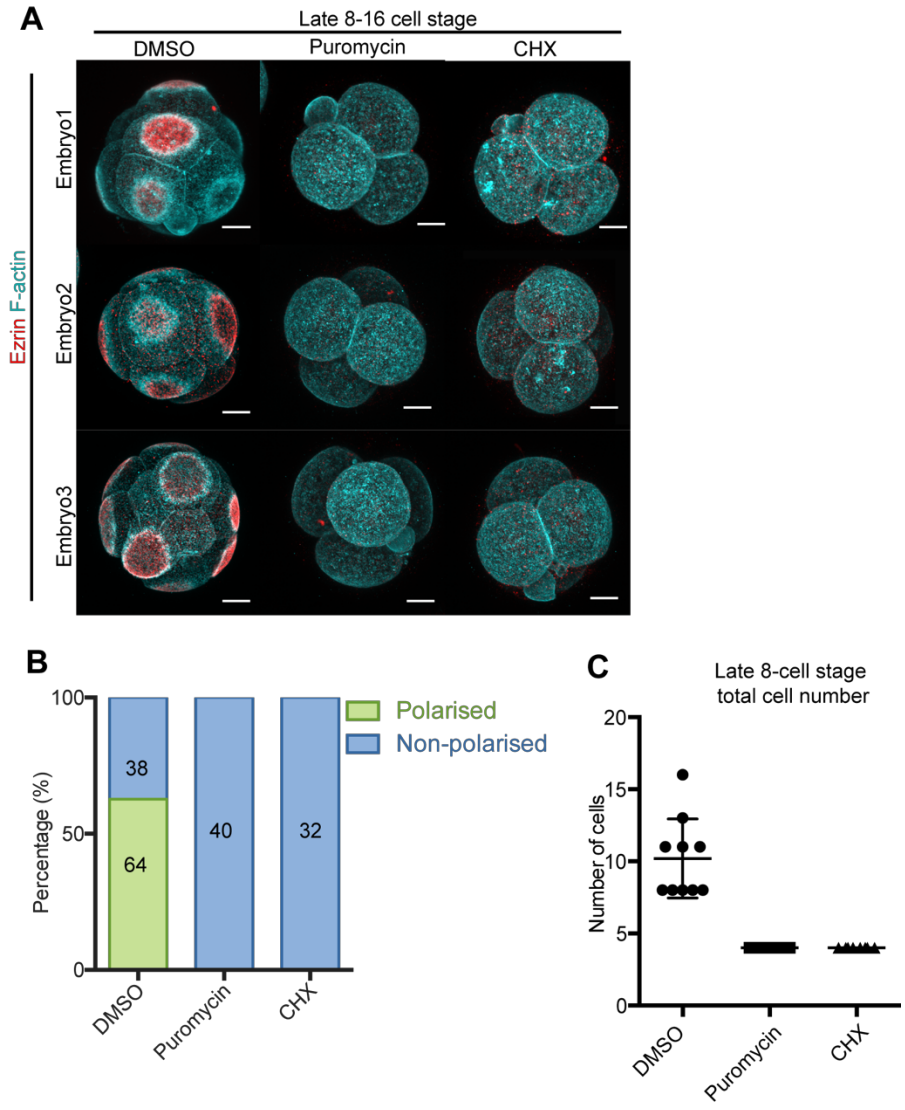

Figure 4.2 Protein synthesis inhibitors caused embryo developmental arrest and the failure of cell polarisation establishment. (A) Embryos with DMSO (as a control), Puromycin or Cycloheximide from the early 4-cell stage were fixed at the late 8-cell stage and stained for Pard6 and F-actin. (B) Quantifications of polarised cell numbers in embryos treated with DMSO, Puromycin or Cycloheximide. Data are shown as a contingency table, the numbers in each bar represent the number of cells analysed. N=2 independent experiments. (C) Quantifications of total cell number at the late 8-cell stage in embryos treated with DMSO, Puromycin or Cycloheximide. Scale bars, 15µm.

4.3 Examining the requirement of zygotic transcripts in triggering cell polarisation by blastomere resection

To fully understand how the timing of cell polarity is regulated, alternative hypotheses have been proposed. Comparisons with other mammalian species have revealed that the temporal correlation between the timing of cell polarity establishment and that of the "maternal-zygotic transition" (MZT), during which maternal proteins are rapidly degraded and the zygotic genome concomitantly is activated in order to generate new zygotic RNA transcripts (Zernicka-Goetz et al., 2009). In the mouse embryo this happens during the 2-cell stage, one day before cell polarity becomes established. Given this close temporal correlation, it is likely that either the maternal degradation releases inhibitory signals to trigger cell polarity, and/or that the zygotic transcripts activate cell polarisation by synthesising activators necessary for cell polarity establishment. If the zygotic activators exist, it is plausible that their action is concentration dependent and that the timing of cell polarity would thus be sensitive to the concentration of such factors (Figure 4.3A). Cell volume has been predicted to correlate with RNA concentration and specifically, smaller cell size would increase the RNA concentration (Padovan-Merhar et al., 2015). Therefore, as an initial attempt to establish whether a zygotic activator exists and if so its potential importance for cell polarity, the cytoplasmic volume of blastomeres from 2-cell stage or 4-cell stage were experimentally reduced by "blastomere resection", a method that does not affect cell fitness or developmental potential (Ciemerych et al., 2000; Zernicka-Goetz, 1998). For 2-cell stage resection, one of the two balstomeres were resected while for 4-cell stage resection, two blastomeres were randomly resected, and the resected or non-resected cells were paired together respectively (Figure 4.3B,E). Indeed, after resection the cells maintained their capacity to form blastocysts with all three lineages (Figure 4.3 C-D, F-G).

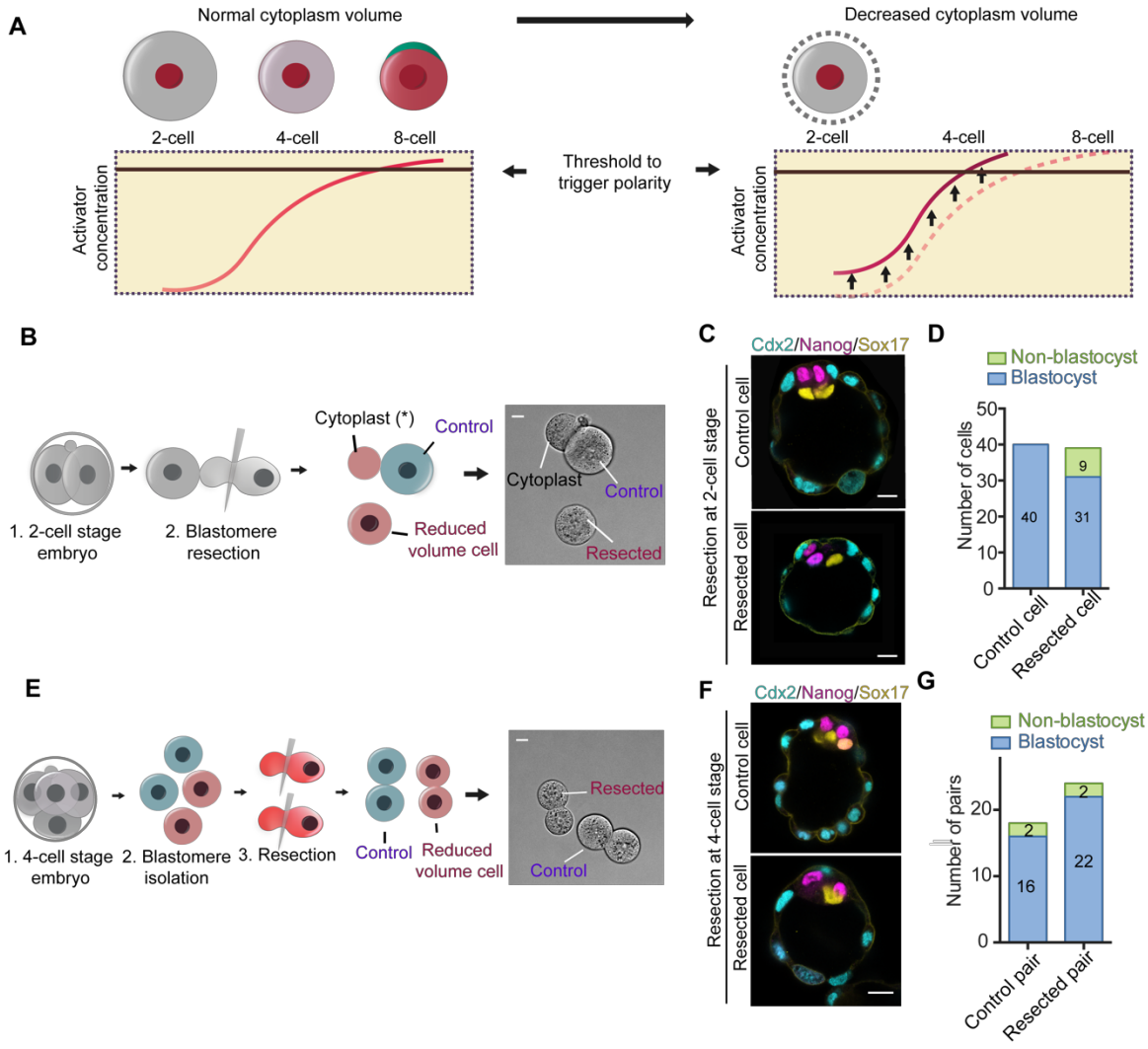

Figure 4.3 Zygotic activator driven hour-glass hypothesis and blastomere resection experiment illustration. (A) According to the zygotic activator driven hour-glass hypothesis, the zygotic transcripts positively regulate cell polarisation and their accumulation beyond a certain threshold triggers cell polarisation. This model also predicts that the elevation of zygotic transcript concentration advances the timing of cell polarisation. (B) Scheme of blastomere resection experiment at the 2-cell stage. One of the blastomeres is resected (30% cytoplasm is removed) resulting in the formation of a resected cell and a control cell attached to part of the cytoplasm of the resected cell. (C) The 2-cell stage resection procedure did not affect cell fitness as the resected cell and control cell were equally capable of forming mini-blastocysts with all three lineages. (D) Quantification of the blastocyst formation rate generated from control or resected cells. (E) Scheme of blastomere resection experiment at the 4-cell stage. The cells were separated and two of the four were resected, the cells were re-aggregated based on the size of their cytoplasm. This resulted in the formation of a resected pair and a control

pair. (F) The 4-cell stage resection procedure did not affect cell fitness as the resected cell and control cell were equally capable of forming mini-blastocyst with all three lineages. (G) Quantification of the blastocyst formation rate generated from control or resected pairs. Data are shown as a contingency table, numbers in each bar represent the number of halved embryos analysed. Scale bars, 15μm.

To track the timing of cell polarity establishment, Ezrin-RFP mRNA was injected into both blastomeres of 2-cell embryos and used as an apical polarity marker and then 2-cell or 4-cell stage embryos were subjected to resection and the dynamics of Ezrin-RFP were monitored by time-lapse imaging until the early blastocyst stage (Figure 4.4A-B; Figure 4.5A-B). This revealed that cell polarity took place faster in the resected cells for both 2-cell stage or 4-cell stage embryos, yet the advance of the timing of polarity was more evident when resection was performed at the 4-cell stage. Specifically, when the bisection was performed at the 2-cell stage, around 59.1% of the cells polarised earlier, compared to only 17.9% of cells with reduced volume which polarised at the same time as sister cells and 23.1% of cells with reduced volume which polarised later than sister cells ($n=39$, $p<0.0001$, hypothetical mean =0, one sample t-test. Figure 4.4A-C). When the resection was performed at the 4-cell stage, 94.5% of the resected cells polarised earlier than their control sister pair cells ($n=35$, $p<0.0001$, hypothetical mean =0, one sample t-test. Figure 4.5A-C).

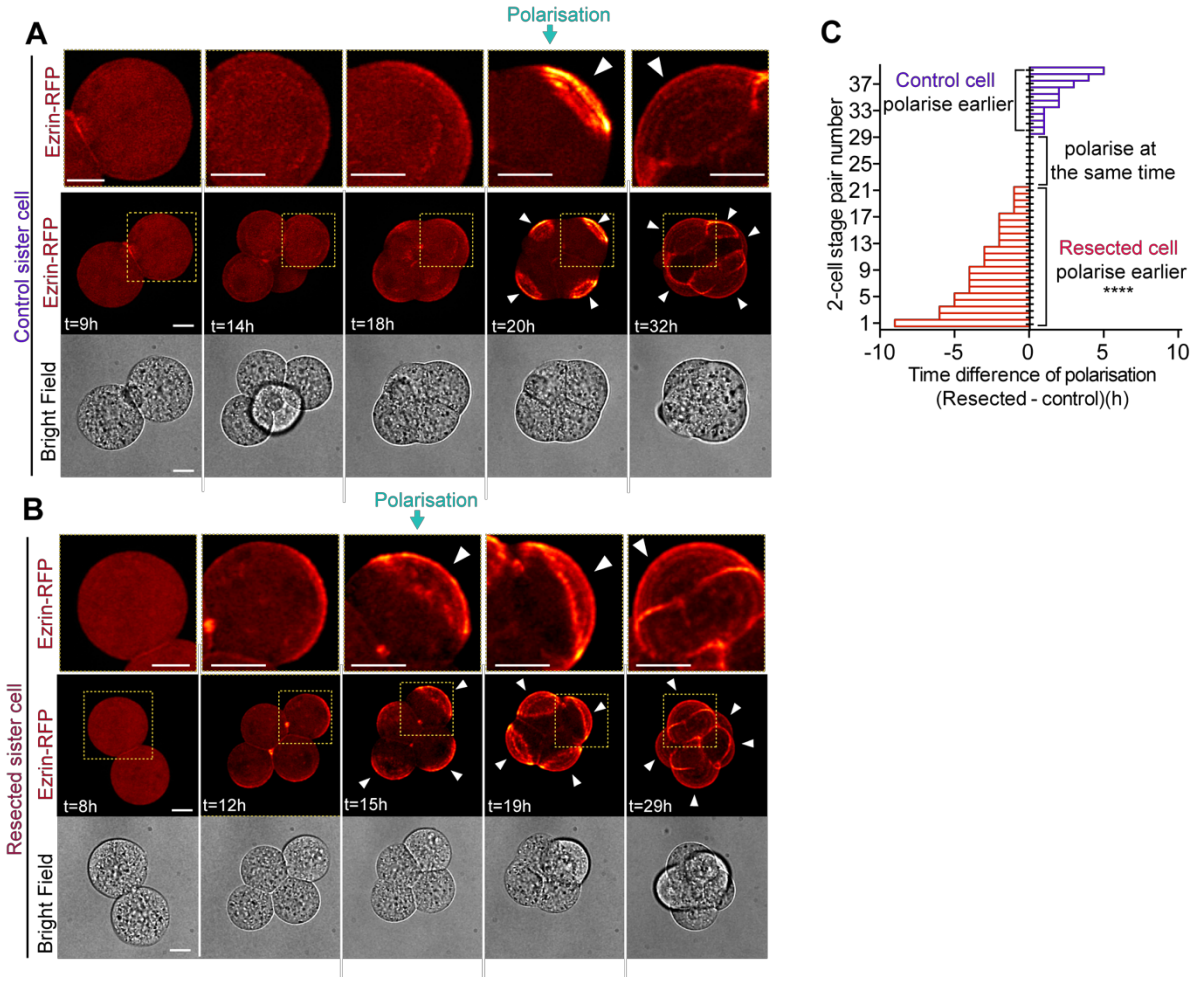

Figure 4.4 Resected cells from 2-cell stage embryo always polarised earlier than control sister cells. (A) Time-lapse imaging of the control sister cells from the 4-cell stage to the morula stage. (B) Time-lapse imaging of resected sister cells from the 4-cell stage to the morula stage. For all images, squares indicate the magnified regions, the arrows indicate the apical domains. (C) Bar chart showing all comparisons of the time difference in polarisation between resected and control sister cells from experiment illustrated in b, each bar represents one comparison. Note that cells with reduced volume polarised earlier in the majority of cases. The time of polarisation is defined as when the first cell becomes polarised in a structure in all experiments. Time difference (in hours, h) is calculated as (time when resected cells polarise – time of control cell polarisation). n=39 pairs analysed. ****$p<0.0001$, one-sample t-test, hypothetical mean =0. Scale bars, 15µm.

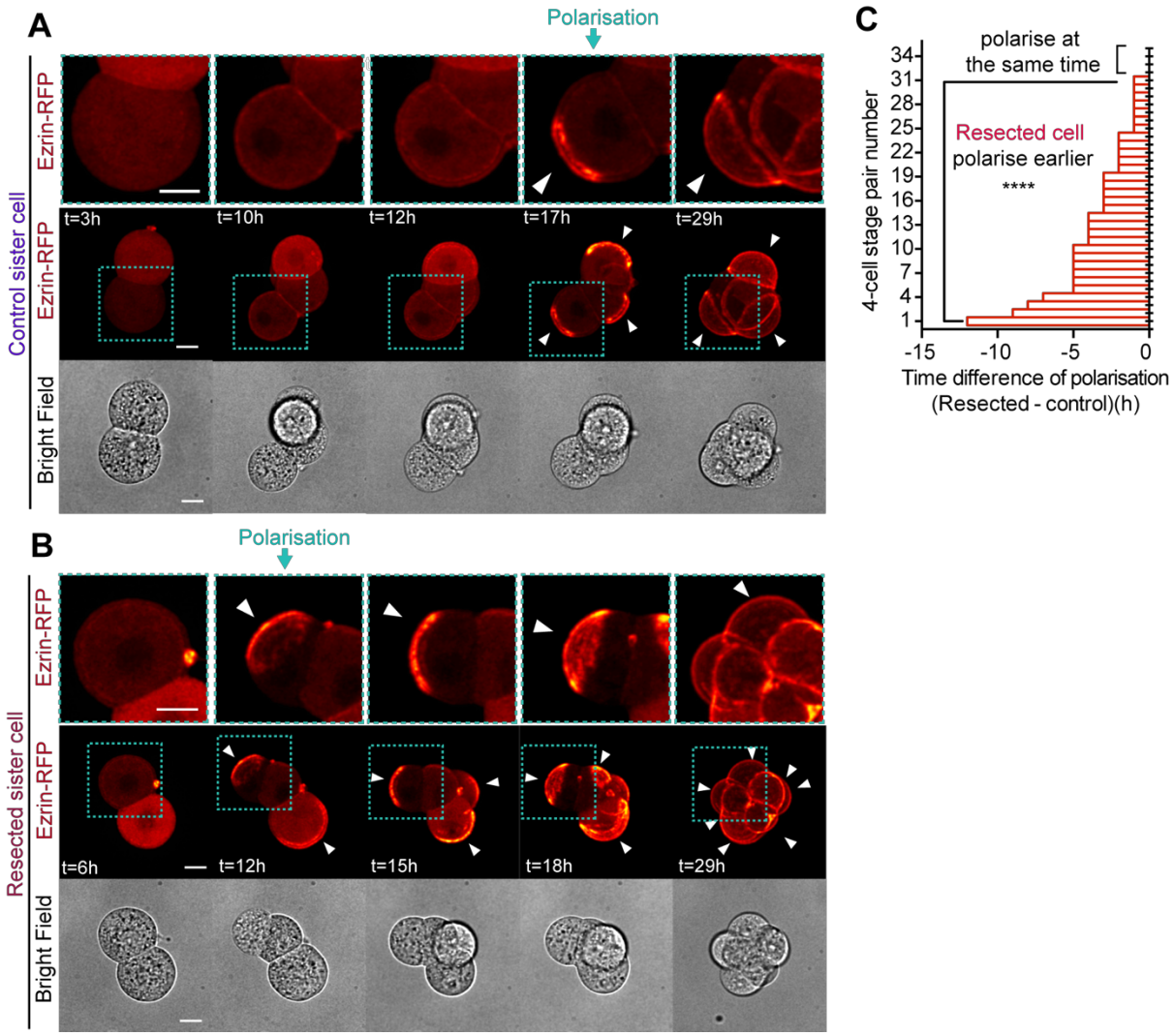

Figure 4.5 Resected cells from 4-cell stage embryo always polarised earlier than control sister cells. (A) Time-lapse imaging of the control pairs from the 4-cell stage to the morula stage. (B) Time-lapse imaging of resected pairs from the 4-cell stage to the morula stage. For all images, squares indicate the magnified regions, the arrows indicate the apical domains. (C) Bar chart showing all comparisons of the time difference of polarisation between resected and control sister cells from experiment illustrated in b, each bar represents one comparison. Note that cells with reduced volume polarise earlier in the majority of cases. The time of polarisation is defined as when the first cell becomes polarised in a structure in all experiments. Time difference (in hours, h) is calculated as (time when resected cells polarise –time of control cell polarisation). n=39 pairs analysed. ****$p<0.0001$, one-sample t-test, hypothetical mean =0. Scale bars, 15µm.

The reduction in blastomere size could potentially affect multiple cellular processes, such as cortical tension. Therefore, to further determine whether the advancement of cell polarisation timing was indeed due to a transcription-dependent effect, the resected cells from the 2-cell stage embryos were subjected to a pulse of 5,6-dichloro-1-beta-D-ribofuranosylbenzimidazole (DRB)(Bensaude, 2011) treatment (Figure 4.6A) from the mid to late 4-cell stage (roughly 3 hours). The timing of cell polarisation was then compared to that of the control sister cells. The analysis of the cell polarity timing between control sister cells and the resected and DRB treated cells revealed that, the short period of DRB treatment repressed the advancement of cell polarity establishment (46%, n=15, ns, one-sample t-test)(Figure 4.6B-D), further strengthening the hypothesis that the zygotic transcripts' concentration is associated with the timing of cell polarity establishment.

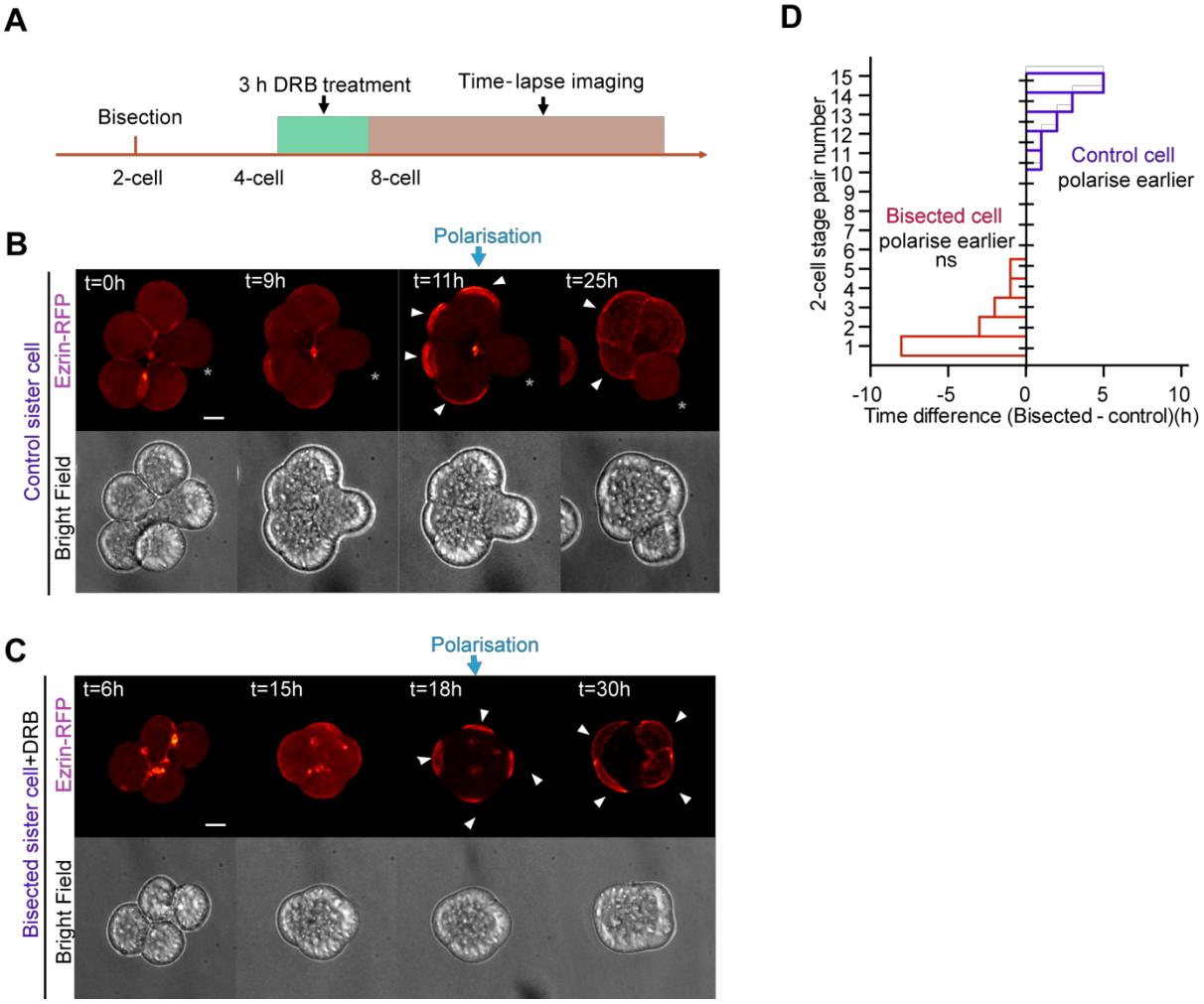

Figure 4.6 Inhibition of transcription prevents advancement of timing of cell polarisation. A. Scheme of pulsed DRB treatment in 2-cell stage resection experiment. Resection was performed at the mid 2-cell stage as indicated in Figure 4.3B. Resected cells were subjected to DRB treatment for 3h at the late 4-cell stage followed by time-lapse imaging. B, C. Time-lapse imaging of control sister cells and resected + DRB-treated sister cells generated from the experiment shown in b. Arrows indicate the apical domain. Asterisks indicate the cytoplasm from resected cells. D. Bar chart shows the time difference between control sister cells and resected+DRB-treated cells, each bar represents one comparison. The time difference (displayed in hours, h) is defined as the time point at which the first cell becomes polarised in a structure, same for all resection related experiments. Time difference (h) is calculated as (the time of resected cells become polarised – the time of control cell become polarised). n=15 pairs analysed. ns, not significant, one-sample t-test, hypothetical mean =0. Scale bars, 15µm.

4.4 Pausing transcription at the early 8-cell stage prevents cell polarity establishment

To further determine the necessity of zygotic transcription for cell polarity establishment, two RNA synthesis inhibitors, DRB and Triptolide (Bensaude, 2011), both of which can effectively inhibit transcription shortly after application, were added to the medium of embryos cultured from the 4-8 cell stage to the 8-16 cell stage (Figure 4.7A). The cell polarisation was examined by Pard6 and F-actin staining. DRB treatment strongly blocked apical domain formation as Pard6 and F-actin failed to organise into apical ring structures in majority of the cells (Figure 4.7B). Interestingly, despite the failure of cell polarity establishment, cytokinesis still occured and the cell number between control and treated groups was not significantly different (Figure 4.7 C-E), suggesting a specific effect of transcription inhibition on cell polarity establishment. As DRB is reversible (Bensaude, 2011), to further determine the specificity of transcription inhibition in preventing cell polarity, the DRB was washed out, and the cell polarisation status as well as the following development were checked every 30 minutes by time-lapse imaging. This revealed that the DRB washout allowed re-establishment of cell polarity within 9 hours (Figure 4.7 F-H). The treatment with triptolide similarly blocked cell polarity establishment without affecting cytokinesis from 8-16 cell stage (Figure 4.8 A-D). These results together suggest that, zygotic transcription was required for cell polarisation establishment at the 8-cell stage, and more importantly, the requirement of transcription is continuous until the early the 8-cell stage is still required for a proper timing of cell polarity establishment.

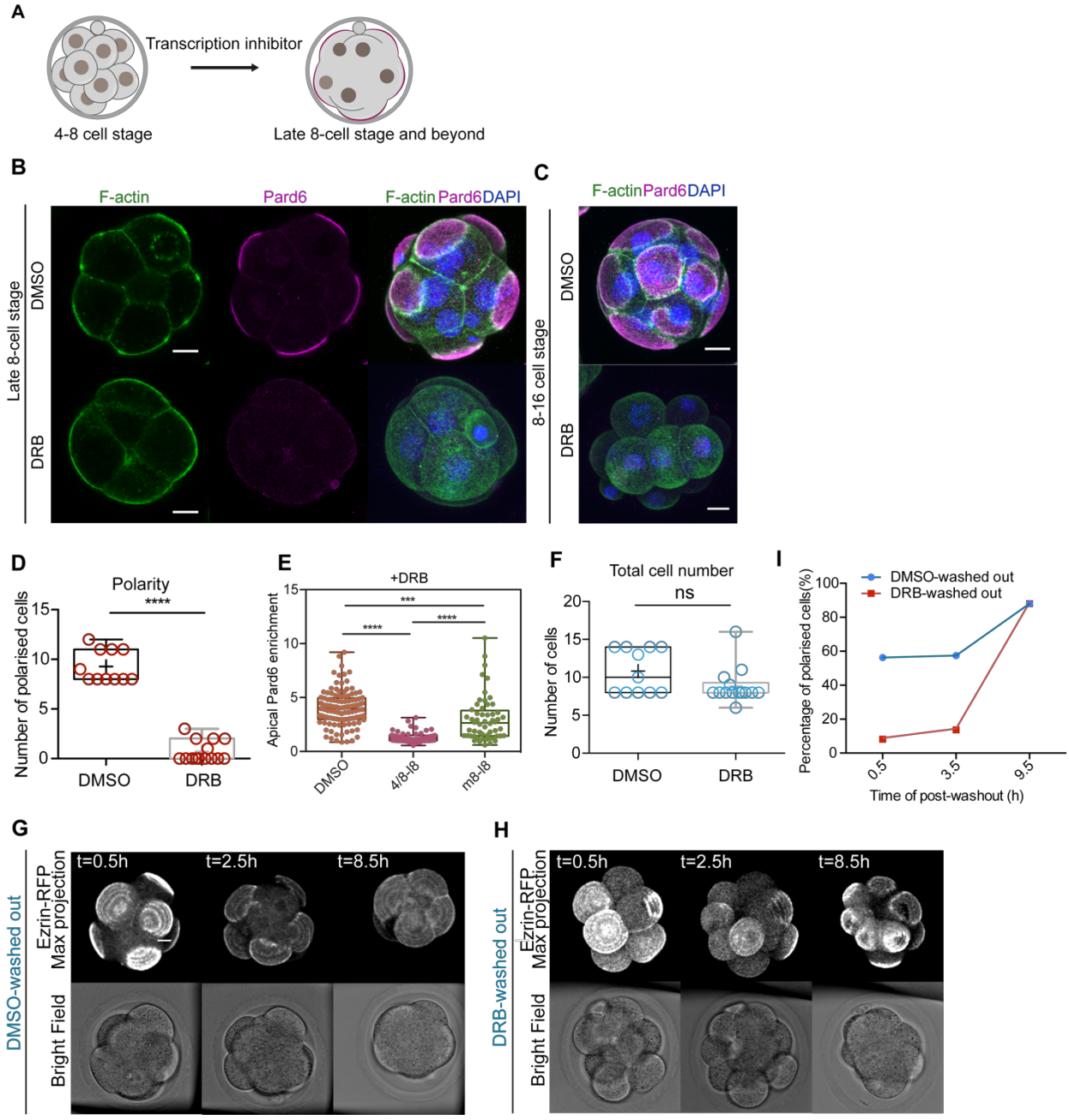

Figure 4.7 DRB treatment blocked cell polarisation. (A) Schematic showing embryos treated from 4-8-cell stage with transcription inhibitors DRB (50µM) or Triptolide (5 µM) and fixed at late 8-cell or 8-16 cell stages (12 hours duration in total). (B) DMSO (control)- or DRB-treated embryos fixed at late 8-cell stage and stained for F-actin, Pard6 and DNA. (C) DMSO- or DRB-treated embryos fixed at 8-16 cell stage and stained for F-actin, Pard6 and DNA. (D) Quantification of Pard6 apical enrichment in cells treated with DMSO or DRB from 4-8 cell stage or mid 8-cell stage to the late 8-cell stage. Each dot represents an analysed cell. Data shown as individual data points with Box and Whiskers plot (bottom: 25%; upper: 75%; line: median; whiskers: min to max). ***p<0.001; **** p<0.0001, One-way ANOVA test. (E)

Numbers of polarised cells in DMSO- and DRB-treated embryos. Data shown as individual data points with Box and Whiskers plot (bottom: 25%; upper: 75%; line: median; whiskers: min to max). **** p<0.0001, Student's t-test. (F) Total cell numbers in DMSO- and DRB-treated embryos. n=11 embryos, DMSO-treated; n=14 embryos, DRB-treated; ns, not significant in Mann-Whitney test. (G, H) Snapshots of time-lapse images of embryos after washing out DMSO (F, control) or (G) DRB from early 8-cell stage to late 8-cell stage. (I) Line chart shows percentage of polarised cells at different post-wash out time-points in DMSO washed-out (control) or DRB washed-out group. For t=0.5h, n=87 cells for DMSO and n=97 cells for DRB group were analysed; for t=3.5h, n=101 cells for DMSO and n=102 cells for DRB group were analysed; for t=9.5h, n=109 cells for DMSO and n=107 cells for DRB were analysed. Scale bars, 15µm.

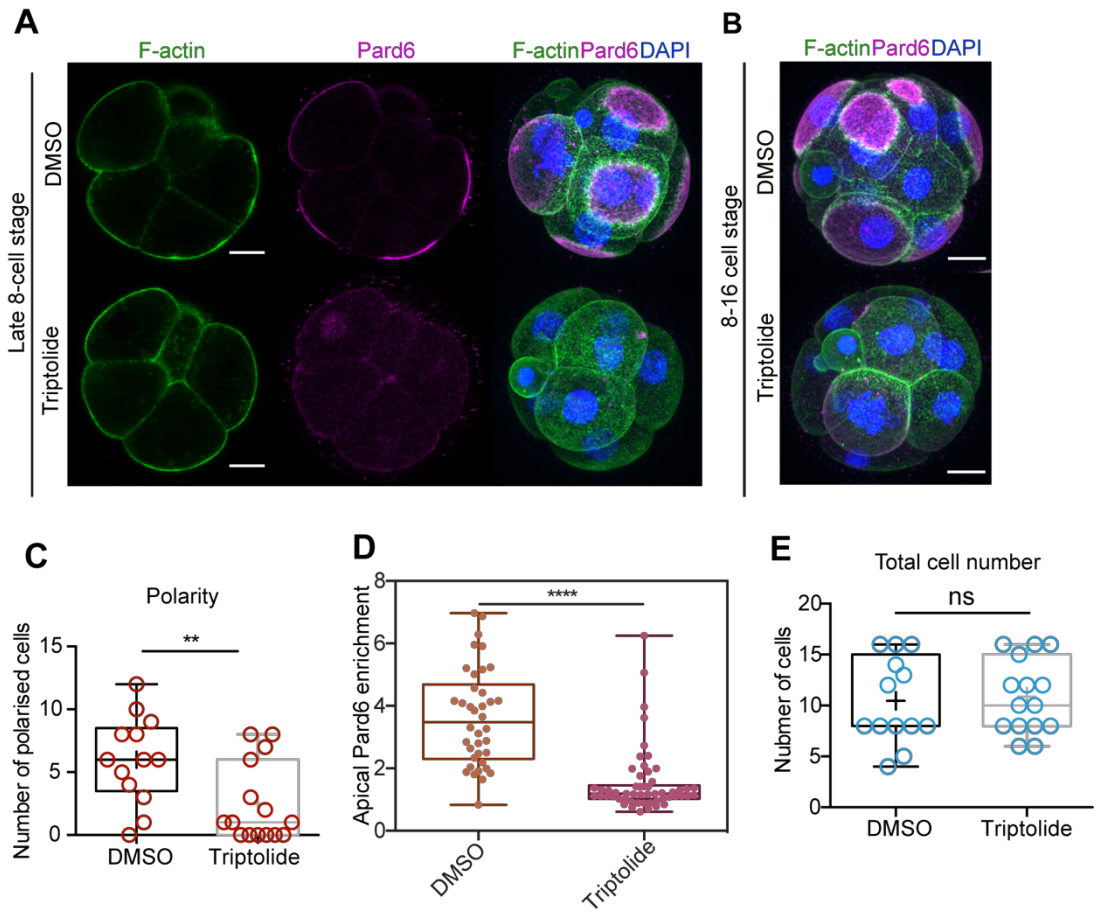

Figure 4.8 Triptolide treatment blocked cell polarisation. (A) Embryos treated with DMSO (control) and Triptolide were fixed at the late 8-cell stage and stained for Pard6 and F-actin. (B) Embryos treated with DMSO (control) and Triptolide were fixed at the late 8-cell stage

and stained for Pard6 and F-actin. (C) Quantifications of polarised cell numbers in embryos treated with DMSO and Triptolide. (D) Quantification of Pard6 apical enrichment in cells treated with DMSO or Triptolide from 4-8 cell stage to the late 8-cell stage. Each dot represents an analysed cell. Data shown as individual data points with Box and Whiskers plot (bottom: 25%; upper: 75%; line: median; whiskers: min to max). **** $p<0.0001$, Mann-Whitney test. (E) Quantifications of total cell numbers in embryos treated with DMSO and Triptolide. Data shown as individual data points with Box and Whiskers plot (bottom: 25%; upper: 75%; line: median; whiskers: min to max). **$p<0.01$; ns, not significant. Student's t-test. Scale bars, 15µm.

4.5 dsRNA screen for candidate zygotic genes for cell polarity establishment at the 8-cell stage

As the blastomere resection and RNA synthesis inhibitor results suggest that ZGA might result in zygotic activators triggering cell polarity establishment, revealing the nature of such factors would be the key step in understanding the mechanism triggering cell polarity establishment, as well as the timing regulation involved. To this end, two different strategies have been used to determine the essential zygotic regulators triggering cell polarity establishment.

4.5.1 Strategy no 1: Screen candidates based on gene expression profile as well as Gene Ontology terminology

The first strategy is based on the hypothesis that certain essential cytoskeleton regulators accumulate immediately after ZGA and keep doing so until the early 8-cell stage. Their action would be concentration dependent, so that once they accumulate beyond a certain threshold this would trigger the establishment of cell polarity. This hypothesis could explain the results of the blastomere resection experiments as well as those of the RNA synthesis inhibitor experiment (as illustrated in the hypothetical model in the blastomere resection experiment, Figure 4.4A). To this end, candidate genes were selected after analysis of two published RNA-seq databases (Deng et al., 2014; Goolam et al., 2016). Two selection criteria were used for the candidate genes: 1) upregulation from the 2-8 cell stage 2) have potential functions in cytoskeletal regulation and cell polarity establishment. To this end, the genes displaying consistent upregulation from the 2-8 cell stage in both databases were filtered out, the GO (gene ontology) term for each gene was determined using the Uniprot website (http://www.uniprot.org) and the genes labelled with cytoskeletal regulation, cell polarity, and Rho GTPase regulation were preferentially selected. Around 5621 genes displayed

upregulation from the 2-8 cell stage (Table 1). Based on the GO terms and previous studies in other systems, 114 genes were selected for the primary screen (Table 1).

Gene Symbol	Gene Symbol	Gene Symbol	Gene Symbol	Gene Symbol
Als2	Celsr2	Igf1r	Plekgh2	Tmem92
Amhr2	Celsr3	Igf2r	Ppp1ca	Trp63
Ap2m1	Cfl1	Itgae	Psap	Vangl1
Arhgap1	Cfl2	Jup	Psen1	Vangl1
Arhgap10	Cttn	Krtcap2	Ptpn18	Vangl2
Arhgap12	Dlg5	Lgr4	Rack1	Wdr83
Arhgap19	Dstn	Llgl2	Rbpj	Xab2
Arhgap28	Efna1	Lpar1	Rhgdia	Ywhab
Arhgap29	Efna2	Lpar5	Ripor1	Ywhae
Arhgap5	Fabp3	Lpar6	Rnd1	Ywhah
Arhgap8	Fabp5	Lrg1	Rnd2	Ywhaq
Arhgdig	Fam89b	Mapt	Rnd3	Zfp740
Arhgef16	Gabpa	Marcks	Rps11	Gata1
Arhgef3	Glrx3	Marcksl1	S1pr2	Gata3
Arpc3	Gmfg	Mark3	S1pr5	Gata4
Arpc5	Gpr136b	Mesdc2	Snx5	Tfap2c
B4galt1	Gpr160	Mybp3	Sphk1	Tead4
Cap1	Gpr160	Net1	Sphk2	Pou5f1
Capzb	Gpr171	Oog1	Spint1	
Ccdc43	Gpr172b	P2y14	Stub1	
Cd9	Gpr19	Pdzd3	Sycn	
Cdc151	Gpr50	Pfn1	Tagln2	
Cdc42ep1	Gprc50	Pkm	Taxbr2	
Cdc42ep5	Gprc5a	Pkn2	Tdgf1	
Celsr1	Hand1	Pkn3	Tm4sf1	

Table 4.1 The selected candidate list for the RNAi screen. The selection criteria were: 1) Upregulation from the 2-8 cell stage in published RNA-seq datasets. 2) Gene ontology terms related to cytoskeletal regulation, cell polarity, Rho GTPase regulation. Highlights show

genes that display a phenotype. Cells coloured in blue = cell proliferation defect. Cells coloured in green = polarisation delay.

One or two dsRNAs were designed to deplete each candidate. Each dsRNA was 300-500nt in length and within the CDS region. For the genes with multiple transcription variants the common CDS region was selected. For the initial screen, 2-3 dsRNAs were grouped together (based on the potential functional redundancy) and injected into the zygote (Table 4.2). The groups that displayed a phenotype were analysed further.

Als2; Ap2m1	Gabpa; Glrx3; Gmfg	Ywhab; Ywhae; Ywhah
Amhr2;	Oog1	Ywahq
Arhgap1; Arhgap5;Arhgap10	Plekgh2	Zfp740
Arhgap12; Arhgap19	Ppp1ca	Gata1
Arhgap28; Arhgap29	Psap	Gata3
Arhgap8;	Psen	Gata4
Arhgef16; Arhgef3	Ptpn18	Tfap2c; Tead4
Arpc3; Arpc5	Rbpj	Pou5f1
B4Galt1;	S1pr2; S1pr5	
Cap1; Capzb	Arhgdig; Arhgdia;Ripor1	
Ccdc43	Rnd1; Rnd2; Rnd3	
Cd9; Cd151	Sphk1; Sphk2	
Cdc42ep1; Cdc42ep5	Stub1	
Celsr1; Celsr2; Celsr3	Spint1	
Cfl1; Cfl2; Dstn	Snx5	
Efna1; Efna2	Sycn	
Fabp3; Fabp5	Tagln2	
Cttn; Rack1	Taxbr2	
Fam89b;Jup	Tdgf1	
Marcks; Marcksl1	Tm4sf1	
Gpr136b; GPR160; Grp172	Tmem92	
Gpr19; Gpr50; Gprc5a	Trp63	
Gpr171; P2y14	Vangl1; Vangl2	
Igf1r; Igf2r	Wdr83	
Pkn2; Pkn3	Xab2	
Als2; Ap2m1	Gabpa; Glrx3; Gmfg	

Table 4.2 The combination of candidate genes for dsRNA injections. The dsRNAs of the candidate genes belonging to the same protein families or implied to have similar biological functions (up to three genes) were pooled together and injected into the zygote. Each cell represents one injection condition.

The initial analysis revealed a couple of candidates the depletion of which resulted in preimplantation phenotypes, including: 1) Xab2, a factor that constitutes a pre-mRNA splicing complex (Kuraoka et al., 2008), and the depletion of which caused a failure of morula to blastocyst transition. 2) Rps11, a ribosomal protein (Lott and Mackie, 1988) whose depletion lead to the failure of embryo cavitation and resulting in cell death at the blastocyst stage (not shown). However, all the remaining candidate failed to show a phenotype and did not affect cell polarisation at the late 8-cell stage.

4.5.2 Strategy no 2: screen transcription factors active around the 8-cell stage based on ATAC-seq data.

The proximate requirement of transcriptional activity for cell polarity establishment suggests that the transcriptional program triggering cell polarity establishment may be under stage specific developmental control. In many embryonic developmental processes stage specific morphogenetic transitions are generally regulated by transcription factor activities (Meech et al., 2005; Shahbazi et al., 2017; Wang et al., 2013). Therefore, it is likely that certain transcription factors are active at the early 8-cell stage or at an earlier stage, and these activate downstream targets necessary for cell polarity establishment. To this end, a recently published ATAC-seq dataset was analysed (Wu et al., 2016), which revealed several transcription factors the activities of which were upregulated from the 2-8 cell stage and appeared highest around the 8-cell stage. These transcription factors included Tead4, Gata1, Gata3, Gata4, Pou5f1 and Tfap2c (Wu et al., 2016). To their potential role in cell polarity establishment, a dsRNA targeting each gene was designed and injected at the zygote stage to deplete protein expression, while Ezrin-RFP was co-injected to visualise polarity dynamics. As a control, dsRNA targeting GFP with Ezrin-RFP was injected. The efficiency for each dsRNA was verified by immunostaining or RT-qPCR (Figure 4.9A-F). The effects on cell polarity establishment were examined by time-lapse imaging. This revealed that the depletion of Gata1, Gata3, Gata4 and Pou5f1 did not significantly affect cell polarity establishment, as by the late 8-cell stage the majority of the cells could successfully polarise, and formed the ring structure on the cell contact-free surface (Figure 4.10 A,F). However, the depletion of Tead4 and Tfap2c significantly reduced the number of polarised cells at the late 8-cell stage, although cytokinesis was not significantly affected (Figure 4.10 B-E, G). However the cell polarity defects caused by Tead4 or Tfap2c depletion seemed to be transient, as by the 16-cell stage the majority of the cells re-established an apical domain (Figure 4.10 B-E, H). To test whether these two

factors could compensate for one another, a dsRNAs targeting the transcripts of both genes was co-injected into the zygote, together with Ezrin-RFP to visualise polarity. The co-depletion caused a more severe phenotype, as the number of cells that polarised with Pard6 and Ezrin at the late 8-cell stage was further reduced, and more importantly, even at the 16-cell stage the majority of cells still failed to form an apical domain (Figure 4.10B-E, H, I-J). Thus the co-depletion of Tfap2c and Tead4 caused a more severe phenotype than single depletion, and therefore it is evident that both Tfap2c and Tead4 are required for cell polarity establishment, and moreover they exhibit functional redundancy. Tfap2c (also known as AP2gamma, Tcfap2c) belongs to the Activating Protein 2 (AP-2) family which has been revealed to be involved widely in early development (Hilger-Eversheim et al., 2000). Tead4 belongs to the transcriptional enhancer factor (TEF) transcription factor family, and it is well known for its role in regulating TE and trophoblast specification and differentiation(Yagi et al., 2007).

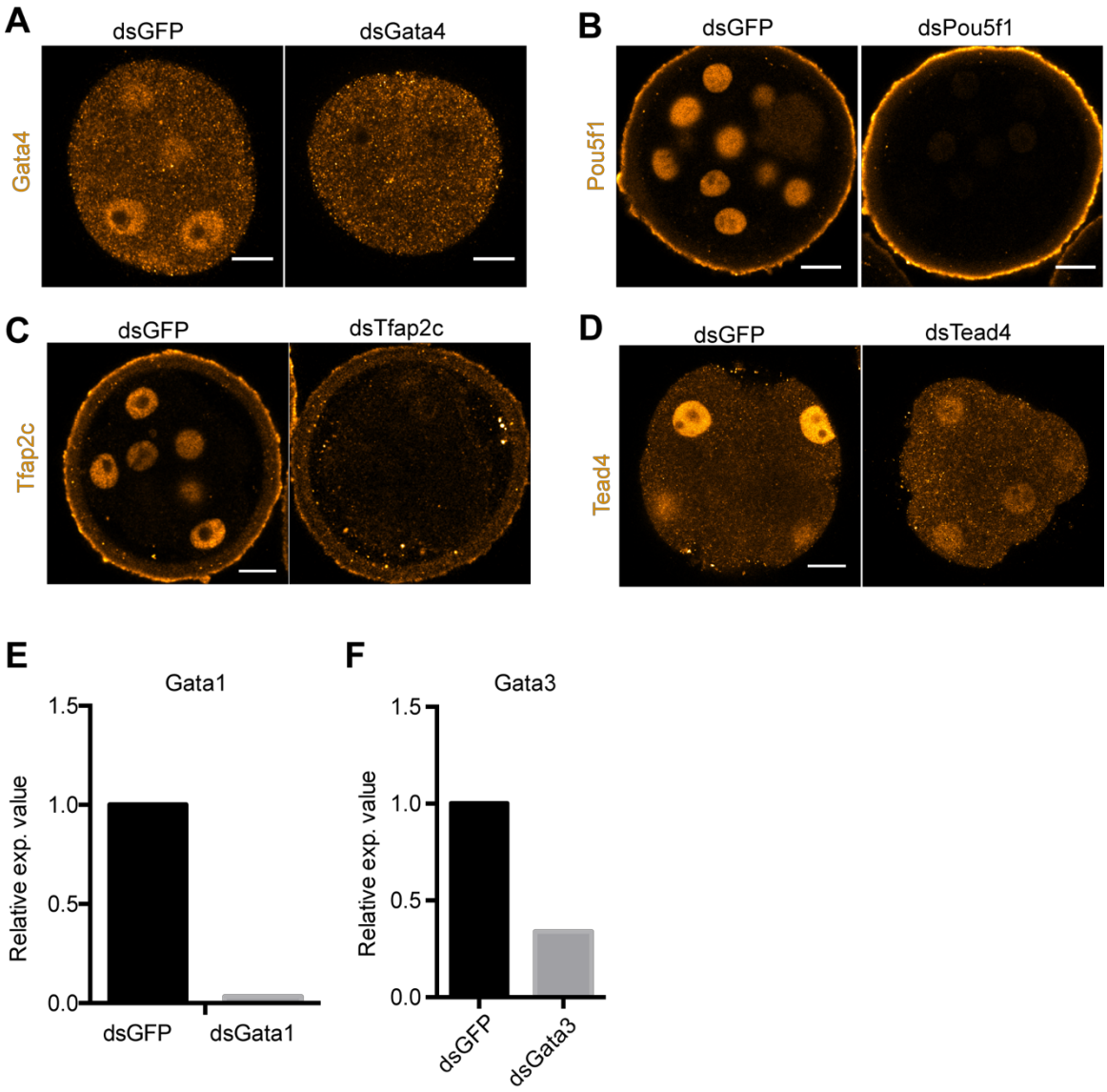

Figure 4.9 Validation of dsRNA targeting different transcription factors active at the 8-cell stage. (A) Embryos injected with dsRNA targeting GFP (control) or Gata4 were fixed at the late 8-cell stage and immunostained for Gata4. (B) Embryos injected with dsRNA targeting GFP (control) or Pou5f1 were fixed at the late 8-cell stage and immunostained for Pou5f1. (C) Embryos injected with dsRNA targeting GFP (control) or Tfap2c were fixed at the late 8-cell stage and immunostained for Tfap2c. (D) Embryos injected with dsRNA targeting GFP (control) or Tead4 were fixed at the late 8-cell stage and immunostained for Tead4. (E) Expression level of Gata1 in embryos injected with dsRNA targeting GFP or Gata1. (F) Expression level of Gata3 in embryos injected with dsRNA targeting GFP or Gata3. Scale bars, 15µm.

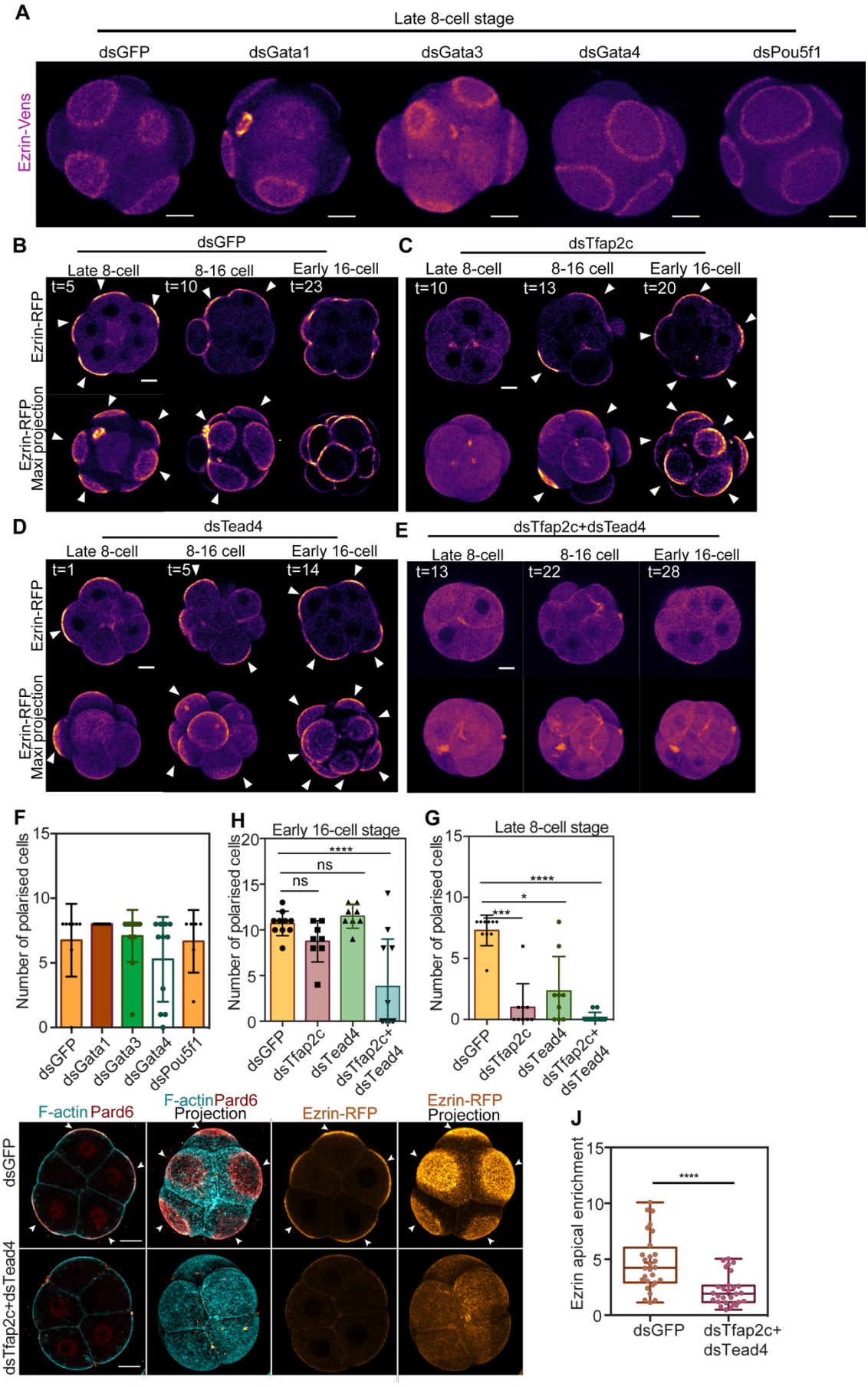
A
Late 8-cell stage
dsGFP
dsGata1
dsGata3
dsGata4
dsPou5f1
Ezrin-Vens
B
dsGFP
Late 8-cell
8-16 cell
Early 16-cell
t=5
t=10
t=23
Ezrin-RFP
Ezrin-RFP Maxi projection
C
dsTfap2c
Late 8-cell
8-16 cell
Early 16-cell
t=10
t=13
t=20
D
dsTead4
Late 8-cell
8-16 cell
Early 16-cell
t=1
t=5
t=14
Ezrin-RFP
Ezrin-RFP Maxi projection
E
dsTfap2c+dsTead4
Late 8-cell
8-16 cell
Early 16-cell
t=13
t=22
t=28
F
Number of polarised cells
dsGFP
dsGata1
dsGata3
dsGata4
dsPou5f1
H
Early 16-cell stage
Number of polarised cells
****
ns
ns
dsGFP
dsTfap2c
dsTead4
dsTfap2c+ dsTead4
G
Late 8-cell stage
Number of polarised cells
****
*
***
dsGFP
dsTfap2c
dsTead4
dsTfap2c+ dsTead4
I
F-actin Pard6
F-actin Pard6 Projection
Ezrin-RFP
Ezrin-RFP Projection
dsGFP
dsTfap2c+dsTead4
J
Ezrin apical enrichment
****
dsGFP
dsTfap2c+ dsTead4

Figure 4.10 dsRNA-mediated knockdown of Tfap2c and Tead4 led to the delay of cell polarisation at the late 8-cell stage. (A) Embryos injected with Ezrin-RFP and dsRNA targeting GFP (control), Gata1, Gata3, Gata4, Pou5f1were scanned at the late 8-cell stage for Ezrin. (B,C,D,E) Snapshots of time-lapse imaging of embryos expressing Ezrin-RFP and dsRNAs targeting GFP (B), Tfap2c (C), Tead4 (D) and Tfap2c+Tead4 (E) from the late 8-cell stage to the early 16-cell stage. Arrows indicate the apical domains. (F) Quantifications of the number of polarised cells in embryos expressing dsGFP, dsGata1, dsGata3, dsGata4 and dsPou5f1 at the late 8-cell stage. (G) Quantifications of the number of polarised cells in embryos expressing dsGFP, dsTfap2c, dsTead4 and dsTfap2c+dsTead4 a the late 8-cell stage. *p<0.05, ***p<0.001, ****p<0.0001; Kruskal-Wallis test. (H) Quantifications of number of polarised cells in embryos expressing dsGFP, dsTfap2c, dsTead4 and dsTfap2c+dsTead4 at the early 16-cell stage. ns, not significant; ****p<0.0001; Kruskal-Wallis test. (I) Embryos injected with dsGFP or dsTfap2c+dsTead4 were fixed at the late 8-cell stage and stained for Pard6, F-actin and DNA. Arrows indicate the apical domains. (J) Quantifications of Ezrin apical enrichment in the cells expressing dsGFP or dsTfap2c+dsTead4. The apical enrichment is calculated as the signal intensity of Ezrin at the cell contact-free domain against the signal intensity of Ezrin at the cell-cell contacts. Data shown as individual data points with Box and Whiskers plot (bottom: 25%; upper: 75%; line: median; whiskers: min to max). ****p<0.0001, Student's t-test. Scale bars, 15µm.

4.6 A CRISPR-Cas9 method to genetically deplete Tfap2c and Tead4

The polarity phenotypes observed as a result of downregulation of Tfap2c and Tead4 were surprising, as no polarity defects were observed for single knockout embryos of Tfap2c or Tead4 at later stages. RNAi methods can potentially give off-target effects (Jackson et al., 2003). To validate the specificity of the phenotype resulting from RNAi targeting of Tfap2c and Tead4, and substantiate the role of these two factors in the regulation of cell polarity, the CRISPR-Cas9 method was employed to genetically deplete Tfap2c and Tead4. To achieve this, three independent sgRNAs targeting a single exon were designed using an optimised CRISPR design website (http://crispr.mit.edu). sgRNAs were spaced out at over 20-50nt intervals. A similar design has been reported to have a very high efficacy at causing genomic mutations (Zuo et al., 2017) (Figure 4.11A). The three sgRNAs for each gene, together with Cas9 mRNA and Ezrin-RFP (to visualise polarisation) were co-injected at the zygote stage, and 8-16 cell stage embryos were collected for immunostaining for the target genes (Figure 4.11A). The

immunostaining for Tfap2c and Tead4 revealed that by the 8-16 cell stage, the cells injected with sgRNAs and Cas9 displayed various levels of expression of Tfap2c or Tead4, in contrast to the control group in which all cells displayed high levels of Tfap2c and Tead4 (Figure 4.11B-C). The cells with a low level of Tfap2c or Tead4 were considered to be Tfap2c-null or Tead4-null cells. Overall, majority of the embryos injected with Cas9 and sgRNA targeting Tfap2c or Tead4 displayed mosaic pattern of Tfap2c or Tead4 expression level at the 8-16 cell stage (80%), only in around 20% of the embryos, all blastomeres remain low level of Tfap2c or Tead4. In embryos injected with only Cas9, all cells have high level of Tfap2c or Tead4 (100%). The quantification of cell polarisation suggested that the percentage of polarised cells in Tead4-null embryos did not differ significantly from the Cas9 only (control) group, suggesting that the Tead4 single knockout cells polarised (Figure 4.11D-F). On the contrary, the Tfap2c-null embryos displayed a reduction in the number of polarised cells, yet there was a certain proportion of cells that polarised (Figure 4.11 D-F), suggesting that Tfap2c depletion alone did not prevent cell polarisation completely.

To test whether the co-depletion of Tfap2c and Tead4 together could yield a more severe phenotype, as suggested by the RNAi experiment (section 3.5), sgRNAs for both Tfap2c and Tead4, together with Cas9 and Ezrin-RFP mRNAs were injected at the zygote stage and the embryos were fixed at the late 8-16 cell stage and stained for Tfap2c and Tead4 (Figure 4.11A). The quantification of cell polarisation in the Tfap2c-, Tead4-null (double depletion) group suggested that none of the cells were able to polarise at the 8-16 cell stage when Tfap2c and Tead4 were both depleted (Figure 4.12A). Together, the gene editing experiments along with the RNAi results, strongly suggest that Tfap2c and Tead4 mediated transcriptional activity is crucial for cell polarity establishment at the 8-cell stage.

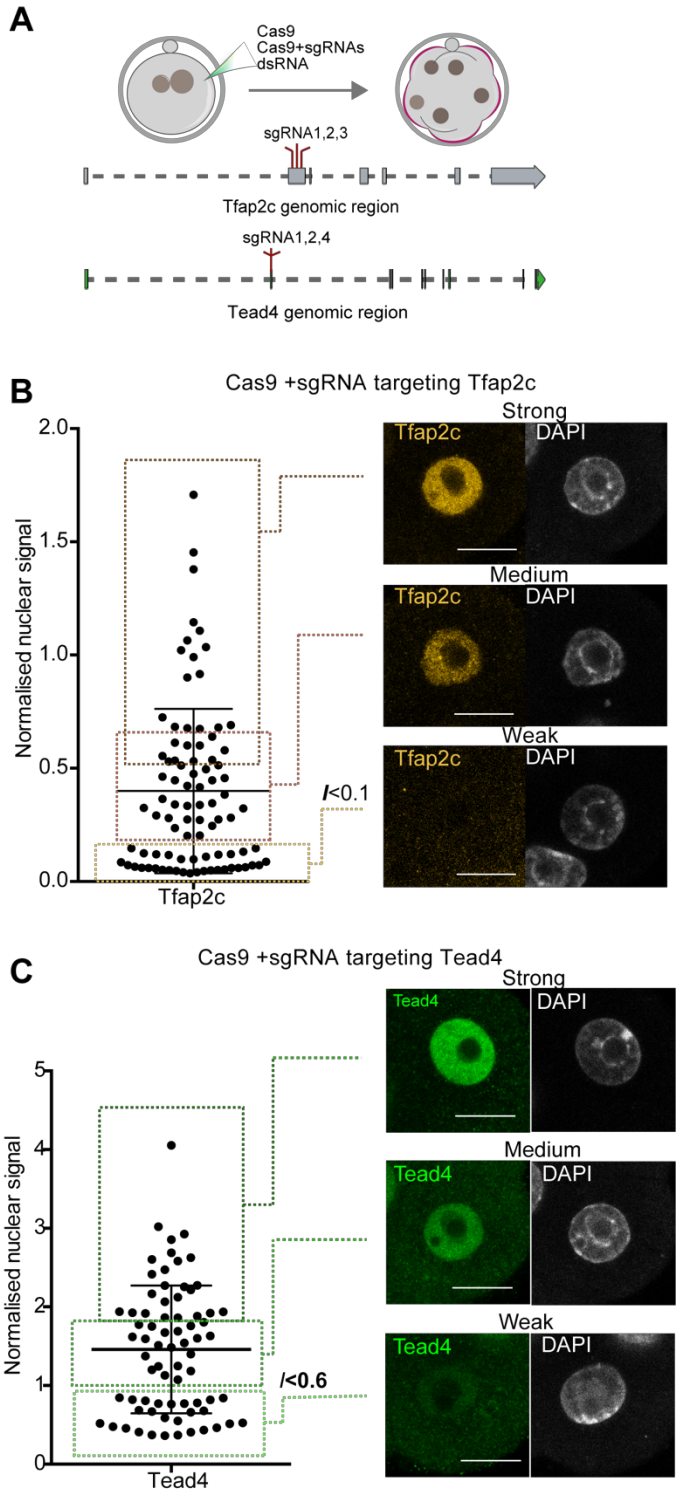

Figure 4.11 CRISPR strategy to deplete Tfap2c and Tead4 from the zygote stage generated cells expressing different levels of Tfap2c and Tead4. (A) Schematic of the CRISPR-cas9 strategy used to deplete Tfap2c and Tead4. (B) Signal intensity quantification in cells that showed a strong, medium or low level of Tfap2c (classification was shown in squares). Representative images of cells expressing different levels of Tfap2c are shown on the

right. Each dot represents a single analysed cell (n=23 embryos). The normalised signal intensity below 0.1 was considered to represent a "Tfap2c-null" cell. All cells were from embryos injected with Cas9 and gRNAs targeting Tfap2c, and immunostained with anti-Tfap2c and DAPI at 8-16 cell stage. b. Quantifications of the signal intensity for cells that showed a strong, medium or low level of Tead4 (classification denoted in squares). Each dot represents a single analysed cell (n=16 embryos). Representative images of cells expressing different levels of Tead4 are shown on the right. Each dot represents a single analysed cell. A cell with a normalised signal intensity below 0.6 was considered a "Tead4-null" cell. All cells are from embryos injected with Cas9 and sgRNAs targeting Tead4 and stained for Tead4 and DNA at the 8-16 cell stage. N=3 independent experiments. Scale bars, 15µm.

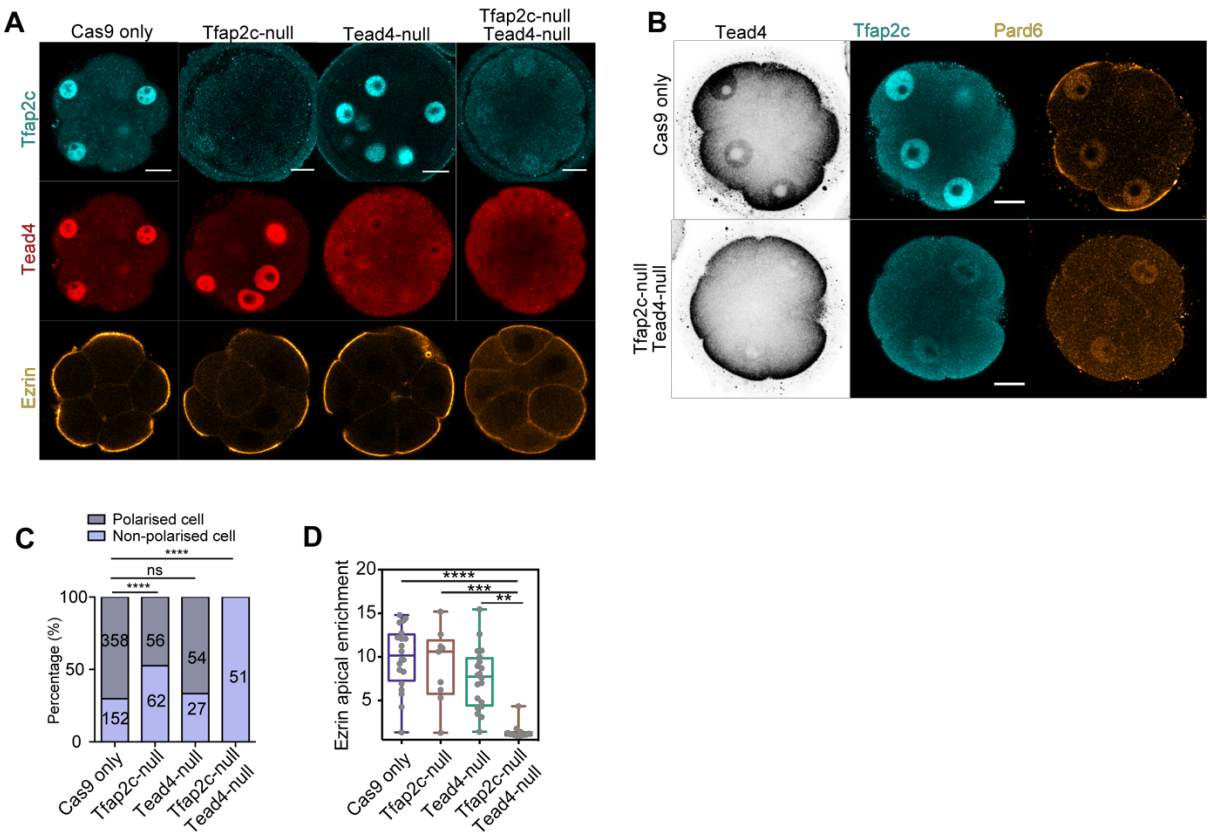

Figure 4.12 Genetic depletion of Tfap2c and Tead4 by CRISPR technology abolished cell polarity at the late 8-cell stage. (A) Representative images of embryos expressing Ezrin-RFP with wild-type (injected with only Cas9 mRNA, control); single depletion of Tfap2c (injected with Cas9 and sgRNAs targeting only Tfap2c); single depletion of Tead4 (injected with Cas9 and sgRNAs targeting only Tead4 sgRNAs); double depletion of Tfap2c and Tead4 (injected

with Cas9 and sgRNAs targeting both Tfap2c and Tead4) fixed at the 8-16 cell stage and stained for Tfap2c and Tead4. (B) Representative images of embryos expressing wild-type (injected with only Cas9 mRNA, control); single depletion of Tfap2c (injected with Cas9 and sgRNAs targeting only Tfap2c); single depletion of Tead4 (injected with Cas9 and sgRNAs targeting only Tead4); double depletion of Tfap2c and Tead4 (injected with Cas9 and sgRNAs targeting both Tfap2c and Tead4) fixed at the 8-16 cell stage and stained for Tfap2c, Tead4 and Pard6. (C) Proportions of polarised blastomeres in different genotypes presented in m. Data presented as contingency table. Number of cells analysed presented within each bar. ns, not significant; ****p<0.0001, Fisher's exact test. Cells showing Ezrin apical enrichment are polarised (quantification of Ezrin apical/basal signal intensity ratio displayed in D). (D) Quantifications of Ezrin apical enrichment in Cas9 only (control), Tfap2c-null, Tead4-null and Tfap2c- and Tead4-null cells. Data shown as individual data points with Box and Whisker plots (lower: 25%; upper: 75%; line: median; whiskers: min to max). n=20 cells for Cas9 only, n=9 cells for Tfap2c-null, n=20 cells for Tead4-null and n=12 cells for Tfap2c and Tead4-null.N=3 independent experiments. Ezrin apical enrichment is calculated as I_{apical}-I_{basal} (Methods). **p=0.0012, ***p=0.0007, ****p<0.0001, Kruskal-Wallis test. Scale bars, 15μm.

4.7 Tfap2c and Tead4 protein showed nuclear accumulation after ZGA and their depletion affected gene expression at the early 8-cell stage.

Both Tfap2c and Tead4 have been implicated in regulating preimplantation development but at later stages than those examined in this study. Tfap2c has been previously shown to promote TE development from pre to post-implantation stages by partially controlling the expression of Pard6b and tight junction components at the blastocyst stage (Cao et al., 2015; Choi et al., 2012). Tead4 is a known master regulator of TE specification and differentiation (Nishioka et al., 2008; Yagi et al., 2007). Therefore, in order for their potential function at earlier developmental stages and their relationship with the establishment of cell polarisation to be examined, the mRNA and protein levels of each gene were analysed using single-cell RNA sequencing data (previously available dataset in the Zernicka-Goetz lab), and immunostaining (Figure 4.13A-C). The single cell RNA-seq data indicated that *Tfap2c* is expressed at the zygote and 2-cell stage, suggesting a maternal contribution, but its expression declines during the 2-4 cell stage transition and subsequently increases between the 4-8 cell stage (Figure 4.13A), in agreement with another report. In contrast, *Tead4* is expressed from the 2-cell stage and its expression steadily increases until the 8-cell stage (Figure 4.13A). Importantly, expression of both Tfap2c and Tead4 proteins is low or barely-detectable at the mid 2-cell stage,

but increases progressively throughout pre-implantation development, indicating a contribution of both transcription factors through ZGA.

The earlier analysis of the single-cell RNA-seq data suggested that several genes encoding cytoskeletal regulatory proteins are dramatically upregulated at the 4-8 cell stage transition (section 3.5.1). Furthermore, it was observed that upon downregulation of either Tfap2c or Tead4, these genes are downregulated further concurring with ATAC-seq data indicating that Tfap2c and Tead4 are active at early stages such as the early 8-cell stage before cell polarity is established.

Together, these data suggest that Tfap2c and Tead4 are upregulated after ZGA, and are active prior to the early 8-cell stage.

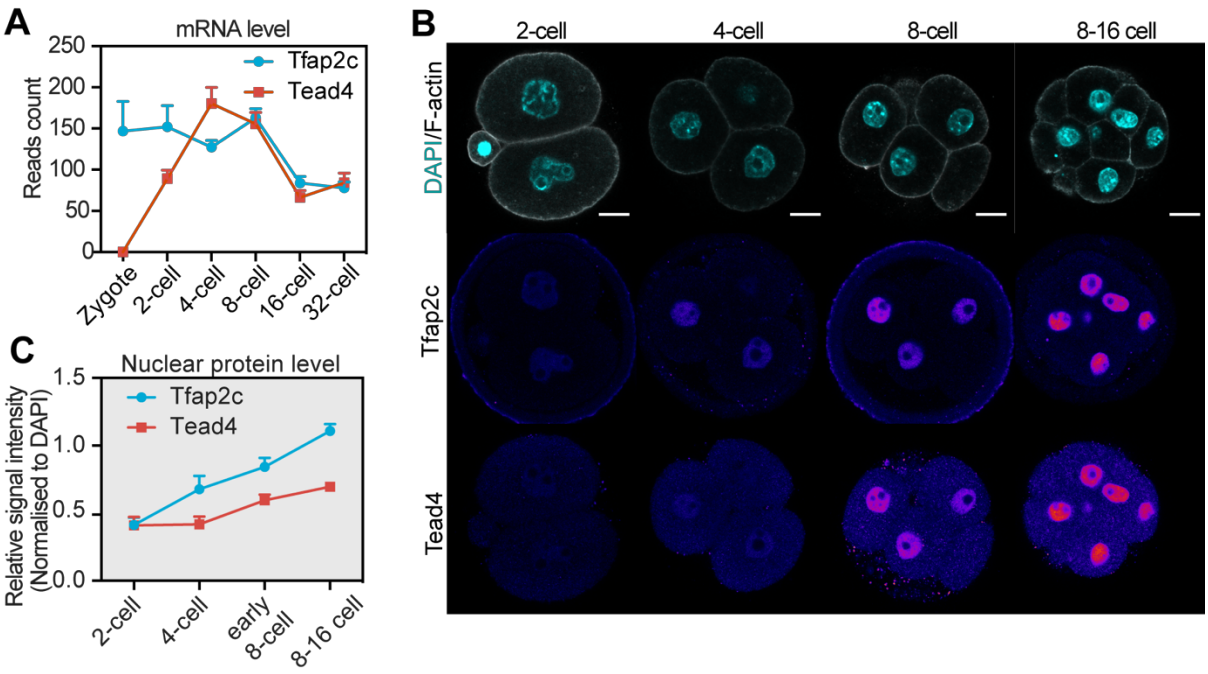

Figure 4.13 Expression profile of Tfap2c and Tead4 from the 2-cell to the 8-16 cell stage. (A) Expression profile of Tfap2c and Tead4. Data are presented as means ± S.E.M. (B) Expression profile of Tfap2c and Tead4 proteins from the 2-cell to the morula stage. (C) Quantification of Tfap2c and Tead4 nuclear protein levels from the 2-cell to the 8-16 cell stage. Data are presented as mean ± S.E.M. n=7 embryos for the 2-cell stage; n=15 embryos for the

4-cell stage; n=26 embryos for early the 8-cell stage; n=17 embryos for the 8-16 cell stage. N=2 independent experiments. Scale bars, 15μm.

4.8 Tead4 expression regulates early Yap nuclear localisation

To activate its downstream targets, Tead4 requires the co-activator Yap/Taz proteins. Paradoxically, the nuclear localisation of Yap/Taz at the late morula stage (16-32 cell stage) is known to be downstream of apical domain activity. However, a recent study revealed that nuclear accumulation of Yap occurs before apical domain formation, and disruption of the apical domain has no significantly effect on Yap's nuclear localisation prior to the 16-cell stage. This suggests that an apical-domain independent mechanism regulates nuclear yap localisation at the early 8-cell stage. To fully understand the manner in which Tead4 regulates downstream gene expression prior to apical domain formation, Yap's nuclear localisation in relation to Tead4 expression was examined. This revealed that, in an agreement with earlier reports, Yap gradually localised to the nucleus (Figure 4.14A-B) prior to apical domain establishment from the 2-8 cell stage onward (Figure 4.14A-B). Moreover, a comparison with the Tead4 nuclear protein level revealed that Yap's nuclear localisation correlated with Tead4 prior to the early 8-cell stage (Figure 4.14C).

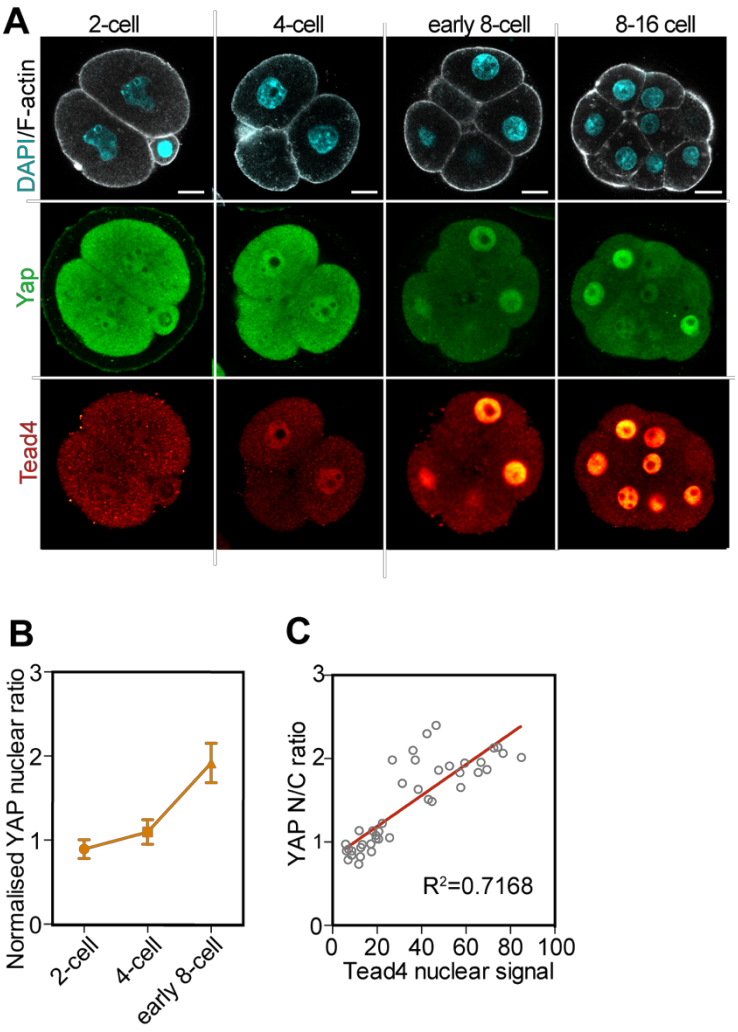

Figure 4.14 Yap nuclear localistaion correlates with Tead4 expression profile from 2-8 ell stage. (A) Expression profile of YAP and Tead4 from the 2-cell to 8-16 cell stage. (B) Quantification of YAP nuclear/cytoplasm (N/C) ratio from the 2-cell to the early 8-cell stage. Data presented as means ± S.E.M. n=10 cells for the 2-cell stage, n=13 cells for the 4-cell stage, n=21 cells for early the 8-cell stage. N=2 independent experiments. (C) Positive correlation between Tead4 nuclear expression and YAP nuclear/cytoplasm ratio, each dot represents one analysed cell. R2 = 0.7168, $p<0.0001$. Scale bars, 15µm.

This correlation raised the question of whether Tead4 plays a role in regulating Yap's early nuclear import. To address this, Tead4 expression was experimentally altered (either through over-expression or knock-down), and the impact on Yap localisation was examined. The reduction of Tead4 expression by RNAi significantly diminished Yap's nuclear localisation at the early 8-cell stage (Figure 4.15A-B) and conversely, Tead4 over-expression resulted in a dramatic up-regulation of Yap's nuclear localisation by the early 8-cell stage (Figure 4.15C-

D). Together, these data suggest that prior to cell polarity establishment, the accumulation of Tead4 protein during the 2-8 cell stage spontaneously leads to the recruitment of its co-activator Yap/Taz into the nucleus thereby facilitating the transcription of genes downstream of Tead4-Yap/Taz.

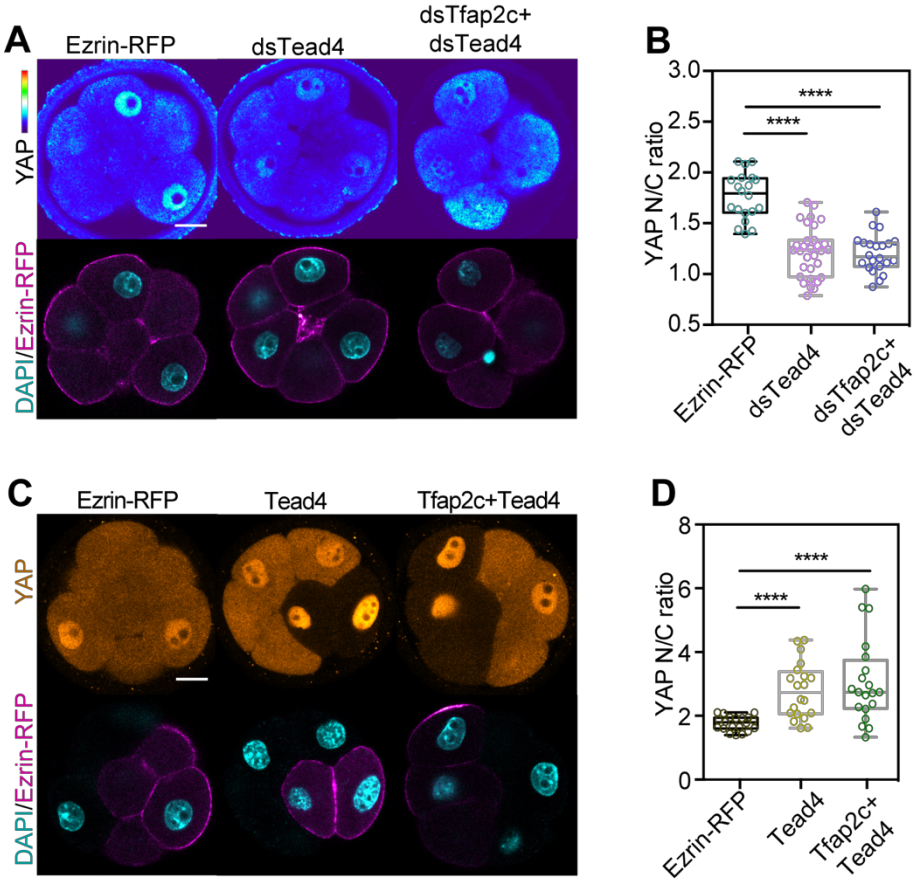

Figure 4.15 Tead4 expression regulates Yap nuclear localisation. (A) Representative images of embryos injected with Ezrin-RFP mRNA only (control), dsTead4 and dsTead4+Tfap2c RNAs, fixed at early 8-cell stage and immunostained to reveal YAP. (B) Quantification of YAP N/C ratio in cells injected with Ezrin-RFP mRNA only, or co-injected with dsTead4, dsTfap2c+dsTead4 RNAs. Data shown as individual data points with Box and Whiskers plot (bottom: 25%; upper: 75%; line: median; whiskers: min to max). n=20 cells for Ezrin-RFP only; n=18 cells for dsTead4; n=27 cells for dsTfap2c+dsTead4. N=2 independent experiments. ****p<0.0001. One-way ANOVA test. (C) Representative images of embryos microinjected with Ezrin-RFP mRNA only, Tead4 and Tead4+Tfap2c mRNAs and analysed for YAP localisation at the early 8-cell stage. Arrows indicate cells overexpressing Tead4. (D)

Quantification of YAP N/C ratio in cells microinjected with Ezrin-RFP mRNA only; with Tead4; or with Tfap2c+Tead4 mRNAs. Data shown as individual data points with Box and Whisker plots (lower: 25%; upper: 75%; line: median; whiskers: min to max). n=20 cells for each group. ****p<0.0001, one-way ANOVA test. Scale bars, 15μm.

4.9 Overexpression of Tfap2c/Tead4/RhoA triggers premature apical domain formation

4.9.1 Overexpression of Tfap2c, with or without Tead4, triggers membrane protrusion and premature compaction at the late 4-cell stage.

To fully dissect the role Tfap2c and Tead4 on the timing of cell polarity formation at the 8-cell stage, it is essential to evaluate the effects of advancing the timing of Tfap2c and Tead4 expression on the establishment of cell polarity. To this end, overexpression of Tfap2c and Tead4 was performed. In the first instance, the concentration of each transcription factor was tested (200ng/ul, 100ng/ul, 15ng/ul). It was noted that the high concentration of Tfap2c (equal or above 30ng/ul) caused developmental arrest in a cell-autonomous manner (Figure 4.16A), yet the overexpression of Tead4 at equal concentrations exhibited no phenotype (data not shown).

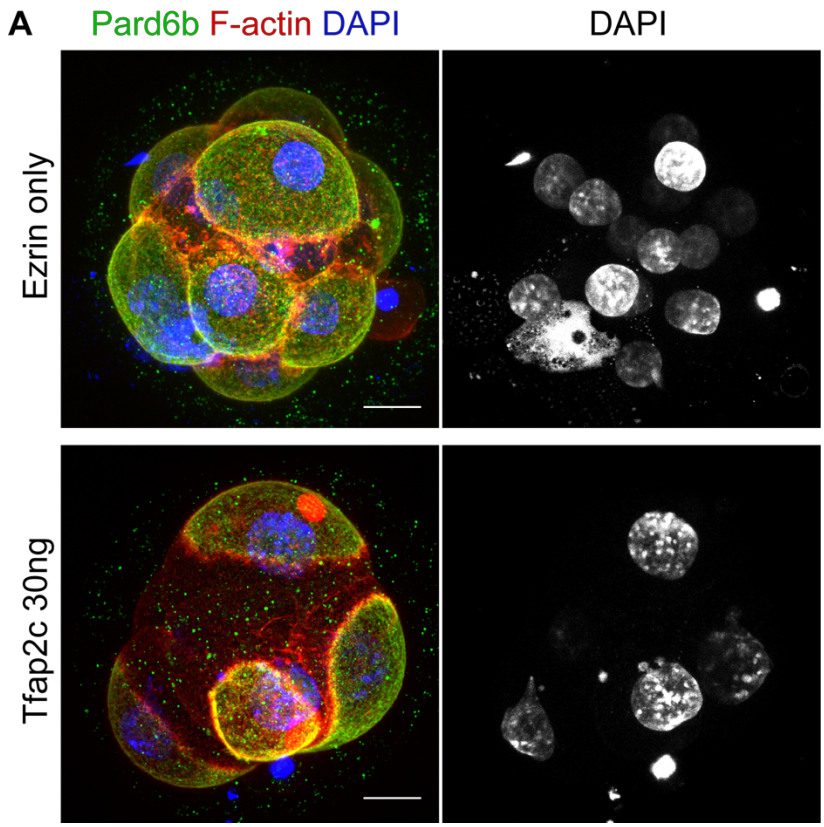

Figure 4.16 A high concentration of Tfap2c leads to cell division defects. (A) Embryos overexpressing Ezrin only (as a control) or 30ng/ul Tfap2c were fixed at the morula stage and stained for Pard6, F-actin and DAPI. The embryos overexpressing Tfap2c fail to proliferate and have only 4 blastomeres at the morula stage. Scale bars, 15µm.

When Tfap2c was expressed at a low concentration (15ng/ul), this triggered membrane protrusion-like structures, accompanied by premature cell compaction (Figure 4.17A-D). At the late 8-cell stage, the cells failed to form a proper apical domain but instead they formed protrusion like structures (Figure 4.17), similar to those observed at the late 4-cell stage. Furthermore, in subsequent cell divisions these cells were engulfed to the inside of the embryo (Figure 4.17).

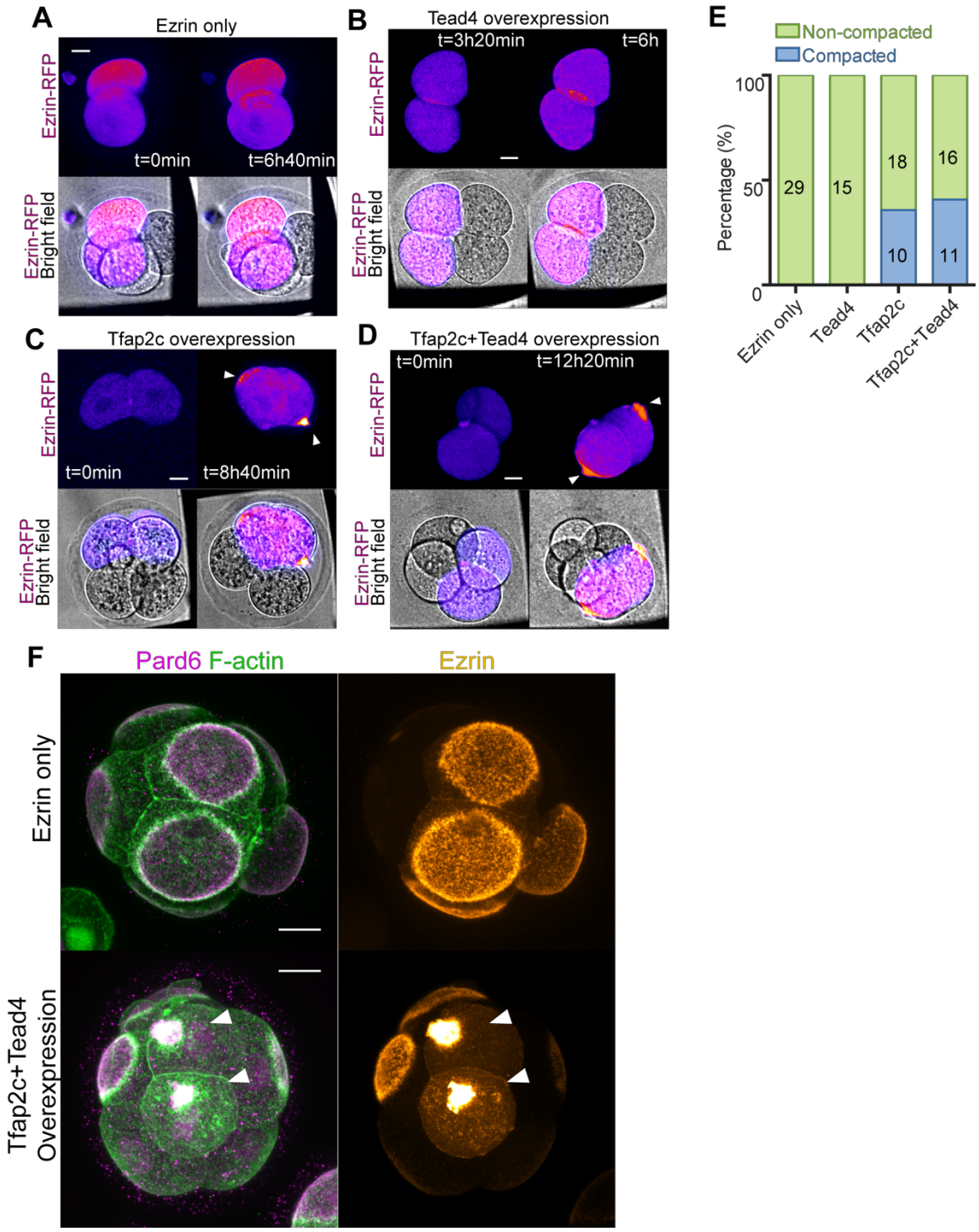

Figure 4.17 Overexpression of Tfap2c or Tfap2c+Tead4 lead to the formation of membrane protrusion like structures at the late 4-cell stage and premature compaction events. (A-D) Time-lapse imaging of embryos overexpressing Ezrin-RFP only (A), or co-expressing Tead4 (B), Tfap2c (C) and Tfap2c+Tead4 (D). Arrows indicate apical domain formation already at the late 4-cell stage. (E) Quantification of the percentage of cell compaction in the various overexpression conditions at the late 4-cell stage. Data are shown

as a contingency table, the numbers in each bar indicate the numbers of embryos analysed. (F) Embryos overexpressing Ezrin-RFP (as a control) or Tfap2c+Tead4 were fixed at the morula stage and stained for Pard6, F-actin and Ezrin. Arrows indicate membrane protrusion structures. N=3 independent experiments. Scale bars, 15µm.

To better understand the extent to which the membrane protrusions induced by Tfap2c/Tead4 overexpression are associated with apical domain formation, the cells were fixed at the late 4-cell stage and immunostained for apical proteins such as Pard6. This revealed that the structures were composed of apical domain proteins, such as Ezrin and Pard6 (Figure 4.18). Additionally, the dynamics forming such structures were filmed by time-lapse imaging, and compared with normal apical domain formation processes. Results in the previous chapter indicate that normal polarisation processes consist of two major steps. The first step, is the actomyosin complex polarisation, followed by apical protein enrichment and the ring domain formation (See Chapter III, results). A detailed analysis of the apical domain formation revealed that, the second step of apical domain formation can be further sub-divided into 2 distinct stages. In stage I, the apical proteins are enriched at the centre of a cell and in stage II, the primary apical domain expands to a proportion of the cell contact-free surface to form a ring-like structure. In the case of Tfap2c and Tead4 overexpression, although the apical enrichment process did occur (step 1, as well as the first stage of step 2) the apical domain expansion did not, but instead the apical domain proteins continued to be concentrated at the centre of the cell contact-free surface ultimately resulting in the formation of membrane protrusions (Figure 4.18).

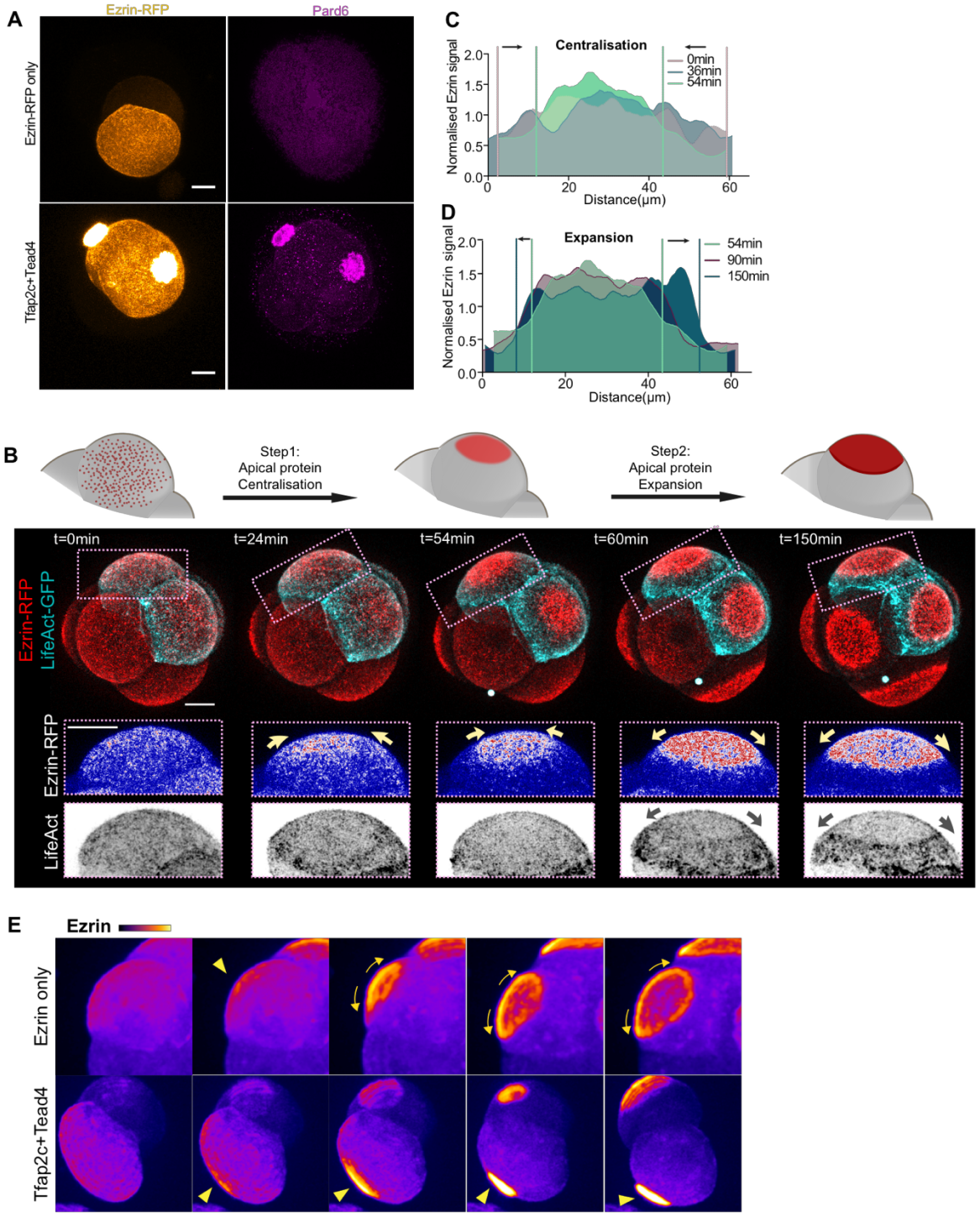

Figure 4.18 Tfap2c and Tead4 overexpression induces apical domain centralisation without apical domain expansion. (A) Embryos overexpressing Ezrin only (as a control) or Tfap2c+Tead4 were fixed at the late 4-cell stage and stained for Pard6. (B) Snapshots of the time-lapse imaging of embryos expressing LifeAct and Ezrin-RFP during the 8-cell stage of development. Arrows indicate the direction of the apical protein movements. (C) Plotting of

the Ezrin-RFP signal during the apical domain centralisation step. (D) Plotting of the Ezrin-RFP signal during the apical domain expansion step. (E) Snapshots of Ezrin dynamics in embryos overexpressing Ezrin only (as a control) or Tfap2c+Tead4. Scale bars, 15μm.

A detailed analysis through time-lapse imaging, together with the immunostaining results suggested that Tfap2c/Tead4 overexpression may promote specific processes of apical domain formation, yet the two factors were not sufficient to trigger apical domain formation. It is clear that other critical factors are necessary for the construction of a complete apical domain.

4.9.2 Actin regulators are activated by Tfap2c and Tead4 and are regulating apical domain concentration step

The examination of Tfap2c and Tead4 knockdown embryos revealed that the cells depleted of Tfpa2c and Tead4 failed to undergo the apical domain centralisation steps, although the embryos were able to undergo compaction. A complete understanding of the regulation of the apical domain centralisation process by Tfap2c and Tead4 requires the identification of their key downstream targets.

The apical domain protein centralisation and expansion process highly resembles T-cell receptor activation. In this system, the activated T-cell receptors first cluster together and subsequently exclude actin to the periphery. The entire process is regulated by dynamic actin cytoskeleton movements that require sufficient levels of Arp2/3, Cofilin/ADF factors, profilin and myosin contractility. Interestingly, all the above factors are dramatically upregulated during the 4-8 cell stage of development, including the Arp2/3 complex component Arpc2/3/4/5; Cofilin/ADF factors Cfl1,2 and Dstn; Pfn1 (Profilin) and Myosin light chain Myl12b. These complexes have been implicated in different systems as generally involved in regulating actin network dynamics. Specifically, Arp2/3 complex, the major components of which are Arp2 and Arp3, is responsible for the actin branching process (Pollard, 2007); Cofilin/ADF factors are necessary for actin severing (Bamburg and Bernstein, 2010); Profilin is an actin binding protein that mediates the actin turn-over process in general (Krishnan and Moens, 2009); Myosin light chain is part of the myosin II complex that is important for actin-myosin contractility (Heissler and Sellers, 2014). To investigate whether Tfap2c and Tead4 could account for the upregulation of the above factors, the expression level of those genes was determined by qPCR in the embryos injected with dsGFP or dsTfap2c+dsTead4. The results showed that Cfl1, Dstn, Aprc5 and Pfn1 were downregulated upon knockdown of Tfap2c and

Tead4 at the early 8-cell stage, suggesting that Tfap2c and Tead4 account for their upregulation between the 4-8 cell stage. More importantly, the inhibition of the Arp2/3 complex by CK666, and Cofilin phosphorylation by Limki-3 equally abolished the apical domain protein centralisation steps (Figure 4.19), suggesting that the regulation of the Arp2/3 complex proteins and Cofilin may be the major downstream mechanism for the Tfap2c/Tead4 mediated apical domain centralisation step.

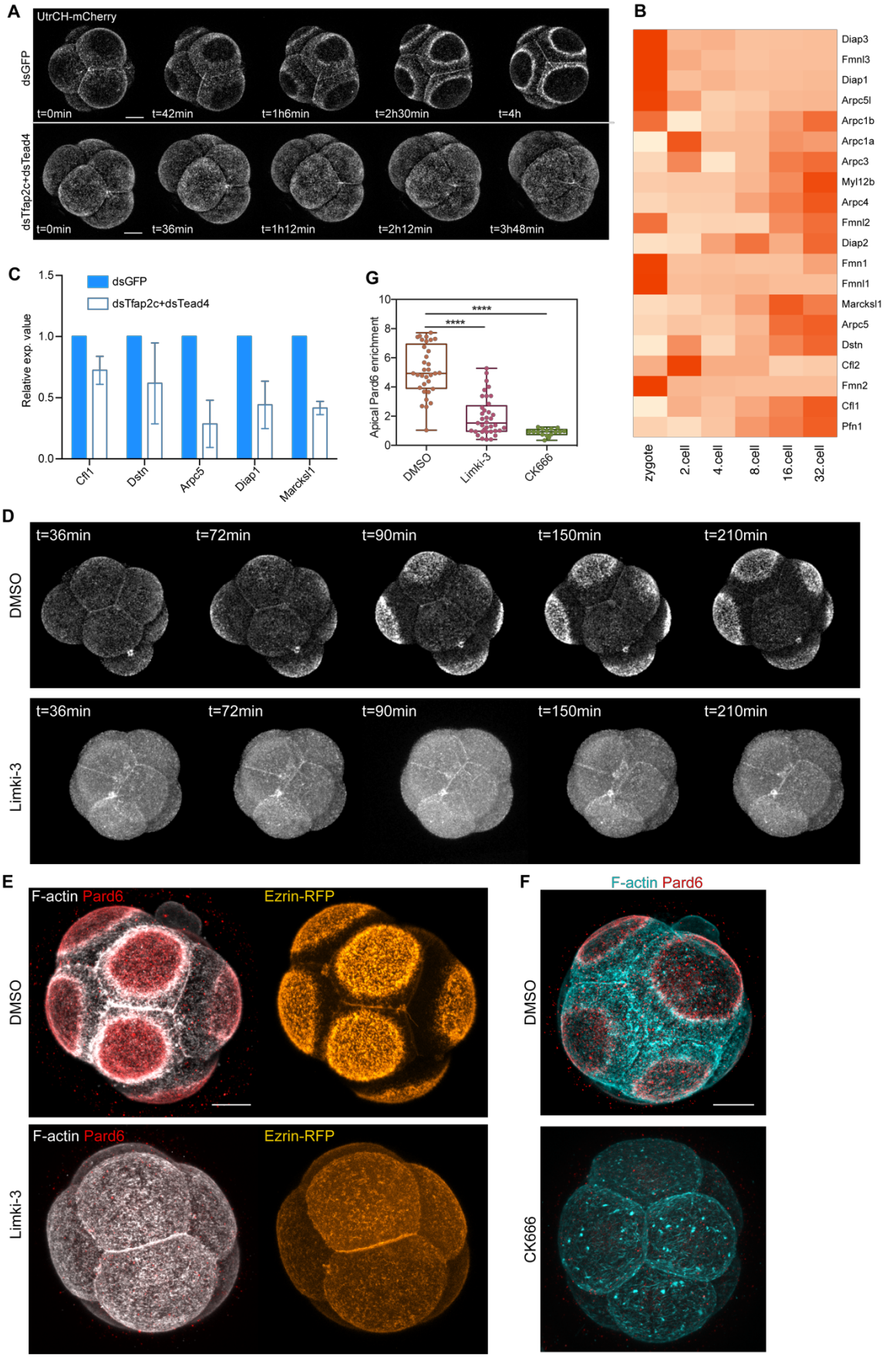
A
UtrCH-mCherry
dsGFP
t=0min
t=42min
t=1h6min
t=2h30min
t=4h
dsTfap2c+dsTead4
t=0min
t=36min
t=1h12min
t=2h12min
t=3h48min
B
Diap3
Fmnl3
Diap1
Arpc5l
Arpc1b
Arpc1a
Arpc3
Myl12b
Arpc4
Fmnl2
Diap2
Fmn1
Fmnl1
Marcksl1
Arpc5
Dstn
Cfl2
Fmn2
Cfl1
Pfn1
zygote
2.cell
4.cell
8.cell
16.cell
32.cell
C
dsGFP
dsTfap2c+dsTead4
Relative exp. value
Cfl1
Dstn
Arpc5
Diap1
Marcksl1
G
Apical Pard6 enrichment
****
****
DMSO
Limki-3
CK666
D
DMSO
t=36min
t=72min
t=90min
t=150min
t=210min
Limki-3
t=36min
t=72min
t=90min
t=150min
t=210min
E
DMSO
F-actin Pard6
Ezrin-RFP
Limki-3
F-actin Pard6
Ezrin-RFP
F
F-actin Pard6
DMSO
CK666

Figure 4.19 Cofilin/ADF factors and the Arp2/3 complex mediate the apical domain centralisation step downstream of Tfap2c and Tead4. (A) Snapshots of the time-lapse movie showing UtrCH-mCherry dynamics in embryos injected with dsGFP (control) or dsTfap2c+dsTead4. In dsGFP injected embryos (control), during the mid to late 8-cell stage, apical polarity proteins become centralised at the cell-contact free surface, and exclude actin to the periphery of apical protein enriched domain to form the apical cap. Embryos depleted of Tfap2c and Tead4 fail to undergo such actin rearrangements as the actin distribution remain homogeneous in cell-contact free surface. (B) Heatmap showing expression profile of various actin regulators from the zygote to the 32-cell stage in the single-cell RNA sequencing dataset (Goolam et al., 2016). (C) Expression level of Pfn1, Arpc5, Cfl1 and Dstn in embryos injected with dsGFP (control) and dsTfap2c+dsTead4. Data are shown as mean ± S.E.M. (D) Snapshots of the dynamics of Ezrin-RFP in the embryos treated with DMSO (control) and Limki-3 (Cofilin phosphorylation inhibitor). (E) Embryos treated with DMSO or Limki-3 were fixed at the late 8-cell stage and stained for Pard6 and F-actin. (F) Embryos treated with DMSO or CK666 were fixed at the late 8-cell stage and stained for Pard6 and F-actin. (G) Quantification of apical Pard6 enrichment. Each dots represent an analysed cell. ****$p<0.0001$, student's t-test. N=8 embryos for DMSO, N=12 embryos for Limki-3 and N=8 embryos for CK666 treated group. N=2 independent experiments. Scale bars, 15µm.

4.9.3 Co-overexpression of Tfap2c, Tead4 and RhoA accelerates the morphogenetic events related to apical domain establishment.

Studies in other systems have suggested that the Arp2/3 complex regulated actin cap domain expansion can be modulated by actomyosin tension downstream of RhoA-ROCK activity (Zenker et al., 2018; Zhang et al., 2018). In support of this, the overexpression of constitutively activated RhoA (RhoA-Q63L) led to apical domain expansion all around the cell membrane at the late 8-cell stage (Figure 4.20A,C). It has also been observed that the RhoA-Q63L overexpression can interfere with cytokinesis processes and led to the bi-nucleation, and affect the formation of blastocyst structures at E3.5 (data not shown). On the contrary, the inhibition of RhoA by C3-transferase led to the formation of membrane protrusions that resembled those induced by Tfap2c+Tead4 overexpression (Figure 4.20B). These results raised the possibility that RhoA could function specifically at the apical domain expansion step. To address this possibility, the co-overexpression of Tfap2c/Tead4 and RhoA were performed. A series of RhoA-Q63L concentrations were tested for RhoA-Q63L co-overexpression experiments. It

was observed that a high dose of RhoA caused the membrane disorganisation in nearly all cells (data not shown), yet when a fairly low concentration of RhoA-Q63L (3ng/ul) was introduced to the early 4-cell stage cells together with Tead4/Tfap2c, this triggered an apical like domain formation at the late 4-cell stage to the early 8-cell stage (Figure 4.21). In contrast, RhoA-Q63L alone, at the same concentration led to either membrane disorganisation, or no phenotype (Figure 4.21).

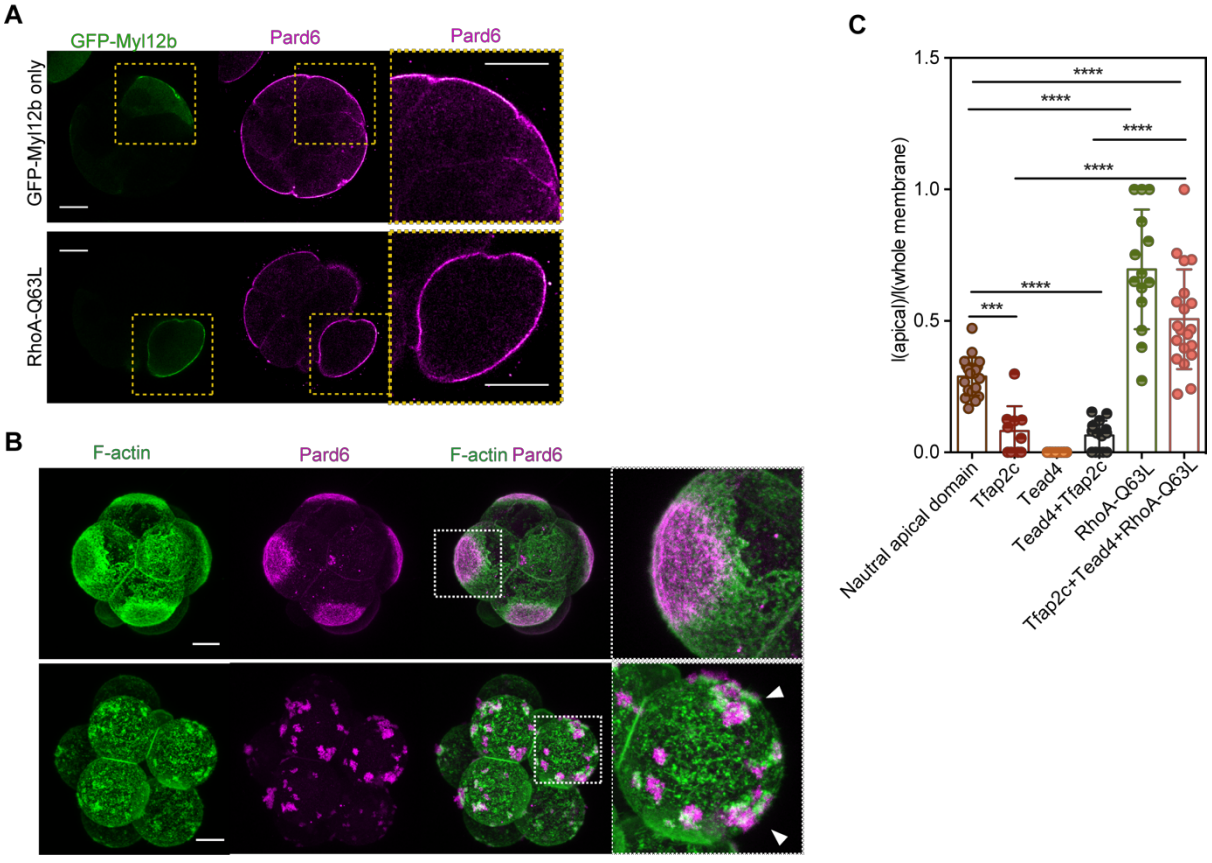

Figure 4.20 RhoA regulates the apical domain size. (A) The overexpression of constitutively active RhoA led to apical domain expansion at the morula stage. (B) RhoA inhibition by C3-transferase treatment led to the formation of membrane protrusions enriched by apical domain proteins at the late 8-cell stage. Arrows indicate the apical protrusions. Squares indicate the magnified regions. (C) Quantifications of apical domain size of various conditions. Each dots represents an analysed cell. N=8 embryos for Ezrin only; N=8 embryos for Tfap2c; N=10 embryos for Tead4; N=13 embryos for Tfap2c+Tead4; N=7 embryos for RhoA-Q63L; N=15 embryos for Tfap2c+Tead4+RhoA-Q63L. Scale bars, 15µm.

A close examination of time-lapse studies revealed that the dynamics of formation of these apical domain-like structures were very similar to those of apical domain assembly in the late 8-cell stage embryo. They led to the apical polarisation of both Ezrin and Pard6 (Figure 4.21A-B) and the induction of the differentiation marker Cdx2 (Figure 4.21C-D), suggesting that Tfap2c/Tead4/RhoA are sufficient to advance cell polarisation.

Together, these results suggest that Tfap2c/Tead4, and a concomitant increase of Rho activity are sufficient to induce apical domain formation, thus they are likely the major components constituting the timer for cell polarity establishment at the 8-cell stage.

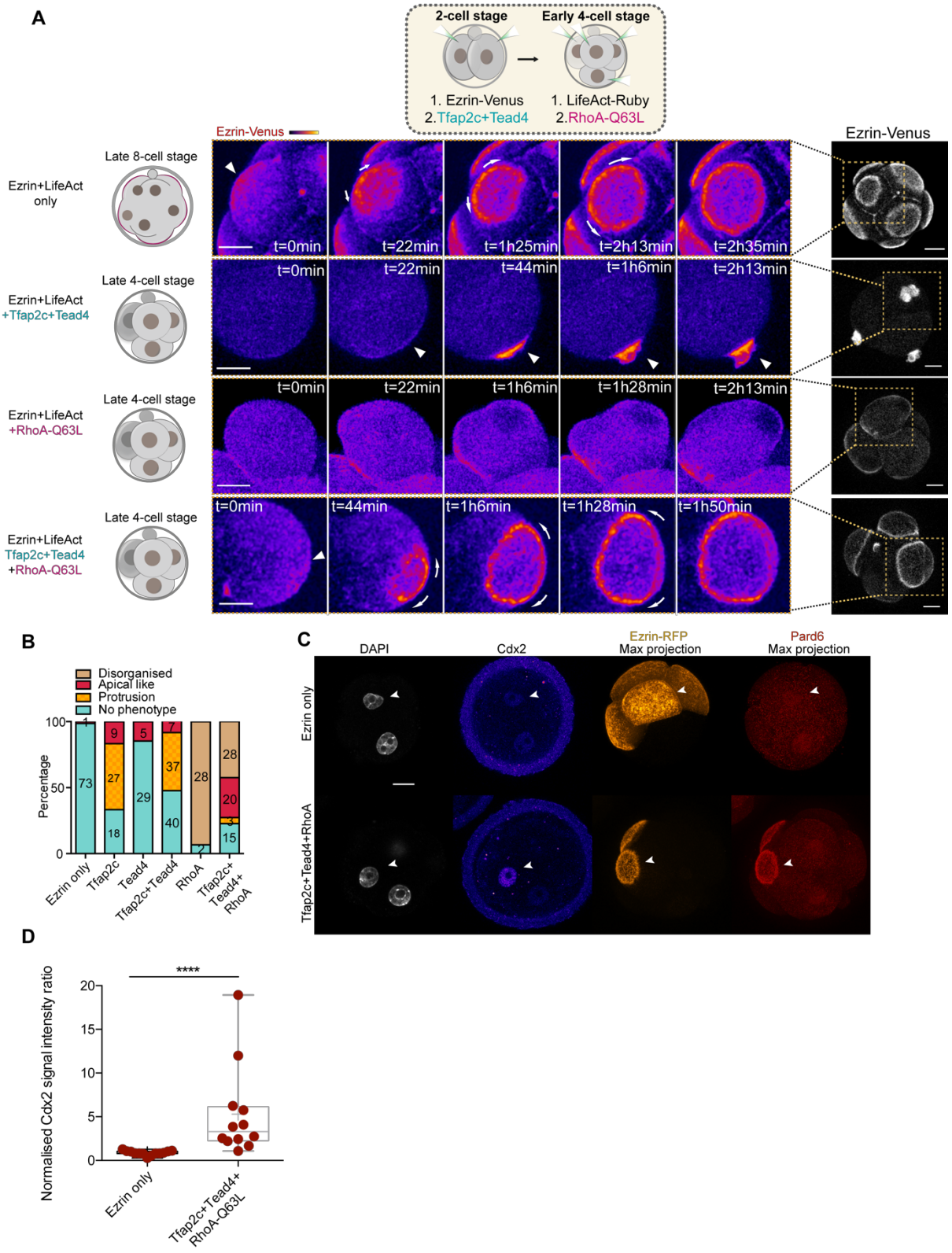

Figure 4.21 RhoA-Q63L together with Tfap2c and Tead4 overexpression led to the formation of a premature apical domain. (A) Scheme of Tfap2c, Tead4, RhoA

overexpression and representative time-lapse snapshots of Ezrin-Venus dynamics during the formation of apical domain structures in 1) natural embryos at late 8-cell stage (from Ezrin-Venus only control group); 2) cells over-expressing Tfap2c+Tead4 showing induced apical domain structure at the late 4-cell stage; 3) cells over-expressing RhoA-Q63L showing membrane protrusion at the late 4-cell stage; 4) cells over-expressing Tfap2c+Tead4+RhoA-Q63L showing induced premature apical domain structure at the late 4-cell stage. Short arrows indicate Ezrin-Venus enrichment at the cell contact-free surface. Long arrows indicate the expansion direction of the Ezrin-Venus enclosed ring domain. Squares indicate the zoomed-in region of each embryo. (B) Quantification of structures induced by various overexpression conditions. Data presented as a stacked bar graph where numbers in each bar indicate the number of cells analysed. (C) Representative images of embryos overexpressing Ezrin-RFP (control) and Tfap2c/Tead4/RhoA-Q63L at the mid 8-cell stage immunostained to reveal DNA, Cdx2 and Pard6. Injected cells (arrows) express Ezrin-GFP (n=8 embryos). (D) Quantification of normalised Cdx2 expression signal intensity in either cells injected with Ezrin-RFP or withTfap2c/Tead4/RhoA-Q63L mRNAs as in a. Intensity of Cdx2 expression in cells of each group is normalised to intensity of DAPI (DNA) staining and for each group injected cells were normalised against non-injected cells. Each dot represents a single embryo. N=5 independent experiments. *p=0.0286, Mann-Whitney test. Overexpression of Tfap2c/Tead4/RhoA-Q63L advanced the timing of apical domain formation and the upregulation of Cdx2. Scale bars, 15μm.

4.10 Tfap2c/Tead4/RhoA co-overexpression accelerated the morphogenetic program in the preimplantation mouse embryo

The results that Tfap2c/Tead4/RhoA activity together can induce premature apical domain formation also provided an opportunity to address whether the timing of apical domain formation is associated with other morphogenetic events taking place at the preimplantation stage, including apical domain zippering with tight junctions (Zenker et al., 2018), and cavitation events.

To this end, long-term time-lapse imaging running from the late 4-cell stage to the early blastocyst stage (E3.5) was performed. This revealed that, in the cells that established the apical

domain earlier (late 4-cell stage), the apical domain zippering process was accelerated and took place at the late 8-cell stage, instead of the early 16-cell stage as normal (Figure 4.22). Moreover, the premature zippering process was linked to tight junction formation, as the zippering sites were enriched by ZO-1 (Figure 4.22).

These results suggest that Tfap2c/Tead4/RhoA overexpression can accelerate the overall morphogenetic events in the preimplantation mouse embryo, and that the timing of apical domain formation may set the timer for apical domain zippering and contribute to tight junction formation processes (Figure 4.23).

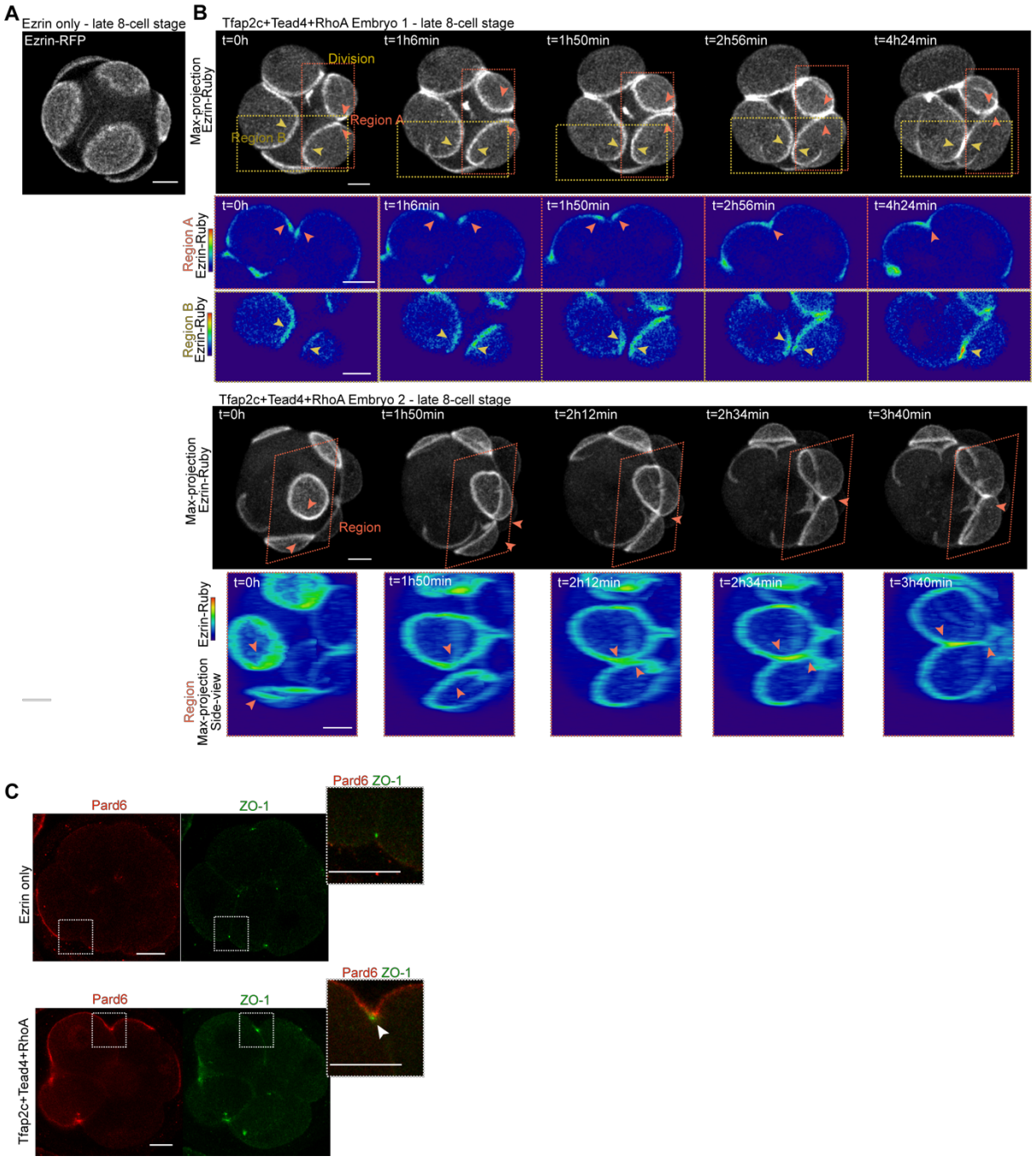

Figure 4.22 RhoA, Tfap2c, Tead4 overexpression led to premature apical domain formation and accelerated the following morphogenetic events. (A) Representative image of a control embryo expressing Ezrin-RFP at the late 8-cell stage (n=12 embryos). (B) Representative images of apical domain zippering in embryos overexpressing Tfap2c/Tead4/RhoA-Q63L at the late 8-cell stage (n=24 embryos). Pink and Yellow rectangular outlines indicate different magnified regions (below). Coloured arrows indicate boundaries of apical domains in different cells. (C) Representative images of embryos overexpressing Ezrin-RFP (control) and Tfap2c/Tead4/RhoA-Q63L at the late 8-cell stage

stained to reveal Pard6 and tight junction marker, ZO-1 (n=8 embryos for Ezrin only, n=12 embryos for Tfap2c/Tead4/RhoA-Q63L). Magnified regions are outlined. Arrows indicate the point of convergence of the apical domain and the tight junction. Tfap2c/Tead4/RhoA-Q63L overexpression advances apical domain formation and accelerates the expansion of the apical domain and its coupling with tight junctions. Scale bars, 15µm.

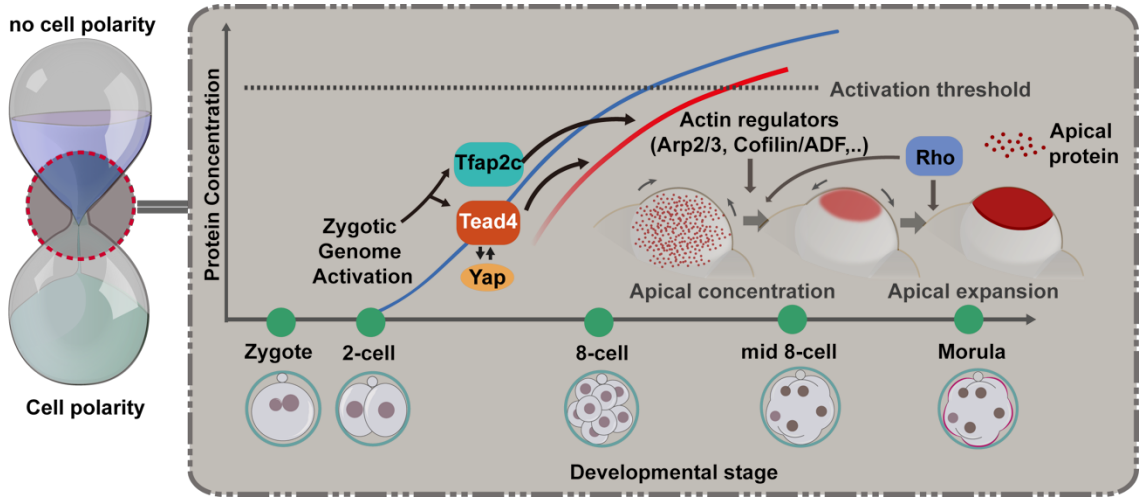

Figure 4.23 Model of the timer regulating polarity formation in the 8-cell stage mouse embryo. The "hourglass" timing model for establishment of de novo cell polarisation in the mouse embryo as a transcriptional cascade initiated by zygotic genome activation. Zygotic transcripts for Tfap2c and Tead4 gradually accumulate from the 2- to 8-cell stage. Tead4 expression spontaneously induces nuclear localisation of YAP promoting the Tead4-YAP transcriptional machinery. Tfap2c and Tead4-YAP induced transcriptional activity, including key actin regulators such as Arp2/3 complex components and Cofilin/ADF factors, drives the central enrichment of apical domain components; Rho protein activity facilitates expansion of the domain to form the final apical ring-like structure. Scale bars, 15µm.

4.11 Discussion

4.11.1 Re-examination of "inhibitor hypothesis": is cell polarity driven by the degradation of inhibitor(s) or the accumulation of zygotic activator(s)?

Given the importance of cell polarity in preimplantation development, coupled with the intriguing fact that mammalian embryos display cellular polarisation at a relatively late

embryonic stage, the mechanism governing the timing of cell polarisation in the mouse has been a topic of study for decades due in part to its far-reaching medical implications. The influential inhibitor hypothesis describes that, the constituents required for cell polarity establishment are already stored at sufficient levels prior to the early 4-cell stage, after which time the barrier for the establishment of cellular polarisation is purely attributed to potential "inhibitors", and the degradation of these inhibitors allows cell polarity to take place. This hypothesis originated form an early experiment in which protein synthesis inhibitors were applied from the late 2-cell stage or the early 4-cell stage, as a result of which the authors consistently observed premature flattening (compaction), and in many cases, precocious cellular polarisation examined by glycoprotein distribution (Concanavalin A immunostaining). However, these observations were not supported by the results in the current study, as cell polarity was examined by the more commonly used markers Pard6 and F-actin. It is fairly challenging to explain the discrepancies between the results, as with time, the culture medium, the methods for drug purification and the mouse strains have changed substantially. Despite the fact that protein synthesis inhibitors gave similar phenotypes in embryos of different genetic backgrounds (author's observations), it is possible that the response of the embryos to the drug varies with culture medium. Keeping all experimental conditions identical to the early studies is not practically feasible. However, it is important to note that although the current results are not sufficient to exclude the potential existence of polarity inhibitors, they provide lines of evidence that strengthen the argument for presence of polarity activators, and reveal the nature of these. Results from the bisection experiments are implicative rather than decisive (as will be discussed later), yet the transcription inhibitor treatments provide a stronger argument that zygotic transcriptional events contribute factors that positively regulate/are necessary for cell polarity establishment. Moreover, the identification of two transcription factors Tfap2c and Tead4, the protein of which is majorly contributed by ZGA, as necessary and partially sufficient factors for cell polarity establishment further strengthens the hypothesis that cell polarity establishment requires activators produced by zygotic transcription. It is unclear whether specific polarity inhibitors (acting on important cytoskeleton regulators) are provided by zygotic genome activation, however it is well-established that maternal protein degradation constitutes an important permissive signal for zygotic genome activation. From this perspective protein degradation may be one of the necessary conditions for cell polarity establishment, although the effects could be indirect. A more genome-wide genetic screen approach may aid in the identification of the nature of potential "polarity inhibitors".

4.11.2 Blastomere resection experiment implicates a role for zygotic RNA concentration in the determination of the timing of cell polarity.

To test the possibility that the zygotic RNA concentration sets the threshold that triggers the timing of cell polarity, the blastomere resection method was used to reduce the cytoplasmic size. RNA concentration is correlated with cytoplasm volume (Padovan-Merhar et al., 2015) and particularly, the reduced cytoplasm size has been shown to lead to a higher RNA concentration. However, the blastomere resection procedure per se may have other effects independent of RNA concentration. For example, the reduction of cytoplasm volume increases the nuclear/cytoplasm (N/C) ratio, a factor that has been implicated in regulating early developmental transitions in other systems (Blythe and Wieschaus, 2015; Collart et al., 2013). However, the N/C ratio is not likely to play a role in determining the timing of cell polarisation, as the prevention of cell cycle by microtubule inhibitors such as nocodazole and colcemid, or DNA replication inhibitors does not significantly affect the timing of cell polarisation (Pratt et al., 1982; Smith and Johnson, 1985). A second possible effect is the increase in cortical tension due to the reduction in cell size. This is also unlikely to explain the effect of blastomere resection on the timing of cell polarisation, as the blebbistatin treatment experiment (Chapter III) suggested that cortical tension does not directly regulate cell polarity, despite its role in driving cell compaction.

Nevertheless, many unknown transcriptional effects could potentially accompany the reduction of cell size, and directly separating these from the effect of RNA concentration could prove challenging. Therefore to unequivocally verify the effect of RNA concentration on the timing of polarisation, the resected cells were treated with DRB to inhibit transcription. Upon DRB treatment the timing of cell polarisation in resected cells was not significantly different from the control (non-resected) sister cells, strongly suggest that the effects on the timing of polarisation observed in the absence of DRB treatment were due to transcription related events.

Another intriguing observation was that the alteration of cytoplasmic volume at the 4-cell stage seemed to cause a more severe phenotype than at the 2-cell stage. This effect could potentially be due to the adaptability of the cells to the altered cellular volume. It has been observed in a variety of cells lines in many species that cells can adapt to changes in cytoplasmic volume through feedback mechanisms regulating chromatin gene expression, although on the whole, mathematical modelling predicts that the decrease in cell size results in a higher concentration of RNA. This suggests that the cells may respond to the resection by upregulating factors that

are sensitive to cell volume. Presumably, this adaptation response is triggered immediately after the resection, and with time the effects of gene dosage compensation become more and more evident. Thus, the nearer the resection is performed to cell polarity establishment, the stronger the effect. To fully verify whether gene dosage compensation takes place as a result of the resection, a more direct method to visualise single RNA molecules such as single RNA fluorescence in situ hybridization could be applied.

4.11.3 Transcription factor Tfap2c and Tead4 activity is required for cell polarity establishment.

Transcription factors with a high activity at the 8-cell stage were screened by RNAi knockdown experiments. Tfap2c and Tead4 were identified as potential regulators of cell polarity formation, as the knockdown of each of them impaired apical domain formation, while their co-depletion resulted in a more pronounced phenotype. One important matter to address is the identification of the downstream factors of Tfap2c/Tead4 which are responsible for triggering cell polarity establishment. The results in Chapter III demonstrate a detailed dissection of the signalling pathways responsible for cell polarity establishment, out of which the actin cytoskeleton dynamics, driven by various actin re-modellers, seem to be critical. A Chip-seq analysis of both transcription factors has been performed in the context of Trophoblast stem cells (Choi et al., 2013; Home et al., 2012). The analysis of the binding domains and potential downstream targets of both factors revealed several actin cytoskeleton regulators, such as Cfl1, Dstn, Marcksl1; and several Rho GTPases regulators, such as Arhgap8, Arhgap17, Arhgap19, Arhgef12, Arhgef18. Preliminary RNAi experiments in which each of the above candidates was knocked down failed to give a strong polarity phenotype as compared to the depletion of Tfap2c or Tead4, yet the dsRNAs' efficacy requires further assessment. Nevertheless, the strategy of screening downstream targets of Tfap2c/Tead4 based on Chip-seq analysis is limited. A potential scenario in which polarity defects are a result of secondary effects (i.e. Tfap2c/Tead4 mediated activation of other transcription factors which in turn activate polarity regulators) would be omitted in this approach. In this regard, the analysis of the global transcriptome changes upon the depletion of Tfap2c and/or Tead4 may be more appropriate. Furthermore, the determination of global transcriptome changes may have other advantages. For example, transcription factors can induce specific morphogenetic changes often via multiplex downstream factors which act in concert, instead of relying on a single target (Moroishi et al., 2015; Shahbazi et al., 2017). This is highly likely to be true for the case of Tfap2c/Tead4. Therefore, the determination of global gene expression changes could result in

a more accurate estimate of the effect on the cytoskeleton or cellular morphology, with the help of a quantitative mathematical model.

The precise role of Tfap2c/Tead4 in establishing the apical domain remains unclear, yet the overexpression experiments indicate that they may promote actin cytoskeleton reorganisation. Results in Chapter III suggest that the first step in apical domain assembly requires a polarised and activated actomyosin system that is regulated by the PKC-Rho GTPase signalling axis. This is followed by apical polarity protein recruitment, concentration and further the expansion of apical domain. The overexpression of Tfap2c/Tead4 triggered membrane protrusion-like structures enriched by apical polarity proteins such as Pard6 and Ezrin (Figure 4.18A). A detailed examination of the dynamics triggering protrusive structure formation upon Tfap2c/Tead4 overexpression revealed that the two factors were linked to the apical domain assembly, by the apical protein centralisation step, despite the lack of the apical expansion step. It seems therefore that Tfap2c/Tead4 mediated transcription activates compaction, actomyosin asymmetry, and the apical domain membrane recruitment and centralisation steps. Although Tfap2c/Tead4 overexpression is capable of triggering premature compaction as well as actomyosin asymmetry, the two factors do not seem to be necessary for this event, as the knockdown or knockout of Tfap2c/Tead4 did not impair cell compaction. As discussed in Chapter III, PKC mediated post-translational modifications are necessary and sufficient for cell compaction as well as actomyosin asymmetry, thus one possibility would be that Tfap2c/Tead4 activate cytoskeleton factors that promote PKC activity, yet other pathways can compensate for Tfap2c/Tead4's role in doing so. On the contrary, Tfap2c/Tead4 are absolutely required for apical domain protein concentration, supported by the findings that knockdown and knockout of Tfap2c/Tead4 abolished the centralisation step (Figure 4.12A), and that the overexpression of Tfap2c/Tead4 consistently triggered apical domain protein centralisation and finally protrusive structure formation. This result echoes the transcription inhibitor experiments, which suggest that the apical domain concentration step requires a proximate transcriptional activity. It is highly possible that the factors affected by transcriptional inhibitors are the downstream targets of Tfap2c/Tead4.

4.11.4 A genetic interaction between Tfap2c and Tead4

The single genetic depletion of Tfap2c or Tead4 does not result in a strong cell polarity phenotype, yet the concomitant depletion of both factors completely abolished cell polarisation. These results suggest a genetic interaction between Tfap2c and Tead4. In an attempt to address

the mechanistic importance of such observations two potential possibilities seem reasonable. Firstly, Tfap2c and Tead4 may bind to a common downstream target but at different enhancers. Both these enhancers may contribute to gene expression, yet the Tfap2c-regulated enhancer region could be more effective in triggering gene expression. This could explain why Tfap2c loss-of- or gain-of-function experiments all display a stronger phenotype over Tead4. Additional evidence could support such an idea: the master TE specifier Cdx2 is a common downstream target for both Tfap2c and the Hippo pathway regulated Tead4/Yap complex. Yet Tfap2c regulates Cdx2 expression by directly binding to a region within intron 1 of the Cdx2 genomic locus (Cao et al., 2015), whereas Taed4/Yap regulates the cis-regulatory enhancer of Cdx2 upstream of the TSS (Rayon et al., 2014). However, overexpression of Tfap2c induces a near 100-fold increase of Cdx2 expression in the embryo (Cao et al., 2015) whereas Tead4/Yap overexpression fails to do so (author's observation). Secondly, it is also possible that Tead4 compensates for Tfap2c by binding to the same loci, yet its binding is only stabilised once Tfap2c is depleted, a mechanism similar to "transcription factor competition" (Domcke et al., 2015; Karreth et al., 2014). Gene activation is always associated with intricate chromatin topology changes, therefore to fully reveal the mechanism of the Tfap2c and Tead4 collaborative regulation of cell polarisation one would need to acquire information pertaining to the changes in chromatin structure of key downstream polarity regulators upon depletion of either or both transcription factors. Several recently developed tools for capturing chromatin conformation, such as Hi-C or 5C, would be useful in addressing this question.

4.11.5 The molecular panorama of cell polarity establishment at the 8-cell stage mouse embryo and its potential implications

Results in this Chapter address some remaining questions concerning apical domain establishment from Chapter III. More importantly, these results provide a demonstration of how diverse signals integrated from post-translational modifications and transcription build the apical domain at a defined time set during mouse embryogenesis.

Results in Chapter III suggest that an asymmetric and active actomyosin network is the first prerequisite for apical domain assembly, yet its role in building the apical domain seems to be permissive, as actomyosin alone is insufficient to recruit apical domain proteins, and the missing factors only appear around the 8-cell stage (Discussion in Chapter III). The results from the current Chapter suggest that such stage dependency relies on the transcriptional input from the 4-8 cell stage downstream of transcription factors Tfap2c and Tead4. Specifically,

such transcriptional activity allows apical proteins to be recruited to the membrane and centralised to a specified region on the cell contact-free surface. Interestingly, RhoA appears to play multiple roles during this process. To begin with, in the very first phase of apical domain assembly, RhoA acts downstream of PKC to activate the actomyosin network and therefore polarises to the apical domain, providing a landmark for apical domain positioning. Secondly, at the subsequent phase of apical domain establishment, RhoA helps to expand the apical proteins to form an apical cap structure. The detailed mechanism underlying the interplay between post-translational activities (PKC, RhoA activity) and transcriptional activity (Tfap2c, Tead4/Yap mediated) calls for substantial future study. Particularly, the description of the molecular details concerning the input from actomyosin polarisation, Tfap2c/Tead4 and RhoA in defining the morphology of the apical domain will be the critical. From the results of gain-of- and loss-of function experiments of Tfap2c/Tead4 and RhoA, it seems likely that Tfap2c/Tead4 and RhoA provide complementary forces for apical domain formation. In other words, the transcriptional programme induced by Tfap2c/Tead4 specifically concentrates apical domain proteins, whereas RhoA expands these proteins, and the competition between these two components defines the dynamics of apical domain formation as well as the size of the apical domain. However the determination of the precise manner in which Tfap2c/Tead4 and RhoA work will require a better understanding of the way in which each factor affects the cytoskeleton environment and apical protein dynamics. In addition, the role of PKC-mediated actomyosin polarisation in this process will need to be better defined. The regulation of apical protein recruitment and the acquisition of a specific polarised pattern are central to cell polarity studies. The finding that PKC, Tfap2c/Tead4, and RhoA induce the self-organisation of apical domain proteins into a limited region provides an opportunity for these important topics to be addressed.

5 Conclusions

The establishment of cell polarity is an important prerequisite for mouse embryo development. It drives the transcriptional direction of outside cells to the acquisition of a trophectodermal fate and structurally prompts the entire epithelisation process including tight junction maturation and blastocoel formation (Alarcon, 2010; Watson et al., 1990; Zenker et al., 2018). Intriguingly, unlike many other model systems, cell polarity in the mouse embryo arises from a specific developmental stage. The timeframe of cell polarity establishment is closely associated with normal developmental progression, as the experimental perturbation of this timing leads to the alteration of embryonic and extra-embryonic lineage ratios (Johnson et al., 1979). Despite decades of study, the effect of timing in the regulation of cell polarisation in the mouse embryo remains poorly understood, as the detailed molecular pathways that trigger cell polarity establishment are largely unclear, and the extent of its reliance on parallel cellular processes, such as transcription and translation is undetermined. With the ultimate aim of understanding the timing regulation of cell polarity establishment, two different strategies were used in this work to tackle this long-standing developmental question.

The results in Chapter III attempted to first characterise the processes driving cell polarity establishment in depth. To this end, the dynamics of the cytoskeleton in relation to apical proteins were examined in live and fixed samples. This revealed two different phases of cell polarity establishment, with the actomyosin complex and apical domain proteins polarising at different times. Furthermore, the requirement of cell polarity establishment for generic cytoskeletal networks, such as the actomyosin network, was determined by pharmacological treatments. The results suggested that actomyosin apical polarisation serves as a scaffold for the apical protein recruitment that follows, but that actomyosin contractility is dispensable. The subsequent pharmacological screen was performed to determine the regulators associated with actomyosin polarisation and permissive for apical domain establishment. This revealed that PLC, PKC and RhoA were the critical determinants for actomyosin activation and its apical polarisation. The inhibition and activation assays using pharmacological treatments, dominant negative forms and overexpression of constitutively active constructs, together with newly developed optogenetics methods, revealed the linear relationship between PLC, PKC and RhoA in regulating actomyosin apical polarisation. Precisely, PLC activates PKC by PIP2 hydrolysis, and subsequently PKC activation triggers active RhoA apical polarisation which directs actomyosin membrane recruitment via a phosphorylation independent pathway. The

fact that actomyosin activation and polarisation happen around the early 8-cell stage implies the possibility that it may contribute to the timing regulation of apical domain establishment. However, activation of actomyosin prematurely via three different methods suggested that actomyosin activation and polarisation per se is insufficient to assemble the apical domains but instead other factors are involved in the recruitment and centralisation of the apical domain components, and these factors likely appear only around the 8-cell stage.

To reveal the mechanism that defines polarisation timing, and also to identify the missing factors complementing actomyosin in building a complete apical domain, a hypothesis-testing method was used (discussed in Chapter V) to explore the precise influence of timing on cell polarity establishment. A hypothesis whereby zygotic genome activation triggers the establishment of cell polarity through the accumulation of positive regulators has been proposed. To test this hypothesis, blastomere resection experiments alongside transcription inhibitor experiments have been performed. These revealed that cell polarity establishment relies on those transcription factors that are actively transcribed until the mid 8-cell stage. Moreover, the protein concentration of polarity activators above a specific threshold defines the timing of polarity establishment. An RNAi screen was performed to identify the key zygotic factors triggering cell polarity establishment. This allowed the detection of two transcription factors, Tfap2c and Tead4, as necessary for cell polarity establishment. The proteins levels of Tfap2c and Tead4 are steadily upregulated after ZGA up until the morula stage, and are responsible for the expression of multiple actin regulators at the early 8-cell stage. RNAi mediated knockdown and CRISPR based knockout experiments demonstrated that Tfap2c and Tead4 regulate the apical domain proteins' centralisation and expansion steps, therefore the transition from phase I to phase II. This is suggestive of the transcriptional programme activated by Tfap2c and Tead4 being responsible for triggering apical domain maturation upon actomyosin polarisation. To experimentally test this Tfap2c, Tead4 and constitutively activated RhoA were overexpressed at the 4-cell stage, and this indeed triggered the formation of apical cap domains that structurally resembled those of the late 8-cell stage, and were capable of accelerating the subsequent associated morphogenetic events such as apical domain zippering and tight junction formation.

Together, this dissertation provides a detailed explanation of the timing regulation of apical domain establishment, which will also aid in the understanding of the temporal regulation of developmental processes in general.

6 References

Abu Shah, E., and K. Keren. 2014. Symmetry breaking in reconstituted actin cortices. *Elife*. 3:e01433.

Aghion, J., C. Gueth-Hallonet, C. Antony, D. Gros, and B. Maro. 1994. Cell adhesion and gap junction formation in the early mouse embryo are induced prematurely by 6-DMAP in the absence of E-cadherin phosphorylation. *Journal of cell science*. 107 (Pt 5):1369-1379.

Ajduk, A., T. Ilozue, S. Windsor, Y. Yu, K.B. Seres, R.J. Bomphrey, B.D. Tom, K. Swann, A. Thomas, C. Graham, and M. Zernicka-Goetz. 2011. Rhythmic actomyosin-driven contractions induced by sperm entry predict mammalian embryo viability. *Nature communications*. 2:417.

Alarcon, V.B. 2010. Cell polarity regulator PARD6B is essential for trophectoderm formation in the preimplantation mouse embryo. *Biology of reproduction*. 83:347-358.

Anani, S., S. Bhat, N. Honma-Yamanaka, D. Krawchuk, and Y. Yamanaka. 2014. Initiation of Hippo signaling is linked to polarity rather than to cell position in the pre-implantation mouse embryo. *Development*. 141:2813-2824.

Arnold, T.R., R.E. Stephenson, and A.L. Miller. 2017. Rho GTPases and actomyosin: Partners in regulating epithelial cell-cell junction structure and function. *Experimental cell research*. 358:20-30.

Avilion, A.A., S.K. Nicolis, L.H. Pevny, L. Perez, N. Vivian, and R. Lovell-Badge. 2003. Multipotent cell lineages in early mouse development depend on SOX2 function. *Genes & development*. 17:126-140.

Bamburg, J.R., and B.W. Bernstein. 2010. Roles of ADF/cofilin in actin polymerization and beyond. *F1000 Biol Rep*. 2:62.

Bedzhov, I., S.J. Graham, C.Y. Leung, and M. Zernicka-Goetz. 2014. Developmental plasticity, cell fate specification and morphogenesis in the early mouse embryo. *Philosophical transactions of the Royal Society of London. Series B, Biological sciences*. 369.

Bensaude, O. 2011. Inhibiting eukaryotic transcription: Which compound to choose? How to evaluate its activity? *Transcription*. 2:103-108.

Blythe, S.A., and E.F. Wieschaus. 2015. Zygotic genome activation triggers the DNA replication checkpoint at the midblastula transition. *Cell*. 160:1169-1181.

Cao, Z., T.S. Carey, A. Ganguly, C.A. Wilson, S. Paul, and J.G. Knott. 2015. Transcription factor AP-2gamma induces early Cdx2 expression and represses HIPPO signaling to specify the trophectoderm lineage. *Development*. 142:1606-1615.

Carvalho, K., J. Lemiere, F. Faqir, J. Manzi, L. Blanchoin, J. Plastino, T. Betz, and C. Sykes. 2013. Actin polymerization or myosin contraction: two ways to build up cortical tension for symmetry breaking. *Philosophical transactions of the Royal Society of London. Series B, Biological sciences*. 368:20130005.

Chazaud, C., and Y. Yamanaka. 2016. Lineage specification in the mouse preimplantation embryo. *Development*. 143:1063-1074.

Choi, I., T.S. Carey, C.A. Wilson, and J.G. Knott. 2012. Transcription factor AP-2gamma is a core regulator of tight junction biogenesis and cavity formation during mouse early embryogenesis. *Development*. 139:4623-4632.

Choi, I., T.S. Carey, C.A. Wilson, and J.G. Knott. 2013. Evidence that transcription factor AP-2gamma is not required for Oct4 repression in mouse blastocysts. *PloS one*. 8:e65771.

Chugh, P., A.G. Clark, M.B. Smith, D.A.D. Cassani, K. Dierkes, A. Ragab, P.P. Roux, G. Charras, G. Salbreux, and E.K. Paluch. 2017. Actin cortex architecture regulates cell surface tension. *Nature cell biology*. 19:689-697.

Ciemerych, M.A., D. Mesnard, and M. Zernicka-Goetz. 2000. Animal and vegetal poles of the mouse egg predict the polarity of the embryonic axis, yet are nonessential for development. *Development*. 127:3467-3474.

Clayton, L., A. Hall, and M.H. Johnson. 1999. A role for Rho-like GTPases in the polarisation of mouse eight-cell blastomeres. *Developmental biology*. 205:322-331.

Collart, C., G.E. Allen, C.R. Bradshaw, J.C. Smith, and P. Zegerman. 2013. Titration of four replication factors is essential for the Xenopus laevis midblastula transition. *Science*. 341:893-896.

De Sousa, P.A., G. Valdimarsson, B.J. Nicholson, and G.M. Kidder. 1993. Connexin trafficking and the control of gap junction assembly in mouse preimplantation embryos. *Development*. 117:1355-1367.

Dejana, E. 2004. Endothelial cell-cell junctions: happy together. *Nature reviews. Molecular cell biology*. 5:261-270.

Deng, Q., D. Ramskold, B. Reinius, and R. Sandberg. 2014. Single-cell RNA-seq reveals dynamic, random monoallelic gene expression in mammalian cells. *Science*. 343:193-196.

Dietrich, J.E., and T. Hiiragi. 2007. Stochastic patterning in the mouse pre-implantation embryo. *Development*. 134:4219-4231.

Domcke, S., A.F. Bardet, P. Adrian Ginno, D. Hartl, L. Burger, and D. Schubeler. 2015. Competition between DNA methylation and transcription factors determines binding of NRF1. *Nature*. 528:575-579.

Ducibella, T., D.F. Albertini, E. Anderson, and J.D. Biggers. 1975. The preimplantation mammalian embryo: characterization of intercellular junctions and their appearance during development. *Developmental biology*. 45:231-250.

Ducibella, T., and E. Anderson. 1975. Cell shape and membrane changes in the eight-cell mouse embryo: prerequisites for morphogenesis of the blastocyst. *Developmental biology*. 47:45-58.

Ebnet, K., A. Suzuki, S. Ohno, and D. Vestweber. 2004. Junctional adhesion molecules (JAMs): more molecules with dual functions? *Journal of cell science*. 117:19-29.

Eckert, J.J., and T.P. Fleming. 2008. Tight junction biogenesis during early development. *Biochim Biophys Acta*. 1778:717-728.

Etter, E.F., M. Eto, R.L. Wardle, D.L. Brautigan, and R.A. Murphy. 2001. Activation of myosin light chain phosphatase in intact arterial smooth muscle during nitric oxide-induced relaxation. *The Journal of biological chemistry*. 276:34681-34685.

Fierro-Gonzalez, J.C., M.D. White, J.C. Silva, and N. Plachta. 2013. Cadherin-dependent filopodia control preimplantation embryo compaction. *Nature cell biology*. 15:1424-1433.

Fleming, T.P., P.M. Cannon, and S.J. Pickering. 1986. The cytoskeleton, endocytosis and cell polarity in the mouse preimplantation embryo. *Developmental biology*. 113:406-419.

Fleming, T.P., D.R. Garrod, and A.J. Elsmore. 1991. Desmosome biogenesis in the mouse preimplantation embryo. *Development*. 112:527-539.

Fleming, T.P., J. McConnell, M.H. Johnson, and B.R. Stevenson. 1989. Development of tight junctions de novo in the mouse early embryo: control of assembly of the tight junction-specific protein, ZO-1. *The Journal of cell biology*. 108:1407-1418.

Frankenberg, S.R., F.R. de Barros, J. Rossant, and M.B. Renfree. 2016. The mammalian blastocyst. *Wiley Interdiscip Rev Dev Biol*. 5:210-232.

Gao, Y., X. Liu, B. Tang, C. Li, Z. Kou, L. Li, W. Liu, Y. Wu, X. Kou, J. Li, Y. Zhao, J. Yin, H. Wang, S. Chen, L. Liao, and S. Gao. 2017. Protein Expression Landscape of Mouse Embryos during Pre-implantation Development. *Cell reports*. 21:3957-3969.

Gonzalez-Garcia, J.R., Z. Machaty, F.A. Lai, and K. Swann. 2013. The dynamics of PKC-induced phosphorylation triggered by Ca2+ oscillations in mouse eggs. *Journal of cellular physiology*. 228:110-119.

Goolam, M., A. Scialdone, S.J. Graham, I.C. Macaulay, A. Jedrusik, A. Hupalowska, T. Voet, J.C. Marioni, and M. Zernicka-Goetz. 2016. Heterogeneity in Oct4 and Sox2 Targets Biases Cell Fate in 4-Cell Mouse Embryos. *Cell*. 165:61-74.

Graham, S.J., K.B. Wicher, A. Jedrusik, G. Guo, W. Herath, P. Robson, and M. Zernicka-Goetz. 2014. BMP signalling regulates the pre-implantation development of extra-embryonic cell lineages in the mouse embryo. *Nature communications*. 5:5667.

Gumbiner, B.M. 2005. Regulation of cadherin-mediated adhesion in morphogenesis. *Nature reviews. Molecular cell biology*. 6:622-634.

Halder, G., S. Dupont, and S. Piccolo. 2012. Transduction of mechanical and cytoskeletal cues by YAP and TAZ. *Nature reviews. Molecular cell biology*. 13:591-600.

Handyside, A.H. 1978. Time of commitment of inside cells isolated from preimplantation mouse embryos. *Journal of embryology and experimental morphology*. 45:37-53.

Handyside, A.H. 1981. Immunofluorescence techniques for determining the numbers of inner and outer blastomeres in mouse morulae. *J Reprod Immunol*. 2:339-350.

Hartsock, A., and W.J. Nelson. 2008. Adherens and tight junctions: structure, function and connections to the actin cytoskeleton. *Biochim Biophys Acta*. 1778:660-669.

Heissler, S.M., and J.R. Sellers. 2014. Myosin light chains: Teaching old dogs new tricks. *Bioarchitecture*. 4:169-188.

Hilger-Eversheim, K., M. Moser, H. Schorle, and R. Buettner. 2000. Regulatory roles of AP-2 transcription factors in vertebrate development, apoptosis and cell-cycle control. *Gene*. 260:1-12.

Hirate, Y., S. Hirahara, K. Inoue, A. Suzuki, V.B. Alarcon, K. Akimoto, T. Hirai, T. Hara, M. Adachi, K. Chida, S. Ohno, Y. Marikawa, K. Nakao, A. Shimono, and H. Sasaki. 2013. Polarity-dependent distribution of angiomotin localizes Hippo signaling in preimplantation embryos. *Current biology : CB*. 23:1181-1194.

Home, P., B. Saha, S. Ray, D. Dutta, S. Gunewardena, B. Yoo, A. Pal, J.L. Vivian, M. Larson, M. Petroff, P.G. Gallagher, V.P. Schulz, K.L. White, T.G. Golos, B. Behr, and S. Paul. 2012. Altered subcellular localization of transcription factor TEAD4

regulates first mammalian cell lineage commitment. *Proceedings of the National Academy of Sciences of the United States of America*. 109:7362-7367.

Horn, T., and M. Boutros. 2010. E-RNAi: a web application for the multi-species design of RNAi reagents--2010 update. *Nucleic acids research*. 38:W332-339.

Howe, K., and G. FitzHarris. 2013. A non-canonical mode of microtubule organization operates throughout pre-implantation development in mouse. *Cell Cycle*. 12:1616-1624.

Huang, J., S. Wu, J. Barrera, K. Matthews, and D. Pan. 2005. The Hippo signaling pathway coordinately regulates cell proliferation and apoptosis by inactivating Yorkie, the Drosophila Homolog of YAP. *Cell*. 122:421-434.

Huang, Y., and J.K. Burkhardt. 2007. T-cell-receptor-dependent actin regulatory mechanisms. *Journal of cell science*. 120:723-730.

Humiecka, M., M. Szpila, P. Klos, M. Maleszewski, and K. Szczepanska. 2017. Mouse blastomeres acquire ability to divide asymmetrically before compaction. *PloS one*. 12:e0175032.

Hyafil, F., D. Morello, C. Babinet, and F. Jacob. 1980. A cell surface glycoprotein involved in the compaction of embryonal carcinoma cells and cleavage stage embryos. *Cell*. 21:927-934.

Jackson, A.L., S.R. Bartz, J. Schelter, S.V. Kobayashi, J. Burchard, M. Mao, B. Li, G. Cavet, and P.S. Linsley. 2003. Expression profiling reveals off-target gene regulation by RNAi. *Nat Biotechnol*. 21:635-637.

Johnson, M.H., J. Chakraborty, A.H. Handyside, K. Willison, and P. Stern. 1979. The effect of prolonged decompaction on the development of the preimplantation mouse embryo. *Journal of embryology and experimental morphology*. 54:241-261.

Johnson, M.H., and B. Maro. 1984. The distribution of cytoplasmic actin in mouse 8-cell blastomeres. *Journal of embryology and experimental morphology*. 82:97-117.

Johnson, M.H., and C.A. Ziomek. 1981. The foundation of two distinct cell lineages within the mouse morula. *Cell*. 24:71-80.

Karreth, F.A., Y. Tay, and P.P. Pandolfi. 2014. Target competition: transcription factors enter the limelight. *Genome Biol*. 15:114.

Kashyap, V., N.C. Rezende, K.B. Scotland, S.M. Shaffer, J.L. Persson, L.J. Gudas, and N.P. Mongan. 2009. Regulation of stem cell pluripotency and differentiation involves a mutual regulatory circuit of the NANOG, OCT4, and SOX2 pluripotency

transcription factors with polycomb repressive complexes and stem cell microRNAs. *Stem Cells Dev*. 18:1093-1108.

Kirton, C.A., and R. Loutzenhiser. 1998. Alterations in basal protein kinase C activity modulate renal afferent arteriolar myogenic reactivity. *Am J Physiol*. 275:H467-475.

Klompstra, D., D.C. Anderson, J.Y. Yeh, Y. Zilberman, and J. Nance. 2015. An instructive role for C. elegans E-cadherin in translating cell contact cues into cortical polarity. *Nature cell biology*. 17:726-735.

Kono, K., D.A. Tamashiro, and V.B. Alarcon. 2014. Inhibition of RHO-ROCK signaling enhances ICM and suppresses TE characteristics through activation of Hippo signaling in the mouse blastocyst. *Developmental biology*. 394:142-155.

Korotkevich, E., R. Niwayama, A. Courtois, S. Friese, N. Berger, F. Buchholz, and T. Hiiragi. 2017. The Apical Domain Is Required and Sufficient for the First Lineage Segregation in the Mouse Embryo. *Developmental cell*. 40:235-247 e237.

Koyama, H., H. Suzuki, X. Yang, S. Jiang, and R.H. Foote. 1994. Analysis of polarity of bovine and rabbit embryos by scanning electron microscopy. *Biology of reproduction*. 50:163-170.

Krishnan, K., and P.D.J. Moens. 2009. Structure and functions of profilins. *Biophys Rev*. 1:71-81.

Kuijk, E.W., L.T. van Tol, H. Van de Velde, R. Wubbolts, M. Welling, N. Geijsen, and B.A. Roelen. 2012. The roles of FGF and MAP kinase signaling in the segregation of the epiblast and hypoblast cell lineages in bovine and human embryos. *Development*. 139:871-882.

Kuraoka, I., S. Ito, T. Wada, M. Hayashida, L. Lee, M. Saijo, Y. Nakatsu, M. Matsumoto, T. Matsunaga, H. Handa, J. Qin, Y. Nakatani, and K. Tanaka. 2008. Isolation of XAB2 complex involved in pre-mRNA splicing, transcription, and transcription-coupled repair. *The Journal of biological chemistry*. 283:940-950.

Laprise, P., and U. Tepass. 2011. Novel insights into epithelial polarity proteins in Drosophila. *Trends Cell Biol*. 21:401-408.

Larue, L., M. Ohsugi, J. Hirchenhain, and R. Kemler. 1994. E-cadherin null mutant embryos fail to form a trophectoderm epithelium. *Proceedings of the National Academy of Sciences of the United States of America*. 91:8263-8267.

Latos, P.A., A.R. Sienerth, A. Murray, C.E. Senner, M. Muto, M. Ikawa, D. Oxley, S. Burge, B.J. Cox, and M. Hemberger. 2015. Elf5-centered transcription factor hub controls

trophoblast stem cell self-renewal and differentiation through stoichiometry-sensitive shifts in target gene networks. *Genes & development*. 29:2435-2448.

Lecuit, T., and P.F. Lenne. 2007. Cell surface mechanics and the control of cell shape, tissue patterns and morphogenesis. *Nature reviews. Molecular cell biology*. 8:633-644.

Leung, C.Y., and M. Zernicka-Goetz. 2013. Angiomotin prevents pluripotent lineage differentiation in mouse embryos via Hippo pathway-dependent and -independent mechanisms. *Nature communications*. 4:2251.

Levayer, R., and T. Lecuit. 2012. Biomechanical regulation of contractility: spatial control and dynamics. *Trends Cell Biol*. 22:61-81.

Levy, J.B., M.H. Johnson, H. Goodall, and B. Maro. 1986. The timing of compaction: control of a major developmental transition in mouse early embryogenesis. *Journal of embryology and experimental morphology*. 95:213-237.

Li, R., and G.G. Gundersen. 2008. Beyond polymer polarity: how the cytoskeleton builds a polarized cell. *Nature reviews. Molecular cell biology*. 9:860-873.

Loh, Y.H., Q. Wu, J.L. Chew, V.B. Vega, W. Zhang, X. Chen, G. Bourque, J. George, B. Leong, J. Liu, K.Y. Wong, K.W. Sung, C.W. Lee, X.D. Zhao, K.P. Chiu, L. Lipovich, V.A. Kuznetsov, P. Robson, L.W. Stanton, C.L. Wei, Y. Ruan, B. Lim, and H.H. Ng. 2006. The Oct4 and Nanog transcription network regulates pluripotency in mouse embryonic stem cells. *Nature genetics*. 38:431-440.

Longenecker, K., P. Read, S.K. Lin, A.P. Somlyo, R.K. Nakamoto, and Z.S. Derewenda. 2003. Structure of a constitutively activated RhoA mutant (Q63L) at 1.55 A resolution. *Acta Crystallogr D Biol Crystallogr*. 59:876-880.

Lott, J.B., and G.A. Mackie. 1988. Sequence of a cloned cDNA encoding human ribosomal protein S11. *Nucleic acids research*. 16:1205.

Louvet, C., S. Djelloul, M.E. Forgue-Lafitte, J. Mester, A. Zimber, and C. Gespach. 1996. Antiproliferative effects of the arotinoid Ro 40-8757 in human gastrointestinal and pancreatic cancer cell lines: combinations with 5-fluorouracil and interferon-alpha. *Br J Cancer*. 74:394-399.

Maitre, J.L., R. Niwayama, H. Turlier, F. Nedelec, and T. Hiiragi. 2015. Pulsatile cell-autonomous contractility drives compaction in the mouse embryo. *Nature cell biology*. 17:849-855.

Maitre, J.L., H. Turlier, R. Illukkumbura, B. Eismann, R. Niwayama, F. Nedelec, and T. Hiiragi. 2016. Asymmetric division of contractile domains couples cell positioning and fate specification. *Nature*. 536:344-348.

Manning, M.L., R.A. Foty, M.S. Steinberg, and E.M. Schoetz. 2010. Coaction of intercellular adhesion and cortical tension specifies tissue surface tension. *Proceedings of the National Academy of Sciences of the United States of America*. 107:12517-12522.

Maro, B., C. Gueth-Hallonet, J. Aghion, and C. Antony. 1991. Cell polarity and microtubule organisation during mouse early embryogenesis. *Dev Suppl*. 1:17-25.

McDole, K., Y. Xiong, P.A. Iglesias, and Y. Zheng. 2011. Lineage mapping the pre-implantation mouse embryo by two-photon microscopy, new insights into the segregation of cell fates. *Developmental biology*. 355:239-249.

Meech, R., D.B. Edelman, F.S. Jones, and H.P. Makarenkova. 2005. The homeobox transcription factor Barx2 regulates chondrogenesis during limb development. *Development*. 132:2135-2146.

Miller, C.J., and L.A. Davidson. 2013. The interplay between cell signalling and mechanics in developmental processes. *Nature reviews. Genetics*. 14:733-744.

Mitsui, K., Y. Tokuzawa, H. Itoh, K. Segawa, M. Murakami, K. Takahashi, M. Maruyama, M. Maeda, and S. Yamanaka. 2003. The homeoprotein Nanog is required for maintenance of pluripotency in mouse epiblast and ES cells. *Cell*. 113:631-642.

Moroishi, T., C.G. Hansen, and K.L. Guan. 2015. The emerging roles of YAP and TAZ in cancer. *Nat Rev Cancer*. 15:73-79.

Morris, S.A., R.T. Teo, H. Li, P. Robson, D.M. Glover, and M. Zernicka-Goetz. 2010. Origin and formation of the first two distinct cell types of the inner cell mass in the mouse embryo. *Proceedings of the National Academy of Sciences of the United States of America*. 107:6364-6369.

Munjal, A., and T. Lecuit. 2014. Actomyosin networks and tissue morphogenesis. *Development*. 141:1789-1793.

Murrell, M., P.W. Oakes, M. Lenz, and M.L. Gardel. 2015. Forcing cells into shape: the mechanics of actomyosin contractility. *Nature reviews. Molecular cell biology*. 16:486-498.

Nance, J. 2014. Getting to know your neighbor: cell polarization in early embryos. *The Journal of cell biology*. 206:823-832.

Nichols, J., B. Zevnik, K. Anastassiadis, H. Niwa, D. Klewe-Nebenius, I. Chambers, H. Scholer, and A. Smith. 1998. Formation of pluripotent stem cells in the mammalian embryo depends on the POU transcription factor Oct4. *Cell*. 95:379-391.

Nishioka, N., S. Yamamoto, H. Kiyonari, H. Sato, A. Sawada, M. Ota, K. Nakao, and H. Sasaki. 2008. Tead4 is required for specification of trophectoderm in pre-implantation mouse embryos. *Mechanisms of development*. 125:270-283.

Nishita, M., S.K. Yoo, A. Nomachi, S. Kani, N. Sougawa, Y. Ohta, S. Takada, A. Kikuchi, and Y. Minami. 2006. Filopodia formation mediated by receptor tyrosine kinase Ror2 is required for Wnt5a-induced cell migration. *The Journal of cell biology*. 175:555-562.

Niwa, H., Y. Toyooka, D. Shimosato, D. Strumpf, K. Takahashi, R. Yagi, and J. Rossant. 2005. Interaction between Oct3/4 and Cdx2 determines trophectoderm differentiation. *Cell*. 123:917-929.

Ohsugi, M., S.Y. Hwang, S. Butz, B.B. Knowles, D. Solter, and R. Kemler. 1996. Expression and cell membrane localization of catenins during mouse preimplantation development. *Dev Dyn*. 206:391-402.

Padovan-Merhar, O., G.P. Nair, A.G. Biaesch, A. Mayer, S. Scarfone, S.W. Foley, A.R. Wu, L.S. Churchman, A. Singh, and A. Raj. 2015. Single mammalian cells compensate for differences in cellular volume and DNA copy number through independent global transcriptional mechanisms. *Molecular cell*. 58:339-352.

Peng, J., F. He, C. Zhang, X. Deng, and F. Yin. 2011. Protein kinase C-alpha signals P115RhoGEF phosphorylation and RhoA activation in TNF-alpha-induced mouse brain microvascular endothelial cell barrier dysfunction. *J Neuroinflammation*. 8:28.

Pey, R., C. Vial, G. Schatten, and M. Hafner. 1998. Increase of intracellular Ca2+ and relocation of E-cadherin during experimental decompaction of mouse embryos. *Proceedings of the National Academy of Sciences of the United States of America*. 95:12977-12982.

Pollard, T.D. 2007. Regulation of actin filament assembly by Arp2/3 complex and formins. *Annu Rev Biophys Biomol Struct*. 36:451-477.

Pratt, H.P., C.A. Ziomek, W.J. Reeve, and M.H. Johnson. 1982. Compaction of the mouse embryo: an analysis of its components. *Journal of embryology and experimental morphology*. 70:113-132.

Ralston, A., B.J. Cox, N. Nishioka, H. Sasaki, E. Chea, P. Rugg-Gunn, G. Guo, P. Robson, J.S. Draper, and J. Rossant. 2010. Gata3 regulates trophoblast development downstream of Tead4 and in parallel to Cdx2. *Development*. 137:395-403.

Ramkumar, N., and B. Baum. 2016. Coupling changes in cell shape to chromosome segregation. *Nature reviews. Molecular cell biology*. 17:511-521.

Rayon, T., S. Menchero, A. Nieto, P. Xenopoulos, M. Crespo, K. Cockburn, S. Canon, H. Sasaki, A.K. Hadjantonakis, J.L. de la Pompa, J. Rossant, and M. Manzanares. 2014. Notch and hippo converge on Cdx2 to specify the trophectoderm lineage in the mouse blastocyst. *Developmental cell*. 30:410-422.

Reeve, W.J., and C.A. Ziomek. 1981. Distribution of microvilli on dissociated blastomeres from mouse embryos: evidence for surface polarization at compaction. *Journal of embryology and experimental morphology*. 62:339-350.

Reima, I., E. Lehtonen, I. Virtanen, and J.E. Flechon. 1993. The cytoskeleton and associated proteins during cleavage, compaction and blastocyst differentiation in the pig. *Differentiation*. 54:35-45.

Riethmacher, D., V. Brinkmann, and C. Birchmeier. 1995. A targeted mutation in the mouse E-cadherin gene results in defective preimplantation development. *Proceedings of the National Academy of Sciences of the United States of America*. 92:855-859.

Rossant, J., and P.P. Tam. 2009. Blastocyst lineage formation, early embryonic asymmetries and axis patterning in the mouse. *Development*. 136:701-713.

Russ, A.P., S. Wattler, W.H. Colledge, S.A. Aparicio, M.B. Carlton, J.J. Pearce, S.C. Barton, M.A. Surani, K. Ryan, M.C. Nehls, V. Wilson, and M.J. Evans. 2000. Eomesodermin is required for mouse trophoblast development and mesoderm formation. *Nature*. 404:95-99.

Samarage, C.R., M.D. White, Y.D. Alvarez, J.C. Fierro-Gonzalez, Y. Henon, E.C. Jesudason, S. Bissiere, A. Fouras, and N. Plachta. 2015. Cortical Tension Allocates the First Inner Cells of the Mammalian Embryo. *Developmental cell*. 34:435-447.

Schneider-Poetsch, T., J. Ju, D.E. Eyler, Y. Dang, S. Bhat, W.C. Merrick, R. Green, B. Shen, and J.O. Liu. 2010. Inhibition of eukaryotic translation elongation by cycloheximide and lactimidomycin. *Nat Chem Biol*. 6:209-217.

Schonegg, S., and A.A. Hyman. 2006. CDC-42 and RHO-1 coordinate acto-myosin contractility and PAR protein localization during polarity establishment in C. elegans embryos. *Development*. 133:3507-3516.

Sefton, M., M.H. Johnson, and L. Clayton. 1992. Synthesis and phosphorylation of uvomorulin during mouse early development. *Development*. 115:313-318.

Shahbazi, M.N., A. Scialdone, N. Skorupska, A. Weberling, G. Recher, M. Zhu, A. Jedrusik, L.G. Devito, L. Noli, I.C. Macaulay, C. Buecker, Y. Khalaf, D. Ilic, T. Voet, J.C. Marioni, and M. Zernicka-Goetz. 2017. Pluripotent state transitions coordinate morphogenesis in mouse and human embryos. *Nature*. 552:239-243.

Siegrist, S.E., and C.Q. Doe. 2007. Microtubule-induced cortical cell polarity. *Genes & development*. 21:483-496.

Smith, R.K., and M.H. Johnson. 1985. DNA replication and compaction in the cleaving embryo of the mouse. *Journal of embryology and experimental morphology*. 89:133-148.

Spindle, A.I. 1978. Trophoblast regeneration by inner cell masses isolated from cultured mouse embryos. *The Journal of experimental zoology*. 203:483-489.

St Johnston, D. 2018. Establishing and transducing cell polarity: common themes and variations. *Curr Opin Cell Biol*. 51:33-41.

Stephenson, R.O., Y. Yamanaka, and J. Rossant. 2010. Disorganized epithelial polarity and excess trophectoderm cell fate in preimplantation embryos lacking E-cadherin. *Development*. 137:3383-3391.

Strumpf, D., C.A. Mao, Y. Yamanaka, A. Ralston, K. Chawengsaksophak, F. Beck, and J. Rossant. 2005. Cdx2 is required for correct cell fate specification and differentiation of trophectoderm in the mouse blastocyst. *Development*. 132:2093-2102.

Tarkowski, A.K., and J. Wroblewska. 1967. Development of blastomeres of mouse eggs isolated at the 4- and 8-cell stage. *Journal of embryology and experimental morphology*. 18:155-180.

Thomas, F.C., B. Sheth, J.J. Eckert, G. Bazzoni, E. Dejana, and T.P. Fleming. 2004. Contribution of JAM-1 to epithelial differentiation and tight-junction biogenesis in the mouse preimplantation embryo. *Journal of cell science*. 117:5599-5608.

Thomas, M.L., D.J. Simmons, L. Kidder, and M.J. Ibarra. 1991. Calcium metabolism and bone mineralization in female rats fed diets marginally sufficient in calcium: effects of increased dietary calcium intake. *Bone Miner*. 12:1-14.

Torres, M., A. Stoykova, O. Huber, K. Chowdhury, P. Bonaldo, A. Mansouri, S. Butz, R. Kemler, and P. Gruss. 1997. An alpha-E-catenin gene trap mutation defines its function in preimplantation development. *Proceedings of the National Academy of Sciences of the United States of America*. 94:901-906.

Varnai, P., and T. Balla. 1998. Visualization of phosphoinositides that bind pleckstrin homology domains: calcium- and agonist-induced dynamic changes and relationship to myo-[3H]inositol-labeled phosphoinositide pools. *The Journal of cell biology*. 143:501-510.

Vestweber, D., A. Gossler, K. Boller, and R. Kemler. 1987. Expression and distribution of cell adhesion molecule uvomorulin in mouse preimplantation embryos. *Developmental biology*. 124:451-456.

Vicente-Manzanares, M., and A.R. Horwitz. 2010. Myosin light chain mono- and di-phosphorylation differentially regulate adhesion and polarity in migrating cells. *Biochem Biophys Res Commun*. 402:537-542.

Vinot, S., T. Le, S. Ohno, T. Pawson, B. Maro, and S. Louvet-Vallee. 2005. Asymmetric distribution of PAR proteins in the mouse embryo begins at the 8-cell stage during compaction. *Developmental biology*. 282:307-319.

Wang, Y., J. Shi, K. Chai, X. Ying, and B.P. Zhou. 2013. The Role of Snail in EMT and Tumorigenesis. *Curr Cancer Drug Targets*. 13:963-972.

Watanabe, T., J.S. Biggins, N.B. Tannan, and S. Srinivas. 2014. Limited predictive value of blastomere angle of division in trophectoderm and inner cell mass specification. *Development*. 141:2279-2288.

Watson, A.J., C.H. Damsky, and G.M. Kidder. 1990. Differentiation of an epithelium: factors affecting the polarized distribution of Na+,K(+)-ATPase in mouse trophectoderm. *Developmental biology*. 141:104-114.

Wedlich-Soldner, R., S. Altschuler, L. Wu, and R. Li. 2003. Spontaneous cell polarization through actomyosin-based delivery of the Cdc42 GTPase. *Science*. 299:1231-1235.

Weiner, J.L., C.F. Valenzuela, P.L. Watson, C.J. Frazier, and T.V. Dunwiddie. 1997. Elevation of basal protein kinase C activity increases ethanol sensitivity of GABA(A) receptors in rat hippocampal CA1 pyramidal neurons. *J Neurochem*. 68:1949-1959.

White, M.D., and N. Plachta. 2015. How adhesion forms the early mammalian embryo. *Curr Top Dev Biol*. 112:1-17.

Wianny, F., and M. Zernicka-Goetz. 2000. Specific interference with gene function by double-stranded RNA in early mouse development. *Nature cell biology*. 2:70-75.

Winkel, G.K., J.E. Ferguson, M. Takeichi, and R. Nuccitelli. 1990. Activation of protein kinase C triggers premature compaction in the four-cell stage mouse embryo. *Developmental biology*. 138:1-15.

Winklbauer, R. 2015. Cell adhesion strength from cortical tension - an integration of concepts. *Journal of cell science*. 128:3687-3693.

Wu, J., B. Huang, H. Chen, Q. Yin, Y. Liu, Y. Xiang, B. Zhang, B. Liu, Q. Wang, W. Xia, W. Li, Y. Li, J. Ma, X. Peng, H. Zheng, J. Ming, W. Zhang, J. Zhang, G. Tian, F. Xu,

Z. Chang, J. Na, X. Yang, and W. Xie. 2016. The landscape of accessible chromatin in mammalian preimplantation embryos. *Nature*. 534:652-657.

Yagi, R., M.J. Kohn, I. Karavanova, K.J. Kaneko, D. Vullhorst, M.L. DePamphilis, and A. Buonanno. 2007. Transcription factor TEAD4 specifies the trophectoderm lineage at the beginning of mammalian development. *Development*. 134:3827-3836.

Zenker, J., M.D. White, M. Gasnier, Y.D. Alvarez, H.Y.G. Lim, S. Bissiere, M. Biro, and N. Plachta. 2018. Expanding Actin Rings Zipper the Mouse Embryo for Blastocyst Formation. *Cell*. 173:776-791 e717.

Zernicka-Goetz, M. 1998. Fertile offspring derived from mammalian eggs lacking either animal or vegetal poles. *Development*. 125:4803-4808.

Zernicka-Goetz, M., S.A. Morris, and A.W. Bruce. 2009. Making a firm decision: multifaceted regulation of cell fate in the early mouse embryo. *Nature reviews. Genetics*. 10:467-477.

Zernicka-Goetz, M., J. Pines, S. McLean Hunter, J.P. Dixon, K.R. Siemering, J. Haseloff, and M.J. Evans. 1997. Following cell fate in the living mouse embryo. *Development*. 124:1133-1137.

Zhang, Y., J.C. Yu, T. Jiang, R. Fernandez-Gonzalez, and T.J.C. Harris. 2018. Collision of Expanding Actin Caps with Actomyosin Borders for Cortical Bending and Mitotic Rounding in a Syncytium. *Developmental cell*. 45:551-564 e554.

Zhao, B., L. Li, Q. Lu, L.H. Wang, C.Y. Liu, Q. Lei, and K.L. Guan. 2011. Angiomotin is a novel Hippo pathway component that inhibits YAP oncoprotein. *Genes & development*. 25:51-63.

Zhao, B., X. Ye, J. Yu, L. Li, W. Li, S. Li, J. Yu, J.D. Lin, C.Y. Wang, A.M. Chinnaiyan, Z.C. Lai, and K.L. Guan. 2008. TEAD mediates YAP-dependent gene induction and growth control. *Genes & development*. 22:1962-1971.

Ziomek, C.A., and M.H. Johnson. 1980. Cell surface interaction induces polarization of mouse 8-cell blastomeres at compaction. *Cell*. 21:935-942.

Ziomek, C.A., and M.H. Johnson. 1981. Properties of polar and apolar cells from the 16-cell mouse morula. *Wilehm Roux Arch Dev Biol*. 190:287-296.

Zuo, E., Y.J. Cai, K. Li, Y. Wei, B.A. Wang, Y. Sun, Z. Liu, J. Liu, X. Hu, W. Wei, X. Huo, L. Shi, C. Tang, D. Liang, Y. Wang, Y.H. Nie, C.C. Zhang, X. Yao, X. Wang, C. Zhou, W. Ying, Q. Wang, R.C. Chen, Q. Shen, G.L. Xu, J. Li, Q. Sun, Z.Q. Xiong, and H. Yang. 2017. One-step generation of complete gene knockout mice and

monkeys by CRISPR/Cas9-mediated gene editing with multiple sgRNAs. *Cell Res*. 27:933-945.

7 Appendix I: original publications and manuscripts

Research articles:

Zhu, M., Zernicka-Goetz, M. (2018) The timing mechanism of de novo cell polarisation and morphogenesis in the early mouse embryo. *Submitted.*

Zhu, M., C.Y. Leung, M.N. Shahbazi, and M. Zernicka-Goetz. 2017. Actomyosin polarisation through PLC-PKC triggers symmetry breaking of the mouse embryo. Nature communications. 8:921.

Review:

Leung, C.Y., M. Zhu, and M. Zernicka-Goetz. 2016. Polarity in Cell-Fate Acquisition in the Early Mouse Embryo. Curr Top Dev Biol. 120:203-234.